

**Multicomponent Network and Linear Polymer Systems:  
Thermal and Morphological Characterization**

by

**Niranjan M. Patel**

Dissertation submitted to the Faculty of the  
Virginia Polytechnic Institute and State University  
in partial fulfillment of the requirements for the degree of

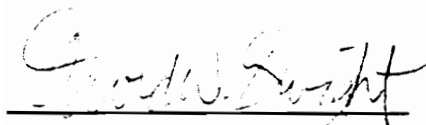
**Doctor of Philosophy**

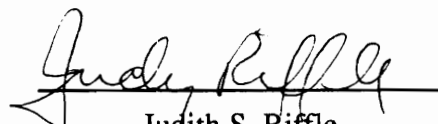
in

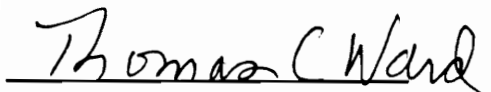
**Materials Engineering Science**

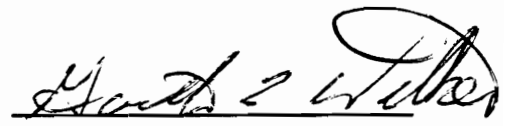
APPROVED:

  
James E. McGrath, Chair

  
David W. Dwight

  
Judith S. Riffle

  
Thomas C. Ward

  
Garth L. Wilkes

October, 1990  
Blacksburg, Virginia

# **Multicomponent Network and Linear Polymer Systems: Thermal and Morphological Characterization**

by

Niranjan M. Patel

James E. McGrath, Chair

Departments of Materials Engineering Science and Chemistry

## **(ABSTRACT)**

Materials comprising of two or more polymeric components have achieved considerable technological significance in the last decade or so due to the unique properties often not attainable in their homopolymeric counterparts. In the present work, two such systems-one involving modified thermosets and the other involving thermoplastic polymer blends, have been studied with regard to their morphological and thermal properties. Both systems take the advantage of not only the physical interactions between the components involved but also their thermooxidative properties, giving rise to novel properties that have both fundamental and practical importance.

The network system consists of a phenolic novolac based epoxy cured in the presence of low molecular weight poly(propylene oxide). The resulting morphology of these polymers has been studied with the help of scanning electron microscopy. It is shown that variables



such as composition, temperature of cure, catalyst concentration, nature of curing agent, molecular weights, and end-group functionality of poly(propylene oxide) can strongly influence the morphological behavior. By changing one or more of these variables, one can obtain a broad spectrum of morphologies having homogeneous to stable microphase separated to grossly phase separated two-phase structures. An attempt has been made to explain the observed morphological behavior on the basis of the combined effects of chemical, thermodynamic, and kinetic aspects of the phase separation process. Complementary to the study of morphology, the cure behavior of this system was also investigated to develop relationships such as those represented by the time-temperature-transformation diagram. Dynamic mechanical analysis was utilized to monitor the thermomechanical properties of neat epoxy as well as poly(propylene oxide)-modified epoxy *in situ* during cure. Results of both isothermal and dynamic cure studies are presented. Finally, degradation behavior of the system has been studied with the help of thermogravimetric analysis. Poly(propylene oxide) undergoes thermooxidative decomposition at relatively lower temperatures than epoxy. Thus once a well-controlled morphology in a cured system consisting of poly(propylene oxide) and epoxy is obtained, the former can be selectively removed by an appropriate heat treatment leaving microporosity in matrix of the latter. This concept has been successfully demonstrated in the form of thin microporous coatings for application in magnetic disks.

The linear system consists of a commercial isotactic polypropylene blended with poly(vinyl methyl ether). Miscibility-immiscibility aspects of this system has been studied with the help of crystallization kinetics and melting point behavior via differential scanning calorimetry and the morphological behavior via scanning electron microscopy. It is shown that although the two polymers do not possess physical miscibility, the thermooxidative

interaction occurring between poly(vinyl methyl ether) and polypropylene may induce *chemical* miscibility. Supporting evidence from fourier transform infra-red spectroscopy and nuclear magnetic resonance spectroscopy suggests the possibility of a free radical mechanism by which poly(vinyl methyl ether) may graft onto polypropylene chains during the processing of the blends. The grafted poly(vinyl methyl ether) is then thought to be responsible for the slower crystallization rates and the depression of melting point, the properties classically displayed by miscible polymers containing one crystallizable component.

## Acknowledgements

---

I must first begin by expressing a deep sense of gratitude and appreciation towards my advisor Professor James E. McGrath for giving me an opportunity to work for him, and for his support, encouragement, and patience throughout my graduate work at Virginia Tech.

Thanks are due to Professors David W. Dwight, Garth L. Wilkes, Thomas C. Ward and Judith S. Riffle for serving in my graduate committee and for their help and suggestions for this research. Acknowledged too are the contributions of Professor Herve Marand through many insightful discussions. Apart from their direct involvement in the research, I would also like to thank them for being excellent teachers and for introducing me to the world of polymer science.

I would also like to thank Dr. R. Bruce Prime for his collaboration from IBM, San Jose on much of what is presented here. The opportunity to work with him at IBM during the summer of 1988 was particularly enjoyable and rewarding. Appreciation is also extended to Connie Moy and Mark Allen for all their help during my stay at IBM.

I wish to thank Jeff Hedrick, Steve Liptak, and Silvia Parisi for sharing the lab with me without many mishaps; Steve McCartney for his technical expertise at SEM; Darlene Alison, Alison Goforth, Guru Sinai-Zingde, Young Tai Yoo and Soner Kilic for their contributions at various stages of my research. The financial support of IBM Corporation and Akzo Corporation for this research are also gratefully acknowledged.

The friendship and love of many during my stay in Blacksburg has played much more important role than one can read from this dissertation. For that, I would like to thank Steve McCartney, Jan Clare, Jan West-Hansen, Eric Sallee, Barb Holcomb, Klaus Hofmann, Emilios Dimitriadis, Vasso Petroussi, Andreas Doulis, and many many more. Blacksburg will always remain a special place for me because of them.

Finally, I would like to thank my parents and my family for their love, support, encouragement, and understanding all these years.

*dedicated to Baa and Bapuji*

*for*

*being there*

# Table of Contents

---

**Abstract** *ii*

**Acknowledgements** *v*

**List of Figures** *xiii*

**List of Tables** *xxii*

## **Chapter I**

**Introduction** *1*

1.1 Multicomponent Polymer Systems *1*

1.2 Miscibility vs Compatibility *4*

1.3 Research Focus *7*

1.4 Dissertation Format *8*

## **Chapter II**

**Poly(propylene oxide)- modified Epoxy:**

**Microporosity in Polymer Films** *9*

2.1 Introduction *9*

2.1.1 Lubrication in Rigid Disk Drives *10*

2.1.2 Proposed Approach for Microporosity Development *14*

2.1.3 Research Objectives *16*

2.1.4 Chapter Organization *18*

2.2 Literature Review *20*

2.2.1 Morphology in Modified Thermosets *20*

2.2.1.1 Phase Separation Process: Thermodynamic Considerations *22*

2.2.1.1.1 Phase Diagram for Polymer Mixtures *22*

2.2.1.1.2	Flory-Huggins Theory	27
2.2.1.1.3	Applicability to Modified Thermosets	30
2.2.1.2	Chemistry-Morphology Relationships	34
2.2.1.2.1	Molecular Nature of the Modifier	37
2.2.1.2.2	Chemical Nature of the Thermoset	44
2.2.1.2.3	Composition	48
2.2.1.2.4	Cure Conditions	50
2.2.1.3	Theoretical Modeling of Phase Separation	55
2.2.1.3.1	Thermodynamics	56
2.2.1.3.2	Kinetics	59
2.2.1.3.3	Model Predictions	61
2.2.1.3.4	Theory-Experiment Correlations	65
2.2.1.4	Summary	66
2.2.2	Cure Behavior of Thermosets	66
2.2.2.1	The Time-Temperature-Transformation Diagram	69
2.2.2.2	Experimental Methods	72
2.2.2.3	Modeling of Cure Behavior	76
2.2.2.4	Summary	80
2.2.3	Thermal Degradation of Poly(propylene oxide)	81
2.2.3.1	General	81
2.2.3.2	Pyrolytic Degradation of Poly(propylene oxide)	85
2.2.3.3	Thermooxidative Degradation of Poly(propylene oxide)	87
2.2.3.4	Effect of End-group on Degradation of Poly(propylene oxide)	90
2.2.3.5	Summary	92
2.3	Experimental	93
2.3.1	Materials	93
2.3.1.1	Thermoset System	93
2.3.1.1.1	Epoxy Resins	93
2.3.1.1.2	Curing Agents	93
2.3.1.1.3	Catalysts	95
2.3.1.2	Poly(propylene oxide)s	95
2.3.1.3	Miscellaneous	98

- 2.3.2 Methods 98
  - 2.3.2.1 Sample Preparation 98
    - 2.3.2.1.1 Morphological Studies 98
    - 2.3.2.1.2 Cure Studies 101
    - 2.3.2.1.3 Degradation and Microporosity Studies 101
  - 2.3.2.2 Analysis 102
    - 2.3.2.2.1 Scanning Electron Microscopy 102
    - 2.3.2.2.2 Dynamic Mechanical Analysis 104
    - 2.3.2.2.3 Thermogravimetric Analysis 107
    - 2.3.2.2.4 Lubricant Retention 107
- 2.4 Results and Discussion 108
  - 2.4.1 Morphology Behavior 108
    - 2.4.1.1 System Variables 108
    - 2.4.1.2 Effect of Cure Chemistry 110
    - 2.4.1.3 Effect of Poly(propylene oxide) End-group 129
    - 2.4.1.4 Effect of Composition 134
    - 2.4.1.5 Effect of Temperature of Cure 138
    - 2.4.1.6 Effect of Poly(propylene oxide) Molecular Weight 150
    - 2.4.1.7 Effect of Catalyst Concentration 155
  - 2.4.2 Cure Behavior 159
    - 2.4.2.1 Neat Epoxy 159
      - 2.4.2.1.1 Isothermal Cure 159
      - 2.4.2.1.2 Dynamic Cure 163
      - 2.4.2.1.3 Glass Transition Temperature of Fully Cured System 169
    - 2.4.2.2 Poly(propylene oxide)- modified Epoxy 172
      - 2.4.2.2.1 Isothermal Cure 172
      - 2.4.2.2.2 Dynamic Cure 175
      - 2.4.2.2.3 Glass Transition Temperature of Fully Cured System 177
    - 2.4.2.3 Time-Temperature-Transformation Diagram 177
  - 2.4.3 Degradation Behavior and Microporosity Development 180
    - 2.4.3.1 Thermogravimetric Analysis 180



2.4.3.1.1 Neat Poly(propylene oxide) 180

2.4.3.1.2 Cured Films 183

2.4.3.2 Dynamic Mechanical Analysis 183

2.4.3.3 Scanning Electron Microscopy 188

2.4.3.3.1 Bulk Film 188

2.4.3.3.2 Disk Coatings 191

2.5 Conclusions 195

2.6 Future Directions for Research 197

Appendices 199

2.I Conversion of Hydroxyl End-groups of Poly(propylene oxide) 199

2.II Thermodynamic Relations for Modified Thermosets 199

2.III Estimation of Solubility Parameters by Group Contribution Method 202

2.IV Conversion at Gelation for Epoxy Cured with Various Curing Agents 205

## **Chapter III**

**Polypropylene - Poly(vinyl methyl ether) Blends 207**

3.1 Introduction 207

3.2 Experimental 211

3.3 Results and Discussion 214

3.3.1 Dynamic Crystallization 214

3.3.2 Isothermal Crystallization 218

3.3.3 Morphology 221

3.3.4 Effect of Solvent Extraction 221

3.3.5 Effect of Heat Treatment 223

3.3.6 Thermooxidative Behavior of Poly(vinyl methyl ether) 225

3.4 Conclusions 237

3.5 Future Recommendations and Implications 238

**References** 240

**Vita** 257

## List of Figures

---

Figure 1.1.1	An example of natural multicomponent, multiphase polymeric system	3
Figure 1.1.2	An example of a human-made multicomponent polymer system	5
Figure 2.1.1	Magnetic disk drive in a modern computer system	11
Figure 2.1.2	Flowsheet for rigid disk fabrication process	13
Figure 2.2.1	Free energy of mixing for binary mixtures which are completely miscible, partially miscible and completely immiscible	24
Figure 2.2.2	T- $\phi$ phase diagram for polymer mixtures	25
Figure 2.2.3	p- $\phi$ diagram for modified thermosets	32
Figure 2.2.4	Cloud point temperature vs mass fraction of CTBN for mixtures of CTBN with epoxy monomers of different molar masses	33
Figure 2.2.5	(a) UCST type phase diagram of epoxy oligomer/CTBN mixture (b) variation of phase diagram with increase in molecular weight of epoxy	35
Figure 2.2.6	(a) Phase diagram of epoxy oligomer/poly(ether sulfone) mixture (b) Schematic representation of the variation of phase diagram and T <sub>g</sub> with curing	36
Figure 2.2.7	Cloud point curves for DGEBA-CTBN system	39
Figure 2.2.8	Morphology of siloxane modified epoxy networks	41

Figure 2.2.9	Effect of modifier molecular weight on phase behavior of an epoxy system containing polysulfone	45
Figure 2.2.10	Effect of type and concentration of hardener on microstructure of an epoxy containing CTBN rubber	47
Figure 2.2.11	Phase inversion in modified thermosets	49
Figure 2.2.12	Models depicting relation between phase separation and cure conditions	52
Figure 2.2.13	Time Temperature Transformation (TTT) diagram inclusive of phase separation for a CTBN modified epoxy system	54
Figure 2.2.14	(a) Gibbs free energy of mixing per unit volume vs modifier volume fraction (b) Gibbs free energy change in the phase separation process vs modifier concentration in the precipitated phase	58
Figure 2.2.15	Evolution of different quantities that characterize the morphology as a function of the thermoset conversion	62
Figure 2.2.16	Final values of different quantities that characterize the morphology as functions of (a) temperature of cure, (b) polymerization rate, and (c) initial modifier concentration	63
Figure 2.2.17	Schematic two-dimensional representation of curing of a thermoset	67
Figure 2.2.18	Schematic time-temperature-transformation (TTT) isothermal cure diagram for a thermosetting system	70
Figure 2.2.19	A typical torsional braid analysis (TBA) spectrum during an isothermal cure showing changes in the relative rigidity and logarithmic decrement vs time	74

Figure 2.2.20	Mechanisms for thermal degradation by pyrolysis	86
Figure 2.2.21	Mass spectrum of volatile fragments of commercial poly(propylene oxide) exposed in air at ~185 °C	89
Figure 2.3.1	The Dupont 982 DMA horizontal clamp assembly with a wire mesh sample for cure studies	105
Figure 2.3.2	A three step DMA method used to study <i>in situ</i> the cure behavior of epoxy systems	106
Figure 2.4.1	Reaction scheme for base catalyzed novolac epoxy - anhydride cure	111
Figure 2.4.2	Reaction scheme for base catalyzed novolac epoxy - Bis-S cure	113
Figure 2.4.3	Reaction scheme for novolac epoxy - amine cure	114
Figure 2.4.4	SEM photomicrographs showing the effect of curing agent on morphology of 5% by weight PPG-1025 modified Quatex-2010 cured at 150 °C for 2 hours	115
Figure 2.4.5	p- $\phi$ diagram of a modified thermoset undergoing cure illustrating the characteristic conversion span $\Delta p$ in which phase separation takes place	119
Figure 2.4.6	Schematic representation of the changes in the viscosity and mobility as a function of conversion in a modified thermoset undergoing cure	121
Figure 2.4.7	Proposed mechanism for co-reaction of hydroxyl terminated PPO during a base catalyzed anhydride - epoxy cure	126
Figure 2.4.8	FTIR spectra of a mixture of PPG-1025, NMA and DMP-30 before and after reaction at 100 °C for 2 hours	127

Figure 2.4.9	FTIR spectra of PPG-1025 and PPG-1025E illustrating the replacement of the hydroxyl functionality of the former with an aromatic ester	130
Figure 2.4.10	SEM photomicrographs showing the effect of PPO end-groups on morphology in Quatrex-2010/NMA/DMP-30 system	132
Figure 2.4.11	SEM photomicrographs showing the effect of PPO end-groups on morphology in Quatrex-2010/NMA/DMP-30 system	133
Figure 2.4.12	SEM photomicrographs showing the effect of PPO content on morphology in Quatrex-2010/NMA/DMP-30 system	135
Figure 2.4.13	Schematic representation of the relation between $\Delta p$ and modifier content	137
Figure 2.4.14	SEM photomicrographs showing the effect of PPO content on morphology in Quatrex-2710/Bis-S/TMAH system	139
Figure 2.4.15	SEM photomicrographs showing the effect of temperature of cure on morphology in Quatrex-2010/NMA/DMP-30 system	140
Figure 2.4.16	Schematic representation of the relation between $\Delta p$ and the temperature of cure	142
Figure 2.4.17	SEM photomicrographs showing the effect of post-cure on the room temperature cured Quatrex-2010/NMA/DMP-30 system	145
Figure 2.4.18	SEM photomicrographs showing the effect of temperature of cure on morphology in Quatrex-2010/NMA/DMP-30 system	148
Figure 2.4.19	SEM photomicrographs showing the effect of post-cure on the room temperature cured Quatrex-2010/NMA/DMP-30 system	149

Figure 2.4.20	SEM photomicrographs showing the effect of temperature of cure on morphology in Quatrex-2710/Bis-S/TMAH system	151
Figure 2.4.21	SEM photomicrographs showing the effect of PPO molecular weight on morphology in Quatrex-2010/NMA/DMP-30 system	152
Figure 2.4.22	SEM photomicrographs showing the effect of PPO molecular weight on morphology in Quatrex-2710/Bis-S/TMAH system	154
Figure 2.4.23	SEM photomicrographs showing the effect of catalyst concentration on the morphology in Quatrex-2010/NMA/DMP-30 system	156
Figure 2.4.24	A $p$ - $\phi$ diagram illustrating the different routes followed by the cure path after it enters the metastable region in accordance with the rate of reaction	158
Figure 2.4.25	Isothermal DMA curing curves of the neat epoxy system	160
Figure 2.4.26	The gelation region of the 60 °C isothermal DMA curves of the neat epoxy system	162
Figure 2.4.27	5 °C/minute dynamic DMA scans as a function of pre-cure temperature in neat epoxy	164
Figure 2.4.28	(a) Model suggesting various stages in which the glass transition temperature of the system competes with the sample temperature in explanation of: (b) dynamic DMA curves after 40 °C isothermal pre-cure	167
Figure 2.4.29	Relationship between the glass transition temperature of the fully cured system and the isothermal pre-cure temperature in neat epoxy	170
Figure 2.4.30	5 °C/minute dynamic TGA scan of previously uncured neat epoxy in nitrogen	171

Figure 2.4.31	Isothermal DMA curing curves of PPO-modified epoxy	173
Figure 2.4.32	Comparison of the 100 °C isothermal curing behavior of neat and PPO-modified epoxy	174
Figure 2.4.33	5 °C/minute dynamic DMA scans as a function of pre-cure temperature in PPO-modified epoxy	176
Figure 2.4.34	Relationship between the glass transition temperature of the fully cured system and the isothermal pre-cure temperature in PPO-modified epoxy	178
Figure 2.4.35	TTT diagram based on the DMA data of neat and PPO-modified epoxies	179
Figure 2.4.36	5 °C/minute dynamic TGA scans of PPG-1025 in air and nitrogen	181
Figure 2.4.37	Isothermal TGA scans of PPG-1025 in air and nitrogen at different temperatures	182
Figure 2.4.38	200 °C isothermal TGA scans in air of neat and 10% PPG-1025 containing epoxy systems cured at 60 °C/12 hours + 150 °C/3 hours	184
Figure 2.4.39	5 °C/minute dynamic DMA scans on wire-mesh films of neat and 10% PPG-1025 containing epoxy systems cured at 60 °C/12 hours + 150 °C/3 hours	186
Figure 2.4.40	5 °C/minute dynamic DMA scans on wire-mesh films of neat and 10% PPG-1025 containing epoxy systems cured at 60 °C/12 hours + 150 °C/3 hours after heat treatment at 200 °C for 12 hours	187



Figure 2.4.41	SEM photomicrographs showing the effect of heat treatment at 200 °C for 12 hours on the bulk morphology of 10% PPG-1025 containing epoxy sample cured at 60 °C for 12 hours + 150 °C for 3 hours	189
Figure 2.4.42	SEM photomicrographs showing the effect of heat treatment at 200 °C for 12 hours on the surface of 10% PPG-1025 containing epoxy sample cured at 60 °C/12 hours + 150 °C/3 hours	190
Figure 2.4.43	Comparison of the morphology of 10% PPG-1025 containing epoxy disk-coating with wire-mesh film of the same composition	192
Figure 2.4.44	Surface morphology of 25% PPG-1025 containing epoxy disk-coating showing microporosity development after heat treatment of 200 °C for 12 hours	194
Figure 3.1.1	Schematic representation of different types of copolymers acting as interfacial agents	209
Figure 3.2.1	DSC methods for study of crystallization and melting behavior in PP/PVME blends	213
Figure 3.3.1	Dynamic crystallization behavior of neat polypropylene and polypropylene-poly(vinyl methyl ether) blends	215
Figure 3.3.2	Melting point behavior of neat polypropylene and polypropylene-poly(vinyl methyl ether) blends after dynamic crystallization	216
Figure 3.3.3	132 °C isothermal crystallization behavior of neat polypropylene and polypropylene-poly(vinyl methyl ether) blends	219
Figure 3.3.4	Melting point behavior of neat polypropylene and polypropylene-poly(vinyl methyl ether) blends after 132 °C isothermal crystallization	220

Figure 3.3.5	SEM photomicrographs showing the morphology of polypropylene-poly(vinyl methyl ether) blends	222
Figure 3.3.6	Effect of solvent extraction on the melting point behavior following 132 °C isothermal crystallization of Blend(210-30)	224
Figure 3.3.7	Effect of 210 °C heat treatment on 132 °C isothermal crystallization behavior of Blend(200-15)	226
Figure 3.3.8	Effect of 210 °C heat treatment on melting point behavior following 132 °C isothermal crystallization of Blend(200-15)	227
Figure 3.3.9	Comparison of the melting point behavior after 132 °C isothermal crystallization of (a) Blend(200-15), (b) Blend(200-15) after 15 minutes at 210 °C, and (c) Blend(210-30)	228
Figure 3.3.10	Effect of 210 °C heat treatment on 132 °C isothermal crystallization behavior of neat polypropylene	229
Figure 3.3.11	Effect of 210 °C heat treatment on 132 °C melting point behavior following 132 °C isothermal crystallization of neat polypropylene	230
Figure 3.3.12	10 °C/minute dynamic TGA scan in air of poly(vinyl methyl ether)	231
Figure 3.3.13	Isothermal TGA scans in air and nitrogen of poly(vinyl methyl ether)	232
Figure 3.3.14	FTIR spectra of poly(vinyl methyl ether) before and after heat treatment at 210 °C for 15 minutes	234
Figure 3.3.15	<sup>13</sup> Carbon CP/MAS NMR spectrum of crosslinked poly(vinyl methyl ether) after 15 minutes at 210 °C	235

Figure 3.3.16 Proposed mechanism for thermooxidative degradation of poly(vinyl methyl ether)

## List of Tables

---

Table 2.2.1	Effect of various end-group functionalities on thermal stability of poly(propylene oxide)	91
Table 2.3.1	Epoxy resins	94
Table 2.3.2	Curing agents	96
Table 2.3.3	Catalysts	97
Table 2.3.4	Poly(propylene oxide)s	99
Table 2.3.5	Spin-coating formulations and conditions for preparation of magnetic disk coatings	103
Table 2.4.1	Comparison of compatibility-incompatibility properties of cured poly(propylene oxide) modified epoxy systems using various catalysts	117
Table 2.4.2	Comparison of various curing agents based on their physico-chemical properties that affect the process of phase separation in poly(propylene oxide) modified epoxy systems	123

# Chapter I

## Introduction

---

### 1.1 MULTICOMPONENT POLYMER SYSTEMS

With polymers coming of age, the requirements demanded from them are becoming more and more stringent. Today's polymers find their usage in virtually every aspect of human life, from toys to aircrafts to microchips. In each application, the selected material is expected to have several specific properties simultaneously, sometimes even those that might seem to be in contrast with each other. For example in the composite matrix application, the polymer not only must possess superior stiffness but should also show considerable "toughness", in addition to other properties such as excellent adhesion to the reinforcing component, resistance to environmental conditions, etc. In order to achieve such diversity in a single system, polymer scientists have at their disposal the possibility of modification of the chemical structure of the polymer backbone itself. However, this route

is found to be increasingly difficult to follow due to restrictions imposed by factors arising from chemistry, economics and environmental concerns. An alternate approach which has become extremely popular more recently is to combine two or more existing polymers to produce the metallurgical equivalent of *alloys*. By this method, the end result is hoped to be materials which are stronger, tougher, more flexible, environmentally more stable, have proper interfacial character and a host of many other desirable properties which would otherwise be difficult to obtain in their homopolymeric counterparts. Of course, nature has exploited the philosophy of multicomponent polymer systems in many elegant ways much before the advent of modern polymer science. For instance, a wool fiber consists of a large number of chemically and structurally different protein macromolecules blended to give an unique material.<sup>1</sup> Figure 1.1.1 shows a cross sectional view of the bulk of this natural fiber, known as alpha-keratin, where crystalline microfibrils derived from a low sulfur protein are hexagonally packed in a crosslinked rubbery matrix made of a high sulfur protein.<sup>2</sup> The idea of utilizing certain characteristic property of one polymer to benefit the overall behavior of the entire system form the basis of the concept of multicomponent polymeric systems.

The multicomponent systems do not display only a combination of properties attributable to their individual components. Quite frequently, synergistic behavior arise that can be traced not to the mere *presence* of the components but more importantly from the way they are brought together, i. e. from their precise *morphological* arrangement. One of the best known examples of this would be rubber toughened thermoplastics such as high impact polystyrene or HIPS. The latter is, incidentally, one of the oldest commercial multicomponent systems and was developed in the 1940's.<sup>3</sup> More mechanical energy is needed to fracture HIPS than either of its pure components, e.g. polystyrene and

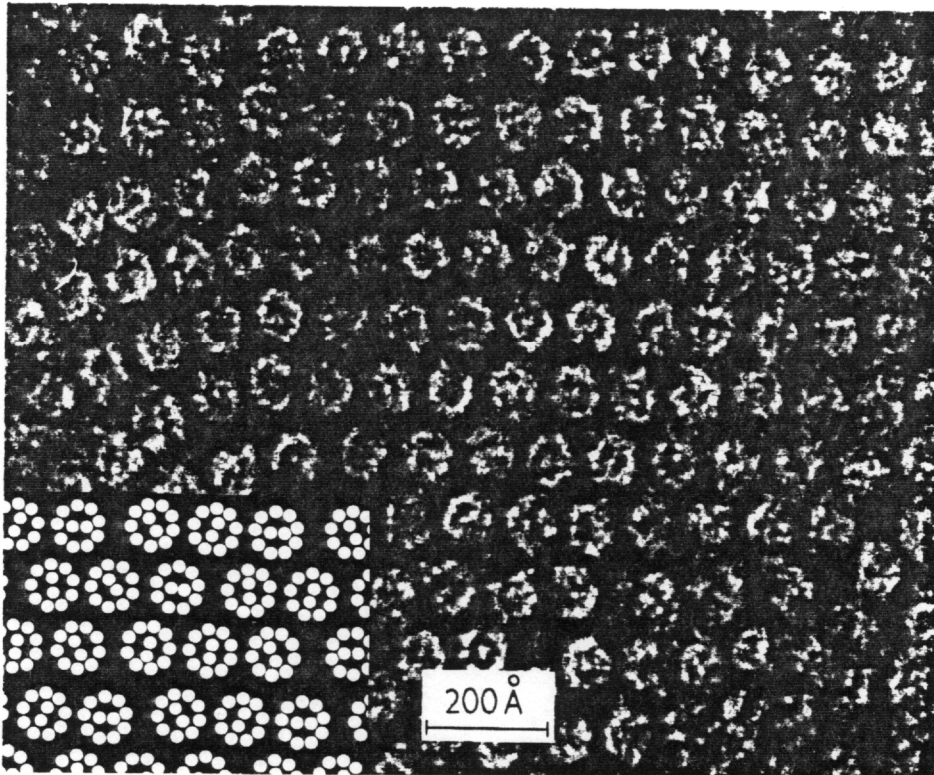


**Figure 1.1.1** An example of natural multicomponent, multiphase polymeric system: Electron micrograph of the cross section of an alpha-keratin fiber. The structure is that of microfibrils separated by more densely stained matrix. Each microfibrils are in turn composed of eleven "protofibrils", with nine in the periphery and two in the center. Insert: a schematic representation of the 9+2 arrangement of the protofibrils. (after reference 2)

polybutadiene. The glassy polystyrene matrix undergoes deformation mechanisms quite different in the presence of rubbery polybutadiene microphases dispersed in the matrix with the help of interfacial grafting.<sup>4</sup> Figure 1.1.2 illustrates the microstructural details of a commercial HIPS displaying its multiphase character.<sup>5</sup>

## 1.2 MISCIBILITY vs COMPATIBILITY

In understanding the behavior of multicomponent systems, two terms need to be clarified, namely, *miscibility* and *compatibility*. These two terms may be found to be used interchangeably as one reviews the early literature.<sup>6-8</sup> However, more recently better and scientifically more consistent definitions have emerged.<sup>9-15</sup> Polymers are said to miscible if they are mixed at the *molecular* level, resulting essentially in a single phase system (excluding crystallinity, if present). Compatibility, on the other hand, is the state in which the polymers form a multiphase system with each phase coexisting in a physically and mechanically stable form. The difference between a miscible and a compatible polymer pair on the macroscopic level may be viewed in terms of how the properties of the individual components are distributed in the final product. In general, in a miscible polymer system, the properties tend to be averaged. For example, the glass transition of a miscible pair may follow weighted average rule such as one represented by the Fox equation.<sup>16</sup> On the other hand, in a compatible system, each component inclines to retain its own properties. Thus, multiple glass transition temperatures would be characteristic of a compatible system.

Relatively fewer high molecular weight polymers are found to be miscible. This is due to the fact that entropic advantages of a single macromolecular phase are usually insignificant, and, therefore, the responsibility for obtaining favorable thermodynamics falls on the



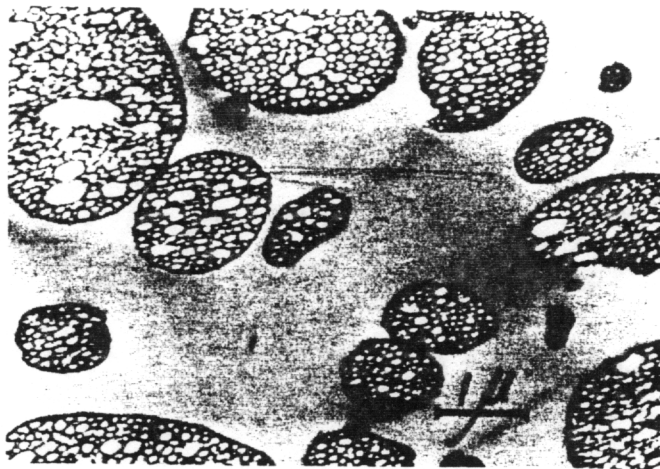


**Figure 1.1.2** An example of a human-made multicomponent polymer system: Commercial high impact polystyrene after osmium tetroxide sectioning, dark regions are polybutadiene phases. (from reference 5)

enthalpic contributions. Van der Waal forces alone are usually not sufficient for this. Hence, some form of "specific interactions", such as hydrogen bonding, are necessary in general to bring about a thermodynamically miscible system. Thus, most polymers are *immiscible*, i.e. they form a multiphase system when mixed.

For a pair of immiscible polymers, the options are that they are either compatible or incompatible. The latter term signifies a gross phase separation of the components resulting into a macroscopically heterogeneous system. In order that a given multicomponent system displays mechanically useful properties, obviously, the components must be compatible. Thus compatibility, if not present under ordinary conditions, must be induced in the system by external means. In HIPS, this is achieved with the help of interfacial grafting that forms in-situ during the polymerization process.<sup>4</sup> In rubber toughened thermosets, which is yet another example of commercially important set of multicomponent systems, this is traditionally achieved by chemical interactions between the thermoset and the end groups of the rubbery component.<sup>17-20</sup> Blends of two thermoplastics can be compatibilized by use of interfacial agents such as block or graft copolymers.<sup>21-23</sup> In fact, these copolymers themselves can be looked upon as two polymers compatibilized by covalent bonding between each other, thereby providing the necessary restriction to gross phase separation that would otherwise occur. The result is polymers with the well established "microphase separated" morphology imparting unique bulk<sup>24-27</sup> and surface properties.<sup>28,29</sup>

### 1.3 RESEARCH FOCUS

The focus of this thesis research is directed towards two such multicomponent systems that have been chosen for study in two somewhat specific applications. The first system, making up the major portion of this thesis, involves poly(propylene oxide) modified epoxy resin thermosets, primarily studied for exploring a novel approach to obtain a microporous polymer matrix. The microporosity development process involves a two step procedure. The first step is the formation of a two component, two phase system by curing an epoxy resin in presence of (optionally co-reactive) poly(propylene oxide). In the second step, the poly(propylene oxide) phase which is thermally less stable is removed from the system by heat treatment at a suitable temperature, which develops porosity in the system. Understanding of the cure behavior of the epoxy resin both by itself and in the presence of poly(propylene oxide), the conditions of compatibility and nature of phase separation, and the thermal and thermooxidative behaviors define the most obvious topics of study for this system. Each has been addressed in detail. The principal material characterization tools for studying of this system are Scanning Electron Microscopy (SEM), Dynamic Mechanical Analysis (DMA), and Thermogravimetric Analysis (TGA).

The second somewhat briefer subject deals with the nature of physical and/or chemical interactions between isotactic polypropylene and poly(vinyl methyl ether). The thrust for this study is based on a broader objective of identifying suitable block or graft copolymer compatibilizers for two important commercial thermoplastics, e.g. Nylon 6 and Polypropylene. The use of poly(vinyl methyl ether) as the block corresponding to the polypropylene phase of this blend was explored by first studying the interactions between these two polymers individually. This allowed one to predict the effectiveness of

poly(vinyl methyl ether) as a potential candidate in a block or graft copolymer where the other component is one that is chemically similar to Nylon 6. With this in mind, the miscibility/immiscibility behavior of the two polymers is studied with the help of crystallization kinetics and melting point behavior via Dynamic Scanning Calorimetry (DSC), with SEM providing the morphological information. TGA, Fourier Transform Infra-red (FTIR) Spectroscopy and Nuclear Magnetic Resonance (NMR) Spectroscopy provide additional insight on the role of thermooxidative processes in the behavior of these blends.

#### **1.4 DISSERTATION FORMAT**

The dissertation is divided in two major chapters addressing the above two research efforts. Chapter II contains the epoxy - poly(propylene oxide) work. Chapter III consists of the study of polypropylene/poly(vinyl methyl ether) blends. Each chapter will be self-sufficient in terms of the development of the research objective, literature review, experimental approach, and the discussion of results.

## **Chapter II**

### **Poly(propylene oxide)- modified Epoxy: Microporosity in Polymer Films**

---

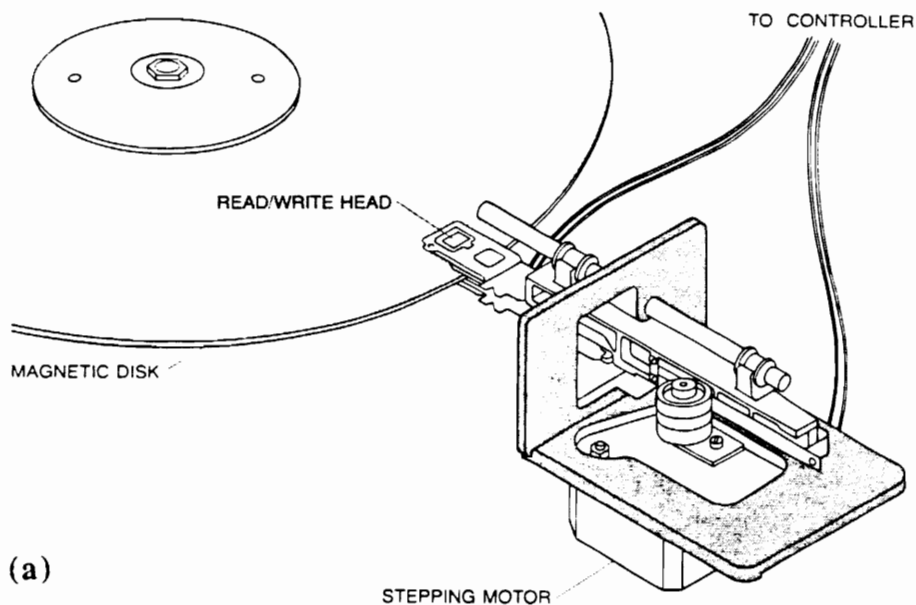
#### **2.1 INTRODUCTION**

As mentioned in Chapter I, the overall goal for studying poly(propylene oxide) (PPO) modified epoxy system is to explore a novel approach for achieving microporosity in crosslinked polymers. Microporosity is a desirable property in many polymer applications such as adsorption and ion-exchange processes, catalysis, and membranes for uses ranging from filtration to desalination. Although the proposed method may well be extended to these conventional areas of use, this work is particularly directed towards its potential for development of new binder matrices for particulate based magnetic coatings in rigid disk drives with enhanced lubrication capability. In this section a background on role of lubrication in rigid disk drives in relation to microporosity in the magnetic coating will be

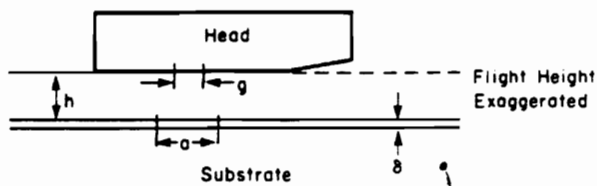
presented. This will be followed by an introduction to the proposed approach for obtaining microporosity in polymers. A brief review of the existing methods of microporosity formation will also be given for comparison. Finally, specific research objectives comprising of the various aspects of the overall effort will be discussed.

### 2.1.1 Lubrication in Rigid Disk Drives.

Figure 2.1.1 displays a schematic representation of a typical disk-head assembly of a rigid disk drive or a Direct Access Storage Device (DASD) such as the Winchester disk drive pioneered by IBM in 1970's.<sup>31</sup> The disk itself is a rigid substrate, generally an aluminium/magnesium alloy, with a thin ( $< 1 \mu\text{m}$ ) magnetic coating. The *particulate* coating (as opposed to the more recent *thin film* coatings) consists of magnetic particles, typically acicular gamma- $\text{Fe}_2\text{O}_3$  or  $\text{CrO}_2$ , together with some load bearing hard particles such as  $\text{Al}_2\text{O}_3$  dispersed in a thermosetting matrix.<sup>32</sup> The most common formulation for the thermoset binder is a combination of an epoxy resin, a phenolic resin, and poly(vinyl methyl ether), the latter serving as a film-forming additive.<sup>33</sup> Data writing and reading are achieved with the electromagnetic head mounted on a mechanical slider. During flight over the rotating disk, air gushes into the head-disk gap area lifting the slider and the head upward. Proper aerodynamic design assures a constant gap between the head and the disk which is an essential feature of these high performance devices. The Winchester technology allowed low-mass, lightly loaded sliders with considerable reduction in the head-disk gap which translated directly into a significant increase in data density over the earlier designs.<sup>31</sup> Also shown on Figure 2.1.1 are the typical operating parameters of a Winchester-type disk drive. As it may be obvious, the sub-micron gap distance and rotational speeds in excess of 3000 rpm put fairly severe conditions on the nature of the



(a)



Head Velocity is  $\sim 100$  miles/hr  
 Flying Height ( $h$ ) is  $\leq 5000 \text{ \AA}$   
 Disk Rotation is  $\sim 3000$  rpm  
 Disk Diameter is 8" and 14"  
 Disk Thickness is 75 and 150 mil  
 Coating Thickness ( $\delta$ ) is  $\leq 1 \mu\text{m}$   
 Width of Data Track is  $\sim 20 \mu\text{m}$   
 Track Density is  $\sim 1000/\text{in. of radius}$   
 Data Transfer Rate is  $\sim 10$  Mbit/s  
 Access Time is  $\sim 10-100$  ms  
 Linear Density is  $\sim 10,000$  bits/in circumference

(b)

**Figure 2.1.1** Magnetic disk drive in a modern computer system. (a) A schematic showing a typical configuration; a motor places the read/write head over data stored on the magnetic coating of the spinning disk (reproduced from ref 30). (b) Characteristic disk operating parameters. (from reference 34)

magnetic coating and its interaction with the head. Small asperities on the surface can cause head "crashes". In addition, as a consequence of the low-load slider design, the head temporarily rubs against the disk during start up from stationary position before it is levitated by aerodynamics. Similarly at the end of the operation, the head comes to rest on the disk. Thus, the tribological character of the head-disk contact during start and stop operations, and occasional crashes, is of critical concern in assuring long term reliability of the disk drives.

The problem of friction between the head and disk is traditionally alleviated with the use of a lubricating medium, mostly a fluorocarbon based polymeric liquid.<sup>31,35,36</sup> Figure 2.1.2 depicts a typical process flow in the manufacture of hard disks based on the particulate magnetic coating technology. In the final step before the performance testing, the lubricating medium is applied to the surface of the disk by spraying it in the form of a solution in solvents such as freon, with the excess being removed using a soft absorbant cloth. The amount of lubricant on the disk must be carefully controlled.<sup>35,36</sup> An inadequate amount of lubricant will give rise to contact wear and "crashes". On the other hand, "puddling" can occur if too much fluid is applied. This can cause "stiction" between the head and the disk at take-off, risking flexure distortion of the former. In addition, once the proper amount of lubricant has been applied, it has the tendency to deplete during usage by flying-off from the disk due to centrifugal force.<sup>37</sup> As a result the effectiveness of lubrication may diminish with operation.

It may seem that an ideal situation for lubrication of the rigid disk would be to have some form of reservoir that replenishes the lubricant as it depletes from the surface. For example, Linder and Mee<sup>36</sup> used ion etching to completely remove the surface lubricant on



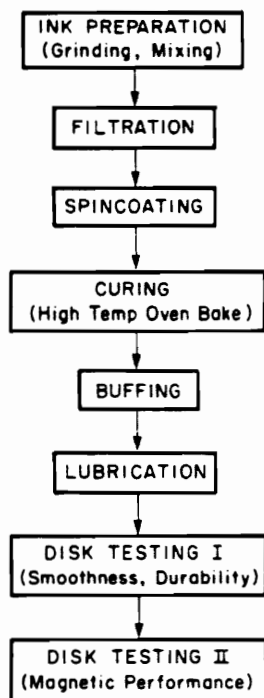


**Figure 2.1.2** Flowsheet for rigid disk fabrication process. (from reference 34)

disks and then monitored its level with the help of x-ray photoelectron spectroscopy. It was found that the amount of lubricant reached back to its original level after a period of time. They ascribed this observation to migration of lubricant from pores existing in the coating. Studies at IBM showed a relationship between lubricant retention on the disks and the coating cure temperature.<sup>37</sup> It was observed that using the same coating formulation, a disk that is cured in air was found to retain more lubricant than one that was cured in nitrogen. The origin of this behavior was thought to be degradation of poly(vinyl methyl ether), the film-forming additive, during cure in the presence of air. Volatile emission of degradation products caused microcracks or voids to form which in turn provided the necessary volume for excess lubricant retention. The formation of porosity due to degradation of poly(vinyl methyl ether) was further confirmed by a microscopy study.<sup>38</sup> From these preliminary investigations, it was recognized that well-controlled self-induced microporosity in the coating binder may attribute to further advancement in the performance of the rigid disk drives. This provided the basic thrust for the current research.

### **2.1.2 Proposed Approach for Microporosity Development.**

Most existing methods of porosity formation in polymeric materials involve a two-phase phenomenon. The procedure can be generalized as follows: a pore forming additive, which may be a solvent, a non-solvent, a polymer, or a combination thereof, forms the second phase in addition to that of the polymer of interest; subsequent removal of the additive phase leaves a porous structure. For instance, microporous styrene-divinylbenzene systems used extensively in ion-exchangers, catalyst supports, and gel chromatography are prepared using this principle. By addition of a solvating diluent such as toluene,<sup>41</sup> t-amyl alcohol,<sup>42</sup> or ethyl-2-hexanoic acid<sup>43</sup> to a copolymerizing mixture of styrene and

divinylbenzene, microporosity develops as a result of a complex mechanism involving inhomogeneity in crosslinking density distribution.<sup>44</sup> On the other hand, if a nonsolvent such as n-heptane<sup>45</sup> is used, porous structure is obtained by precipitation of the reacting medium as its molecular weight increases due to crosslinking. Similarly a non-reacting polystyrene may be added to the monomers to form the required second phase which can be solvent extracted to give porosity.<sup>46,47</sup> A host of other possibilities exist when two types of diluents are used simultaneously.<sup>48</sup> Pore sizes in these copolymers may range from few angstroms to micron level depending on the type of diluent(s), the composition of the reactants, and the conditions of polymerization.

Membranes for separation processes such as microfiltration, dialysis, and reverse osmosis make up another major group of commercially important polymeric microporous media.<sup>49-52</sup> The membranes used in these various applications differ considerably in their structure and their function. However, majority of these membranes can be said to be prepared by the same basic mechanism referred to by Kesting<sup>53</sup> as *phase inversion*, again a two-phase process, first conceived by Loeb and Saurirajan<sup>54</sup> in preparation of their now-famous asymmetric membrane. Phase inversion can be described as the conversion of liquid homogeneous solutions of two or more components into a two-phase system with a solid, polymer-rich phase forming the rigid membrane structure and a liquid, polymer-poor phase forming the membrane pores. Analogous to the styrene-divinylbenzene copolymers, there are a number of ways phase inversion can be brought about. Among them are solvent evaporation, non-solvent precipitation, and thermally induced precipitation of the polymer component.<sup>55</sup>

The method proposed in the current work comprises of a two step procedure to create microporosity in crosslinked polymer films based on similar basic approach. However, the differences lie in the manner of formation and control of the second phase and the mechanism of its removal. In the first step, the thermoset resin such as an epoxy is cured in presence of a thermoplastic modifier which phase separates by the process reminiscent of rubber-toughened thermosets. In the second step, the system is heat treated at an elevated temperature where the thermoplastic additive degrades selectively leaving a porous or microporous crosslinked system. Poly(propylene oxide), PPO, is used here as the pore forming additive to an epoxy based thermoset. PPO is an attractive candidate for this purpose due to its well controlled degradation behavior. Previous research has shown that by carefully selecting the end group functionality, these polymers can be designed to degrade at various temperatures ranging from 160 °C to 350 °C.<sup>56,57</sup> One of the necessary requirements for maximizing the selectivity in the degradation step is that there is a sufficient gap between the degradation temperatures of the modifier and the matrix polymer. Accordingly, the flexibility in degradation temperature of PPO would make it a more general modifier for different matrix polymers with varying degrees of thermal stability.

### **2.1.3 Research Objectives.**

The overall goal of this research is to explore the approach described above involving phase separation followed by selective degradation to obtain microporosity in a thermosetting matrix. Clearly, in order to obtain a microporous system of predictable porosity by this concept, one has to study both aspects of the process, i.e. the phase separation of PPO from the epoxy during cure, and the degradation behavior of the PPO while incorporated in

the epoxy matrix. The process of phase separation will control the morphology of the two-phase intermediate and hence, ultimately, the size and extent of porosity that can be achieved. The nature of phase separation will be affected by numerous variables, some of which are composition, temperature of cure, and rate of cure, based on both thermodynamic and kinetic considerations. In addition, the curing process itself, both of the neat as well as the PPO-modified epoxies, will be an important aspect to study on a fundamental basis. Events such as gelation and vitrification can be expected to influence the phase separation process, in addition to providing practical information on optimum cure conditions. On the other hand, once the two-phase system has been obtained, the final porosity development would be governed by the mechanisms of PPO degradation and the efficacy of removal of the resulting species from the epoxy matrix. Thickness of the film may be expected to play a role in this step. It would also be of interest to know whether the film thickness is of importance in the morphological development itself, i.e. films of thickness comparable to the expected phase sizes may behave different from films of bulk thickness.

From the above arguments, the following three major areas of study were identified:

*Phase separation process and morphology control.* Approaching from a fundamental point of view, a range of variables that can influence the nature of phase separation were studied. It was shown that by manipulation of these variables, one can obtain systems which transform from being one-phase miscible to two-phase immiscible/incompatible with a range of compatible two-phase systems possessing well controlled morphology in-between. Experimental results also will be accompanied by theoretical explanation based

on the thermodynamic and kinetic criteria. The principal tool for this study was scanning electron microscopy (SEM).

*Cure behavior of neat epoxy and PPO modified epoxy.* Time-temperature relationships such as Gillham's Time Temperature Transformation (TTT)<sup>58</sup> diagram were utilized in this part to elucidate the fundamental nature of the neat thermosetting system at hand, both during and after cure. Further, the behavior of the neat epoxy system will be compared with that when PPO is added to the reacting mixture. Both isothermal and dynamic cure behaviors were studied. Dynamic Mechanical Analysis (DMA) was the chosen analytical technique for this study. Pyrolytic contribution to cure were also examined with the help of Thermogravimetric Analysis (TGA).

*Degradation process and the microporosity development.* Degradation behavior of neat PPO, followed by neat and PPO-modified epoxy will be presented with the help of TGA. The question of microporosity development was probed with the help of SEM and DMA. Also results of field trials performed at IBM, San Jose, California, to verify the practical applicability of the approach in disk coatings of submicron thickness will be presented along with SEM and lubricant retention studies.

#### **2.1.4 Chapter Organization.**

In the next section, literature review of subjects related to each of the above three areas will be given. This will be followed by the details of the experimental approach including the materials and methods used in the study. Results and discussion, again divided into three subsections will be given in Section 2.4. Finally, a review of major conclusions that can

be drawn from this research and some comments on future work will be presented in Section 2.5 and 2.6.

## 2.2 LITERATURE REVIEW

This section is divided into three major parts. The first part addresses the topic of morphology, including the phase separation process that determines the morphology, in modified thermosetting systems. This will be followed by a discussion of cure behavior of neat and modified thermosets. Finally, a brief review of degradation processes in poly(propylene oxide) will be given.

### 2.2.1 Morphology in Modified Thermosets.

Thermosetting polymers, most notably epoxies, provided for a need of high strength, high modulus materials for structural adhesives and composite matrices during the initial development of these technologically important areas. However, since most thermosets are inherently brittle, a requirement to introduce toughness in these materials was quickly recognized. Earlier attempts to meet this additional requirement were mostly confined to a number of patented industrial formulations utilizing such polymeric additives as nitrile rubber, nylon, vinyl acetals etc.<sup>59,60</sup> They were not described in open literature until McGarry *et al.*,<sup>61-64</sup> and, soon after that, Siebert and coworkers<sup>65-67</sup> and others<sup>68-70</sup> reported results of systematic studies on epoxy resin systems containing carboxyl terminated butadiene-acrylonitrile (CTBN) elastomers. They found by electron microscopy that CTBN separated into a second phase in the epoxy matrix *in situ* during the cure reaction in the form of particles whose size ranged from 1 to 5 microns. This two-phase structure was then thought to be responsible for the several-fold increase in toughness of the cured resins.



Two decades or so since these earlier findings, an extensive amount of research has been done in exploiting the phase-separated morphology to enhance the energy absorbing properties of various thermosets, including polyimides,<sup>71-73</sup> polyesters,<sup>74,75</sup> and acrylics,<sup>76,77</sup> in addition to the more widely studied epoxy resins. Benefits of modification of thermosets in this manner have been realized in applications other than toughening of adhesives and composite matrices as well; some examples are improvements in friction and wear properties,<sup>78</sup> thermal and humidity resistance in encapsulants,<sup>79</sup> corrosion control in sheet molding compounds<sup>80</sup> and adhesion of coatings with metals.<sup>81</sup> Furthermore, the use of butadiene-acrylonitrile rubbers has been extended to alternative rubbery materials such as polysiloxanes,<sup>19,78,78b,82,83</sup> polyacrylates,<sup>84,84b,85</sup> polyisobutylene,<sup>86</sup> poly(propylene oxide),<sup>87</sup> and polycaprolactone.<sup>87</sup>

In most of these rubber modified systems, increased toughness is generally obtained at the expense of a certain degree of reduction in the modulus. In addition, the low glass transition temperature of the rubbery phase limits the performance of these materials in the elevated temperature range. Recently, attempts have been made to overcome these disadvantages by use of functionalized high performance thermoplastic modifiers instead of the rubbery modifiers. A number of glassy polymers have been used successfully for this purpose, among them being poly(ether sulfone)s,<sup>88-91</sup> poly(ether ketone)s,<sup>92,93,93b</sup> poly(ether imide)s,<sup>94</sup> and a variety of other proprietary materials.<sup>95-97</sup>

On a review of the body of published literature, it becomes quite apparent that, indeed not unlike other multiphase polymer systems, there is a strong relationship between the morphology/structure and the end-use attributes of modified thermosets. Along this direction, several mechanisms are put forward to explain the fracture behavior of these

systems *vis-a-vis* their morphology.<sup>99-100</sup> Furthermore, quantitative models relating the toughness to structural parameters have also been proposed.<sup>101-103</sup> The fracture resistance and other mechanical properties have been experimentally found to be dependent on a combination of matrix characteristics (crosslink density, glass transition temperature, and amount of dissolved rubber) and the rubbery phase parameters (volume fraction, particle size, particle size distribution, interfacial adhesion, and the glass transition temperature).<sup>104</sup> Thus, an in-depth understanding of the nature of phase separation and the resulting morphological character becomes critically important in optimization of final material properties.

Since the objectives of the current research do not include mechanical property aspects *per se* but rather the control of morphology, the emphasis in the further discussion will be placed on the latter. First a brief background on the thermodynamic concepts of phase separation in relation to modified thermosets will be developed. A review of the published literature on various methods utilized for controlling the phase behavior and, hence, the morphology of these systems will follow. Finally, an analysis of a theoretical treatment for modeling the phase separation process will be presented.

### **2.2.1.1 Phase Separation Process: Thermodynamic Considerations.**

#### ***2.2.1.1.1 Phase Diagrams for Polymer Mixtures.***

From elementary equilibrium thermodynamics, whose foundation was laid by Gibbs<sup>105</sup>, the necessary conditions for a binary system to be miscible at a particular composition are:

$$\Delta G_m < 0 \quad (2.2.1)$$

$$(\partial^2 \Delta G_m / \partial \phi_2^2) > 0 \quad (2.2.2)$$

where  $\Delta G_m$  is the free energy of mixing per unit volume and  $\phi_2$  is the volume fraction of the component 2. Figure 2.2.1 shows three possible events in a binary polymer system. Curve I satisfies both criteria of equations 2.2.1 and 2.2.2, therefore it represents one-phase miscibility in all proportions. On the other hand, curve III satisfies neither and is typical of completely immiscible system. A system characterized by curve II has a miscibility gap in the intermediate region because the second condition is not satisfied in that range. In a given polymer system, the Gibbs free energy characteristics can display transition from I to II to III (or the reverse) by change of an independent variable. In a blends of two thermoplastic polymers, such a variable would typically be the temperature as shown in Figure 2.2.1 by  $T_1$ ,  $T_2$ , and  $T_3$  for the behaviors of type I, II, and III respectively.

The information from Gibbs free energy-composition curves can be organized on phase, or T- $\phi$ , diagrams according to regions where the miscibility criteria are satisfied or not satisfied. Depending on the relation between the three temperatures, one may have a Upper Critical Solution Temperature (UCST) or a Lower Critical Solution Temperature (LCST) behavior as illustrated on Figure 2.2.2(a) and (b) respectively. The UCST is obtained when  $T_1 < T_2$ . Similarly, the LCST is obtained when  $T_1 > T_2$ . The line dividing the single-phase and the two-phase regions is called the *binodal curve*. Each temperature having the free energy behavior similar to the curve II in Figure 2.2.1 provides a pair of binodal points at which the chemical potentials of individual components in the two phases are the same.

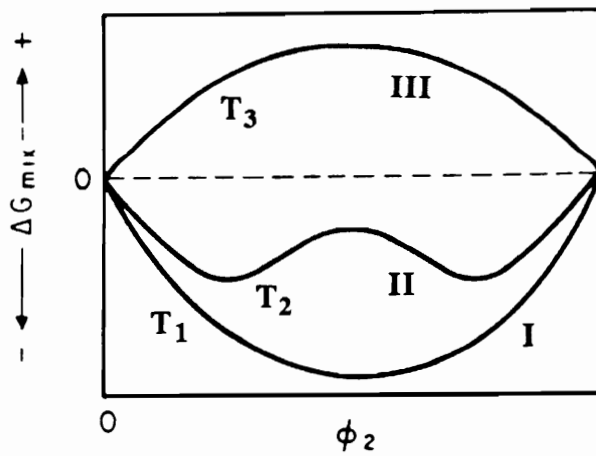


**Figure 2.2.1** Free energy of mixing for binary mixtures which are completely miscible (curve I, temperature  $T_1$ ), partially miscible (curve II, temperature  $T_2$ ) and completely immiscible (curve III, temperature  $T_3$ ). (after reference 13)

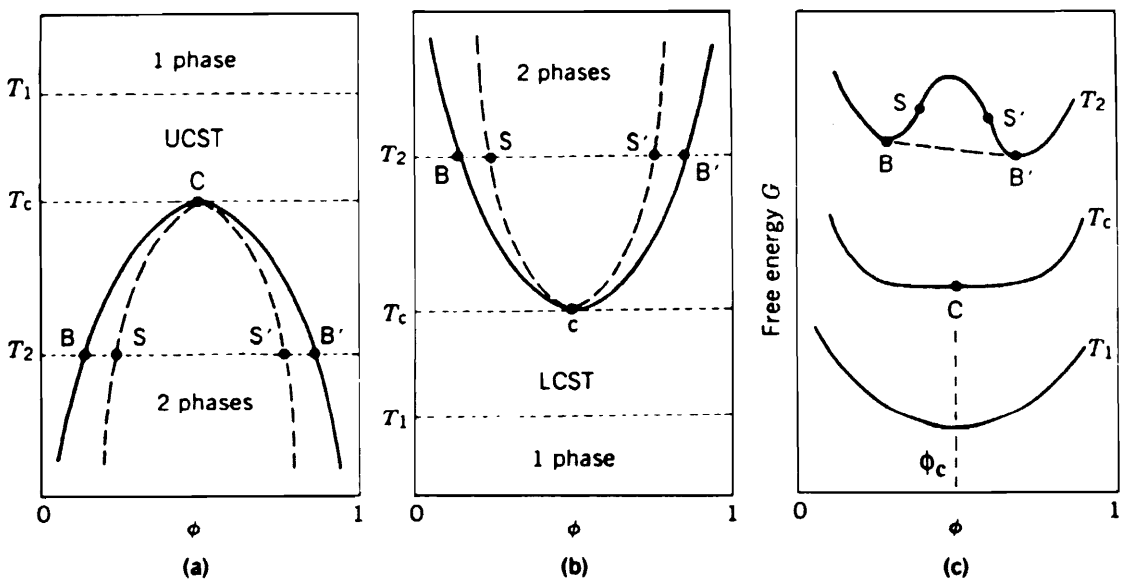


**Figure 2.2.2**  $T$ - $\phi$  phase diagram for polymer mixtures. (a) upper critical solution temperature (UCST) behavior; (b) lower critical solution temperature (LCST) behavior; (c) Temperature dependence of free energy-composition relation for temperatures above and below the critical value.  $T_c$  is the critical temperature, and  $\phi_c$  is the critical composition. (after reference 10).

These are shown on Figure 2.2.2(c) as points B and B'. The state of equilibrium between the two phases stipulates the following condition for the binodal points:

$$\mu_i |_{\text{B}} = \mu_i |_{\text{B}'} \quad (2.2.3)$$

where  $\mu_i$  is the chemical potential of component  $i$  as defined by:

$$\mu_i = \left( \frac{\partial G}{\partial n_i} \right) |_{T,P,n_j \neq i} \quad (2.2.4)$$

The inflexion points S and S' define the *spinodal* curve which satisfies the following relation:

$$\left( \frac{\partial^2 \Delta G_m}{\partial \phi_2^2} \right) = 0 \quad (2.2.5)$$

The binodal curve defines the equilibrium conditions. The spinodal curve and the *metastable* region between the binodal and the spinodal are significant with respect to the mechanism and kinetics of phase separation.<sup>9,106,107</sup> The two curves meet at the critical point C characterized by two parameters: the critical temperature  $T_c$  and the critical composition  $\phi_{2c}$ . The critical temperature (UCST or LCST) represents the minimum (or maximum) temperature at which the two components will be miscible in *all* proportions. The critical composition  $\phi_{2c}$  divides the composition range into two regions; for an initial composition  $\phi_2 < \phi_{2c}$ , the minor precipitating phase will be rich in the component 2 and when  $\phi_2 > \phi_{2c}$ , it will be rich in the component 1. This gives rise to the important phenomenon of *phase-inversion* in polymer blends.<sup>108,109</sup>

The model shown here is quite simplistic recognizing that more complex diagrams such one having UCST and LCST simultaneously, one where the UCST and LCST merge or one in which the binodal and spinodal curves are bimodal instead of unimodal are possible.<sup>9,110,111</sup>

### 2.2.1.1.2 *Flory-Huggins Theory.*

The free energy of mixing is given by:

$$\Delta G_m = \Delta H_m - T\Delta S_m \quad (2.2.6)$$

where  $\Delta H_m$  is the enthalpy of mixing,  $\Delta S_m$  is the entropy of mixing and  $T$  is the absolute temperature. According to the lattice theory developed by Flory<sup>112,113</sup> and Huggins<sup>114</sup> the entropy of mixing is given by:

$$\Delta S_m = -R(N_1 \ln \phi_1 + N_2 \ln \phi_2) \quad (2.2.7)$$

where  $N_i$  is the number of moles and  $f_i$  is the volume fraction of component  $i$  and  $R$  is the gas constant. The enthalpy of mixing is given by :

$$\Delta H_m = RT\chi_{12}N_1\phi_2 = BV_1N_1\phi_2 = (v_1+v_2) B\phi_1\phi_2 \quad (2.2.8)$$

where  $v_1$  and  $v_2$  are the actual volumes of the components,  $V_1$  is the molar volume of component 1,  $B$  is the interaction energy density and  $\chi_{12}$  is the interaction parameter (per

mole of component 1), popularly known as Flory-Huggins *chi* parameter. The interaction parameter can be expressed as:

$$\chi_{12} = BV_1/RT = z\Delta w_{12}N_A/RT \quad (2.2.9)$$

where  $N_A$  is Avogadro's number,  $z$  is the coordination number of the lattice and  $\Delta w_{12}$  is the energy for formation of an unlike contact pair which can be given by:

$$\Delta w_{12} = w_{12} - (w_{11} + w_{22})/2 \quad (2.2.10)$$

where  $w_{11}$ ,  $w_{22}$  and  $w_{12}$  are the energies of the respective pair attractions. In case of interactions between nonpolar or slightly polar it is possible to replace  $w_{12}$  by geometric means of  $w_{11}$  and  $w_{22}$ , in which case the following may be deduced:

$$\Delta w_{12} = (w_{11}^{1/2} - w_{22}^{1/2})^2/2 \quad (2.2.11)$$

The above assumption allows one to relate the *chi* parameter to a more commonly used Hildebrand's solubility parameter approach<sup>114b,114c</sup> by:

$$\chi_{12} = v_1(\delta_1 - \delta_2)^2/RT \quad (2.2.12)$$

where  $\delta_i$  is the solubility parameter of the component  $i$ .

The following observations can be made from the lattice model put forward by Flory and Huggins. Firstly, the enthalpy of mixing is independent of the molecular weights of the



components. However, the entropy of mixing is not. This means that for a fixed mass of the system (or volume, considering no volumetric change on mixing), the entropy of mixing becomes increasingly smaller as the molecular weights of the components increase (the number of moles  $N_i$  in Equation 2.2.7 decreases as the molecular weight of component  $i$  increases), ultimately becoming zero as they approach infinity. Thus for a pair of high molecular weight polymers, the burden of satisfying Equation 2.2.1 falls on the enthalpy of mixing. Endothermic mixing (for B,  $\chi_{12}$ ,  $\Delta w_{12} > 0$ ) does not favor miscibility. On the other hand, for exothermic mixing, the F-H theory predicts that conditions for miscibility are satisfied no matter how large the molecular weights are. Thus as a simple rule, miscibility of high molecular weight polymers is assured only if the mixing is exothermic. For this to occur, generally some form of specific interactions such as dipole-dipole or hydrogen bonding are required. Origins of different interactions that can contribute to the enthalpy of mixing have been reviewed by Olabisi, Robeson and Shaw.<sup>9</sup>

A number of extensions to this basic theory have been worked out to account for additional possibilities such as polydispersity<sup>115</sup> and dependence of interaction parameter on temperature as well composition.<sup>9,116,117</sup> Also more advanced Equation of State theories<sup>9,118-121</sup> consider the additional contributions to the free energy due to volumetric changes accompanying mixing which are ignored in the F-H theory. For most purposes, nevertheless, the F-H theory seems to suffice, qualitatively at least, for elucidation of the phase behavior in multicomponent polymer systems.

### 2.2.1.1.3 *Applicability to Modified Thermosets.*

As discussed earlier, molecular weights of the components affect the entropy of mixing. This becomes the key mechanism in bringing about a phase transformation in thermosets modified with thermoplastics. In a mixture of the thermoset and the modifier before curing, the former, being essentially in its monomeric state, contributes favorably to the free energy. A miscible mixture may be obtained at this stage provided that the positivity of the enthalpy of mixing is not high enough to impose a condition otherwise. However, with the commencement of curing reaction, the entropic contributions become monotonically smaller as the thermoset gains molecular weight, finally reaching a point when the miscibility condition of Equation 2.2.2 is no longer satisfied. Phase separation follows as a result. Thus, analogous to the temperature as an independent variable in a blend of thermoplastics, it is the molecular weight that causes the change in free energy-composition character in a thermoset-thermoplastic mixture driving it to a metastable or unstable state.

Williams and coworkers<sup>122</sup> have utilized this concept by use of F-H theory modified to replace the molecular weight of the thermoset by the extent of reaction using the statistical relationships of Flory<sup>123,123b,124</sup> and Stockmayer.<sup>125</sup> Taking the case of a self-crosslinking monomer with a functionality of 4 (component 1) in presence of a modifier (component 2), they presented the Gibbs free energy expression in the following form:

$$\begin{aligned} \Delta G_m^V / (RT/V_{1,0}) = & (1-2p) (1-\phi_2) \ln(1-\phi_2) \\ & + (\phi_2/z_0) \ln\phi_2 + \chi_{12,0} \phi_2 (1-\phi_2) \end{aligned} \quad (2.2.13)$$

where  $\Delta G_m^V$  is the Gibbs free energy of mixing per unit volume,  $p$  is the thethermoset conversion, and  $z$  is the ratio of molar volumes i.e.  $V_2/V_1$ . The additional superscript 0 denotes the initial conditions *before* polymerization begins.

The resulting Gibbs free energy curves together with the binodal and spinodal curves are reproduced in Figure 2.2.3. Note the here that the parameter that changes as one goes from one free energy curve to another is the extent of reaction  $p$  rather than the temperature in contrast with Figure 2.2.1. Instead of the conventional  $T$ - $\phi$  diagram to represent the phase behavior in thermoplastic blends, a  $p$ - $\phi$  diagram represents the same in a thermoset-thermoplastic blend undergoing cure. The shape of binodal curve resembles the LCST behavior in thermoplastic blends. However, the term LCST for the  $p$ - $\phi$  behavior would be a misnomer, and, a more appropriate term here perhaps will be Lower Critical Solution *Conversion*, or the LCSC.

An alternative way to look at the same phenomenon is to obtain the conventional  $T$ - $\phi$  diagram and shift it to higher or lower temperature as a function of molecular weight. Figure 2.2.4 illustrates this concept as employed by Pascault and coworkers<sup>126</sup> where cloud point curves, representing the equilibrium binodal curves,<sup>9,111</sup> are shown as a function of the molar mass of epoxy based on homologues of diglycidyl ether of bisphenol A (DGEBA) in a mixture with CTBN rubber. The curves shift upward as the molar mass of the epoxy is increased implying a reduction in the miscibility between the epoxy and the rubber.

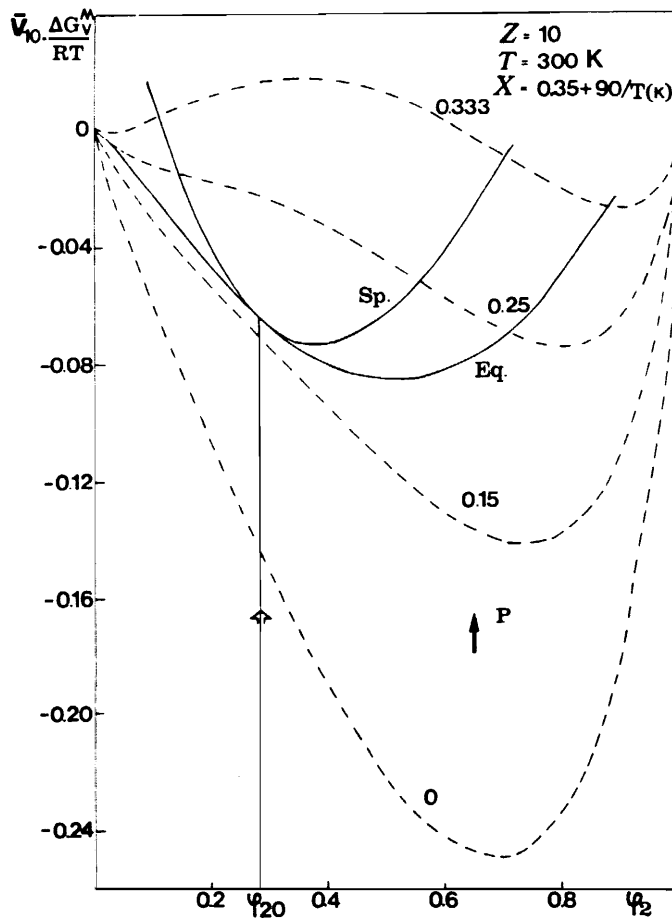


**Figure 2.2.3**  $p$ - $\phi$  diagram for modified thermosets: dimensionless free energy of mixing per unit volume as function of rubber volume fraction for different thermoset conversions. Eq = equilibrium or binodal curve, Sp = spinodal curve. (from reference 122)

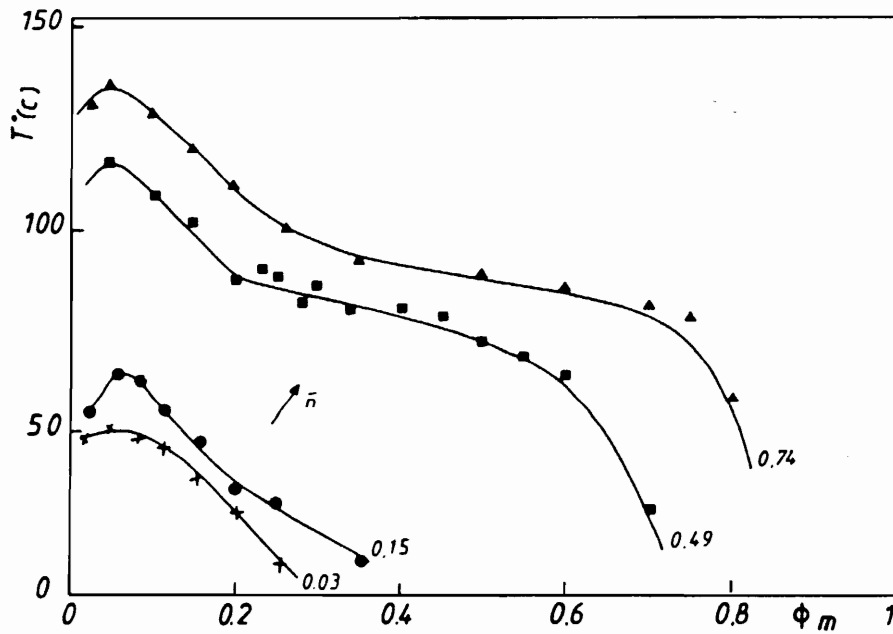


**Figure 2.2.4** Cloud point temperature vs mass fraction of CTBN for mixtures of CTBN with epoxy monomers of different molar masses.  $\bar{n}$  denotes the average number of repeat units in the epoxy based on DGEBA structure.  $\bar{n} = 0.03$  to  $0.74$  corresponds to  $M_n$  of 349 to 550.gm/mole. (from reference 126)

From experimental cloud point curve at a given molecular weight, Yamanaka and Inoue<sup>127</sup> estimated the temperature dependence of the interaction parameter in a mixture of epoxy and CTBN in the form:

$$\chi_{12} = A + B/T \quad (2.2.14)$$

where A and B are temperature-independent quantities. From this information, they calculated the T- $\phi$  behavior at other molecular weights. Figure 2.2.5 depicts their results; Figure 2.2.5 (a) is the cloud point curve with UCST type behavior obtained by optical microscopy, Figure 2.2.5 (b) illustrates the upward shift of calculated spinodal curves as the molecular weight of the epoxy is increased. In a similar fashion they also demonstrated shifts in T- $\phi$  diagram of a poly(ether sulfone)/epoxy mixture<sup>91</sup> as displayed on Figure 2.2.6. Here, they claimed that the nature of the equilibrium curve is of LCST type rather than a UCST type unlike in the case of CTBN/epoxy system described previously. The effect of curing reaction can be interpreted on Figure 2.2.6 (b) by looking at the location of the bimodal curve with respect to the point ( $T_{\text{cure}}, \phi$ ), which is fixed for a given composition and the cure temperature. Initially the point is outside the binodal implying one-phase miscibility. But as reaction proceeds, the binodal moves towards the lower right, with phase separation commencing as the binodal crosses ( $T_{\text{cure}}, \phi$ ).

### 2.2.1.2 Chemistry - Morphology Relationships.

The main factors that affect the final morphology in modified thermoset are the characteristics of the modifier and the thermoset (including the resin, hardener and catalyst), composition, and the cure conditions, i. e., time and temperature of cure.

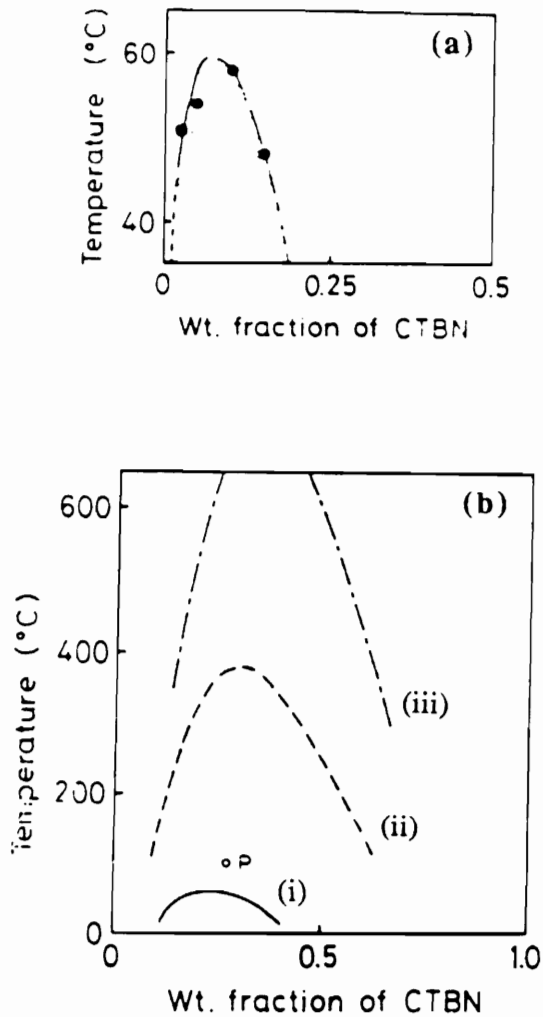


**Figure 2.2.5** (a) UCST type phase diagram of epoxy oligomer/CTBN mixture. (b) variation of phase diagram with increase in molecular weight of epoxy: (i) calculated spinodal curve having the same critical point as that of (a), (ii) and (iii) predicted spinodal curves for systems having double and triple molecular weights of epoxy respectively. (from reference 127)

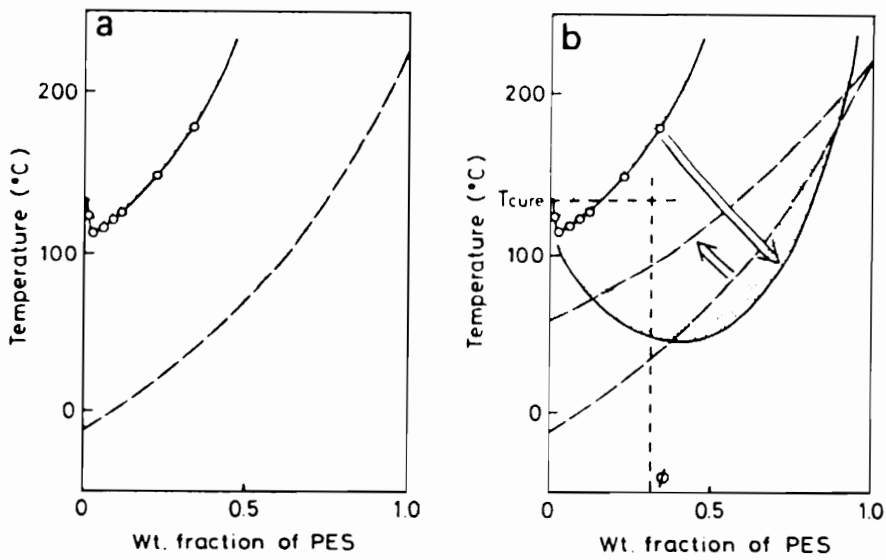


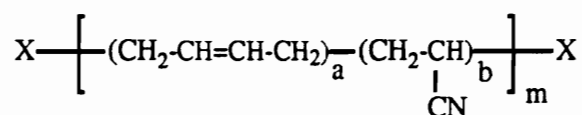
**Figure 2.2.6** (a) Phase diagram of epoxy oligomer/poly(ether sulfone) mixture. (b) Schematic representation of the variation of phase diagram and  $T_g$  with curing. (from reference 91)



### 2.2.1.2.1 *Molecular Nature of the Modifier.*

In order to obtain a stable two-phase morphology in a modified thermoset, a necessary requirement is that the reactants form a homogeneous solution before polymerization commences. As the polymerization progresses, the phase separation must begin at relatively lower conversions, before gelation or vitrification occurs, while there is still enough mobility in the system. This means that there must be sufficient affinity between the modifier and the thermoset to fulfil the requirement of initial miscibility, but not quite so high as to cause the miscibility to continue well into the cured state. As an additional requirement, adequate interfacial adhesion should exist between the separated phases to assure good mechanical performance. A certain amount of chemical reactivity between the modifier and the thermoset will help impart the requisite interfacial character. However, excessive chemical reactivity will also hinder phase separation and the development of subsequent two-phase morphology. Thus, the optimum molecular structure of the modifier is determined by a delicate balance of its interactions, physical as well as chemical, with the matrix.

The various molecular parameters of a modifier at disposal to achieve the above compatibility balance may be illustrated with the help of butadiene- acrylonitrile rubbers, CTBN being one specific case that has been studied the most. The structure of these random copolymers, where butadiene and acrylonitrile form segments of short sequences along the chain, can be generalized by the following:



Three main molecular parameters are evident: a and b determine the ratio of butadiene to acrylonitrile contents and hence, the polarity of the copolymer; m gives the molecular weight of the polymer; and X is a moiety of choice that may or may not be reactive with the thermoset. In the following paragraphs a review of how each of these parameters affect the morphology in systems containing butadiene acrylonitrile, and, analogously, other modifiers as well is presented.

Variation of the relative amounts of acrylonitrile and butadiene components provides the first effective way to change the compatibility of butadiene acrylonitrile copolymers with the resin system. The aim is to match the respective values of solubility parameters of the resin and the modifier,  $\delta_{\text{resin}}$  and  $\delta_{\text{modifier}}$ , fairly closely to minimize the enthalpy of mixing, as expressed through Equations 2.2.8 and 2.2.12, so that the miscibility criteria of Equations 2.2.1 and 2.2.2 are satisfied. For example, the solubility parameter of CTBN's change from 8.04 with no acrylonitrile (i.e in carboxyl terminated butadiene, or CTB) to 9.16 with 28.5% by weight acrylonitrile at which point it matches the solubility parameter of DGEBA epoxy.<sup>65,128</sup> Thus, the compatibility of the CTBN with DGEBA may be expected to be a strong function of the acrylonitrile content. This has been demonstrated thermodynamically by Wang and Zupko<sup>129</sup> by constructing cloud point plots for the DGEBA-CTBN system with CTBN's having two different acrylonitrile contents (10% and 17% by weight). As shown on Figure 2.2.7, the cloud point curve shifted upwards, implying a reduction in the compatibility of CTBN with DGEBA, as the acrylonitrile content of the copolymer decreased from 17 to 10%. Similarly Hsich's<sup>130</sup> Raleigh-Bernoulli laser light scattering experiments on CTBN-DGEBA system also produced shifts in binodal curves towards higher temperatures as the acrylonitrile content decreased.

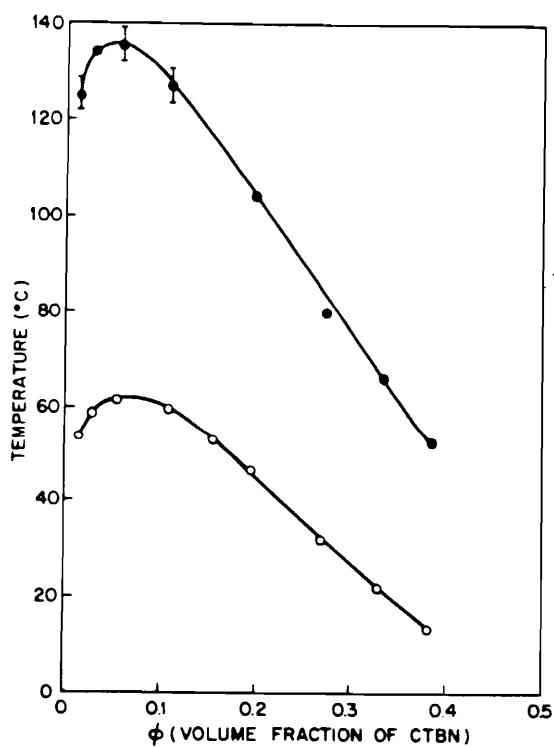


**Figure 2.2.7** Cloud point curves for DGEBA-CTBN system. (a) CTBN containing 10% acrylonitrile; and (b) CTBN containing 17% acrylonitrile. (from reference 129)

The thermodynamic characteristics via T- $\phi$  diagrams of *unreacted* modifier/resin corroborate well with the effect the acrylonitrile content is found to have on the size of rubber domains after cure. As one may anticipate, the relation between the acrylonitrile content and the phase size has been found to be that of inverse as observed by several workers.<sup>68,128,131,132</sup> For instance, In a study by Drake and Siebert,<sup>65,128</sup> a wide range of particle sizes varying from microns to few angstroms were obtained as the acrylonitrile content of CTBN was varied from 10 to 28% by weight. At the same time, the use of CTB resulted in complete incompatibility with formation of two separate layers of epoxy and copolymer each at the end of cure.

Among the modifiers other than butadiene-acrylonitrile copolymers, successful use of siloxanes has also been attained by balancing interactions through manipulation of polar/non-polar moieties in the backbone structure. Tran and coworkers<sup>19,78,78b</sup> studied a series of siloxane copolymers where the solubility parameter of the polydimethylsiloxane (PDMS) was raised from 7.5 to values nearer to that of DGEBA by introduction of more polar species such as trifluoropropylmethylsiloxane or diphenylsiloxane as comonomers. PDMS by itself is found incompatible with the epoxy initially and therefore not useful as a modifier without appropriate molecular structure modification.<sup>82</sup> The effect of introducing additional polarity in the system directly correlated with the size of the domains in modified resins as shown in Figure 2.2.8. Similar modification of PDMS with methylphenylsiloxane by Saito *et al.*<sup>83</sup> resulted in an increase in compatibility as suggested by smaller phase sizes in the cured systems. The compatibility of poly(n-butyl acrylate) with epoxy has also been shown to be enhanced by introduction of acrylonitrile as a comonomer.<sup>84b</sup>

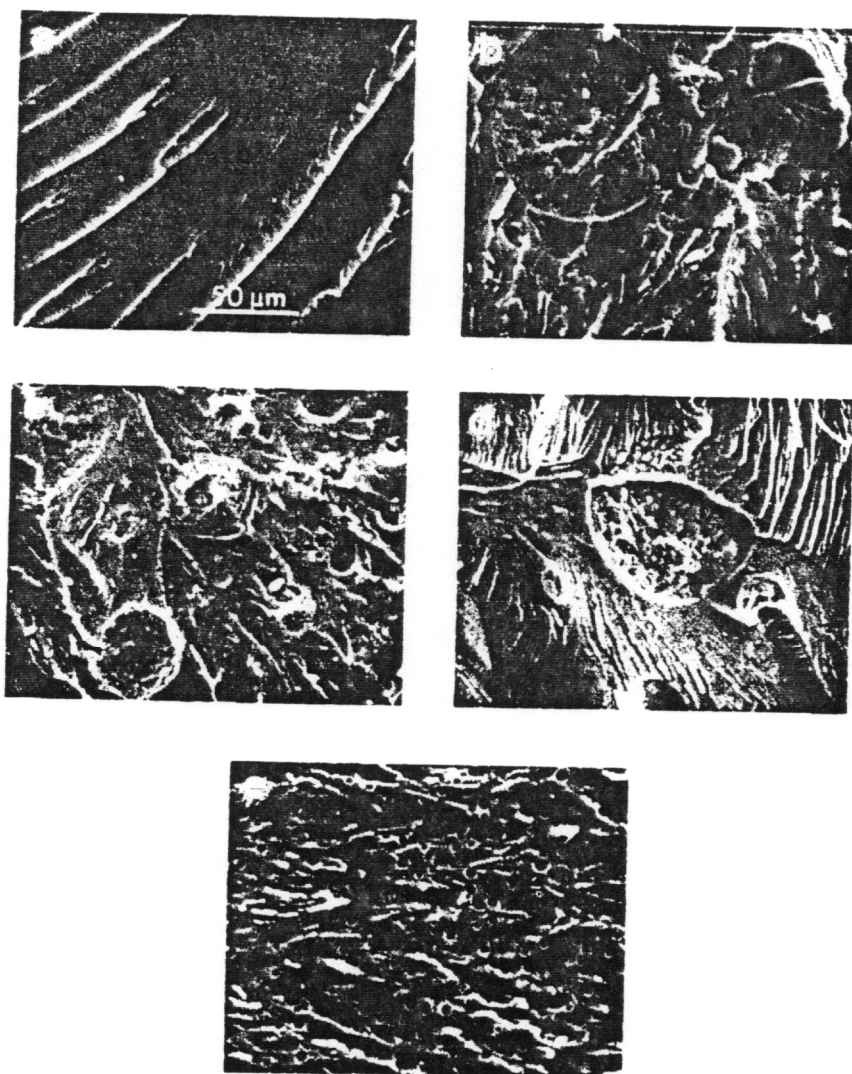


**Figure 2.2.8** Morphology of siloxane modified epoxy networks (a) neat epoxy; (b) to (e) contain overall 15% by weight poly(dimethylsiloxane-co-trifluoropropylmethylsiloxane) with (b)5%, (c) 20%, (d) 40%, and (e) 70% by weight respectively trifluoropropylmethyl siloxane in the copolymer. (from reference 78)

In addition to domain size, the nature of morphology itself can also be controlled by changing the character of the modifier backbone. This was demonstrated by Sefton and coworkers<sup>97</sup> who synthesized several thermoplastic polymers by systematically varying their backbone structure and used them to modify an epoxy novolac resin. They showed that using identical composition and cure conditions, altering the modifier chemistry produced a range of different morphologies, starting from a homogeneous single phase through a co-continuous "spinodal" type to the more frequent discrete phase separated structure.

The chemistry of the end groups in the modifier constitute an another important variable to control the phase separation behavior. The higher the reactivity of the functional groups with the resin, the greater is the tendency of the modifier to be incorporated in the matrix instead separating into domains. In a systematic study, Riew *et al.*<sup>67</sup> studied the effect of various end groups, namely, carboxyl, phenolic hydroxyl, epoxy, aliphatic hydroxyl and mercaptan. These functionalities are in the order of increasing reactivity towards epoxy, and this was reflected in the observed reverse order in the efficiency of phase separation. Kirshenbaum and coworkers<sup>84,84b</sup> varied the reactivity of poly(n-butyl acrylate) by introducing various quantities of acrylic acid as a comonomer. In these modifiers now one has reactive moieties in the backbone rather than at the end. The tendency to phase separation and the resulting domain size and volume fraction decreased as more of acrylic acid was incorporated into the modifier.

The use of functional end group to enhance the compatibility of the modifier can be facilitated by use of a two step curing procedure instead of one step procedure. Riffle *et al.*<sup>82</sup> circumvented the problem of gross phase separation of PDMS modifier by first

prereacting the amine functionality of the oligomers with a DGEBA based epoxy resin, EPON-828,<sup>®</sup> at a lower temperature of 60 °C for two hours prior to introduction of the curing agent. At this point the oligomers were essentially capped with epoxy end groups. Finally the required amount of curing agent was added and cure completed at an elevated temperature to obtain a compatible two-phase system. Similar two-step procedure was also used later by Tran, Yorkgitis and coworkers<sup>19,78,78b</sup> for their poly(dimethylsiloxane-co-trifluoropropylsiloxane) and poly(dimethylsiloxane-co-diphenylsiloxane) modified epoxies described previously. The capping of the modifier with epoxy prior to the final cure played also a major role in successful utilization of thermoplastic modifiers such as polysulfone<sup>88,89,92</sup> and poly(ether ketone),<sup>92,93,93b</sup> both in terms of stable two-phase morphology as well as toughness enhancement that was absent when nonreactive modifiers were used.<sup>90,94</sup>

The reactivity of the end groups has also been shown to affect the nature of interface. Kunz and coworkers<sup>133</sup> investigated interfacial region between the rubber domain and the epoxy matrix in CTBN and amine terminated butadiene acrylonitrile (ATBN) modified systems with the help of TEM coupled with energy dispersive X-ray analysis (EDAX). TEM results suggested that a gradually changing rubber concentration was present at the phase/matrix interface in ATBN modified epoxy whereas the CTBN modified epoxy had sharp interface. However, further investigation with NMR and DSC indicated that segmental mixing did not occur in either of the two systems. They attributed the diffuse nature of the interface to an irregular particle shape rather than phase mixing. No explanation for this difference in particle shape was however offered. Similar diffuse interface was also observed in amine terminated butadiene acrylonitrile system in a later study by Chan et. al.<sup>134</sup>

An additional modifier parameter one can adopt for morphology control is its molecular weight. Again from the thermodynamic arguments one can expect that lower molecular weight modifier will have lower tendency for phase separation. Early work by McGarry<sup>64</sup> on CTBN's showed that with similar compositions and curing conditions, the domain size can be modulated by changing the molecular weight of the modifier. A molecular weight of 3500 g/mol was found to have the domain size distribution that seem to maximize the toughening performance. Perhaps this preliminary study was responsible for the fact that typical commercial CTBN's have molecular weight in the range of 3500 gm/mole. Noshay and Robeson<sup>87</sup> found that a critical molecular weight of at least 3000 g/mol was required for the formation of a two-phase morphology in poly(propylene oxide) containing epoxy systems, below which single phase system is obtained. Similarly, Saito *et al.*<sup>83</sup> reported that in case of Poly(methyl phenyl siloxane), a lower molecular weight oligomer was completely miscible in the cured epoxy system whereas two phase system was obtained with higher molecular weight oligomers using the same loading and curing conditions. Other systematic studies on effect of molecular weights on the morphology and hence on the mechanical properties were performed by Hedrick *et al.*<sup>88,89</sup> and Cecere *et al.*<sup>92,93,93b</sup> for polysulfone and poly(ether ketone)s respectively. Figure 2.2.9 depicts an example of the effect of polysulfone molecular weight on domain size.

#### **2.2.1.2.2 Chemical Nature of the Thermoset.**

The chemical properties of the thermoset component, which includes the resin, the curing agent and the catalyst if any, obviously will have an effect on the compatibility and the extent of phase separation. However, in most cases the choice of resin system is usually determined by the such factors as availability, the end-application, cost, pot life etc.



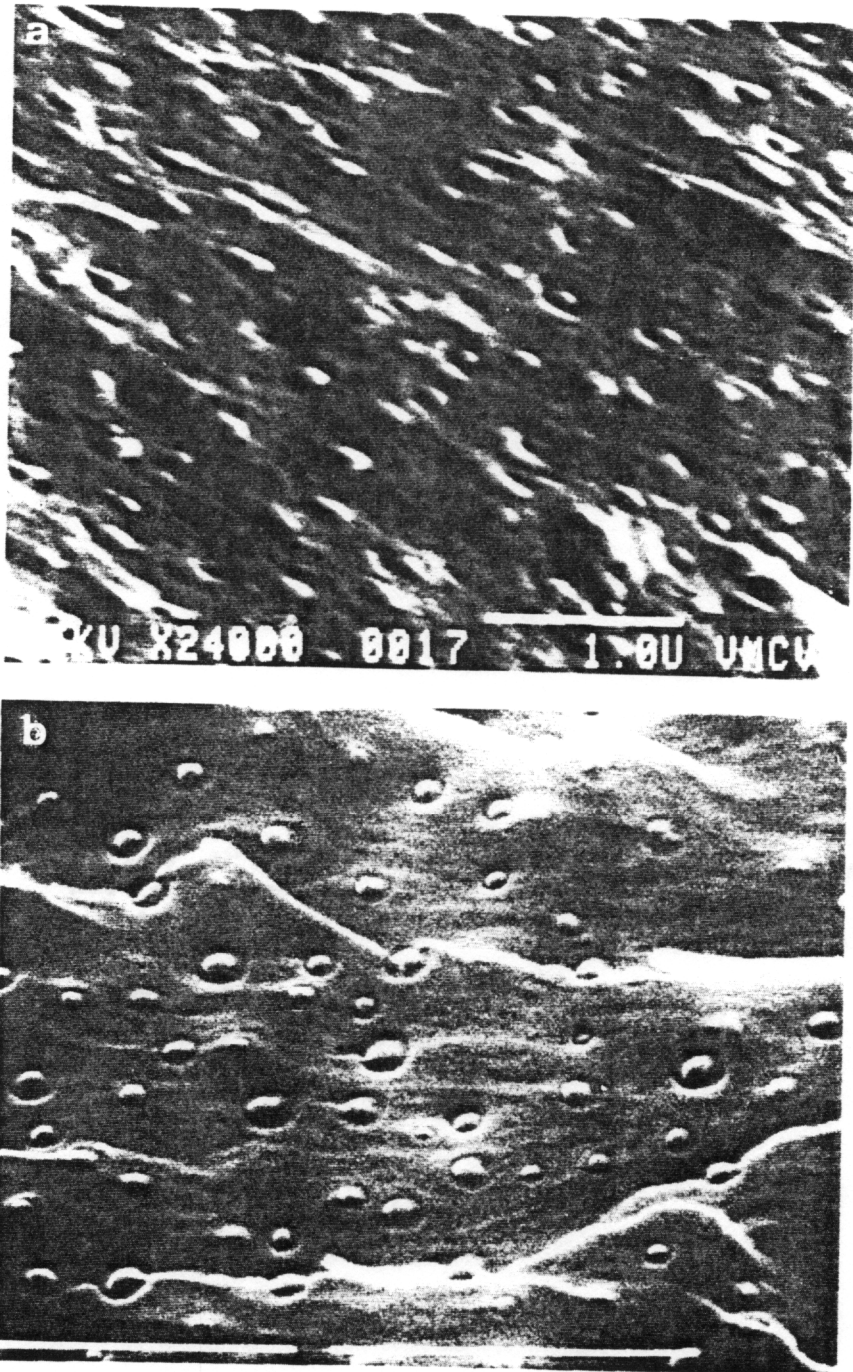


**Figure 2.2.9** Effect of modifier molecular weight on phase behavior of an epoxy system containing polysulfone. 15% by weight of polysulfone of molecular weights (a) 5300 gm/mole; and (b) 8200 gm/mole. (from reference 88)

Therefore, the research performed in the area of changing the nature of the thermoset has been somewhat limited compared to that regarding modifier chemistry described in the previous section.

The chemical nature of the thermoset can be changed by either using different types and amounts of curing agent and/or catalyst or by changing the structure of resin in terms of its functionality or molecular weight. The most detailed study on the effect of hardener type and concentration was performed by Bucknall and Yoshii<sup>135</sup> who examined the microstructure of an epoxy/CTBN system using a variety of curing agents ranging from anhydride to primary amines to tertiary amines and their salts. At any given hardener concentration the largest rubbery particle size was obtained with the least reactive hardener used, i. e. piperidine. As shown in Figure 2.2.10, with increasing hardener reactivity the particle size reduced and increasing the hardener content for a given type also reduced the particle size. This is also reflected on the total volume fraction of the rubber phase. At high concentrations of the more reactive hardener such as 2,4,6-Tris(dimethylaminomethyl) phenol and its salt with Tris(2-ethyl hexanoic acid), the rubber remained dissolved in the matrix with no phase separation. Effect of curing agent was also observed in a study by Meeks<sup>69</sup> in which a comparison was made between the morphology obtained by various amines and anhydrides.

Bucknall and Yoshii<sup>135</sup> also showed that the extent of phase separation can be controlled by adding bisphenol A which acts as a chain extension agent, thus, increasing the molecular weight of the resin between crosslinks. The tendency for phase separation increased as a result. Similar results were obtained when a higher molecular weight resin instead of DGEBA was used. An additional effect of adding bisphenol A (typically when

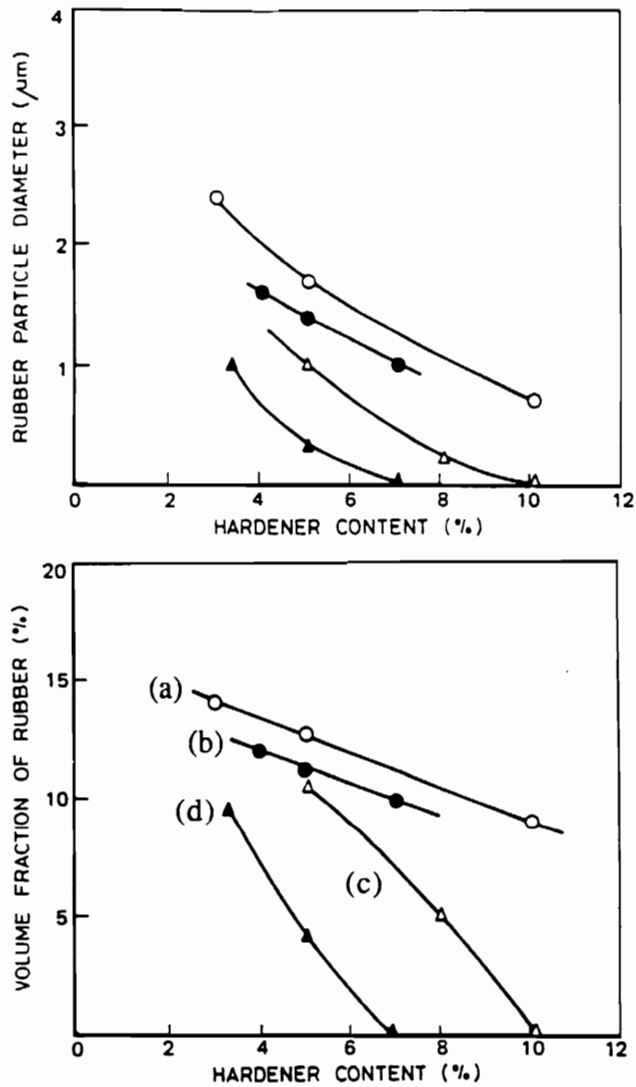


**Figure 2.2.10** Effect of type and concentration of hardener on microstructure of an epoxy containing CTBN rubber. (a) Piperidine; (b) Tri(2-ethyl hexanoic acid) salt of 2,4,6 tris(dimethylaminomethyl) phenol; (c) Triethylene tetramine; and (d) 2,4,6 tris(dimethylaminomethyl) phenol. (from reference 135)

in the ratio of 24:100 with the epoxy) has been seen on the particle size distribution. A distinctive bimodal particle size distribution was observed in these systems<sup>67,100,135</sup> with one family of particles around 0.1 μm and a second in the range of 1-5 μm. The detailed mechanism behind such a bimodal distribution is not clearly understood but a possible reaction sequence has been suggested by Riew *et al.*<sup>67</sup>

The functionality of the epoxy also has been shown to be important in control of morphology. For example, Bucknall and Partridge<sup>90</sup> used a trifunctional and a tetrafunctional epoxies in various ratios. Under identical conditions and rubber composition, the higher amount of tetrafunctional epoxy resulted in lesser phase separation and smaller particles. Similarly, Nae<sup>136</sup> also observed marked difference in morphologies developed when using epoxies of various functionalities.

#### **2.2.1.2.3 Composition.**

In general, as one may expect, the addition of larger amount of the modifier would result in an increase in size as well the number of domains. However, both from morphological as well as mechanical property points of view, a more interesting effect of composition develops when at a certain point phase inversion occurs whereby epoxy becomes the discrete phase instead of the modifier.<sup>68,137</sup> An example of this is given on Figure 2.2.11(a) where a 9% CTBN modified epoxy is compared with one containing 28%.<sup>137</sup> The latter has the rubber as the continuous phase. For rubber modified systems, phase inversion is not particularly sought after (unless the aim is to obtain reinforced rubber rather than toughened thermoset) since this obviously occurs with a considerable loss in modulus. However, in case of thermoplastic modified systems, the phase inverted morphology

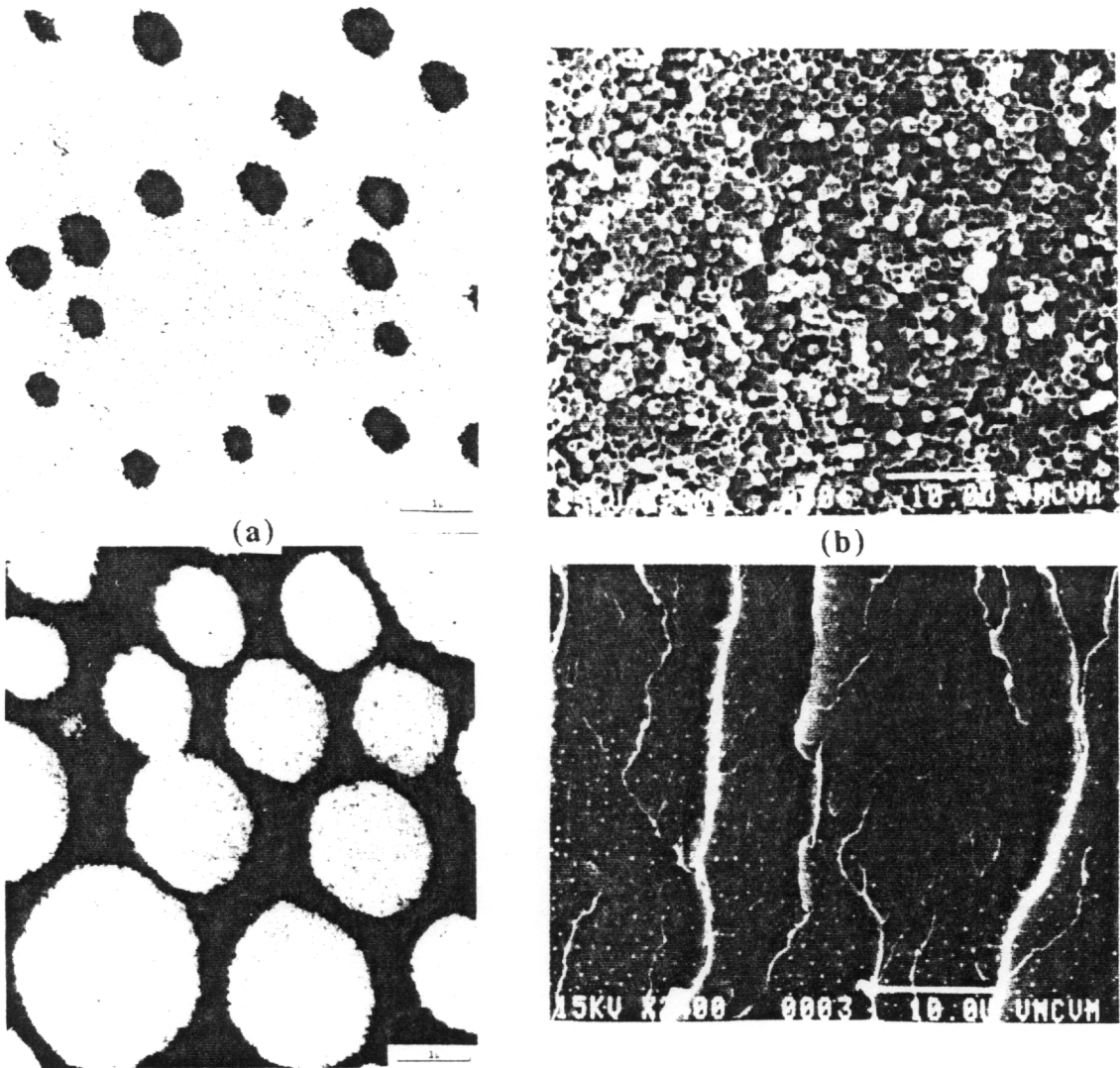


**Figure 2.2.11** Phase inversion in modified thermosets. (a) CTBN as modifier, 9% (top) vs 28% (bottom). (reproduced from reference 137); (b) Polysulfone as modifier, 15% (top) vs 30% (bottom). (from reference 92)

promises better performance in terms of both toughness and modulus.<sup>92,93,93b</sup> Figure 2.2.11(b) shows phase inversion in a 30% by weight in a amine terminated polysulfone modified epoxy. The enhanced utilities of thermoplastic modified systems via phase inversion have also been realized by others as well.<sup>95,96</sup>

#### **2.2.1.2.4 Cure Conditions.**

The curing of the thermoset/modifier mixture involves three processes: phase separation, gelation, and vitrification. The time and temperature employed for the overall cure will affect both the kinetics and thermodynamics of the system differently through each of these processes and, in turn, govern the extent to which these processes occur. Thus, cure conditions, i.e. time and temperature of cure, play a profound role in control of the microstructure development.

Levita and coworkers<sup>138</sup> studied the effect of temperature of cure on 10% ATBN modified epoxies. Three cure temperatures, 60 °C, 100 °C , and 140 °C, displayed a marked difference in the domain size of the rubber phase- starting from about 1 μm at 60 °C to 5 μm at 140 °C. In a similar fashion, Shaw and Tod<sup>139</sup> also observed increase in domain size of 15% CTBN modified DGEBA epoxy cured with piperidine at several temperatures ranging from 120 °C to 160 °C. However, an increase in domain size with the temperature of cure is not always necessarily the case. Chan *et al.*<sup>134</sup> observed that while a CTBN system showed an increase in the average domain size with temperature of cure, the reverse was true for an ATBN modified system. Inoue and coworkers<sup>91,127,140</sup> have also studied the effect of cure conditions on rubber modified as well as thermoplastic poly(ether

sulfone) modified epoxies and reported that morphology of varying sizes as well as shapes i. e. discrete morphology to interconnected globule type are possible.

The extent of phase separation as a function of temperature was found to go through a maximum by Gillham and coworkers<sup>131</sup> as measured by both the size as well as the total volume fraction of the rubber phase. Based on their results they proposed that phase separation was influenced by competing effects of incompatibility, rate of nucleation and growth of the phases, and quenching of morphological development by gelation. With these arguments they put forward a generalized representation of morphology as a function of cure temperature as depicted in Figure 2.2.12(a). It conveys two important points: the volume fraction of phase separated rubber has a maximum in an intermediate temperature range and the morphology remains unchanged after gelation. Gillham *et al.*<sup>131</sup> also explained the volume fraction maxima in terms of kinetic and thermodynamic factors involved in phase separation by drawing a parallel to crystallization in linear polymers. Analogous to the  $(T_g-T_m)$  window with crystal growth maxima at an intermediate temperature, they proposed a  $(T_{s0}-T_s)$  window for phase separation as shown in Figure 2.2.12(b) where  $T_{s0}$  is the minimum temperature at which the components are initially miscible and  $T_s$  is the minimum temperature at which the phase separation will begin prior to gelation.

The question of whether there is any substantial phase separation activity following gelation was further addressed in several publications after the initial work by Gillham *et al.*<sup>131</sup> One of the most definitive study was that by Wang and Zupko<sup>129</sup> on CTBN modified epoxy in a composition range of 3 to 38% rubber. A combination of light transmission and viscosity measurements allowed them to monitor the phase separation and the crosslinking reaction

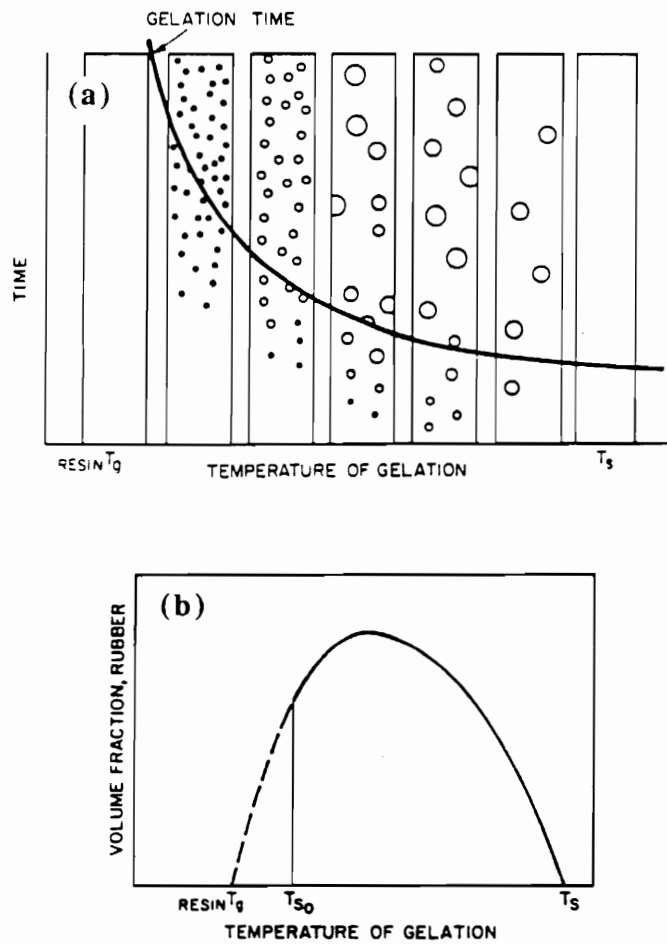


**Figure 2.2.12** Models depicting relation between phase separation and cure conditions. (a) morphology map on cure time/temperature axes; and (b) cure temperature window for phase growth. (from reference 131)



simultaneously. From the comparison of viscosity and scattering data, they observed that even after the viscosity has risen sharply, the light intensity continued to drop at a steady rate and did not level off long after the samples had gelled. These results were particularly interesting since microscopic examination of the samples during cure revealed that the physical growth of phase domains ceased approximately at the same time when the viscosity began to rise rapidly. Considering that even after gelation there should be sufficient mobility in the network for the molecular segments to migrate in a limited range, they suggested that the post-gelation light transmission behavior might be associated with localized changes in composition within the sample. Such localized changes could result in formation of more well-defined boundaries, for example.

Visconti and Marchessault<sup>137</sup> also studied the dynamics of phase behavior in an epoxy-CTBN system by means of small angle light scattering and detected further increase in the scattered intensity after gelation. However, ruling out any phase changes, they ascribed this behavior due to artifacts from the evolution of small gas bubbles in the sample cell at the glass-solid interface. A more direct observation of phase separation after gelation was reported by Romanchick *et al.*<sup>132</sup> They examined samples cured isothermally at several time intervals with TEM and found that in a 7.5% CTBN modified epoxy, the phase dimensions continued to grow to a considerable extent several minutes after gelation had occurred.

Following up on their previous work Gillham and coworkers<sup>134</sup> further explored the relation between phase separation, gelation and vitrification with the use of torsional braid analysis (TBA) and light transmission techniques. A typical example of their results in the form of a Time Temperature Transformation (TTT) diagram is displayed in Figure 2.2.13.

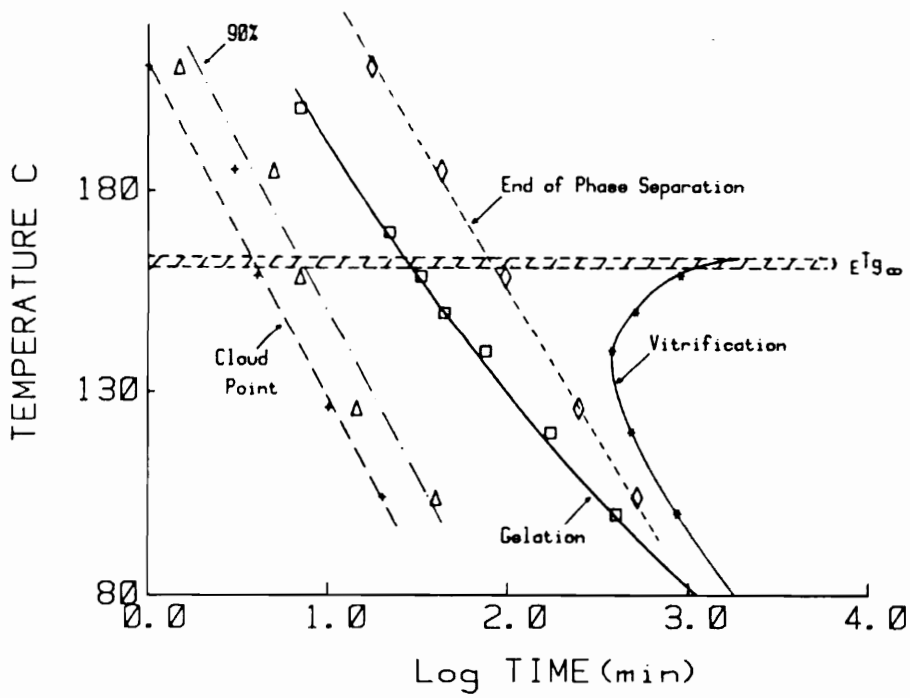


**Figure 2.2.13** Time Temperature Transformation (TTT) diagram inclusive of phase separation for a CTBN modified epoxy system. (from reference 134)

It is evident that although 90% of the total decrease in the transmitted light occurred before gelation, there was still further change observed well after gelation, particularly in the case of higher cure temperatures.

Finally, the role of cure conditions has very recently been demonstrated by use of microwave energy to cure thermoplastic modified epoxies. Although the subject is still in its infancy, the indications so far point towards significant and sometimes dramatic difference between morphologies obtained via microwave cure and those obtained by conventional thermal cure.<sup>141-143</sup>

### **2.2.1.3 Theoretical Modeling of Phase Separation.**

The only significant comprehensive theoretical treatment of the phase separation process in modified thermoset has been developed by Williams and coworkers.<sup>122</sup> In this section a brief review of their approach and the predictions based on the theory will be given. It would be out of the scope of this review to give *all* details of this theory and the reader is referred to their original publication for further information.

As it is quite evident from the discussion so far that phase separation is a combination of two processes: thermodynamics (statics) and kinetics (dynamics). Thermodynamic changes evolving from polymerization of the thermoset create the free energy conditions conducive to phase separation. However, the extent to which this is accomplished will depend on the kinetics. Which of the two processes is dominant in governing the final outcome is a function of how fast or slow the system is changing, i. e. on the rate at which

the cure takes place. The Williams' theory takes this basic concept of relation between statics and dynamics to predict various paths that the phase separation process may take.

A simplifying assumption made in this approach is that the modifier does not take part in the polymerization reactions occurring in the system. Taking the case of CTBN modified epoxy, this amounts to assuming that the reaction between the carboxyl end-groups and the epoxide are negligible and have no effect on the kinetic as well as statistical parameters of epoxy cure reaction. The treatment is also based on a second order kinetics for cure rate. Furthermore, the thermoset is taken to comprise a tetrafunctional monomer, such as DGEBA epoxy, crosslinking in presence of a catalyst, such as piperidine. Thus, the system consists of a pseudo-binary mixture of the thermoset (component 1) that includes monomer and catalyst and an inert modifier (component 2).

#### **2.2.1.3.1 Thermodynamics.**

The thermodynamics in this treatment is based on the Flory-Huggins theory modified to take into account the changing molecular weight of the thermoset as discussed earlier in the section 2.2.1.1. With the help of free energy expression given by Equation 2.2.13 and its derivatives, binodal and spinodal curves ( $p$ - $\phi$  diagrams) defining the metastable region can be constructed as shown in Figure 2.2.3. Equation 2.2.13 also gives the free energy-composition relation at any conversion during polymerization which can be used to define a number of energetic and compositional quantities that in turn can be used further in the development of kinetic equations.

*Driving Force for Phase Growth.* Phase separation commences when the system enters the metastable region. Figure 2.2.14(a) shows a free energy-composition curve for a system in the metastable state at a certain conversion  $p$ . At this conversion, there are two equilibrium compositions  $\phi_{2\alpha}$  and  $\phi_{2\beta}$ , also known as conjugate points on the binodal curve;  $a$  denotes the phase rich in modifier (component 2) and  $b$  denotes the phase rich in the thermoset (component 1). Also,  $\phi_{2c}$  defines the actual modifier concentration in the continuous thermoset-rich phase. Initially  $\phi_{2c}$  would be the same as  $\phi_{20}$ , the composition of mixture before polymerization. Then, at a certain conversion  $p$ , when the system reaches the binodal curve,  $\phi_{2c} = \phi_{20} = \phi_{2\alpha}$ . At this point, the value of  $\phi_{2c}$  starts to deviate from the corresponding equilibrium value  $\phi_{2\alpha}$ . The extent to which this deviation occurs depends upon the relative rates of phase separation and polymerization. A considerable divergence from the equilibrium, as it is the case on Figure 2.2.14(a), originates from relatively faster rates of reaction. Similarly, for slower rates of reaction, the actual composition of the continuous phase will remain close to the equilibrium value. The difference  $(\phi_{2c} - \phi_{2\alpha})$  provides the driving force for phase growth at any time during phase separation.

*Maximum Free Energy Gain by Precipitation.* From the partial free energy concepts, it can be shown that for a given concentration  $\phi_{2n}$  as the composition of the new precipitating phase from the mother phase having composition  $\phi_{2c}$ , the Gibbs free energy change,  $\Delta G_n$ , is the distance between the tangent at  $\phi_{2c}$  and the free energy curve  $\Delta G_m^V$ , as illustrated in Figure 2.2.14(a). The value of  $\Delta G_n$  will depend on the chosen position of  $\phi_{2n}$ . A plot of  $\Delta G_n$  vs  $\phi_{2n}$  is given on Figure 2.2.14(b). It shows that at  $\phi_{2n} = \phi_{2N}$ , the maximum possible decrease in free energy is obtained. The significance of this is that the  $\phi_{2N}$  will be the preferred composition of the precipitated phase from the continuous phase of

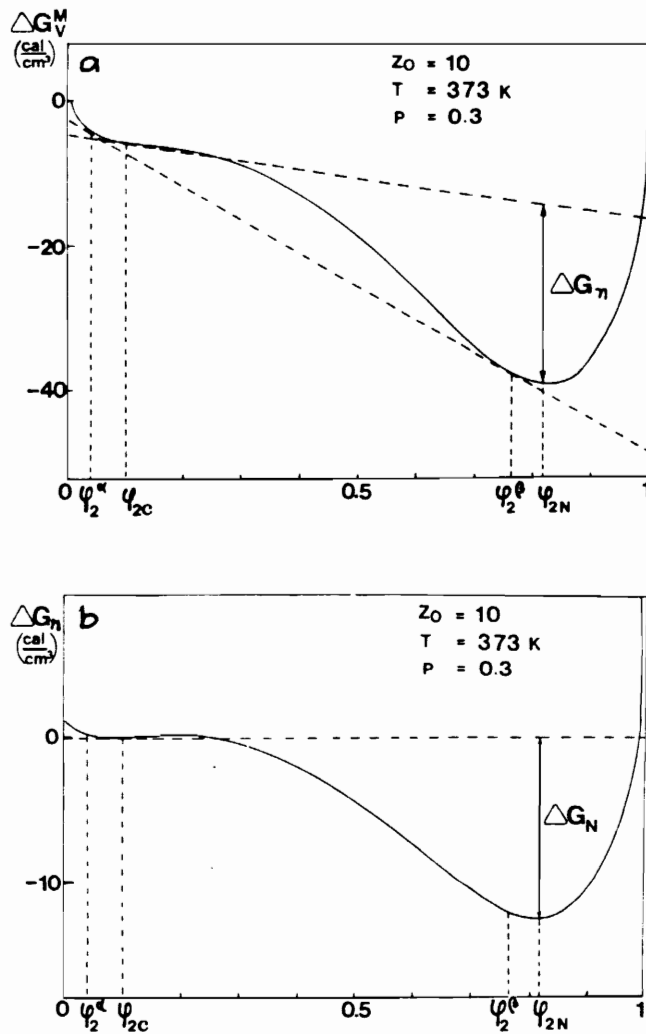


**Figure 2.2.14** (a) Gibbs free energy of mixing per unit volume vs modifier volume fraction. (b) Gibbs free energy change in the phase separation process vs modifier concentration in the precipitated phase. (after reference 122)

composition  $\phi_{2c}$  under the given conditions of Figure 2.2.14. The negative value of  $\Delta G_N$  provides the necessary impetus for precipitation.

*Activation Energy for Composition Fluctuations.* To precipitate a phase of composition  $\phi_{2N}$  from the continuous phase of composition  $\phi_{2c}$ , there must be some form of composition fluctuations. Figure 2.2.14(b) shows that the path from  $\phi_{2c}$  towards  $\phi_{2N}$  encounters a region in which  $\Delta G_n$  increases slightly to a maximum value,  $E_F$ , and then decreases continuously. Thus,  $E_F$  may be regarded as an energy barrier for phase separation. It can be shown that  $E_F$  reaches a maximum value when the system is completely in equilibrium, and is zero if the system is at the spinodal curve. The latter situation corresponds to having no energy barrier for precipitation and hence, the system at the spinodal goes into spontaneous demixing.

#### 2.2.1.3.2 Kinetics.

Williams *et al.* consider that, in general, the mechanism of phase separation is that of nucleation and growth. They contend that spinodal demixing occurs only in special circumstances when the rate of reaction is extremely high, the temperature is low, and the composition in the vicinity of the critical point.

*Nucleation.* The following expression for rate of formation of new nuclei,  $N$ , using conversion,  $p$ , as the independent variable is arrived at by the use of appropriate relations for reaction kinetics and diffusion coefficient:

$$\frac{dN}{dp} = \frac{F_0 T}{A} \left[ \frac{(1-3p)}{(1-p^2)} \right]^2 \exp\left[\frac{(E-E_\eta-E_F-\Delta G_c)}{RT}\right] \quad (2.2.15)$$

where,  $F_0$  is an adjustable parameter,  $A$  is the pre-exponential factor in the polymerization rate equation,  $E$  is the activation energy of polymerization,  $E_\eta$  is the activation energy of viscosity, and  $\Delta G_c$  is the free energy of the formation of critical nucleus as given by:

$$\Delta G_c = 16\pi\sigma^3 / (3 |\Delta G_N|^2) \quad (2.2.16)$$

Consideration of disappearance of particle through coalescence gives the following expression for  $P$ , the rate of variation of particles per unit volume:

$$\frac{dP}{dp} = \frac{dN}{dp} - \frac{4}{3} \frac{kT}{A\eta} P^2 \left[ \frac{\exp(E/RT)}{(1-p^2)} \right] \quad (2.2.17)$$

Here,  $\eta$  is the viscosity of the continuous phase.

*Particle Growth.* The total increase in volume fraction of the separating phase is the sum of that through formation of new nuclei and that by growth of the existing particles via mass transfer process taking place due to the difference  $(\phi_{2c}-\phi_{2a})$ . The expression for the  $V_D$ , the volume fraction of the discrete phase is found to be:

$$\frac{dV_D}{dp} = \frac{4\pi}{3} (r_{cp})^3 \frac{dN}{dp} + k_\phi 4\pi R^2 P (\phi_{2c}-\phi_{2a}) dt/dp \quad (2.2.18)$$



where,  $r_{cp}$  is the radius of the critical nucleus,  $k_{\phi}$  is a mass transfer coefficient, and  $R$  is the mean radius of the dispersed phase.

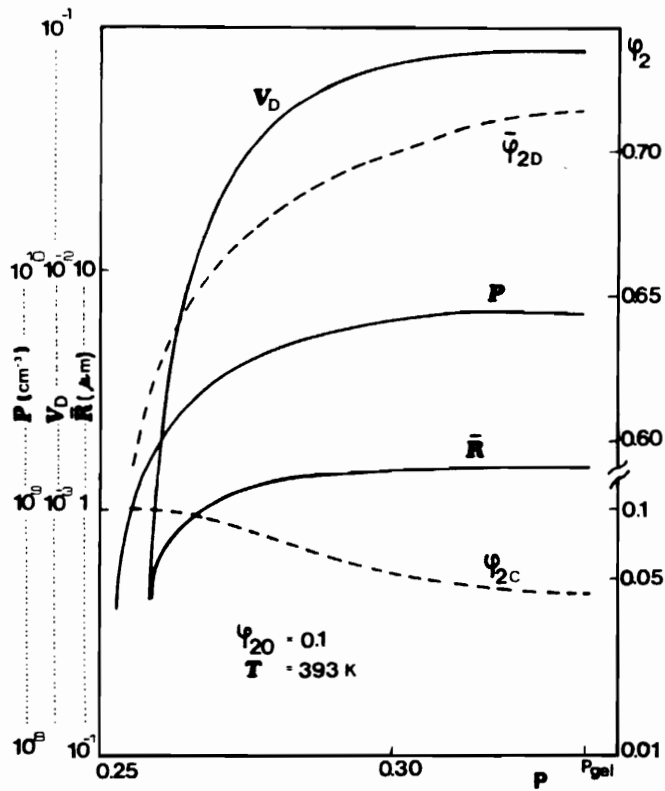
### 2.2.1.3.3 Model Predictions.

Using model parameters to fit the CTBN modified epoxy/piperidine system similar to that studied by Manzione *et al.*,<sup>131</sup> Williams and coworkers<sup>122</sup> solved the key differential equations 2.2.15, 2.2.17, and 2.2.18 with the help of numerical methods to obtain quantities that define the morphology:  $P$ , the number of dispersed phase particles per unit volume;  $V_D$ , the volume fraction of dispersed phase; and  $R$ , the average radius of the particles.

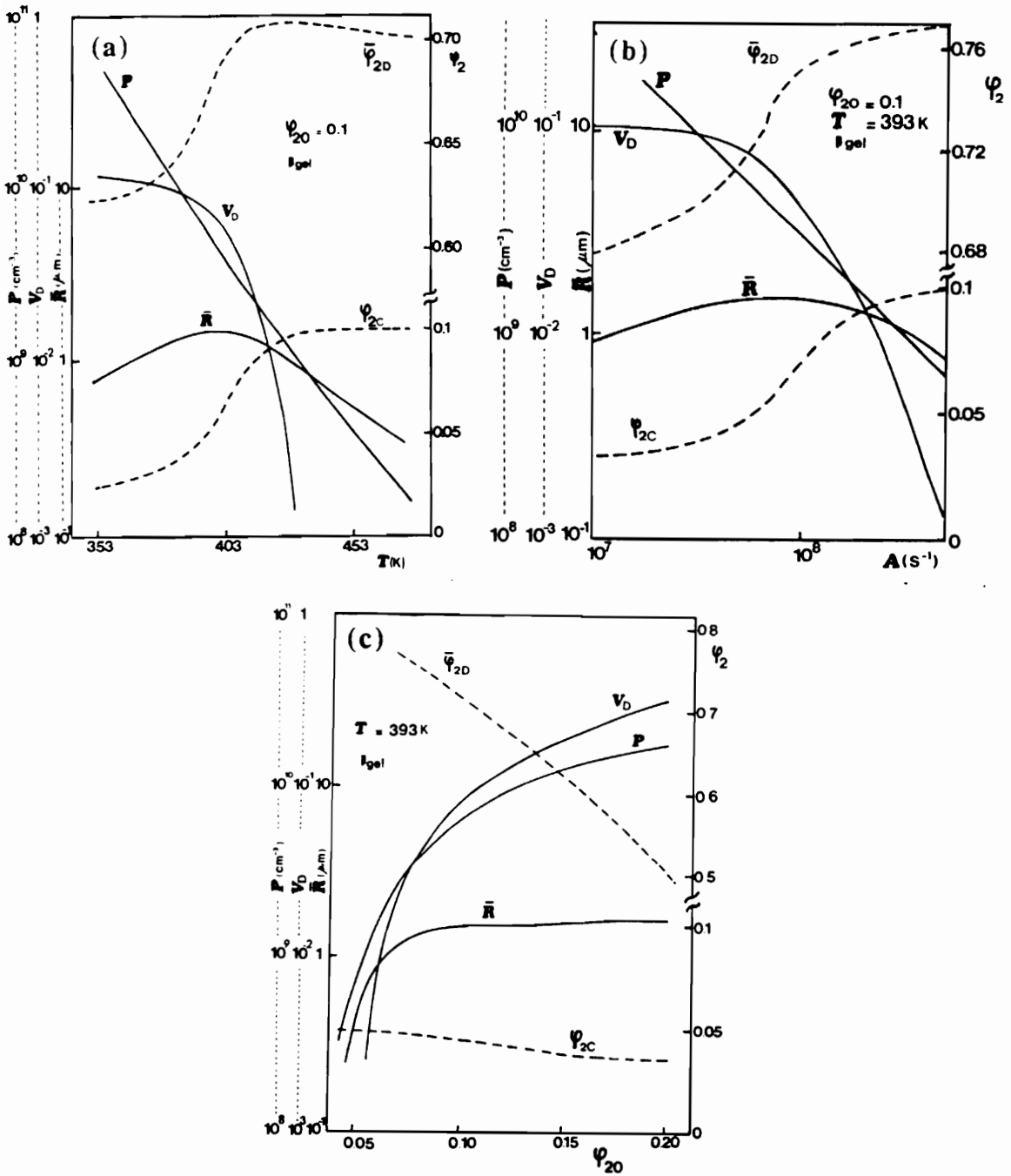
Figure 2.2.15 displays the evolution of these parameters as a function of conversion at given temperature of cure and initial composition. As seen, the mean radius of particles attains its maximum value well before gelation, a prediction not far from experimental observations. Analogously, the total volume fraction as well as the number of particles also level off as they approach the gel point.

Figure 2.2.16 (a) through (c) show the final values of  $P$ ,  $V_D$ , and  $R$  obtained as functions of cure temperature, rate of polymerization, and initial modifier concentration, respectively. The observations made from each case can be summarized as follows.

*Effect of Cure Temperature.* The concentration of dispersed phase particles decreases monotonically with increase in temperature. This is a consequence of using the activation energy of reaction  $E > E_{\eta} + E_F + \Delta G_c$ . (For this situation, the exponential term in



**Figure 2.2.15** Evolution of different quantities that characterize the morphology as a function of the thermoset conversion. (from reference 122)



**Figure 2.2.16** Final values of different quantities that characterize the morphology as functions of (a) temperature of cure, (b) polymerization rate, and (c) initial modifier concentration. (from reference 122)

Equation 2.1.15 contains a positive coefficient and the rate of nucleation becomes a strong function of the inverse of temperature.) The volume fraction  $V_D$  is nearly constant in the limit of lower temperatures since in this region, reaction rates are slow and the phase separation is restricted only by the position of the binodal and the conversion at gelation. The situation is reverse at higher temperatures, though, because of high polymerization rates where the kinetics becomes the controlling factor. The volume fraction, therefore drops dramatically at higher temperatures. The mean radius, which is dependent on the ratio of  $V_D$  to  $P$ , as a result goes through a maximum. One can divide the temperature range into two regions, one on each side of the maximum on the curve for  $R$ . On the left hand side, the thermodynamics controls the phase separation and on the right, kinetics is the limiting mechanism.

*Effect of Polymerization Rate.* Figure 2.2.16(b) shows the effect of increasing the polymerization rate represented by the pre-exponential factor  $A$  in the rate equation. From experimental point of view, this can be achieved by using various catalyst to resin ratios or by employing catalysts of differing activities. The trends here are similar to the ones observed from temperature increase. Again it may be proposed that for the lower polymerization rates the thermodynamics is the controlling factor, and at higher polymerization rates kinetics limits the extent of phase separation.

*Effect of Initial Modifier Concentration.* Increasing the initial modifier concentration leads to increase in both the number of particles as well as the total volume of dispersed phase. However, more interestingly, the model predicts that the mean radius of the particles, after an initial increase, levels off. Thus it seems that the increases in  $V_D$  and  $P$  tend to compensate each other at higher values of  $\phi_{20}$ .

#### **2.2.1.3.4 Theory-Experiment Correlation.**

Most of the trends predicted by the above model seem to agree fairly closely with experimental observations made by other workers.<sup>131,133,134</sup> Particularly the effects of gelation and cure temperature have been well represented by the model. Williams *et al.*, in a more recent publication,<sup>144</sup> further improved upon their approach and utilized it to predict the particle size distribution of the dispersed domains in a DGEBA based epoxy cured with diaminodiphenyl sulfone (DDS) with CTBN as the modifier. They also developed all necessary experimental steps to illustrate the applicability of their model to any given system under study. A preliminary comparison of the predicted and experimental cumulative particle size distribution gave reasonable agreement.

In the final analysis, the above model has been successful in building a complete framework based on thermodynamic and kinetic equations describing the process of phase separation in modified thermosets. However, in order for the model to be most effective in predicting the behavior in real systems, a number of further considerations seem warranted. Particularly important among them is the dependence of the F-H interaction parameter, in addition to the temperature, on composition of the system which has not been taken into account so far. Also of significance would be the effect of modifier interaction with the thermoset via reactive end-groups. In conjunction with these, better empirical and experimental means to estimate physical quantities such as diffusion coefficients, viscosity, and interfacial properties will make the model applicable to a broader range of systems. Finally careful experiments under well-controlled conditions using model systems will be necessary to evaluate further the validity of this theory.

#### **2.2.1.4 Summary.**

The review of morphology in modified thermoset has touched upon three major aspects. First an understanding of the thermodynamic concepts describing the phase separation process was developed. This was followed by an analysis of experimental literature in relation to morphology control via various chemical and physical means available to affect both thermodynamic as well as kinetic processes in the system. Finally, salient features of an elaborate theoretical model have been discussed. This model depicts major components of the phase separation process and provides an excellent basis for interpretation of the experimental observations.

#### **2.2.2 Cure Behavior of Thermosets**

The properties of a thermoset depend greatly on the cure path the system takes to reach its final state. This is specially true in the case of modified thermosets where the phase separation process goes hand-in-hand with the cure, as demonstrated amply in the preceding section. Thus, understanding the cure behavior of thermosets, both in the neat as well as the modified forms, becomes critically important in order to establish their optimum utilization.

Several steps comprise the process of cure, which is in general defined as the transformation of a low molecular weight liquid into a crosslinked, high molecular weight polymer solid. Figure 2.2.17 illustrates some of the basic steps involved. Cure begins by the reaction between the molecules to give rise to linear growth and branching of chains that

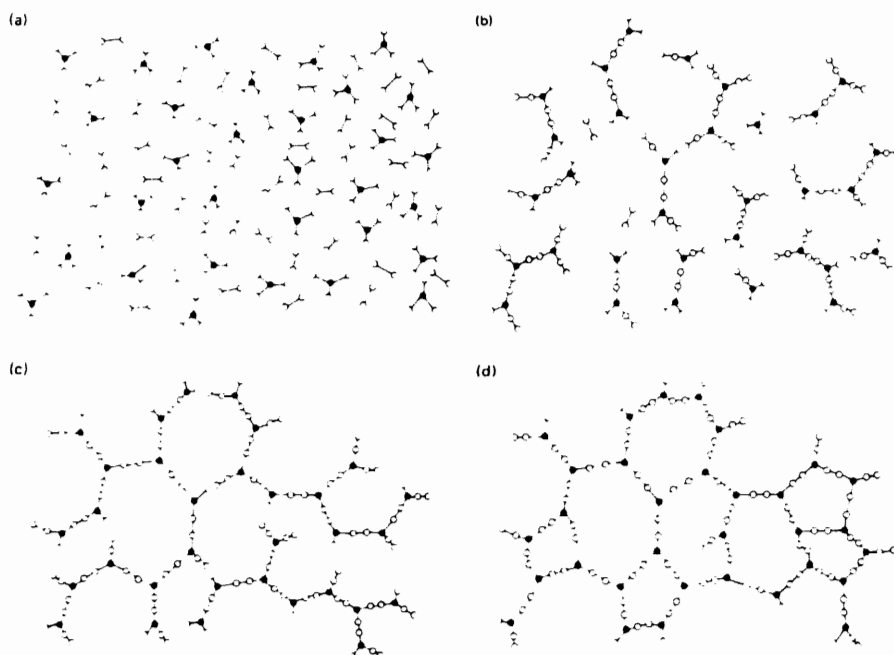


**Figure 2.2.17** Schematic two-dimensional representation of curing of a thermoset. (a) starting monomers, (b) linear growth and branching, (c) formation of gelled but incomplete network, and (d) fully cured material. (from reference 145)

soon begin to crosslink, the condition for this being that at least one of the reacting species has the functionality of greater than 2. As the reaction proceeds, the molecular weight of the system increases rapidly leading to the incipient formation of an infinite network by the phenomenon known as *gelation*. Continued incorporation of the remaining reactive species into the network results eventually into the fully cured system.

Prior to gelation, the system is soluble and fusible, but after gelation both soluble (sol) and insoluble (gel) fractions are present. As gelation is approached, the viscosity increases dramatically, and the weight average molecular weight goes to infinity while the number average molecular weight remains small. Flory<sup>123</sup> showed first that gelation is a statistical event and can be predicted based solely on the functionality and stoichiometry of the reacting species. A second important phenomenon that may occur at any point during the course of reaction is *vitrification*, which is the transition in the material from a liquid or rubbery state to a glassy state. This occurs when the  $T_g$  of the system, increasing monotonically as the reaction proceeds, coincides with the cure temperature. Controlled mainly by diffusion limited kinetics, further reaction in the glassy state is extremely slow and thus, for all practical purposes, vitrification brings an abrupt halt to cure. In addition to gelation and vitrification, other events of importance in the thermosetting process include changes in viscosity and conversion with time, thermal degradation, and the onset and termination of phase separation in case of modified thermosets.

By far the most useful tool to develop the intellectual framework for understanding and comparing the various aspects of the cure process is the Time Temperature Transformation (TTT) diagrams. The concept of TTT diagrams have been in use extensively in materials science for studying the phase changes in metals and metal alloys for quite some



time.<sup>146,147</sup> Its application to the thermosets is however more recent. The majority of the work published in this area, including the very first, has originated from Gillham and his group<sup>58,148-155</sup> at Princeton University over the last decade or so. Analogous to their counterparts in metallurgy, the TTT diagrams for thermosets allow one to choose specific time-temperature paths so that gelation, vitrification, and phase separation occur in a controlled manner and the final properties of these systems may be predicted. The rest of this section will be devoted to a brief review of the salient features of a generalized TTT diagram, experimental methods for its construction, and other related concepts. For more in-depth treatment of the most of the topics covered here, the reader is referred to some of the many excellent reviews available in literature.<sup>150,153,155</sup>

#### **2.2.2.1 The TTT Diagram.**

A generalized TTT diagram that includes the majority of the important features of the cure of neat as well as modified thermosets is displayed in Figure 2.2.18. In the most simple terms, a TTT diagram may be looked upon as a map showing the existence of various states of the material arising from different combinations of temperature and time of cure. These states include liquid, sol/gel rubber, gel rubber, sol/gel glass, gel glass, sol glass and char. Various changes occurring in the material during an isothermal cure are characterized by contours of times to reach these events. Relevant contours seen on Figure 2.2.18 include: gelation (corresponding to a unique conversion), vitrification (corresponding to the glass transition temperature equalling the temperature of cure,  $T_{\text{cure}}$ ), devitrification (corresponding to the  $T_g$  decreasing to  $T_{\text{cure}}$  because of thermal degradation), and char formation (corresponding to  $T_g$  increasing to  $T_{\text{cure}}$  because of thermal degradation).

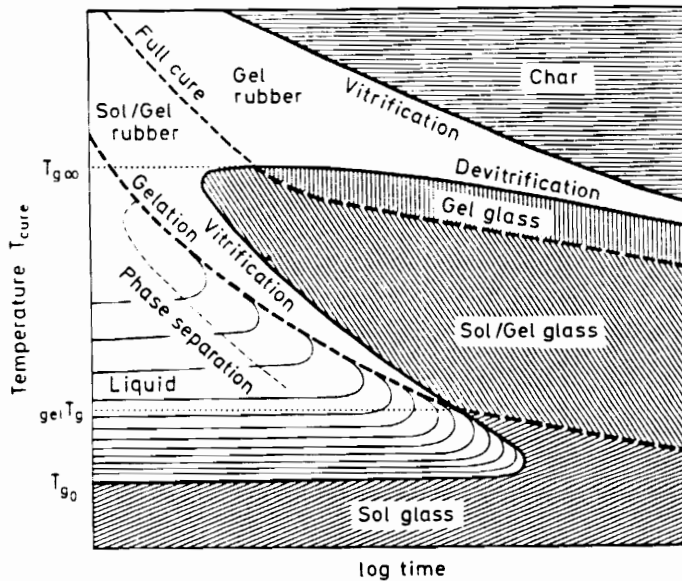


**Figure 2.2.18** Schematic time-temperature-transformation (TTT) isothermal cure diagram for a thermosetting system. Shown are three critical temperatures ( $T_{g0}$ ,  $_{gel}T_g$ , and  $T_{g\infty}$ ) and distinct regions of matter (liquid, sol/gel rubber, gel rubber, sol/gel glass, gel glass, sol glass, char). The full cure line ( $T_g = T_{g\infty}$ ) separates the sol/glass from the gel glass region, and the sol/gel rubber from gel elastomer region, respectively. Also displayed are degradation events of devitrification and char formation, isoviscous lines, and the onset of phase separation. (from reference 155)

Additional secondary events such as the onset of phase separation, isoviscosity, and full cure may also be represented on this diagram.

There are three critical temperatures that have important physical significance:  $T_{g0}$ ,  $_{gel}T_g$ , and  $T_{g\infty}$ .  $T_{g0}$  is the glass transition temperature of the initial uncured reactant mixture. Being in the glassy state, the system may be presumed to be nearly non-reactive below  $T_{g0}$ . From practical standpoint, this temperature is the upper limit for a safe storage of the reactant mixture for long periods of time.  $_{gel}T_g$  is the cure temperature at which the gelation and vitrification occur at the same time. Between  $T_{g0}$  and  $_{gel}T_g$ , the system will vitrify before gelation. In this temperature range, the system, not having gelled yet, is of low molecular weight. Therefore, subsequent heating and processing of this material, frequently known as a B-stage resin in industry, at a higher temperature is possible. Finally,  $T_{g\infty}$  is the maximum glass transition temperature achievable in the system corresponding to the state in which complete reaction has taken place without thermal degradation. Between  $_{gel}T_g$  and  $T_{g\infty}$ , gelation occurs prior to vitrification. Thus if a system is cured in this range of temperatures, it will be set irreversibly. If the system is cured at a temperature above  $T_{g\infty}$ , on the other hand, no vitrification takes place and it will remain in the gelled rubber state unless thermal degradation increases the  $T_g$  up to the  $T_{cure}$ .

The shape of the gelation and vitrification curves may require further explanation. The time to gel,  $t_{gel}$ , monotonically decreases as the temperature of cure is increased. This follows from the premise that, under ideal conditions, the conversion at which gelation occurs is determined by the chemistry of the reactants alone and is independent of the cure temperature. With the exothermic nature of a typical thermoset curing reaction, higher temperature then corresponds to shorter gel times according to the Arrhenius dependence of

the reaction rate. The vitrification curve is, by contrast, "S"-shaped. At temperature immediately above  $T_{g0}$ , the time to vitrification,  $t_{vit}$ , passes through a maximum as a consequence of the opposing influences of the temperature dependence of the reaction rate and the extent of conversion required to meet the criterion of  $T_g = T_{cure}$ . At higher temperatures, the time to vitrification goes through a minimum which is the result of the competing effects of the temperature dependence of the reaction rate and the decreasing concentration of reactants at vitrification as temperature of cure approaches  $T_{g\infty}$ .

#### **2.2.2.2 Experimental Methods for Construction of TTT diagrams.**

To characterize completely the curing phenomenon of thermosetting resins, several complementary thermoanalytical techniques can be used to obtain information on macroscopic as well as molecular levels.<sup>145</sup> One of the most convenient methods that determines both gel and vitrification times simultaneously, however, is dynamic mechanical analysis. Gillham and coworkers<sup>150,156-160</sup> developed the technique of Torsional Braid Analysis (TBA) based on the principle of a freely oscillating torsion pendulum to study in-situ the progress of cure. In a TBA experiment, a small sample is supported on a multifilament glass braid which becomes a part of the torsional pendulum system. The elastic and loss moduli of the composite specimen (resin plus the braid) are calculated from the damped oscillation of each wave and the changes are interpreted in terms of the properties of the supported material. The TBA technique has the distinct advantage of being able to take measurement throughout the cure process, since properties can be recorded above the load-limiting temperatures of the reactants. This ability to monitor the entire cure process is essential for the construction of a TTT diagram.

The results of a typical isothermal cure as studied by TBA is shown on Figure 2.2.19 where the relative rigidity ( $\sim 1/P^2$ , where  $P$  is the period of oscillation) and the log decrement  $\Delta$  ( $= \ln[\theta_i/\theta_{i+1}]$  where  $\theta_i$  is the amplitude of the  $i$ th oscillation of the freely damped wave) are plotted against time. The relative rigidity is related to the elastic or in-phase shear modulus  $G'$ . The log decrement  $\Delta$  is proportional to the ratio  $G''/G'$  or  $\tan\delta$  where  $G''$  is the loss or out-of-phase shear modulus and  $\delta$  is the phase angle between the cyclic stress and the cyclic strain. In general, three events can be distinguished in the  $\Delta$  vs  $t$  plot: a shoulder and two peaks. The first peak is associated with gelation and the second peak with vitrification. The pregel shoulder may be attributed to an isoviscous event that is due to the interaction of the liquid and the support.<sup>155</sup> The peaks in the  $\Delta$  curve are located approximately midway through the transitions in the relative rigidity plots. The relative rigidity ( $\sim$ modulus) increases abruptly at each transitions, first due to the transformation of liquid to rubbery state at gelation and the second from rubbery to glassy state at vitrification. The generation of the complete gelation and vitrification curves of the TTT diagram can be accomplished by conducting the above isothermal experiment at a number of temperatures ranging from  $T_{g0}$  to above  $T_{g\infty}$  to giving a set of  $t_{vit}$  and  $t_{gel}$  (or only  $t_{vit}$  or only  $t_{gel}$  depending on the location) for each  $T_{cure}$ .

The TBA technique gives an unambiguous assignment of vitrification in terms of the time (and frequency) at which a peak occurs in the mechanical damping (log decrement  $\Delta$ ) in conjunction with an increase in modulus. Attention may be drawn, however, to the identification of the first damping peak to gelation. In one of their early publications, Enns and Gillham<sup>154</sup> make a distinction between *molecular* gelation and *macroscopic* gelation. The former is the true gelation brought about according the statistical definition of Flory, dependent only on the chemical nature of the system. The latter is based on the

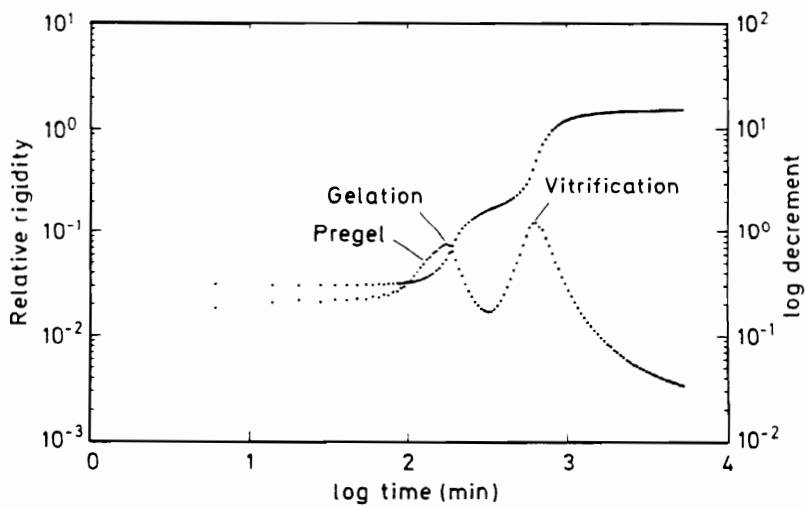


**Figure 2.2.19** A typical torsional braid analysis (TBA) spectrum during an isothermal cure showing changes in the relative rigidity and logarithmic decrement vs time. (from reference 155)

mechanically observable liquid-to-rubber transition. Enns and Gillham<sup>154</sup> assigned this viscoelastic transition to the mechanical loss peak occurring immediately prior to that for vitrification. They calculated the molecular gel point with the help of FTIR and gel fraction experiments. A Comparison between TBA liquid-to-rubber transitions and the gel points obtained through chemical means revealed an agreeable correspondence between the two. This was considered to be an adequate justification for assignment of the TBA peak to the gel point. Recently, Stutz and Mertes<sup>161</sup> have published a report that specifically addresses the validity of this assignment. With a combination of TBA, DSC and viscosity measurements, they showed that the peak in TBA always occurred slightly *before* the true gel point. From the results of this study, they explained that the TBA peak may be a consequence of the flow characteristics of the resin between the fibers during oscillation in the following manner. When the resin-impregnated glass braid is forced into oscillation, the liquid resin can reduce mechanical stresses by being able to flow between the braid fibers. The extent to which this reduction takes place is dependent on the viscosity and its increase with time as cure progresses. At a certain time close to gelation, however, a state is reached where the relaxation time for viscous flow becomes equal to half of the period of oscillation. At this point the purely viscous flow ceases and the whole oscillating composite system changes its damping characteristics. This change gives rise to the observed maximum in damping. Data on several samples suggested that the viscosity of the thermoset was similar, in the range of 6000-8000 (MPa s), at the point where the maximum in damping occurred *regardless of the cure temperature*. From these observations, Stutz and Mertes<sup>161</sup> claim that the peak in TBA measurements is really an *isoviscous* event rather than a true gel point. This finding does indeed have significance from the fundamental point of view. However, for practical purposes, one may still consider the TBA peak to be a "qualitative" gel point as suggested by Gillham since a

physical definition of the latter is also the time at which the viscosity reaches a certain arbitrary high value.

In addition to TBA, other dynamic mechanical techniques have also been utilized to study the cure behavior of thermosets. For example, Lee and Goldfarb have developed Torsion Impregnated Torsion Analysis (TICA), a method similar to TBA but with the capability of constant or multifrequencies, and reported its utility in cure studies.<sup>161b,161c,161d</sup> Hofmann and Glasser<sup>162,163</sup> have demonstrated the use of Dynamic Mechanical Thermal Analysis (DMTA) instrumentation, manufactured by Polymer Laboratories, to generate TTT characteristics of an amine cured epoxy. Zukas et al<sup>164</sup> have shown that another technique called Dynamic Spring Analysis (DSA) may also be used to detect gelation and vitrification processes along the same principles as TBA. A "viscoelasticimeter" based on a piston-and-cylinder arrangement has been able to provide comparable information to Toussaint and coworkers.<sup>165</sup> Yet another group of researchers<sup>166-170</sup> are actively pursuing the applicability of the conventional parallel plate type rheometer for cure studies (without the "benefit" of a support such as the glass braid in TBA) which includes the location of the gel point by a highly debated concept of the so-called "cross-over point"<sup>168</sup> between  $G'$  and  $G''$  during the experiment.

### **2.2.2.3 Modeling of Cure Behavior.**

Considerable progress has been made over the last few years in modeling of the thermoset cure behavior to further support the experimental understanding provided by the methods described above. Attempts have been made to predict processes such as gelation, vitrification, and advancement of  $T_g$  with respect to time and conversion during cure.



Some of the basic approaches reported in the literature are reviewed here in brief with details left to the referenced publications.

*Time to Gelation and Vitrification.* The calculation for the time to gelation is fairly straightforward if gelation is assumed to be an isoconversion state and if the kinetics of the reaction are known.<sup>154,155</sup> Disregarding the role of diffusion, the rate equation for thermoset cure may be written in the following general form:

$$dp/dt = k(T) f(p) = A \text{Exp} [ -E_A/RT ] f(p) \quad (2.2.19)$$

where  $p$  is the conversion,  $k(T)$  is the Arrhenius rate constant defined by the pre-exponential factor  $A$  and the activation energy  $E_A$ , and  $f(p)$  is a function of conversion based on the reaction mechanism. Equation 2.2.19 can be reduced to give the time for gelation,  $t_{gel}$ , as:

$$t_{gel} = k^{-1} \int_0^{p_{gel}} dp/f(p) \quad (2.2.20)$$

where  $p_{gel}$  is the conversion at gel point. Time to gelation may be obtained by performing the integration in Equation 2.2.20 with the knowledge of  $p_{gel}$ , which can be derived from theoretical relations such as those by Flory.<sup>123</sup>

Similarly, for the time to vitrification,  $t_{vit}$ :

$$t_{vit} = k^{-1} \int_0^{p_{vit}} dp/f(p) \quad (2.2.21)$$

where  $p_{vit}$  is the conversion at which vitrification occurs, i. e. at the point where  $T_g = T_{cure}$ . Here the calculation of  $p_{vit}$  requires a relation between  $T_g$  and conversion. One may use experimental data for this purpose, if available. An alternative empirical method based on the DiBenedetto Equation<sup>171,172</sup> is frequently used which helps to predict  $p_{vit}$  in terms of physical parameters. The DiBenedetto equation is expressed as:

$$(T_g - T_{g0})/T_{g0} = (E_x/E_m - F_x/F_m) p_{vit} / [ 1 - (1 - F_x/F_m) p_{vit} ] \quad (2.2.22)$$

where  $E_x/E_m$  is the ratio of lattice energies for crosslinked and uncrosslinked polymers, and  $F_x/F_m$  is the corresponding ratio of segmental mobility. In order to use Equation 2.2.22, the values of the two characteristic ratios must be determined. Adabbo and Williams<sup>173</sup> assumed  $E_x/E_m = 1$  and found that  $F_x/F_m = 0.733$  was an acceptable value for fitting  $p_{vit}$  vs  $T_g$  for several epoxy systems. Enns and Gillham<sup>154</sup> found that  $E_x/E_m$  of 0.34 and  $F_x/F_m$  of 0.19 fitted their data on the Epon 828/PACM-20 system better. Using these parameters, they went on to determine the time for vitrification by Equation 2.2.20 assuming a first order reaction mechanism. The "S"-shaped curve obtained by this model seemed to represent well the experimental data obtained from TBA measurements. Hofmann and Glasser<sup>162,163</sup> also found a good agreement between the model derived by following a similar procedure and DMTA data in an epoxy/amine system.

*Tg and Conversion vs Time Behavior and Diffusion Control During Cure.* In the modeling approach so far, the reaction kinetics have been assumed to be free of diffusion limitations. However, the effect on reaction rates of restrictions arising from the lack of mobility in the system around and beyond vitrification may be quite significant.<sup>174,175,176</sup> More recently, generalized models that incorporate these effects have been worked out. Two

examples of elaborate studies in this area are those by Matsuoka et al<sup>177</sup> and by Wisanrakkit and Gillham.<sup>178</sup>

Matsuoka et al<sup>177</sup> considered a model that include a thermodynamic parameter for the molecular mobility, which changes as the reaction proceeds. They based their approach on the similarity between the crosslinking process and physical aging of thermoplastic glassy polymers. In both cases, chain mobility decreases, with conversion in the former and with time in the latter, leading to increased relaxation times. They included the relaxation time in the rate equation by assuming that the overall rate constant  $k$  is the reciprocal of the sum of two terms as per the Rabinowich model:<sup>179</sup> (i)  $1/k_1$ , where  $k_1$  is the conventional chemical reaction constant, and (ii)  $1/k_2$ , where  $k_2$  is the diffusion rate constant. Matsuoka et al<sup>177</sup> equated  $1/k_2$  to  $\tau$ , where  $\tau$  is the conversion-dependent relaxation time. Effectively, the reaction rate constant in Equation 2.2.19 becomes a function of not only the temperature based on Arrhenius relationship, but also the conversion. In the initial stage of reaction,  $\tau$  is very small. As a result, the  $k_1$  term dominates the reaction, i. e. the reaction is chemically controlled. In the latter stages of cure near or beyond vitrification,  $\tau$  becomes significantly large and the reaction becomes diffusion controlled. To evaluate  $\tau$ , Matsuoka et al<sup>177</sup> used the formula suggested by Adam and Gibbs.<sup>180</sup> The resulting general model was able to predict conversion vs time behavior of an epoxy system isothermally cured in the entire range from the beginning to post-vitrification period.

Wisanrakkit and Gillham<sup>175</sup> also used the above concept of considering the overall reaction kinetics to be a parallel combination of the diffusion kinetics and the Arrhenius kinetics. However, they expressed the diffusion rate constant  $k_2$  according to the Williams-Landel-Ferry (WLF) approach<sup>181</sup> modified to cover both glassy as well rubbery state:

$$\log [ k_2(T) / k_2(T_g) ] = C_1 (T - T_g) / [ C_2 + | T - T_g | ] \quad (2.2.23)$$

Here,  $k_2(T_g)$  is a constant independent of the temperature and conversion which can be calculated empirically from a known set of data in the post-vitrification region where diffusion is the controlling mechanism. With the help of fairly involved numerical procedures, Wisanrakkit and Gillham have successfully demonstrated the applicability of thus combining chemical and diffusion kinetics to the thermoset cure process. Their theoretical predictions also matched well with experimental  $T_g$  vs time data obtained from DSC measurements.

#### 2.2.2.4 Summary.

The cure behavior of thermosets has been discussed with a particular emphasis to Gillham's TTT diagrams. These diagrams not only provide practical guide to find the optimum conditions to achieve specific material properties, but also give a fundamental insight into the process of cure. Dynamic mechanical techniques such as TBA can be utilized to observe the critical cure phenomena of gelation and vitrification. Finally, theoretical models, the most elaborate being those combining both chemical as well as diffusion kinetics, may be used to predict the cure behavior.

### 2.2.3 Thermal Degradation of Poly(propylene oxide).

Degradation of polymers under normal use conditions is a major factor limiting the application of these otherwise versatile materials. Therefore, understanding the mechanisms involved in degradation processes and, subsequently, developing effective methods of stabilization to prolong the useful life of polymers have become important areas of study as substantiated by the numerous books and monographs<sup>182-187</sup> published on the subject over the years. The context in which degradation behavior is alluded to in this dissertation is however slightly different. Here the degradation characteristics of the polymer in question, i. e. poly(propylene oxide), are to be utilized in a *positive* manner as a means to develop microporosity in a host matrix. Keeping this in mind, this section briefly reviews some of the basic concepts of polymer degradation with further emphasis given on the mechanisms, kinetics, and conditions related to the degradation of poly(propylene oxide)s.

#### 2.2.3.1 General.

Polymer degradation may be defined as an irreversible change in the chemical structure resulting into property deterioration in the material. The degradation processes may be classified according to the modes of initiation such as: thermal, mechanical, photochemical, radiation chemical, biological, chemical etc.<sup>186</sup> Thermal degradation, which is the focus of this review, refers to the case where the polymer at elevated temperatures starts to undergo chemical changes without the simultaneous involvement of another compound. Often it is rather difficult to distinguish between thermal and thermo-chemical degradation because polymeric materials are seldom chemically "pure".

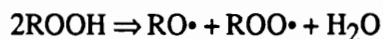
Impurities and additives present in the material as well as the environment in which the material is may take part in the degradation mechanism. Thus, the definition of thermal degradation is in general broadened to include the role of these external agents as well. Accordingly, two distinct types of thermal degradation processes may be identified. Pyrolysis is the term used for polymer degradation occurring in complete absence of any external reactant. Thermo-oxidative degradation, on the other hand, as the name suggests, takes advantage of oxidation reactions to give rise to degradation. In a typical situation, however, thermal degradation usually results from the combined effect of pyrolysis and thermal oxidation.

*Pyrolysis.* When a polymer is exposed to high temperatures, energy is absorbed and distributed through the molecules. Eventually, a point is reached at which the energy concentrated at one bond in the molecule exceeds its dissociation energy. When this occurs, the bond ruptures and, unless it can reform, an irreversible change takes place. Therefore, pyrolytic degradation is thought to be closely related to the dissociation energy of the molecular bonds. Polymers pyrolyze by one or more of three general mechanisms.<sup>187</sup> Random scission occurs through breakage of bonds along the backbone chain. As the term implies, this is a statistical event, and polymer molecules are first broken into large macroradicals. There is a rapid decrease in the molecular weight and almost no monomer is formed in the early stages. This mechanism is predominant in pyrolysis of polyolefins. Depolymerization is the second general mechanism of pyrolysis. This is usually initiated at the chain ends. Monomer units are split off sequentially, and the reaction proceeds until the molecule is depolymerized completely. Polymers such as polyacetals and poly(methyl methacrylate) pyrolyze by depolymerization. A third general mechanism is characterized by the elimination of a low molecular weight fragments other

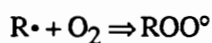
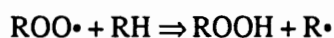
than monomer such as a side chain group, an example being elimination of hydrogen chloride from poly(vinyl chloride). The molecular chain is not cleaved, but there is a significant decrease in molecular weight as volatile products are given off.

*Thermo-oxidative Degradation.* Combined action of heat and oxygen comprises one of most frequently encountered modes of degradation. Therefore, a number of studies have been directed towards thermal oxidation of polymers. Emphasis has been placed on autoxidation, which is a thermal oxidation under mild conditions up to about 200 °C. Based on studies on model compounds for rubber, Shelton<sup>188</sup> has proposed the following kinetic scheme for autoxidation of hydrocarbon polymers:

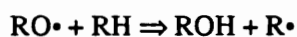
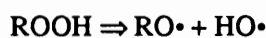
Initiation:



Propagation:



Oxidative Chain Branching:



Initiation of polymer autoxidation is quite complex. Hydroperoxides are generally assumed to be the primary source of radicals that are required to initiate the oxidation, but various additives including stabilizers may also be involved. Propagation is a chain reaction in which a single initiation event could lead to further reaction in a multitude of other

molecules. Chain reactions of propagation and oxidative chain branching are responsible for rapid degradation that takes place during autoxidation.

The chemical structure of the polymer is an important parameter in thermal oxidation. For example, linear polyethylene, branched polyethylene, and polypropylene each display measurably different degradation behaviors. The dissociation energy of the bond between a hydrogen atom attached to a tertiary carbon at a branch point is lower than that between hydrogen and carbon in the main chain methylenes. These labile hydrogens are more susceptible to become points of thermo-oxidative initiation. Thus, branched polyethylene is less stable than linear polyethylene, and polypropylene, with a methyl branch at every other carbon along its backbone, is less stable than either of the polyethylenes.<sup>187</sup> In general whenever branched groups are present, the polymer may be expected to have poorer resistance to oxidative degradation. Polystyrene is an exception to this conclusion: its superior thermo-oxidative stability is thought to result either from steric protection of the labile hydrogen by the bulky aromatic rings<sup>189</sup> or from the loss of resonance energy caused by unfavorable orientation of phenyl group in the structure.<sup>190</sup> In addition to structural factors, morphology also plays a role in degradation. For example, semicrystalline materials show higher resistance to oxidative degradation since the oxygen molecule can not easily penetrate into the crystallites. This is evident in linear polyethylene where the rates above and below melting point are significantly different.<sup>187</sup> In some cases the crystallites may be permeable to oxygen, as with poly(4-methylpentene-1) where the oxidation pattern for amorphous and crystalline forms are essentially the same.<sup>191</sup>

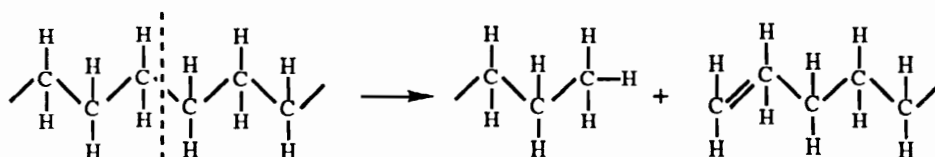


### 2.2.3.2 Pyrolytic Degradation of Poly(propylene oxide).

Incorporation of oxygen in the backbone of an aliphatic chain should cause a lowering of the thermal stability as C-O bonds are less stable than C-C bonds. Based on this, Madorsky and Straus<sup>192</sup> undertook an investigation of degradation behaviors of poly(ethylene oxide) and poly(propylene oxide), both isotactic and atactic, for comparison with those of polymethylene, polyethylene, and polypropylene. Pyrolysis was conducted in a vacuum chamber to eliminate thermo-oxidative contribution to degradation. The volatile fractions from pyrolysis were collected by a cold trap and analyzed by mass spectrometer. Among the polymers studied, poly(propylene oxide)s were the least stable, whereas polymethylene was the most stable. Of the two poly(propylene oxide)s, the atactic form volatilized faster than the isotactic variety which was thought to be due to the lower molecular weight and the possibility of more chain branching in the former. The possibility of crystallinity playing a role in the isotactic poly(propylene oxide) was ignored, perhaps due to the fact that the temperatures utilized were well beyond its melting temperature (70-80 °C). The major components of the volatiles in poly(propylene oxide)s were propylene oxide, acetaldehyde, propene, and acetone with the last three being the most abundant.

In their analysis, Madorsky and Straus<sup>192</sup> recognized the possibility of two types of scission processes that governed the nature and relative amounts of the various pyrolytic products: (a) type I scission in which an intermolecular transfer of hydrogen takes place, resulting in one end becoming saturated and the other unsaturated; and (b) type II scission in which an intermolecular transfer of hydrogen does not take place, giving rise to free radical ends which subsequently break up into monomer or monomer size fragments by unzipping reaction. The two mechanisms are illustrated in Figure 2.2.20. Whether type I

## TYPE I



## TYPE II

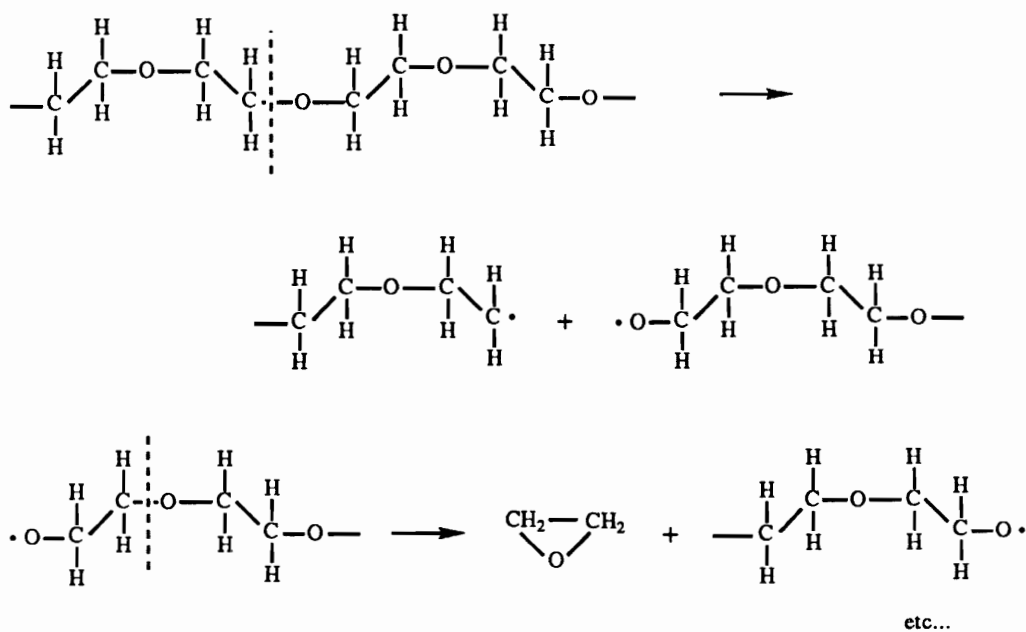


**Figure 2.2.20** Mechanisms for thermal degradation by pyrolysis. The type I and II are illustrated by taking the examples of polyethylene and poly(ethylene oxide) respectively. (from reference 192)

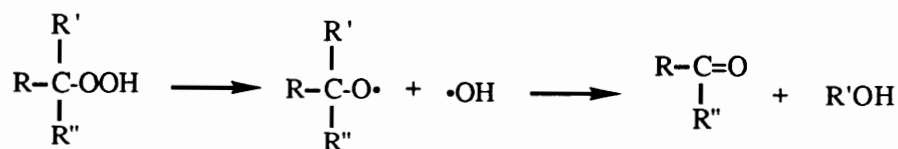
or type II scission will take place depends on the supply of hydrogen in the immediate vicinity of the ruptured bond. For example, only type I takes place in polyethylene. In case of Poly(propylene oxide) in which the supply of hydrogen is somewhat limited, both type of scission may be expected to occur. This was evident from the fact that the yield of monomer and monomer size fragments was greater in case of poly(propylene oxide) than that in polypropylene.

Vo Van et al<sup>193</sup> studied the kinetics of thermal decomposition of poly(propylene oxide) in nitrogen atmosphere with the help of dynamic scanning calorimetry (DSC) and thermogravimetric analysis (TGA). DSC yielded a zeroth order kinetics while the data obtained from TGA were suitable for a first order kinetics. According to the DSC study the activation energy of thermal degradation increased with the molecular weight of the polymer. However, dynamic thermogravimetric scans showed insignificant variation in thermal degradation behavior of different molecular weights. The activation energy of degradation from TGA ranged between 8 and 25 kcal/mol depending on the rate of heating. The discrepancies in the results were explained by the argument that DSC provided activation energy applicable to chain ruptures as well as volatile product evaporation, whereas TGA furnished activation energy only for the second step.

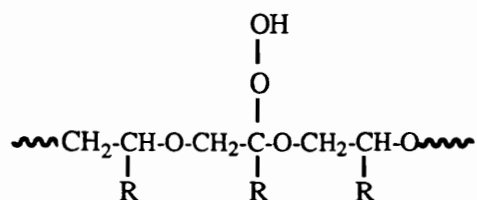
### **2.2.3.3 Thermooxidative Degradation of Poly(propylene oxide).**

A study of the thermal oxidation of poly(propylene oxide), poly(butene-1-oxide), and poly(styrene oxide) has been reported by Dulog and Storck.<sup>194</sup> The polymers were autoxidized in bulk and volatile reaction products were identified by gas chromatography. The major degradation products from poly(propylene oxide) oxidized at 110 °C were

methanol, acetone, isopropanol, and acetic acid. The investigators postulated a thermo-oxidative mechanism based in part on the analogous decomposition of alkyl peroxides:



Dulog and Strock<sup>194</sup> proposed the initial formation of an ether hydroperoxides as :



which can then decompose in a number of different ways to give the above listed reaction products.

A slightly different reaction products were reported by Yoo<sup>57</sup> from an analysis by mass spectrum of the volatile fragments of poly(propylene oxide) exposed to air at 185 °C as shown in Figure 2.2.21. In this investigation, the composition of the degradation products was found similar to that obtained under pyrolytic conditions by Madorsky and Straus<sup>192</sup>: major fractions were acetaldehyde, acetone, propene, and propylene oxide. From this it may be hypothesized that at a relatively higher temperature, significant extent of pyrolysis could also be occurring simultaneously with the oxidative reactions. The kinetics of thermo-oxidative degradation of poly(propylene oxide) were reported by Kilic and McGrath.<sup>195</sup> Both isothermal and dynamic thermograms were obtained by TGA and analyzed by Arrhenius type relationships. A zeroth order of reaction was found to fit the

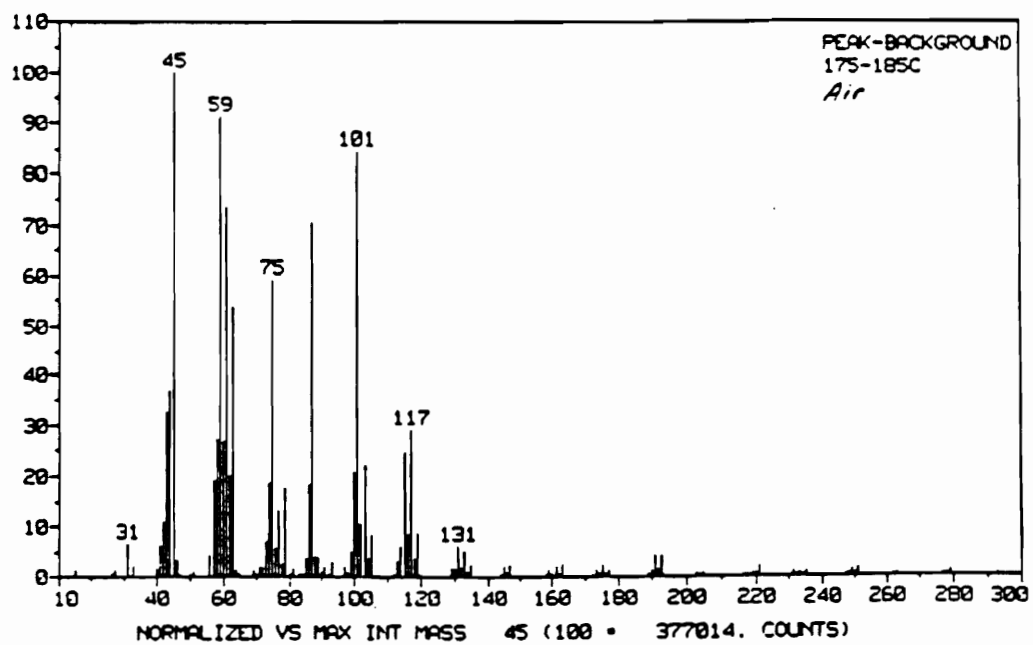


**Figure 2.2.21** Mass spectrum of volatile fragments of commercial poly(propylene oxide) exposed to air at ~185 °C. (from reference 57)

data. The activation energies for decomposition calculated from isothermal experiments were found to be lower than those from dynamic experiments (17.8-19.5 kcal/mol in the former vs 24.0-28.5 kcal/mol in the latter).

#### **2.3.3.4 Effect of End-group on Poly(propylene oxide) Degradation.**

The thermal degradation of poly(propylene oxide) in the studies discussed so far has been seen to depend on variables such as tacticity, molecular weights, environment, heating rates etc. However, all of these studies were carried out on commercial polymers mostly having hydroxyl end-group functionality. The only reported systematic study that has addressed the question of effect of the end-group chemistry on thermal stability of poly(propylene oxide) was performed by Yoo, Kilic, and McGrath.<sup>56,57,196</sup> They prepared a series of well-characterized poly(propylene oxide)s containing a variety of end-groups via coordination polymerization using aluminum porphyrin catalyst and by modifying commercially available hydroxyl terminated polymers. Table 2.2.1 summarizes the results of their study in the form of the initial degradation temperature over 3-8% weight loss region. Quite clear from the figures on Table 2.2.1 is that by changing the nature of the end-group, one may have the degradation temperature to span more than 200 °C.

Some of the other specific findings were as follows. Hydroxyl terminated poly(propylene oxide) prepared by the porphyrin chemistry was considerably more stable than its commercial counterpart. This was thought to be due to the fact that the anionic route of polymerization used commercially inherently generates 3.0-3.5 milliequivalents of unsaturated end-groups<sup>197</sup> which may provide additional source for radical generation. This was consistent with the lower stability of poly(propylene oxide)s prepared deliberately

**Table 2.2.1** Effect of various end-group functionalities on thermal stability of poly(propylene oxide). (from reference 57)

POLYMER	MOLECULAR WEIGHT	DEGRADATION * TEMPERATURE, °C
$\text{H}-\text{O}-\underset{\text{CH}_3}{\text{CH}}-\text{CH}_2-\text{O}-\text{O}-\text{CH}_2-\text{CH}(\text{CH}_3)-\text{O}-\text{H}$	1000	190-210
(COMMERCIAL PPG)	2000	190-210
$\text{H}-\text{O}-\underset{\text{CH}_3}{\text{CH}}-\text{CH}_2-\text{O}-\text{O}-\text{CH}_2-\text{CH}(\text{CH}_3)-\text{O}-\text{CH}_2-\text{CH}(\text{CH}_3)-\text{O}-\text{H}$	700	160-180
$\text{HOC}-\text{C}_6\text{H}_4-\text{C}(=\text{O})-\text{O}-\underset{\text{CH}_3}{\text{CH}}-\text{CH}_2-\text{O}-\text{O}-\text{CH}_2-\text{CH}(\text{CH}_3)-\text{O}-\text{H}$	800	170-200
$\text{CH}_2=\text{C}(\text{CH}_3)-\text{C}(=\text{O})-\text{O}-\underset{\text{CH}_3}{\text{CH}}-\text{CH}_2-\text{O}-\text{O}-\text{CH}_2-\text{CH}(\text{CH}_3)-\text{O}-\text{H}$	5000	180-200
$\text{HOC}-\text{C}_6\text{H}_4-\text{C}(=\text{O})-\text{O}-\underset{\text{CH}_3}{\text{CH}}-\text{CH}_2-\text{O}-\text{O}-\text{CH}_2-\text{CH}(\text{CH}_3)-\text{O}-\text{C}_6\text{H}_4-\text{C}(=\text{O})-\text{OH}$	2300	170-190
$\text{O}_2\text{N}-\text{C}_6\text{H}_4-\text{C}(=\text{O})-\text{O}-\underset{\text{CH}_3}{\text{CH}}-\text{CH}_2-\text{O}-\text{O}-\text{CH}_2-\text{CH}(\text{CH}_3)-\text{O}-\text{C}_6\text{H}_4-\text{NO}_2$	2400	270-290
$\text{HO}-(\text{PO})_n-\text{C}_6\text{H}_4-\text{C}(\text{CH}_3)_2-\text{C}_6\text{H}_4-(\text{PO})_n-\text{OH}$	1000	250-270
	2000	220-240
$\text{HO}-(\text{PO})_n-\text{C}_6\text{H}_4-(\text{PO})_n-\text{OH}$	1000	250-270
$\text{H}_2\text{N}-\text{C}_6\text{H}_4-\text{O}-\underset{\text{CH}_3}{\text{CH}}-\text{CH}_2-\text{O}-\text{O}-\text{CH}_2-\text{CH}(\text{CH}_3)-\text{O}-\text{C}_6\text{H}_4-\text{NH}_2$	2000	350-365
$\text{O}_2\text{N}-\text{C}_6\text{H}_4-\text{O}-\underset{\text{CH}_3}{\text{CH}}-\text{CH}_2-\text{O}-\text{O}-\text{CH}_2-\text{CH}(\text{CH}_3)-\text{O}-\text{C}_6\text{H}_4-\text{NO}_2$	2000	350-365
$\text{H}_2\text{N}-\text{C}_6\text{H}_4-\text{C}(=\text{O})-\text{O}-\underset{\text{CH}_3}{\text{CH}}-\text{CH}_2-\text{O}-\text{O}-\text{CH}_2-\text{CH}(\text{CH}_3)-\text{O}-\text{C}_6\text{H}_4-\text{NH}_2$	2300	225-245
PHYSICAL BLEND OF COMMERCIAL PPG AND BISPHENOL A (15 WT. %)	2000	260-280
PHYSICAL BLEND OF COMMERCIAL PPG AND ANTIOXIDANT (IRGANOX 1 WT. %)	2000	230-250
PHYSICAL BLEND OF COMMERCIAL PPG AND ANTIOXIDANT (IRGANOX 5 WT. %)	2000	265-275

\* DEGRADATION TEMPERATURES OF EACH OLIGOMER HAVE BEEN MEASURED IN THE 3-8% WEIGHT LOSS REGION DURING THE DYNAMIC TGA SCANS(10°C/MIN).

with unsaturated end-groups such as allyl and acrylate. Lower degradation temperatures by about 20-30 °C were observed in these polymers. An another means of improving the thermal stability was demonstrated by introduction of an aromatic nitro end-group. Remarkable increase in in the temperature of degradation was evident, up to ~150 °C, over the commercial hydroxyl terminated polymer. This stabilization effect may be due to the radical trapping capability of the nitro group. The nitroxide radical may inhibit the propagation of decomposition by eliminating alkyl radicals in the initial stage, thereby reducing the tendency for thermal degradation. Significant improvements were also found by use of phenolic hydroxyl and aromatic amine groups.

#### **2.2.3.5 Summary.**

Due to the presence of C-O bonds in the backbone, the thermal stability of poly(propylene oxide) is considerably lower than analogous hydrocarbon polymers. On degradation, the polymer is converted into low molecular weight volatile products. The factors such as tacticity, molecular weights, heating rate, and more importantly, the end-group functionality have been observed to influence the degradation behavior. By carefully selecting the end-group, the temperature for onset of thermo-oxidative degradation may be controlled to vary between 160-370 °C. These characteristics of poly(propylene oxide) make it a good candidate for use as an agent for microporosity development.



## 2.3 EXPERIMENTAL

### 2.3.1 Materials.

#### 2.3.1.1 Thermoset System.

The thermoset system consisted of an epoxy resin, a curing agent, and a catalyst, when necessary. The following sections describe the details of the individual components utilized.

##### 2.3.1.1.1 *Epoxy Resins.*

The epoxy resins used in this study were principally based on novolac chemistry. They were obtained from Dow Chemicals, Midland, Michigan, as their products Quatrex-2010<sup>®</sup>, and Quatrex-2710<sup>®</sup>. These oligomers are electronic grade multifunctional epoxy novolac resins with structures and other details as shown in Table 2.3.1. The essential difference between the two resin grades is their average molecular weights, and accordingly, the average number of epoxide groups per chain and the functionality.

##### 2.3.1.1.2 *Curing Agents.*

Three different curing agents, were utilized in this thesis. Methyl-5-norbornene-2,3-dicarboxylic anhydride, more commonly known as nadic methyl anhydride (NMA), was used in the major portion of the study. It was obtained from Buffalo Color Corporation, Parsippany, New Jersey, and had a specified purity of 99%+ (less than 1% free acid). It

**Table 2.3.1** Epoxy Resins.

<p style="text-align: center;"><b>Epoxy Novolac Resin</b></p>					
<b>Designation<sup>†</sup></b>	<b>&lt;n&gt;<sup>§</sup></b>	<b>f<sup>¥</sup></b>	<b>EEW<sup>¶</sup></b>	<b>&lt;M<sub>n</sub>&gt;<sup>‡</sup></b>	<b>Physical Character</b>
Quatrex-2010	1.6	3.6	178.4	570	highly viscous liquid
Quatrex-2710	4.5	6.5	190.8	1040	solid, softning point: 78-95 °C

<sup>†</sup> registered trade mark of Dow Chemicals Company

<sup>§</sup> specified by manufacturer

<sup>¥</sup> f = average number of epoxide groups per chain = <n> + 2

<sup>¶</sup> epoxy equivalent weight measured by titration procedure suggested by Jay<sup>201</sup>

<sup>‡</sup> gm/mol, calculated from <n>

was used without further purification. The other two curing agents were a bisphenol- 4,4' sulfonyldiphenol (also known as Bis-S), and an amine- 4,4' Diaminodiphenyl Sulfone (DDS). Each were received from Aldrich Chemicals in 98%+ purity and were used as such. Table 2.3.2 summarizes further particulars of the curing agents.

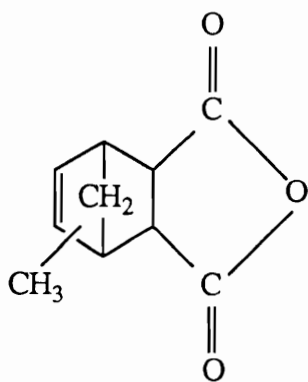
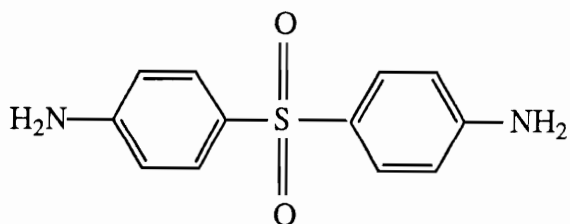
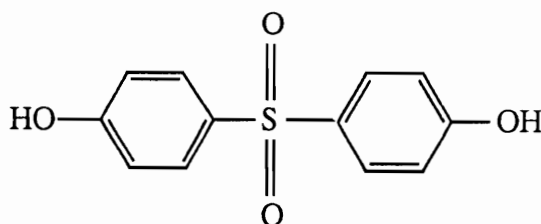
#### **2.3.1.1.3 Catalysts.**

The anhydride cured epoxy required the use of a tertiary amine catalyst. This was purchased from Aldrich Chemicals as 2,4,6 Tris(dimethyl aminomethyl)phenol. It is commercially known as DMP-30, and was supplied in a purity of 96%+. Tetramethylammonium hydroxide (TMAH) was used as the catalyst for Bis-S cured epoxy. This was obtained from Aldrich Chemicals in the form of a 25% solution in methanol. Both catalysts were used as received. The details are given on Table 2.3.3.

#### **2.3.2.2 Poly(propylene oxide)s.**

A series of commercially available poly(propylene oxide)s (PPO)s with three different molecular weights were used as modifiers. These were obtained from Union Carbide Corporation, Danbury, Connecticut under the trade name NIAX<sup>®</sup> polyols PPG-425, PPG-1025, PPG-2025. The specified number average molecular weights of the three polymers are  $5 \times 10^2$ ,  $1 \times 10^3$ ,  $2 \times 10^3$  gm/mol respectively.

Niax<sup>®</sup> polyols have hydroxyl functionality as their end groups. For comparison, chemical modification was carried out on PPG-1025 to replace the hydroxyl end groups with an

**Table 2.3.2** Curing Agents.**Nadic Methyl Anhydride (NMA)****4, 4' Diaminodiphenyl sulfone (DDS)****4,4' Sulfonyldiphenol (Bis-S)**

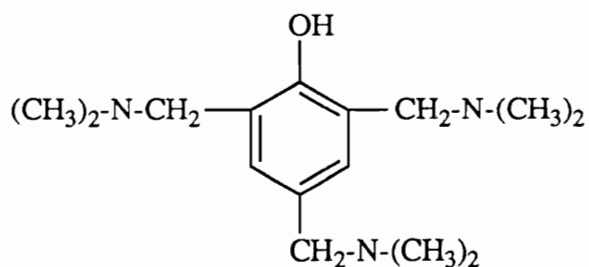
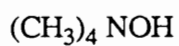
Curing Agent	f/g <sup>¶</sup>	Formula Weight	Physical Character
NMA	2/2=1.00	178.2	low viscosity yellowish liquid
DDS	1/4=0.25	248.3	crystalline solid, melting.point: 176 °C
Bis-S	1/2=0.50	250.3	crystalline solid, melting point: 246 °C

¶ f = number of reactive sites per epoxide group in relation to the curing agent;

g = number of reactive sites per molecule of the curing agent;

f/g gives the ratio of mole equivalent of epoxy to mole of curing agent for stoichiometric reaction

Table 2.3.3 Catalysts.

**2,4,6-Tris(dimethylaminomethyl)phenol (DMP-30)****Tetramethylammonium hydroxide (TMAH)**

<b>Catalyst</b>	<b>Physical Character</b>
DMP-30	low viscosity yellowish liquid
TMAH	25% by weight solution in methanol

ester moiety. This is redesignated as PPG-1025E. The procedure for preparation has been given in the Appendix 2.I.

More information on these oligomers can be found on Table 2.3.4.

#### **2.3.2.4 Miscellaneous.**

The following miscellaneous materials were used at different instances in the research:

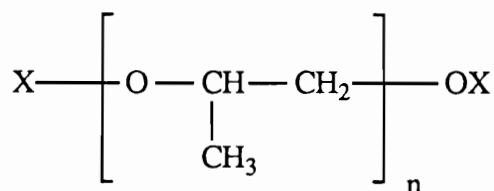
- *Solvents*- Methyl ethyl ketone (MEK), xylene, ethyl amyl ketone (EAK), tetrahydrofuran (THF), and hexane purchased from various sources
- *Flow Agent*- PA-57<sup>®</sup> purchased from Dow Chemicals used at IBM, San Jose
- *Lubricant*- a fluorocarbon based polymeric liquid used at IBM for disk lubrication

### **2.3.2 Methods.**

#### **2.3.2.1 Sample Preparation.**

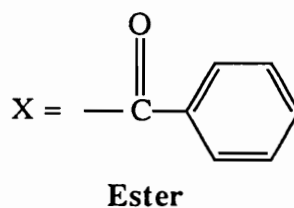
##### **2.3.2.1.1 Morphological Studies.**

For the study of morphological behavior, "bulk" films of ca. 1 mm thickness were prepared by curing about 2 gm mass of the reaction mixture in covered aluminium dishes in a gravity or convection oven set at the desired temperature. The procedure for preparing

**Table 2.3.4** Poly(propylene oxide)s.

**Poly(propylene oxide)**

X = H  
Hydroxyl



Designation	$\langle M_n \rangle^{\S}$	End-group	Physical Character
PPG-425 <sup>†</sup>	$5 \times 10^2$	hydroxyl	viscous liquid
PPG-1025 <sup>†</sup>	$1 \times 10^3$	hydroxyl	viscous liquid
PPG-2025 <sup>†</sup>	$2 \times 10^3$	hydroxyl	viscous liquid
PPG-1025E	$1 \times 10^3$	ester	viscous liquid

<sup>§</sup> manufacturer specification

<sup>†</sup> registered trademark of Union Carbide Corporation

the reaction mixtures varied according to the curing agents used taking in account the differences in their physical character.

*NMA cured systems.* The epoxy and NMA in stoichiometric ratio were mixed thoroughly at 60 °C. In absence of a catalyst, the epoxy-anhydride reaction is extremely sluggish even at temperature as high as 200 °C.<sup>202</sup> After cooling this mixture to room temperature, an appropriate quantity of PPO was added and mixed in. The catalyst, DMP-30, was added last to minimize any premature reaction that may take place before curing at the proper temperature.

*DDS and Bis-S cured systems.* In the case of Bis-S and DDS cured systems, reaction mixtures required the use of a solvent to facilitate proper mixing without having to use high temperatures. The epoxy and the curing agent (in stoichiometric ratio), the catalyst TMAH in case of Bis-S (none for DDS), and an appropriate amount of PPO were dissolved in an equal amount by weight of MEK. The solutions were then weighed into aluminium dishes and kept in a hood overnight to allow a partial removal of the solvent. Finally, they were transferred to a vacuum oven set at ~40°C for approximately 2 hours to remove the remaining MEK from the mixtures, leaving about 2 gm of the reaction mixture for further curing. Again, it was assumed that the amount of reaction occurring under these conditions so far is negligible and does not contribute to the final morphological properties of the samples when they are subsequently cured at higher temperatures.



### **2.3.2.1.2 Cure Studies.**

*Reaction Mixtures.* For cure studies, about 10 gm of the reaction mixtures were prepared according to the procedure described above, and frozen immediately to  $-40\text{ }^{\circ}\text{C}$  in small quantities in sealed glass vials. The samples were then thawed to room temperature only minutes before being used for analysis. This provided both consistency and convenience in the experiments.

*DMA Samples.* A suitable method to perform dynamic mechanical analysis on thermosetting polymers systems undergoing cure utilized wire-mesh as a support to hold the reaction mixture (which is initially in the liquid state) at the temperature of cure<sup>203</sup>. In this study, ribbons of an 84x84 stainless steel mesh (wire diameter of 0.0035"), measuring approximately 12x30 mm were coated with the epoxy mixture of interest. The excess amount was wiped off with a glass rod to provide an uniformly coated mesh. The ends of the ribbon were covered with aluminium foil, to avoid contact between the reaction mixture and the DMA clamps.

### **2.3.2.1.3 Degradation and Microporosity Studies.**

The degradation behavior and the microporosity development studies in cured systems were performed on films of varying thicknesses prepared in different forms including the bulk films described above.

*Wire-mesh Coatings.* A stainless steel mesh similar to the one used in cure studies was used as a support to obtain impregnated films of approximately 0.125 mm thickness. This

was done by coating a rectangular sheet of the wire-mesh with the reaction mixture, prepared in the manner described above, and placing it in the oven vertically in a clamp. Excess material collected at the bottom of the sheet, leaving an uniformly coated area at the top which was used subsequently for analysis.

*Magnetic Disk Coatings.* Films on highly polished and precleaned 10.5" aluminium disks were prepared by spin-casting from solutions of the epoxy systems in a 50/50 mixture of xylene and EAK. The solutions were filtered through disposable 0.5  $\mu\text{m}$  Nucleopore<sup>®</sup> filters before using for spin-coating. A small percentage of the flow agent PA-57, was necessary to add to the solution to ensure an uniform coating. After the spin coating the disks were transferred to a forced convection oven and taken through the desired time/temperature schedule. The complete procedure was carried out in a clean room to eliminate undesirable contamination by air-borne particles. The resulting films were uniform with thicknesses assumed to be in the sub-micron range as judged by the interference pattern on the disks. More details regarding the formulations, spin coating and curing condition are summarized on Table 2.3.5.

### **2.3.2.2 Analysis.**

#### ***2.3.2.2.1 Scanning Electron Microscopy.***

A Philips EM420 STEM or a Hitachi S-800 SEM operating at 20 kV were used to probe the morphological features. The bulk films were fractured at room temperature to reveal their cross sections. In case of wire mesh samples, the use of liquid nitrogen temperature and a pair of scissors was found helpful to obtain a good fracture surface. The thin

**Table 2.3.5** Spin-coating formulations and conditions for preparation of magnetic disk coatings.

<b>Disk</b>	<b># 1</b>	<b># 2</b>	<b># 3</b>	<b># 4</b>
Quatrex-2010 + NMA, part	100	100	100	100
DMP-30, parts	2	2	2	2
PPG-1025, parts	0	10	0	25
Solvent, parts	100	100	100	100
PA-57, parts	0.1	0.1	0.1	0.1
Spin speed, rpm	4000	4000	4000	4000
Cure Schedule, pre-cure	----- 60 °C/12 hrs -----		----- RT/7 days -----	
post-cure	----- 150 °C/3 hrs -----			
Heat Treatment	----- 200 °C/12 hrs -----			

coatings on aluminium disks were analyzed simply at their air surface. Square pieces of approximately 1"x1" were cut from the disks for this purpose. All samples were sputter-coated with gold or gold-palladium to make them conductive before analysis.

#### **2.3.2.2.2 *Dynamic Mechanical Analysis.***

A DuPont 982 Dynamic Mechanical Analyzer in the resonant frequency mode with horizontal clamps was used for this study. The DMA was controlled via the DuPont 9900 Thermal Analyzer. The spacing between the passive and the active arms was fixed at 6.5 mm. An 0.1 mm oscillation amplitude was used in all runs. A nitrogen purge rate of 2 liter/min was used during data collection.

For wire-mesh samples that were cured externally, ribbons were cut with dimensions of 12x30 mm and dynamic runs at 5 °C/min were performed in the range of -150 °C to 250 °C.

For cure behavior study, the ribbons coated with the reaction mixture prepared in the manner described above were inserted between the horizontal clamps as shown on Figure 2.3.1. Each run consisted of three steps as schematically displayed on Figure 2.3.2. The first step was of an isothermal cure at a desired temperature that was continued until the sample reached vitrification point as suggested by leveling of the signals. The second step of a 5 °C/min dynamic scan completed the residual cure remaining from the first step. Finally, the last 5 °C/min scan provided the dynamic mechanical behavior of fully cure system.

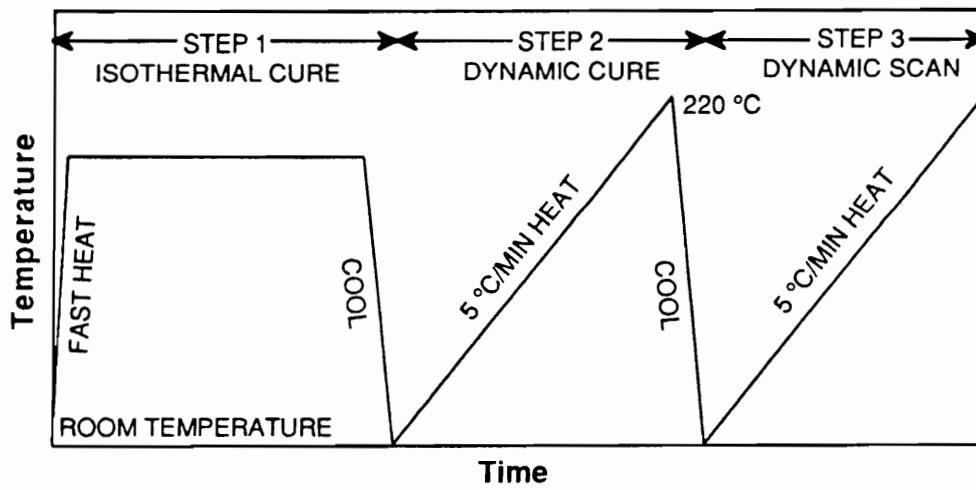


**Figure 2.3.1** The Dupont 982 DMA horizontal clamp assembly with a wire mesh sample for cure studies.

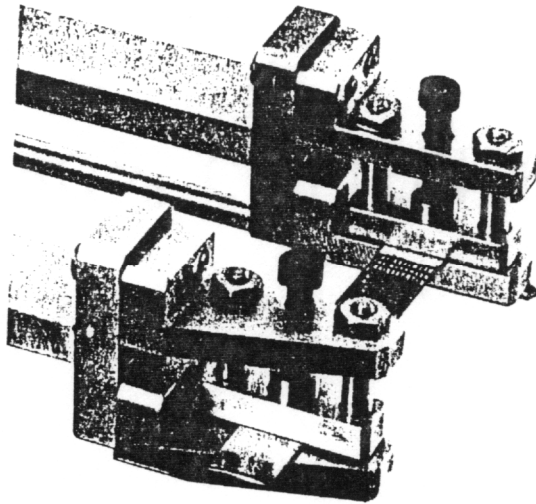


**Figure 2.3.2** A three step DMA method used to study *in situ* the cure behavior of epoxy systems.

#### **2.3.2.2.3 *Thermogravimetric Analysis.***

Measurements were performed on Perkin Elmer TGS-2 TGA which was programmed with a System-4 microprocessor controller or with an Omnitherm 35053 Three Module Controller/Data System. Air and nitrogen purge rates were monitored at ~100 cc/min. At least five minutes of initial purge at the beginning of each run was allowed to ascertain that the atmosphere in the system was replaced with the required gas before the heating began.

#### **2.3.2.2.4 *Lubricant Retention.***

A proprietary fluorocarbon-based lubricating medium was applied to the disks coatings by a standard IBM procedure. The quantitation of lubricant retention was achieved by extracting the lubricant remaining on the coating after the application procedure with the help of freon and then weighing the extract after evaporation of the solvent. The results are given as mg of lubricant extracted per side of the disk.

## 2.4 RESULTS AND DISCUSSION

### 2.4.1 Morphology Behavior.

#### 2.4.1.1 System Variables.

Before discussing the morphological behavior of the PPO modified epoxy system at hand, it is appropriate to review the system variables that are likely to influence the phase separation process, both through the thermodynamics as well as kinetics.

Starting with thermodynamics, a generalized form of the Flory-Huggins Gibbs free energy equation for a thermosetting polymer (component 1) at a certain point during cure with a average degree of polymerization  $\langle DP_n \rangle$  in presence of a modifier (component 2) can be written as (the derivation is presented in Appendix 2.II):

$$\Delta G_m^V = RT \left[ (1-\phi_2) \ln(1-\phi_2) / (\langle DP_n \rangle V_{1,0}) + (\phi_2 / V_{2,0}) \ln \phi_2 + \chi_{12,0} \phi_2 (1-\phi_2) / V_{1,0} \right] \quad (2.4.1)$$

The above equation can be utilized to identify the variables that affect the thermodynamics of the system. The first and the most obvious variable is the composition which influences the free energy change through the term  $\phi_2$ , the volume fraction of the modifier. Molecular weights of the two components contribute to the entropic terms via the molar volumes,  $V_{1,0}$ , and  $V_{2,0}$ . On the other hand, the interactions between the thermoset and the modifier become important in the enthalpic term due to its effect on the chi parameter,  $\chi_{12,0}$ . The



temperature of cure also plays a role in the phase separation thermodynamics through its relationship with the chi parameter.

Some of the above variables may simultaneously affect the kinetics of the system as well. For example, the molecular weights, temperature, and the composition associatively determine the viscosities and diffusion properties in the system which figure prominently in phase separation kinetics as demonstrated by Williams' theoretical treatment<sup>122</sup> discussed in Section 2.2.1.3. In addition, the nature of cure chemistry will govern the extent of reaction at gelation which can cause a drastic reduction, if not complete halting, of subsequent phase separation. Lastly, the rate of thermoset polymerization will play a dominant role in determining the importance of kinetics in relation to thermodynamics in the phase separation process.

From the above arguments, the following variables are qualitatively expected to influence the phase separation process, hence, lending themselves to be good candidates for morphology control in the study of PPO modified epoxy novolacs:

- Curing chemistry
- End groups of PPO
- Composition
- Temperature of cure
- Molecular weight of PPO
- Catalyst Concentration

In the following discussion the effect on morphology by each of the above variables is presented. The basis for comparison of morphology is two-fold. First is the question of *compatibility*, as defined in Chapter I, i. e. whether the system forms a stable, two-phase morphology without gross phase separation. If so, then a qualitative analysis of the sizes and concentration of the phases through SEM photomicrographs will provide a further evaluation of the morphological behavior under different conditions. No attempt is made for quantitative assessment in terms of size distributions or volume fractions, mainly due to the lack of reliability, in author's opinion at least, in such calculations from photomicrographs of fracture surfaces.

#### **2.4.1.2 Effect of Cure Chemistry.**

The reaction between epoxide and anhydride in presence of a basic catalyst, such as DMP-30 used here, primarily gives rise to esterification. With the anhydride in equimolar ratio, or in excess, the literature suggests that the possibility of forming ether linkages by way of epoxy homopolymerization is not likely.<sup>203-208</sup> Fisher<sup>205</sup> proposed the following mechanism for catalytic copolymerization of epoxide and anhydride. The base opens the anhydride ring, forming a carboxylate ion, which in turn reacts with an epoxide ring yielding an alkoxide. The alkoxide anion then reacts with another anhydride to form an ester. In addition, the alkoxide anion can also displace the amine on the activated anhydride to give an ester. Continuation of these alternating steps would yield a polyester network as depicted in Figure 2.4.1. No doubt that the temperature, catalyst type and concentrations are also of importance.

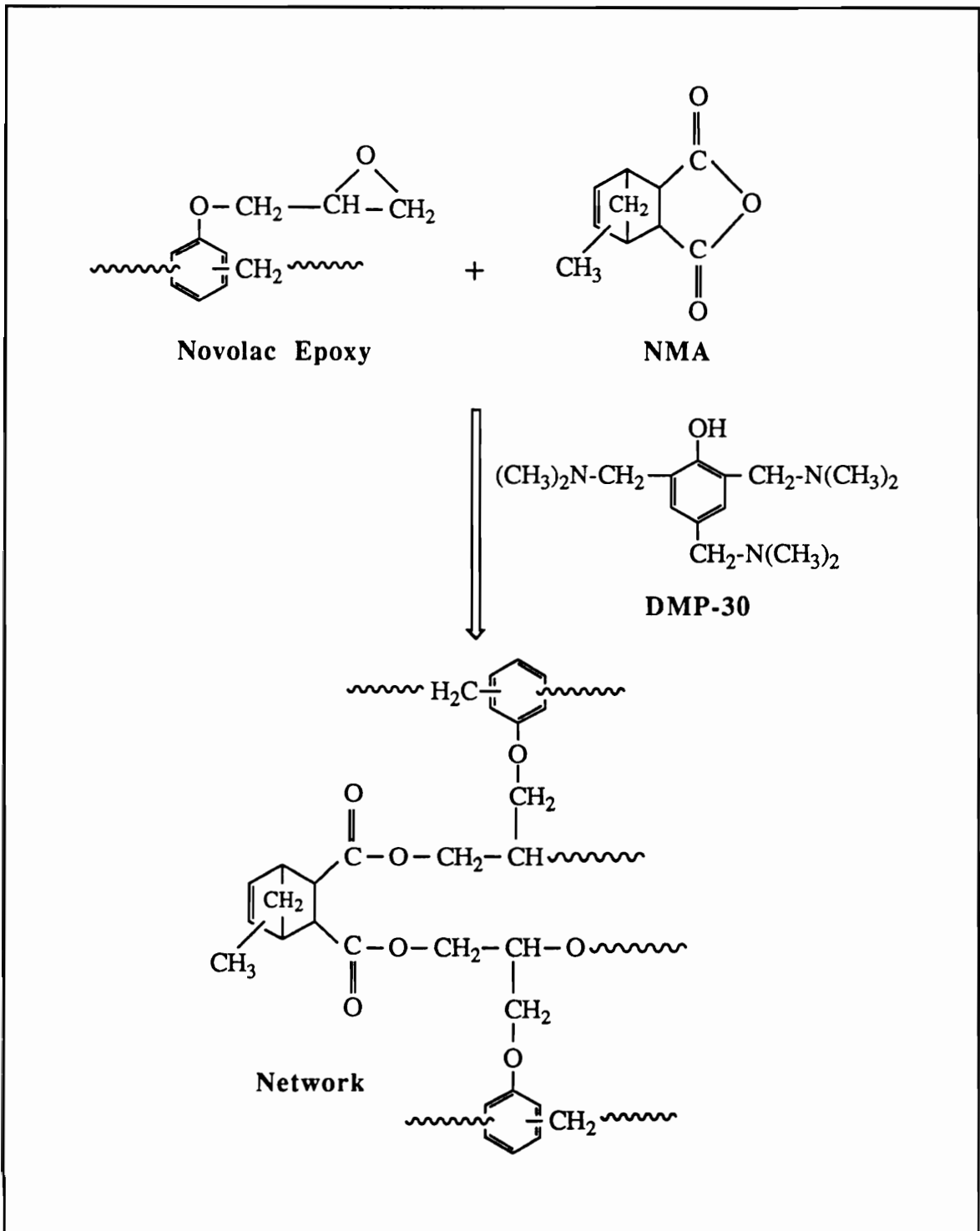


**Figure 2.4.1** Reaction scheme for base catalyzed novolac epoxy - anhydride cure.

The reaction scheme for Bis-S cured epoxy is shown on Figure 2.4.2. Two steps are possible in the case of the overall reaction between base-catalyzed phenolic hydroxyl and epoxide- that of hydroxyl with epoxide and that of resulting aliphatic hydroxyl with epoxide. Shechter and Wynstra,<sup>203</sup> based on their study on reaction between phenol and phenyl glycidyl ether, have shown that in a base catalyzed equimolar reactions between phenolic hydroxyl and epoxide essentially consists of the first step, to the exclusion of any alcohol-epoxide reaction.

The chemistry of cure using less reactive aromatic primary amines such as 4, 4' DDS as the curing agent comprises first the reaction of the primary amine with the epoxide group to form a secondary hydroxyl group and a secondary amine. The secondary amine can then react with an another epoxide to give one more secondary hydroxyl group and a tertiary amine group. Again, the possibility of the reaction between the secondary hydroxyl and epoxide leading to polyetherification has been found to be negligible,<sup>209,210</sup> and the resulting structure may be thought to contain the residue of the diamine acting as a central molecule with four branches representative of the epoxy monomer as depicted in Figure 2.4.3.

A comparison of the three curing agents with regards to their effect on the morphological behavior of PPO modified systems is given on Figure 2.4.4 which displays the SEM photomicrographs of Quatrex-2010 epoxy containing 5% by weight PPG-1025 cured by (a) NMA, (b) Bis-S, and (c) DDS. The cure conditions were 150 °C for 2 hours, and the catalyst concentrations used were 2% by weight of DMP-30 and 1% by weight of TMAH in the NMA and Bis-S cured systems respectively. As seen, the morphology obtained in the NMA cured system was single-phase; no domain structure was visible even at

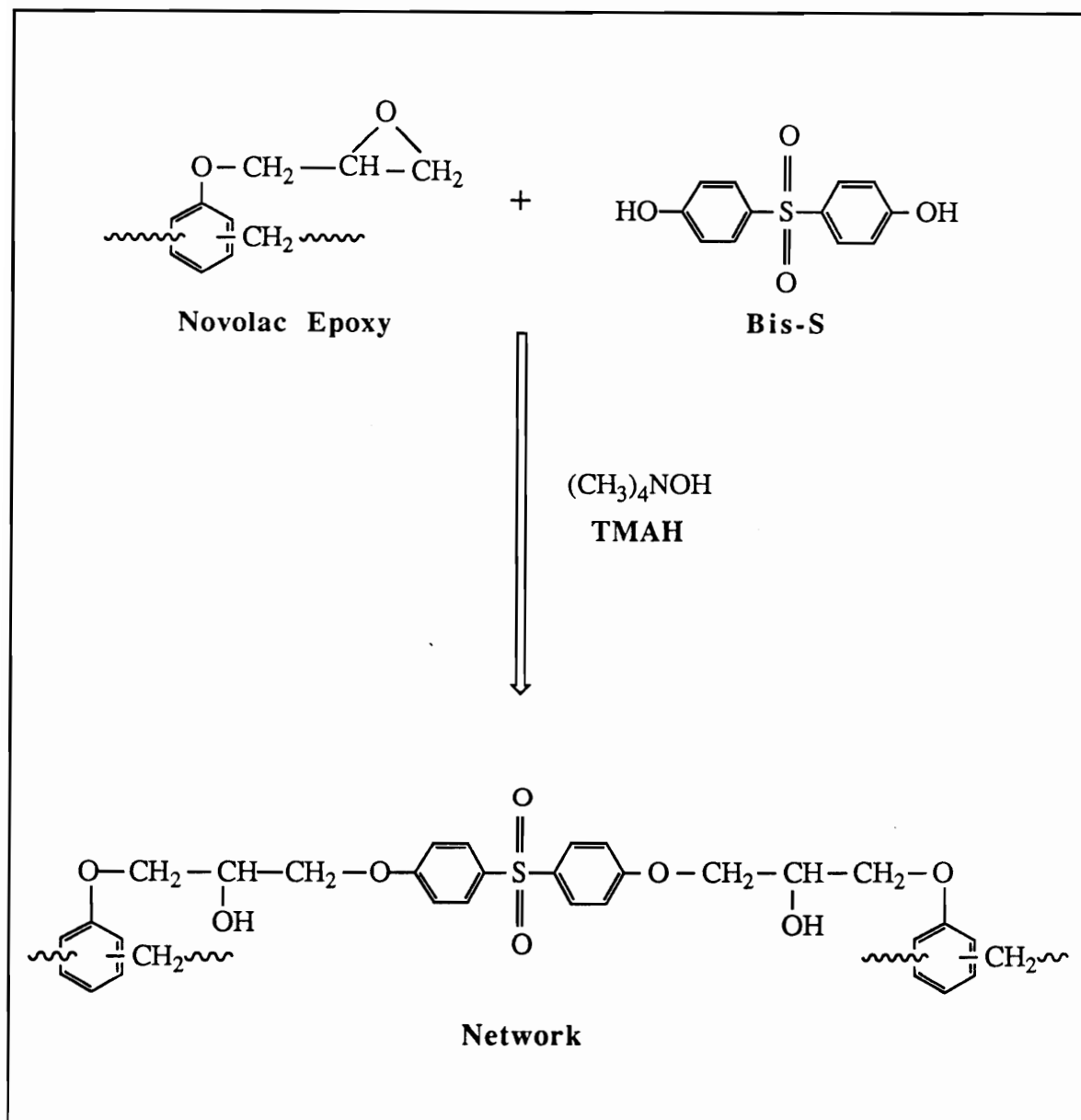


Figure 2.4.2 Reaction scheme for base catalyzed novolac epoxy - Bis-S cure.

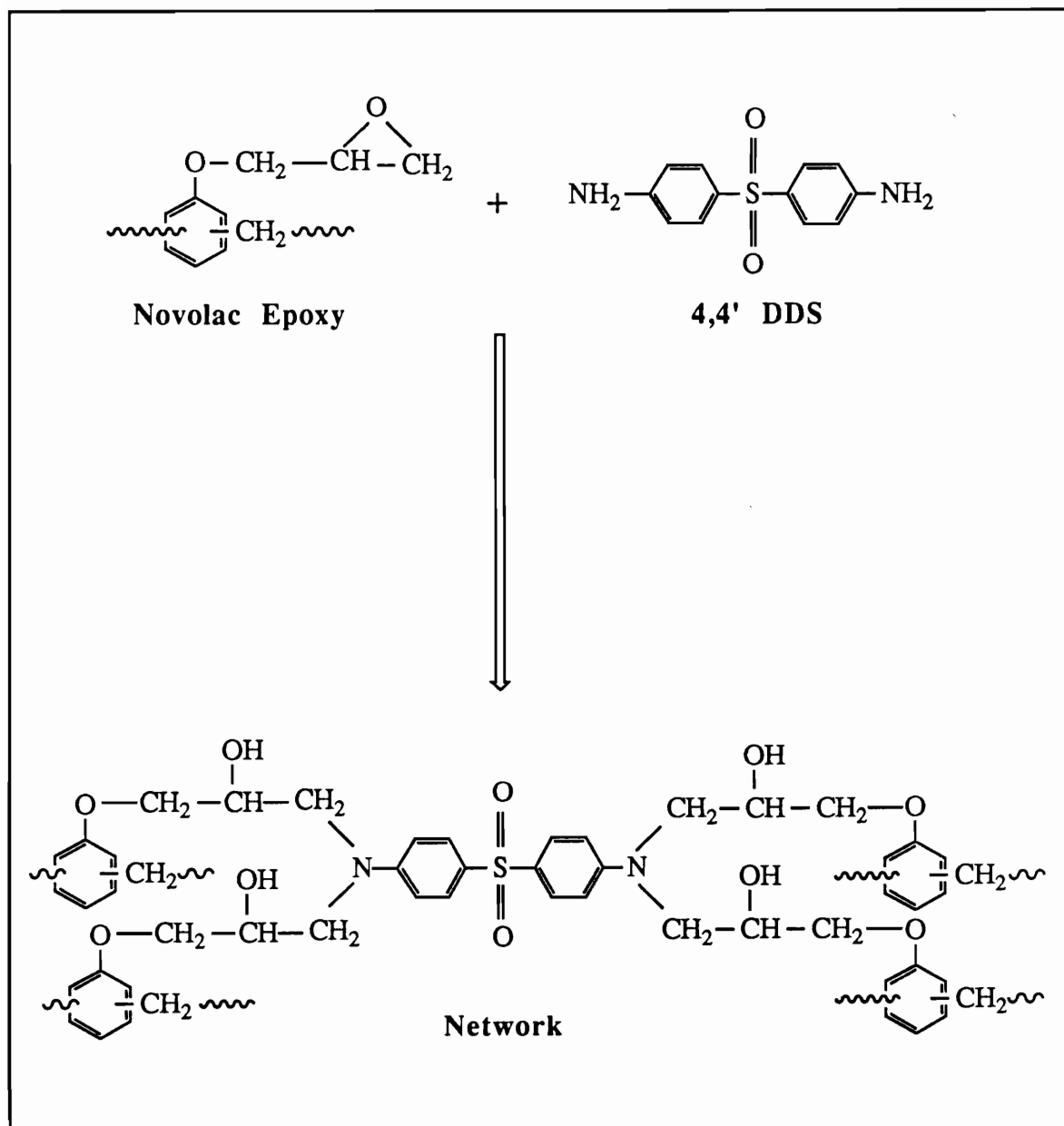
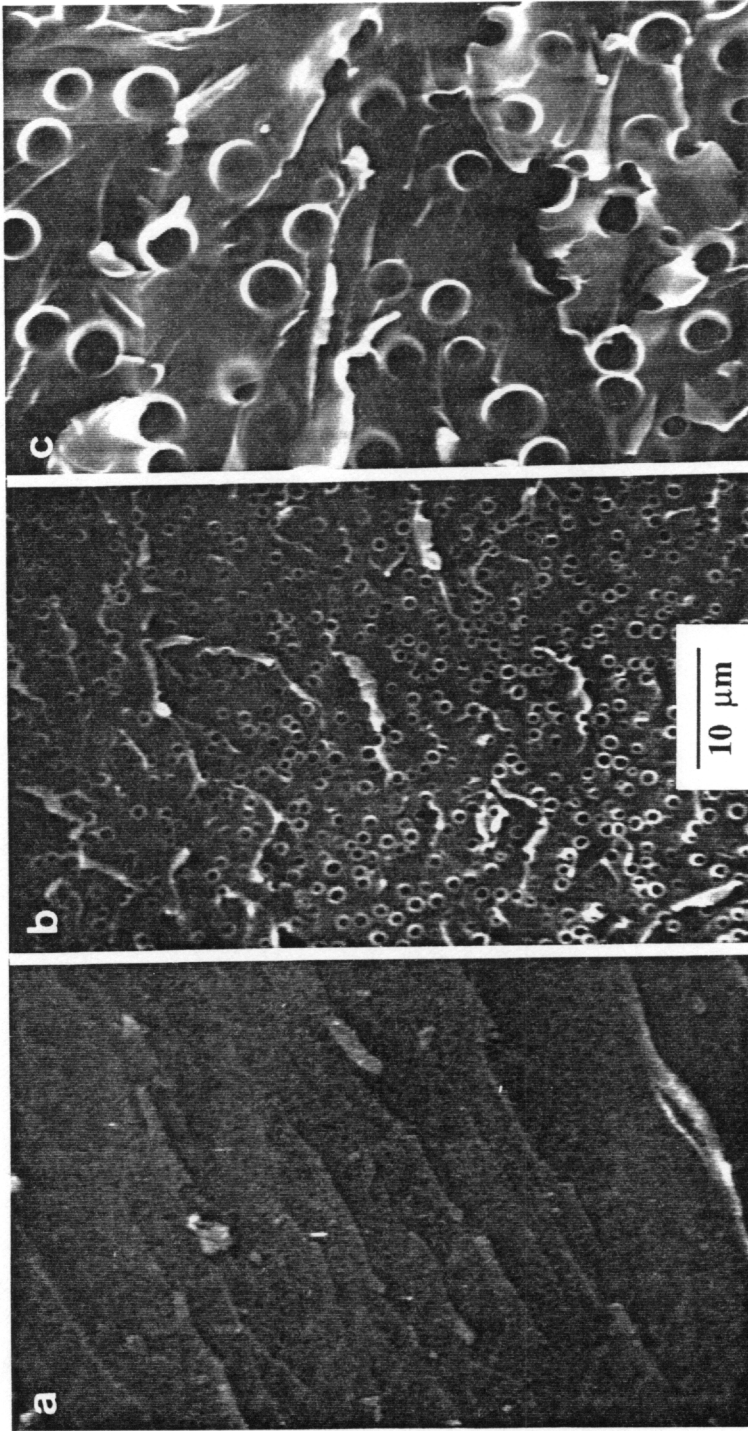


Figure 2.4.3 Reaction scheme for novolac epoxy - amine cure.



**Figure 2.4.4** SEM photomicrographs showing the effect of curing agent on morphology of 5% by weight PPG-1025 modified Quatrex-2010 cured at 150 °C for 2 hours. The curing agents are (a) NMA with 2% DMP-30 as catalyst, (b) Bis-S with 1% TMAH as catalyst, and (c) DDS.

magnifications as high as 100,000X. On the other hand, in the case of Bis-S and DDS cured systems, a two-phase morphology is evident on the photomicrographs with discrete, well defined PPO domains of sizes in the range of 1-1.5  $\mu\text{m}$  and 4-6  $\mu\text{m}$  respectively.

None of the above 5% PPG-1025 containing samples displayed gross phase separation, i. e. they were compatible. At higher PPG-1025 contents, however, Bis-S and DDS cured systems exhibited incompatibility, typically witnessed as a layer of viscous PPO at the surface of the cured sample. A summary of compatibility-incompatibility properties of several compositions for each curing agents are given on Table 2.4.1. In case of Bis-S, compositions above 10% PPG-1025 were incompatible, whereas the same was true in the case of DDS at compositions above 5% PPG-1025. In comparison, at the same cure temperature of 150 °C, the anhydride cured systems showed compatibility with PPG-1025 contents as high as 30%. Although a single set of conditions (cure temperature, PPO molecular weight, etc.) have been used so far, these preliminary results clearly suggest the greater practical viability of the NMA cured systems relative to the Bis-S and DDS cured systems.

Note that the 5% PPG-1025 sample cured with NMA is termed as *compatible*, although it qualifies for being labeled as *miscible* by virtue of its one-phase morphology as per the definition of Chapter I. This is more appropriate because the one-phase state here, even with molecular level mixing of PPO within the epoxy matrix, is not in thermodynamic equilibrium. The homogeneously dispersed PPO chains are frozen in the crosslinked epoxy network, being unable to phase separate due to diffusion limitations. In this respect, a further distinction may be made between miscibility and compatibility in addition to those



**Table 2.4.1** Comparison of compatibility-incompatibility properties of cured PPO modified epoxy systems<sup>‡</sup> using various curing agents.

Weight % PPO	Curing Agent		
	NMA <sup>¶</sup>	Bis-S <sup>†</sup>	DDS
5	C	C	C
10	C	C	I
15	C	I	I
20	C	I	I
25	C	I	I

C = Compatible; I = Incompatible

<sup>‡</sup> Epoxy resin = Quatrex-2010; PPO = PPG-1025;

Cure conditions = 150 °C for 2 hours

<sup>¶</sup> DMP-30 as catalyst, 2% of the total weight of resin and curing agent

<sup>†</sup> TMAH as catalyst, 1% of the total weight of resin and curing agent

based on single phase and single  $T_g$ , that the former is an equilibrium condition whereas the latter is a non-equilibrium state forced on the system by kinetic means.

The scenario in which the above mentioned gross phase separation or incompatibility occurs may be visualized as follows. In the beginning the system is miscible, with its location in the one-phase region of the  $p$ - $\phi$  diagram as illustrated in the Figure 2.4.5. As the cure progresses, at a certain conversion,  $p_b$ , the thermodynamic conditions for phase separation are satisfied or the cure path meets the binodal. At this point, the system enters the metastable state and phase separation commences via nucleation and growth mechanism (unless the reaction rate is extremely fast and the cure path bypasses the metastable region and reaches the spinodal curve). Once the phases start growing, they will have a tendency to migrate to the surface due to the density difference, PPO being lighter than epoxy ( $\rho_{PPO} = \sim 1.0 \text{ g/cc}$  vs  $\rho_{\text{epoxy}} = \sim 1.2 \text{ g/cc}$ ). An additional impetus for gross phase separation comes from the fact that, indeed, the lowest free energy state is the one in which there are two separate layers of PPO-rich and epoxy-rich phases, thus eliminating the interfacial energy costs involved in creating discrete domains. Williams et al<sup>144</sup> alluded to the gross phase separation as a consequence of a high degree of phase coalescence, a description that may not be too different from the one given here if coalescence is considered to be a step in the overall process of phase migration. The occurrence of phase coalescence, however, is not a sufficient condition for gross phase separation, the latter being dependent on a number of other considerations as well.

First consideration is the mobility in the system. Lower mobility will impose restrictions on diffusion of the phases through the matrix and, therefore, on their migration towards the surface. The mobility, quantitatively described by the diffusion coefficient, in the system is

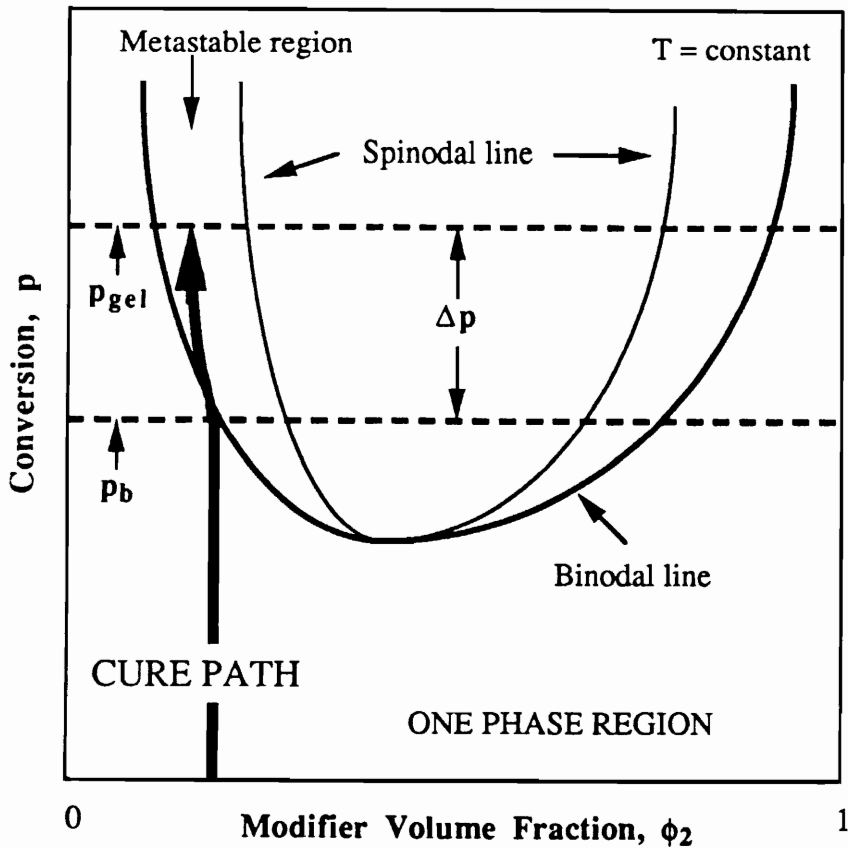


**Figure 2.4.5**  $p$ - $\phi$  diagram of a modified thermoset undergoing cure illustrating the characteristic conversion span  $\Delta p$  in which phase separation takes place.  $p_{gel}$  is the conversion at gelation, and  $p_b$  is the conversion for onset of phase separation corresponding to the modifier composition  $\phi_{2,0}$  of the initial reaction mixture. The cure path traces the composition of the continuous phase.

inversely dependent on the viscosity as shown by such relations as the Stokes-Einstein equation. Now the viscosity at a given temperature in a thermosetting polymer is a function of the conversion. As shown on Figure 2.4.6, the viscosity increases slowly as cure progresses until the system nears gelation at which time it rises rapidly towards infinity. Analogously, the mobility in the system decreases slowly before it falls abruptly towards zero as gelation occurs. Based on this, a characteristic conversion difference  $\Delta p$  may be defined as suggested by Williams *et al.*<sup>144</sup>

$$\Delta p = p_{gel} - p_b \quad (2.4.2)$$

Referring to both Figures 2.4.5 and 2.4.6, the parameter  $\Delta p$  may be looked upon as the span of thermoset conversion in the metastable region in which mobility necessary for phase migration exists. The wider this span, which can occur due to a low  $p_b$  or a high  $p_{gel}$  or both, the more favorable it is for the migration of the phases to the surface, and hence, for incompatibility. The second consideration is the time the system spends in the metastable region which is a complementary condition for the mobility. Here, the rate of reaction will determine whether sufficient time is available for migration of the phases. Finally, the tendency for gross phase separation will also be influenced, perhaps in the most effective way, by the presence of some form of chemical interactions between the separating phase and the matrix. These interactions provide an anchoring mechanism by which the phases are restricted within the matrix, thereby stabilizing them against migration.

By influencing one or more of the above factors, a curing agent may play a significant role in determining the overall compatibility-incompatibility character of a particular thermoset-

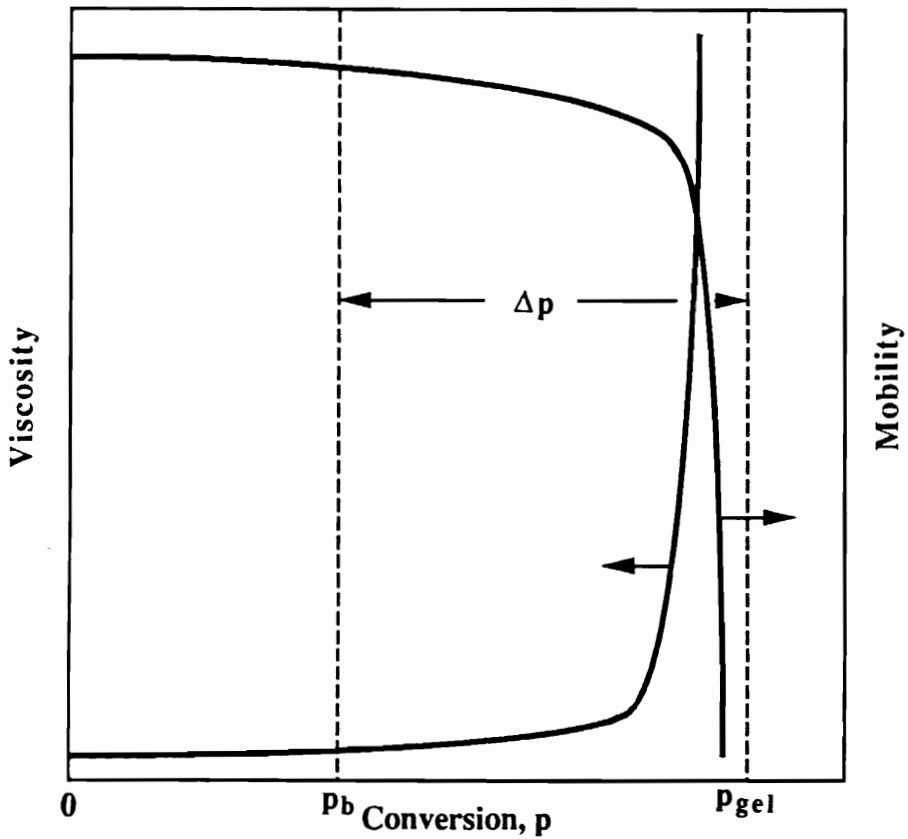


**Figure 2.4.6** Schematic representation of the changes in the viscosity and mobility as a function of conversion in a modified thermoset undergoing cure.  $p_b$  is the conversion for onset of phase separation,  $p_{gel}$  is the conversion at gel point, and  $\Delta p$  is the distance between the two.

modifier system. First, each curing agent will have different contributions to the enthalpic interactions between the thermoset and the modifier. Keeping all other variables constant, this amounts to changing the value of the interaction parameter  $\chi_{12,0}$  in Equation 2.4.1. The lowering of the interaction parameter results into a shifting of the binodal on Figure 2.4.5 towards higher conversions and vice versa. Therefore, for any given composition, the binodal conversion,  $p_b$ , will be a function of whether the presence of the curing agent increases or decreases the interactions between the resin and the modifier. Exact determination of the chi parameter between the thermoset system and the modifier involves elaborate cloud point experiments and the accompanying calculations<sup>126,127,144</sup> which have not been attempted here. An approximation can be made instead by comparing the solubility parameters of the three thermoset systems, each composed of the epoxy resin and one of the curing agents, with respect to the solubility parameter of PPO which is cited<sup>211</sup> to be  $7.2 \text{ (cal/cc)}^{1/2}$ . The solubility parameters of the particular thermoset systems were not available in the literature. Hence, an exercise was carried out to calculate the same by using the concept of group contributions.<sup>211-213</sup> Appendix 2.III provides the details of these calculations. The results summarized on Table 2.4.2(a) indicate that the solubility parameter of the NMA cured epoxy system is closest to that of PPO.

Secondly, due to different functionalities involved in the cure reactions, the conversion at gel point,  $p_{gel}$ , will be different for the three systems. Appendix 2.IV presents the calculations for prediction of  $p_{gel}$ 's for Quatrex-2010 cured with NMA, Bis-S, and DDS respectively using the relations provided by Flory<sup>123</sup> and their extensions by Tanaka and Kakiuchi.<sup>214</sup> The results are listed on Table 2.4.2(b). Here the system containing DDS has the lowest  $p_{gel}$  followed closely by that cured with NMA and finally by the Bis-S cured system.

**Table 2.4.2** Comparison of various curing agents based on their physico-chemical properties that affect the process of phase separation in PPO modified epoxy systems.

(a) Solubility Parameters<sup>§</sup>

System	$\delta$ , (cal/cc) <sup>1/2</sup>
Quatrex-2010/NMA	9.1
Quatrex-2010/Bis-S	11.2
Quatrex-2010/DDS	12.4
PPO	6.9

(b) Conversion at Gelation<sup>¶</sup>

System	P <sub>gel</sub>
Quatrex-2010/NMA	0.38
Quatrex-2010/Bis-S	0.58
Quatrex-2010/DDS	0.33

§ see Appendix 2.III

¶ see Appendix 2.IV

Table 2.4.2 continued..

**(c) Coreactivity with hydroxyl terminated PPO**

<b>System</b>	<b>Yes/No</b>
Quatrex-2010/NMA	Yes
Quatrex-2010/Bis-S	No
Quatrex-2010/DDS	No



In addition to the solubility and functionality characters, the reactivity of the curing agent may also affect the tendency for gross phase separation. Curing agents that offer faster reactions under similar conditions may be expected to promote compatibility. Due to the lack of kinetic data, a comparison of the three curing agent based on reactivity will not be made here. However, it might suffice to emphasize that the rate of reaction is indeed an important component for morphology control as will be shown later under the effect of catalyst concentration in NMA cured systems.

Finally, a further important contribution by the curing agent to the overall compatibility between the resin and the modifier may be made via chemical interactions. From the reaction schemes presented on Figures 2.4.1 through 2.4.3, it may be deduced that while Bis-S and DDS curing chemistries offer no reactivity with the hydroxyl terminated PPO, the anhydride cure does. As shown on Figure 2.4.7, the PPO hydroxyl functionality can react with an anhydride to form a carboxylic acid group, which in turn can react with an available epoxide. Figure 2.4.8 shows FTIR spectra of a mixture of PPG-1025, NMA and DMP-30 before and after 2 hours at 100 °C. A diminished hydroxyl peak at 3480 cm<sup>-1</sup>, and appearance of two new peaks- a broad one in the region of 2900-3250 cm<sup>-1</sup> for carboxylic acid hydroxyl stretching and a sharp one at 1740 cm<sup>-1</sup> for the ester carbonyl absorbance, clearly corroborate the possibility of the first step in the co-reaction of PPO in the anhydride cured system. Although, the extent of this co-reaction may not be significant, on a molar basis, in comparison to the competing main reaction of epoxy and anhydride, its influence can be envisaged in two ways. First, due to chemical interactions during the early stage of cure, PPO will tend to remain in solution a little longer until thermodynamic conditions stipulate the onset of phase separation. In effect, this may be seen as a decrease in the interaction parameter  $\chi_{12,0}$  and consequently, an increase in the

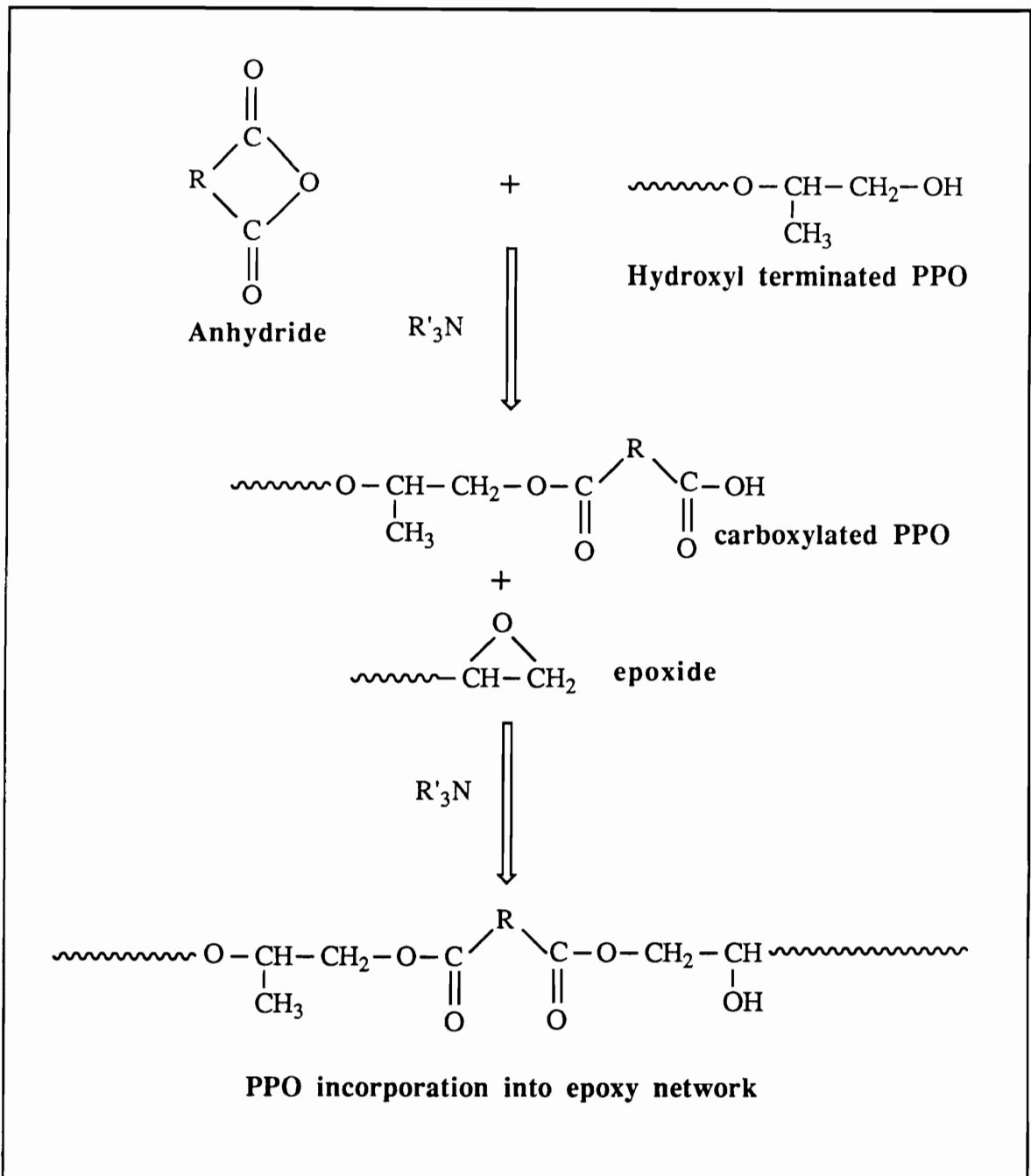


**Figure 2.4.7** Proposed mechanism for co-reaction of hydroxyl terminated PPO during a base catalyzed anhydride-epoxy cure.

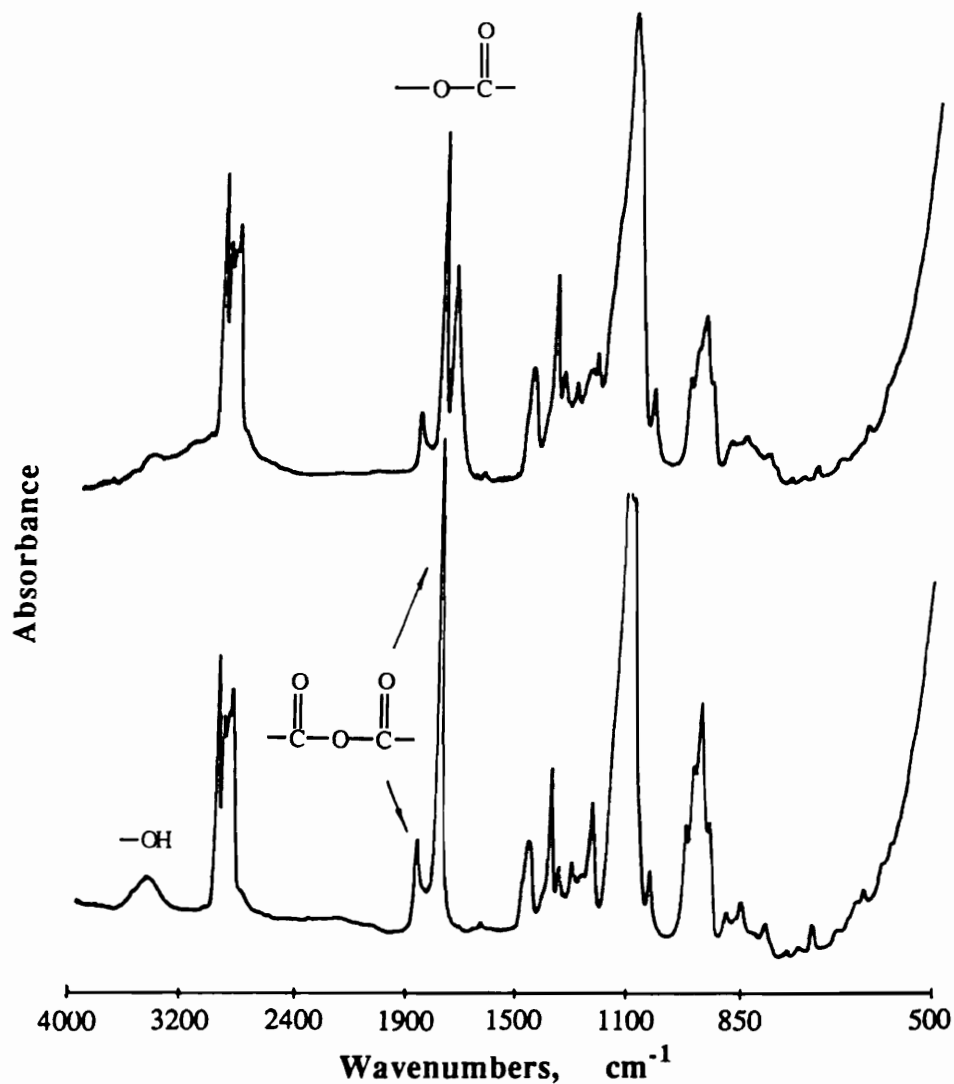


**Figure 2.4.8** FTIR spectra of a mixture of PPG-1025, NMA and DMP-30 before (bottom) and after (top) reaction at 100 °C for 2 hours. The amount of NMA was in 10% excess based on the hydroxyl content of PPG-1025, and the amount of DMP-30 was chosen as 1% by weight of the total amount of PPG-1025 and NMA.

critical conversion,  $p_b$ . Additionally, once the phase separation has begun, the groups can still react at the interface of the growing phase, thus stabilizing it against its migration towards the surface that may otherwise give rise to macroscopic phase separation. Of course, an added advantage of these interfacial interactions will be in providing the necessary energy transfer mechanism for toughening applications.

From the above analysis, it is evident that the attributes typifying a curing agent, e. g. solubility, functionality, reactivity, and co-reactivity, influence various aspects of the phase separation process which in turn collectively determine the overall compatibility-incompatibility character of a given system. Based on a qualitative analysis it would be difficult to predict just which one of these attributes, if any, dominates the final behavior. Nevertheless, a general observation can be made that under similar conditions, the NMA cured system seems to promise the greatest compatibility among the three systems under study, the two of its most favorable properties being the possibility of co-reaction and a better-matched solubility parameter with PPO.

The discussion so far has been focussed on how the compatibility of a modified thermosetting system can be influenced merely by use of different curing agents. However, it might be realized that the same parameters that affect the compatibility also control the tendency towards phase separation itself. For example, the assumption that  $p_{gel}$  provides the upper limit for phase *migration* may be extended to phase *growth* as well. Although, some controversy exists in literature regarding the efficacy of gelation to completely arrest phase separation, this presupposition may not be too far off, at least for the purpose of qualitative comparisons. This means that a small  $\Delta p$  which reduces the possibility of incompatibility will also be responsible for minimizing the tendency of the

system to phase separate. Similarly, fast curing reactions and chemical interactions between PPO and epoxy will also act to reduce the extent of phase separation. Since a two-phase structure is a prerequisite for the usefulness of the PPO modified epoxies with regards to the subsequent microporosity development, an optimization of various conditions must be performed to give a *maximum* amount of phase separation *without* gross phase separation. Along this reasoning, it is clear that the 5% PPG-1025 modified epoxy/NMA system of Figure 2.4.4(a), in spite of being compatible, needs to be worked on further with the help of the other system variables so that it attains a two-phase morphology. Similarly, it should be possible that a greater range of compatibility can be induced in Bis-S and DDS cured systems also by choosing proper conditions. Hopefully, this will be demonstrated during the course of the present work.

#### 2.4.1.3 Effect of PPO End-group.

In the last section, it was postulated that PPG-1025 may take part in the anhydride-epoxy reaction via its hydroxyl end-group functionality. To what extent it influences the overall phase separation process in terms of compatibility and domain size and concentration can be investigated by comparing PPG-1025 modified system with that containing PPG-1025E. The latter was obtained by replacing the hydroxyl groups of the former via their reaction with benzoyl chloride by the procedure outlined in Appendix 2.I. Figure 2.4.9 shows the FTIR spectra of PPG-1025 before and after this conversion. The disappearance of the peak due to hydroxyl end-group in the region of  $3480\text{ cm}^{-1}$  and emergence of a peak at  $1721\text{ cm}^{-1}$  from ester carbonyl absorbance indicate a nearly complete replacement of the hydroxyl functionality by aromatic ester in PPG-1025E. The ester moiety is unable to take

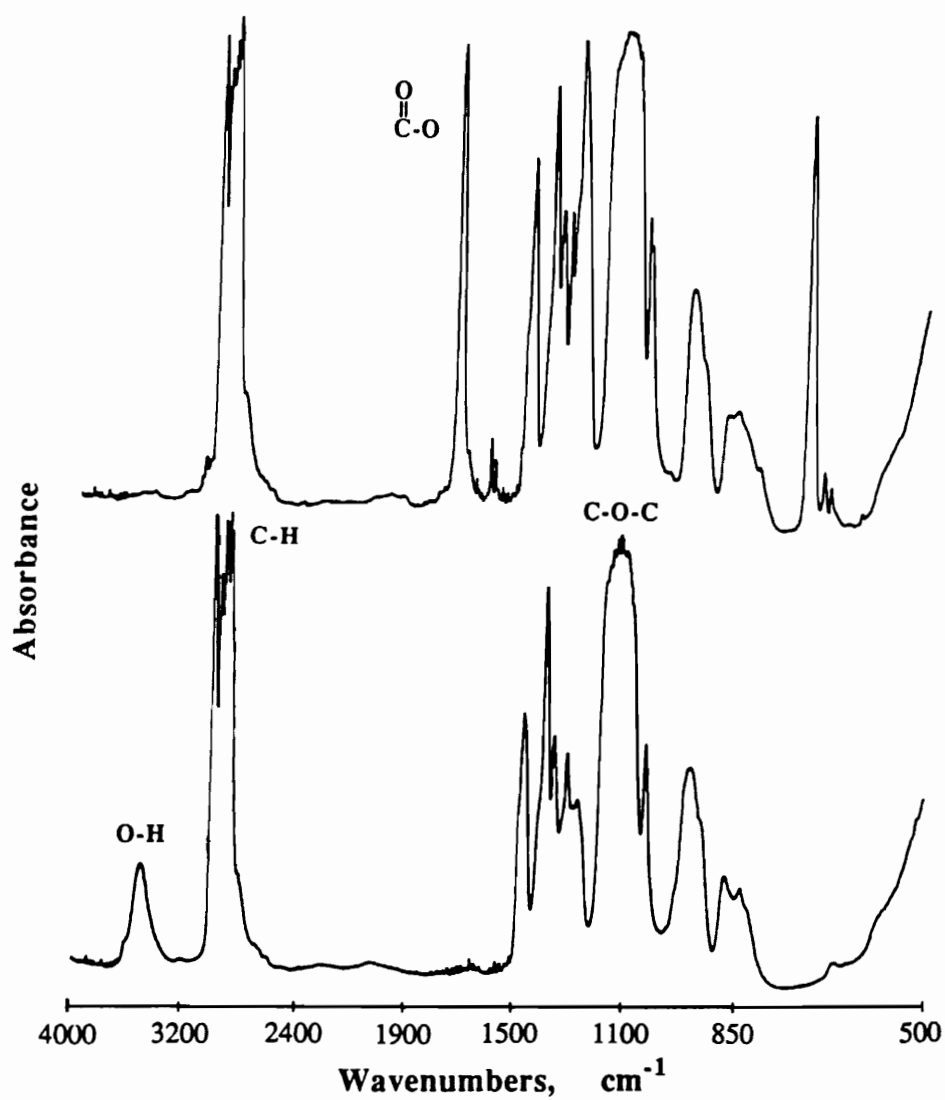


**Figure 2.4.9** FTIR spectra of PPG-1025 (bottom) and PPG-1025E (top) illustrating the replacement of the hydroxyl functionality of the former with an aromatic ester.

part in the reaction between anhydride and epoxy and, therefore, provide a suitable means of comparison for the role of end-groups in morphology control.

Figure 2.4.10 displays the SEM photomicrographs of the room temperature fracture surfaces of Quatrex-2010/NMA samples modified with 5% by weight of (a) PPG-1025 and (b) PPG-1025E. The amount of DMP-30 used was 2% by weight based on total amount of epoxy and NMA, and the curing conditions used were 60 °C for 12 hours. Both of the samples displayed stable two-phase morphology. However, it can be clearly seen from the photomicrographs that the PPG-1025E modified system has a greater tendency for phase separation than the PPG-1025 modified system. The domain size is in the range of 1.5-2  $\mu\text{m}$  in the former compared to slightly smaller domains of  $\sim 1 \mu\text{m}$  in the latter. A more pronounced difference is observed in the concentration of domains: PPG-1025E modified system possesses considerably more numerous domains than the PPG-1025 modified system.

Similar trends were observed at higher PPO contents also. Figure 2.4.11 compares the morphology of 10% PPG-1025 and PPG-1025E modified systems cured under same conditions as above. Interestingly, the domain sizes in the two samples are comparable, in the region of 2  $\mu\text{m}$  or so, with those in PPG-1025E modified sample in fact slightly smaller. However, the PPO phase concentration is much higher in the PPG-1025E system, to the extent that the phases seem to be on the verge of coalescence, than the PPG-1025 system. On further increasing the amount of PPO to 15%, the PPG-1025E sample displayed gross phase separation whereas PPG-1025 sample did not.

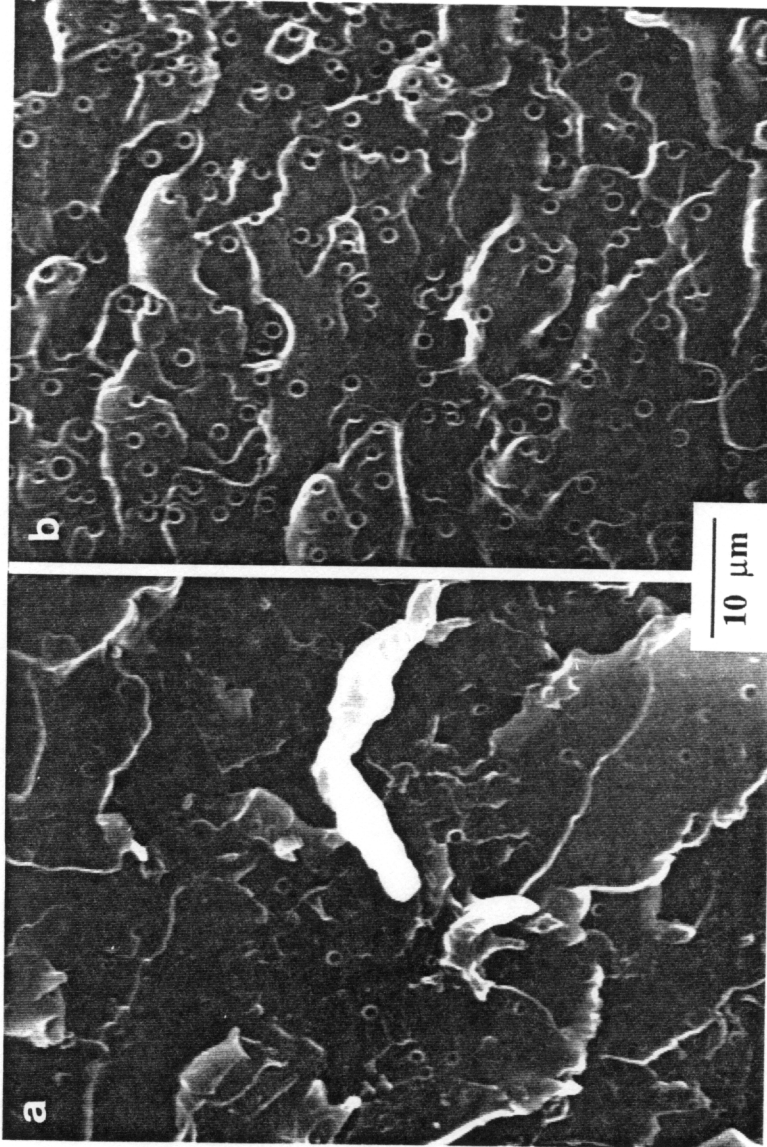


**Figure 2.4.10** SEM photomicrographs showing the effect of PPO end-groups on morphology in Quatrex-2010/NMA/DMP-30(2%) system containing 5% by weight of PPO cured at 60 °C for 12 hours. (a) PPG-1025E, and (b) PPG-1025E.



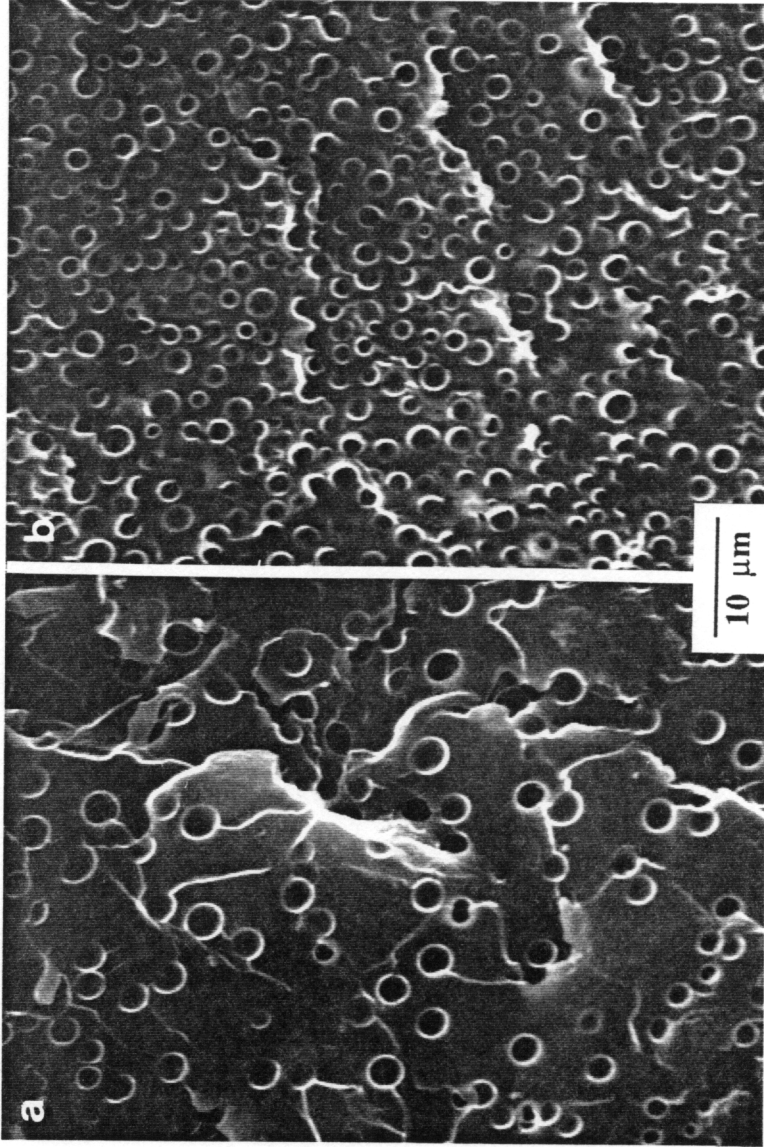


**Figure 2.4.11** SEM photomicrographs showing the effect of PPO end-groups on morphology in Quatex-2010/NMA/DMP-30(2%) systems containing 10% by weight of PPO cured at 60 °C for 12 hours. (a) PPG-1025E, and (b) PPG-1025E.

The above results suggest quite convincingly that the reaction of hydroxyl functionality with epoxide via carboxyl formation plays a substantial role in the process of phase separation. As a consequence of this co-reaction, there is an enhancement in compatibility accompanied by some loss in the overall extent of phase separation as measured by combination of the size and concentration of the PPO domains.

#### **2.4.1.4 Effect of Composition.**

Figure 2.4.12 displays the SEM photomicrographs of fracture surfaces of Quatrex-2010/NMA/DMP-30 system containing various amounts of PPG-1025 ranging from 2% to 30% by weight. Again, all samples were cured at 60 °C for 12 hours with a catalyst concentration of 2% based on the total weight of Quatrex-2010 and NMA (thus the 5% and 10% PPG-1025 samples here are the same as in Figures 2.4.10(a) and 2.4.11(a) respectively).

Several observations can be made from Figure 2.4.12. The 2% PPG-1025 sample has a single phase morphology with no domain structure. All other samples display phase separation. As evident on the photomicrographs, there is an increase in domain size from ~1  $\mu\text{m}$  to ~2  $\mu\text{m}$  to ~3  $\mu\text{m}$  as PPO content is varied from 5% to 15%. All samples so far were compatible. In contrast, the 20% PPG-1025 was found to be incompatible. This is also reflected in its morphology as seen on the Figure 2.4.12(e): the domains are less well-defined and there is a greater variation in phase sizes, some as large as 10  $\mu\text{m}$ . The morphology of 25% PPG-1025 sample, which is not shown on Figure 2.4.12, was similar with the extent of gross phase separation even more severe. On increasing the PPO content to 30%, there was a distinct change in morphology. First, the discrete phase was no longer

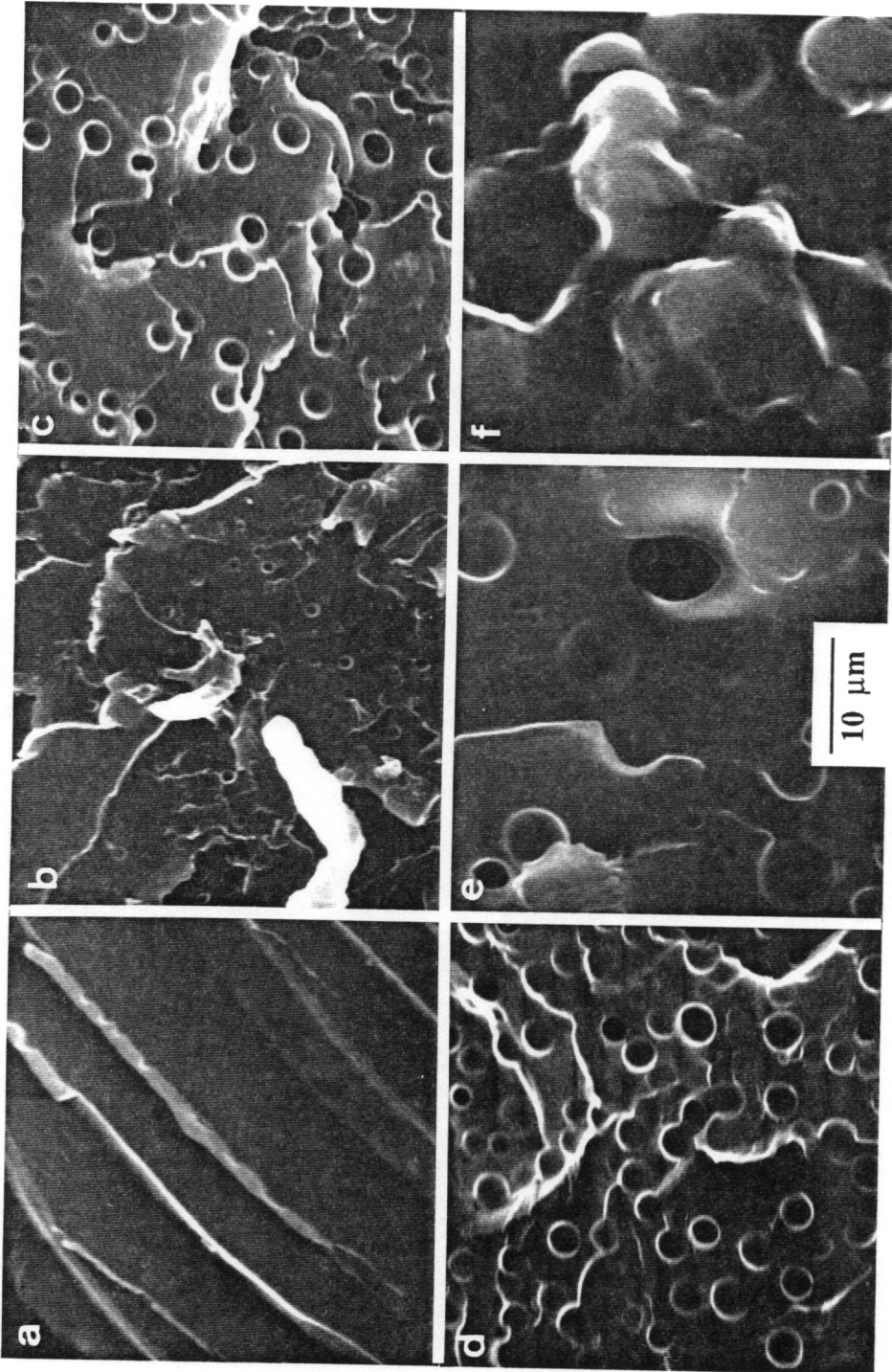


**Figure 2.4.12** SEM photomicrographs showing the effect of PPO content on morphology in Quatex-2010/NMA/DMP-30(2%) system cured at 60 °C for 12 hours containing various percentages by weight of PPG-1025. (a) 2, (b) 5, (c) 10, (d) 15, (e) 20, and (c) 30.

PPO, rather it was the epoxy network, i. e. phase inversion occurred at this composition. Domains of epoxy, though with a high degree of coalescence, in the size range of 10-15  $\mu\text{m}$  are visible on Figure 2.4.12(f). The second difference was in the fact that this sample, although lacking mechanical strength (understandably so since the continuous phase is PPO with a  $T_g$  below room temperature), did not display any evidence of gross phase separation unlike its predecessors, the 20% and 25% PPG-1025 containing samples.

The concept of  $\Delta p$ , the characteristic conversion span defined by Equation 2.4.2, can be utilized to describe the observed effect of composition on morphological behavior. For the above system,  $p_{gel}$  is the same for all samples, assuming that there is a negligible effect of PPO co-reaction on gel point. However, referring to Figure 2.4.5,  $p_b$  increases as one increases the initial PPO content,  $\phi_{2,0}$ . This continues until the critical composition  $\phi_{2c}$  is reached at which time the phase inversion takes place and  $p_b$  starts increasing. The resulting relation between  $\Delta p$  and PPO content is depicted on Figure 2.4.13. There is a maximum in  $\Delta p$  at the critical point. Thus, considering  $\Delta p$  as the measure for extent of phase separation, the phase size and concentration as well as the tendency for gross phase separation may be expected to increase until phase inversion occurs and then the reverse is true. Three regions are marked on Figure 2.4.13. Region of type I at the two extremes of the composition scale, where  $\Delta p \leq 0$ , gives a one-phase behavior; whereas Region II, where  $\Delta p > 0$ , represents the two phase compatible behavior. An finally, the region III may be identified in the intermediate composition range around the critical point in which conditions of incompatibility prevail. By comparison, it can be noted that the 2% PPG-1025 sample belongs to region I, the 5, 10, 15, and 30% samples to region II, and the 20 and 25% samples to region III.

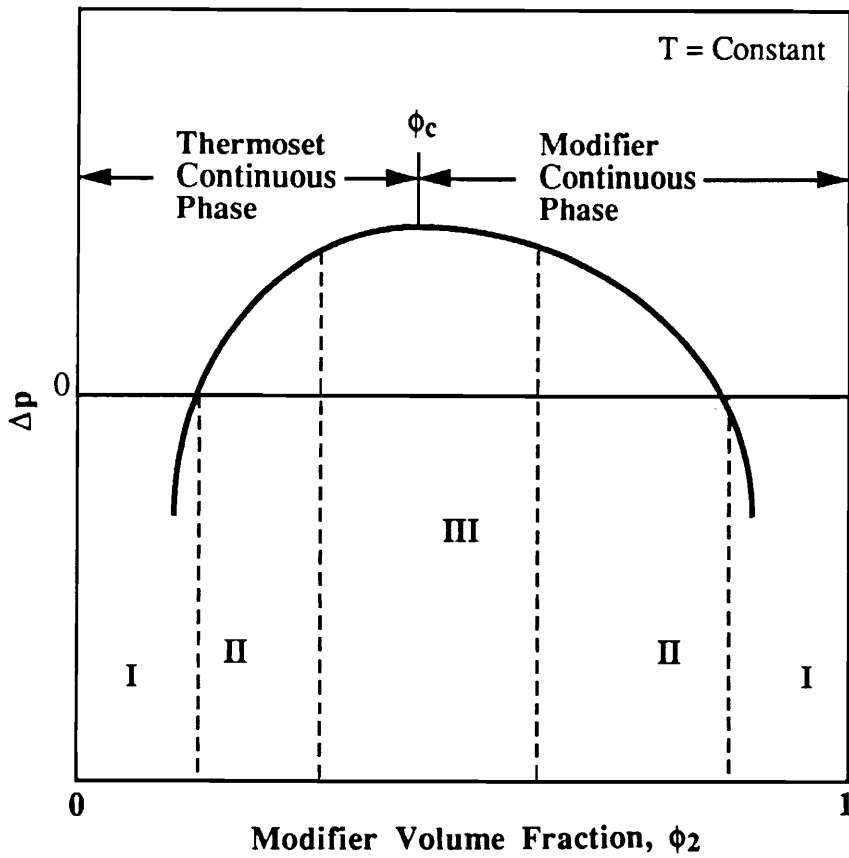


**Figure 2.4.13** Schematic representation of the relation between  $\Delta p$  (the difference between conversion at gelation,  $p_{gel}$ , and conversion at the onset of phase separation,  $p_b$ ) and modifier content.  $\phi_c$  = critical modifier volume fraction at which phase inversion occurs; the three regions marked are I = one-phase *compatible*, II = two-phase *compatible*, and III = two-phase *incompatible*.

The effect of PPO content was also studied in the Bis-S cured systems. Figure 2.1.14 displays the photomicrographs of PPG-425 modified Quatex-2710 cured with Bis-S and TMAH (1%). The size of PPO domains changes from extremely small (less than 0.1  $\mu\text{m}$ ) at 15% PPG-425 to slightly larger ( $\sim 0.2 \mu\text{m}$ ) at 25% PPG-425. The photomicrograph of the 30% PPG-425 sample, by contrast, displays domains of size in the vicinity of 0.5  $\mu\text{m}$  many of which can be seen to merge into each other. This would be an example in which the conditions of phase separation were such that phase coalescence occurred without gross phase separation. A morphology of this type would be of interest from the point of view of microporosity development where open or interconnected pores are required.

#### 2.4.1.5 Effect of Temperature of Cure.

One of the attractive features of the anhydride cure in comparison of the other chemistries, specifically aromatic amines such as DDS, is its flexibility in the temperature of cure. A finite amount of cure takes place even at room temperature in the presence of the catalyst. Therefore, there is a broader range of temperatures available in anhydride cure which can be effectively used for morphology control. Figure 2.1.15 displays photomicrographs of the fracture surface of three Quatex-2010/NMA/DMP-30(2%) samples having identical PPO content, 10% by weight of PPG-1025, but cured at different temperatures. The three cure time/temperature schedules utilized were: (a) room temperature for 7 days, (b) 60 °C for 12 hours, and (c) 150 °C for 3 hours. The results of changing the cure temperature were immediate as evident on Figure 2.4.15: the phase size varied from very small  $\sim 0.1 \mu\text{m}$  to nearly 2  $\mu\text{m}$  in going from room temperature cure to 60 °C cure; the 150 °C cured sample in contrast displayed no domain structure which was in agreement with its clear homogeneous appearance. In addition, the concentration of domains in the room

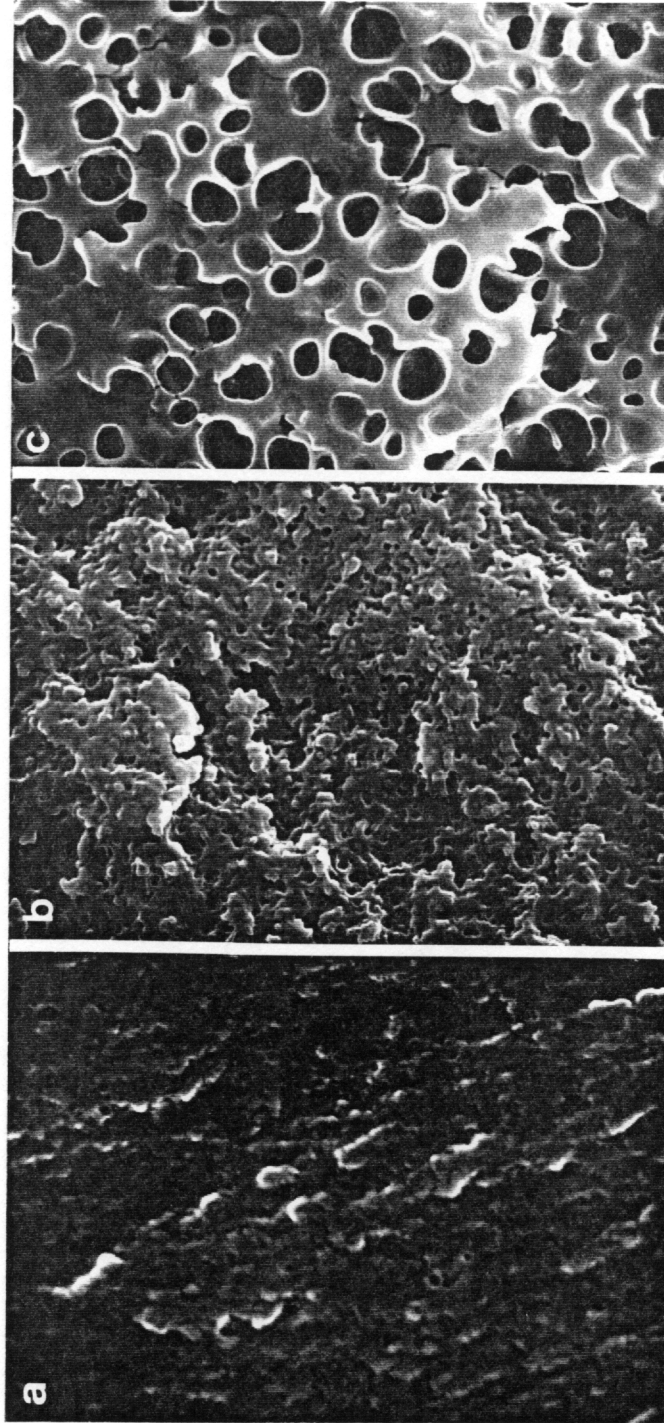


**Figure 2.4.14** SEM photomicrographs showing the effect of PPO content on morphology in Quatex-2710/Bis-S/TMAH(1%) system cured at 150 °C for 2 hours containing various percentages by weight of PPG-425. (a) 15, (b) 25, and (c) 30.



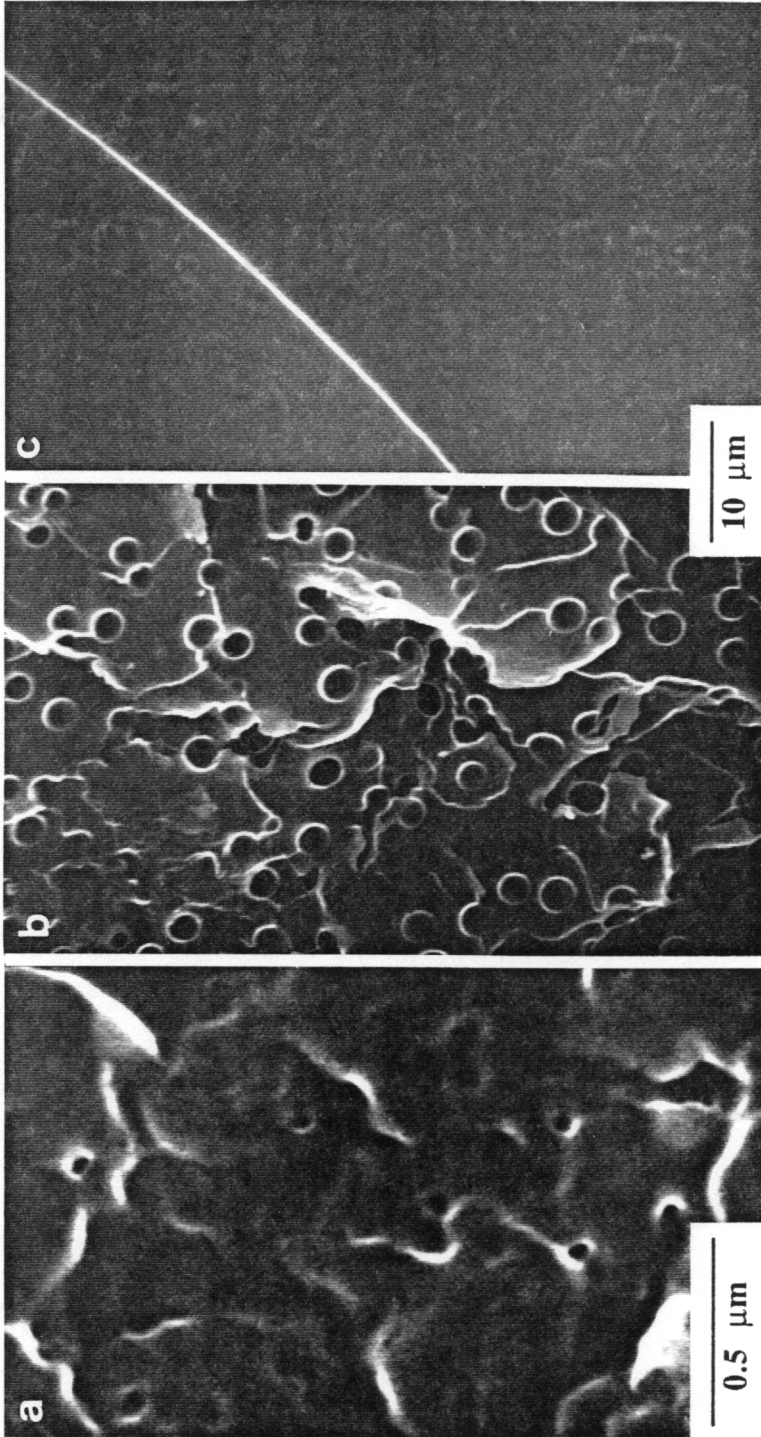


**Figure 2.4.15** SEM photomicrographs showing the effect of temperature of cure on morphology in Quatrex-2010/NMA/DMP-30(2%) system containing 10% by weight of PPG-1025. Cure schedules: (a) room temperature for 7 days, (b) 60 °C for 12 hours, and (c) 150 °C for 3 hours.



temperature cure sample also was considerably higher than that in the sample cured at 60 °C, considering that magnification in Figure 2.4.14(a) is 50,000x compared to 1,600x in case of Figure 2.4.14(b).

The observed dependence of morphology on the temperature of cure may be analyzed as follows. First of all, solubility of PPO in the epoxy increases as the temperature is increased. This may be expected if one considers the initial interaction parameter,  $\chi_{12,0}$ , between the two components to be a function of the inverse of temperature. One such empirical relationship suggests a linear dependence<sup>122,127,144</sup> given by:

$$\chi_{12,0} = A + B/T \quad (2.4.3)$$

where A and B are constants that can be derived from experimental cloud point data. Consequently,  $p_b$ , the conversion needed for commencement of phase separation increases with temperature. Therefore, assuming that  $p_{gel}$  remains unchanged, there will be a decrease in  $\Delta p$  as the temperature of cure is raised. At a sufficiently high temperature, the  $\Delta p$  will become zero and then negative (which, as far as phase separation is concerned, is effectively the same as zero) if the temperature is increased even further as illustrated on Figure 2.4.16. Thus, in the high temperature region, the system remains in the metastable region only for a short conversion before it encounters gelation. Furthermore, higher temperatures also promote faster polymerization rates. Combination of small  $\Delta p$  and higher reaction rates then may be expected to allow little or no phase separation, latter being the case in the 150 °C cure sample here.

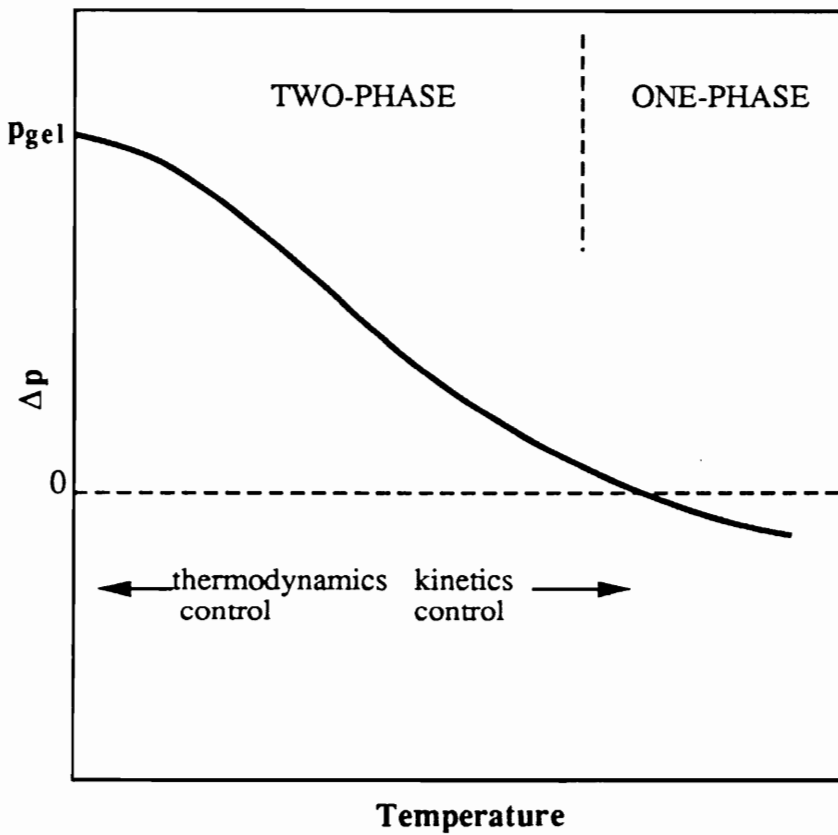


**Figure 2.4.16** Schematic representation of the relation between  $\Delta p$  (the difference between conversion at gelation,  $p_{gel}$ , and the conversion at the onset of phase separation,  $p_b$ ) and the temperature of cure.

As the cure temperature is lowered, the changes in  $\Delta p$  and the rate of reaction together increase the tendency for phase separation. Thus in general the total volume fraction of phase separated domains may be anticipated to increase when the cure temperature is lowered, first rapidly and then leveling off as the gap between  $p_{gel}$  and  $p_b$  becomes wide enough to ensure that most of the phase separation is completed before gelation. Accompanying the increased tendency for phase separation at low temperature also is an enhancement in the nucleation rates. The critical size of the nucleus for phase growth is smaller at lower temperature. Therefore, more nuclei can be activated and, accordingly, there would be a greater concentration of domains at lower temperatures. Since, the domain size is proportional to the ratio of volume fraction to the number of domains, it can be easily seen that as the temperature is lowered the domain size would initially increase, reach a maximum and then, continue to decrease. This explains the results of Figure 2.4.15 that by changing the cure temperature from 150 °C to 60 °C, the phase size increased (from 0 to ~2  $\mu\text{m}$ ) and then from 60 °C to room temperature, the phase size decreased (from ~2 to ~0.1  $\mu\text{m}$ ). The behavior displaying a maximum in domain size as a function of temperature is fairly typical; it has been previously observed experimentally by Gillham in CTBN modified epoxy systems<sup>131</sup> and also predicted theoretically by Williams *et al.*<sup>122</sup> A convenient way to look at this behavior is to consider the phase separation to be kinetically controlled in the high temperature side and thermodynamically controlled in the lower temperature side of the maximum.

In the room temperature cure, an additional factor also comes into play that further restricts the phase growth from what may be expected from the preceding explanation. This originates from the fact that the room temperature sample, in this particular case, vitrified before gelation (as confirmed by its solubility in methylene chloride). The effect of

vitrication may be considered to be similar to that of gelation, i. e. it arrests further phase separation. The result is that the domains in the room temperature sample do not fully grow to the size they would have had if they were allowed to continue until gelation. If this is the case, then, it should be possible to resume the phase separation process by increasing the temperature. In order to check the validity of this statement, the sample of Figure 2.4.15(a) was post-cured at two different higher temperatures: 60 °C for 12 hours, and 150°C for 3 hours. The results can be observed on Figure 2.4.17 which compares the morphology of the original room temperature cured sample with those of the two post-cured samples. From Figure 2.4.17(a) and Figure 2.4.17(b), it can be noted that little change occurs after the 60 °C post-cure, except for a slight increase in the number of domains whose size remains in the vicinity of 0.1  $\mu\text{m}$  as before. On the contrary, the 150 °C post-cure produces a dramatic change: the phase size increases nearly ten-fold to  $\sim 1 \mu\text{m}$  while retaining a fairly high domain concentration at the same time. The difference in the morphological behaviors of two post-cured systems seems to reinforce the importance of mobility during phase separation. The viscosities may be expected to be much higher at 60 °C than those encountered during the 150 °C cure. The result is that in the former case, although there may be some new nucleation, the phase growth is restricted due to kinetic limitations. On the other hand, sufficient mobility is present in the latter for the growth of the phases which are already present in the system from the room temperature cure.

The effect of temperature of cure on 25% PPG-1025 containing Quatex-2010/NMA/DMP-30(2%) system was also studied. Figure 2.4.18 displays the photomicrographs of samples cured at (a) room temperature for 7 days, and (b) 150 °C for 3 hours. The morphological change as a function of cure temperature for the 25% PPG-1025 system seems to be quite different from that observed earlier in the 10% PPG-1025 system. Here, instead of

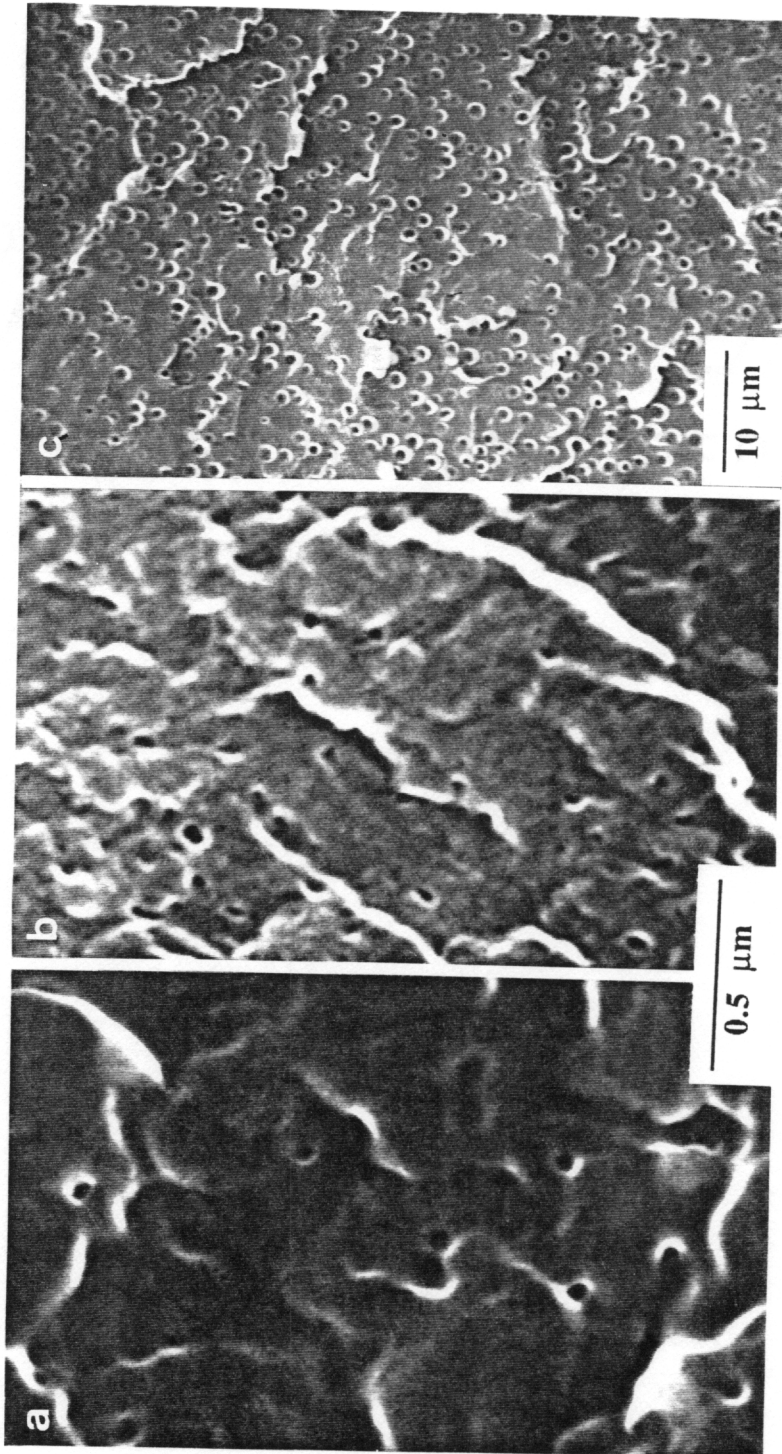


**Figure 2.4.17** SEM photomicrographs showing the effect of post-cure on the room temperature cured Quatrex-2010/NMA/DMP-30(2%) system containing 10% PPG-1025. (a) room temperature for 7 days, (b) room temperature for 7 days + 60 °C for 12 hours, and (c) room temperature for 7 days + 150 °C for 3 hours.

variation in the phase size or phase concentration, the nature of phase structure itself changes. For room temperature cure, PPO is the discrete phase. On the other hand, epoxy forms the discrete phase when the cure temperature is 150 °C. In other words, the critical composition,  $\phi_{2c}$ , where phase inversion takes place decreases from *above 25% PPG-1025* to *below 25% PPG-1025* when the temperature of cure is increased from room temperature to 150 °C. It would of interest to know if this observation is agreement with what may be predicted by Flory-Huggins thermodynamics.

Theoretically, the critical point can be obtained by equating the second and third derivatives of the Gibbs free energy expression to zero,<sup>9</sup> i. e.

$$\partial^2(\Delta G_m^V) / \partial \phi_2^2 = 0 \quad (2.4.4)$$

$$\partial^3(\Delta G_m^V) / \partial \phi_2^3 = 0 \quad (2.4.5)$$

Using the expression for  $\Delta G_m^V$  from Equation 2.4.1 in the Equations 2.4.4 and 2.4.5 and solving them simultaneously, one can arrive at the following relation for the critical composition  $\phi_{2c}$  (see Appendix 2.II for detailed derivation):

$$\phi_{2c} = [V_{1,0} / (2 V_{2,0} \chi_{12,0})]^{1/2} \quad (2.4.6)$$

Equation 2.4.6 predicts that for a given system of epoxy and PPO (i. e. keeping  $V_{1,0}$  and  $V_{2,0}$  constant), the critical composition will increase as the interaction parameter decreases. Assuming that the inverse relation of Equation 2.4.3 between the chi parameter and the

temperature holds, this means that  $\phi_{2c}$  should increase with temperature- in contrast with the observations from Figure 2.4.18.

This discrepancy between the experimental results and theory may possibly be related to the assumption in the latter that the modifier does not chemically interact with the thermoset to appreciably influence the process of phase separation. As seen in Section 2.4.1.3, hydroxyl end-group reaction in the NMA cured epoxy does play a significant role in morphology control. From the point of view of thermodynamics, as mentioned earlier, the overall effect of this co-reaction may be looked upon as a reduction in the interaction parameter. The extent to which this co-reaction occurs in comparison to the main epoxy-NMA reaction must also depend on the temperature as well as the composition. Given these additional complexities,  $\chi_{12,0}$  may no longer expected to be a simple linear function of  $1/T$  as given by Equation 2.4.3, and consequently, it may not always increase as the temperature is reduced. This may be particularly true when the PPO content is fairly high, as it is in the case under discussion.

In a manner similar to the 10% PPG-1025 system, the room temperature cured sample of the 25% PPG-1025 system was also post-cured at a higher temperature to see if further phase growth occurs. Figure 2.4.19 shows the photomicrographs of the sample before and after post-cure at 150 °C for 3 hours. Once again, the post-cure effected a sharp change in the morphology. The phase size can be seen on the photomicrographs to increase from  $\sim 0.2 \mu\text{m}$  to nearly  $1 \mu\text{m}$ . Moreover, a dense closed-packed domain structure is obtained which could become an excellent candidate for an open-pore microporous system after effective removal of PPO.

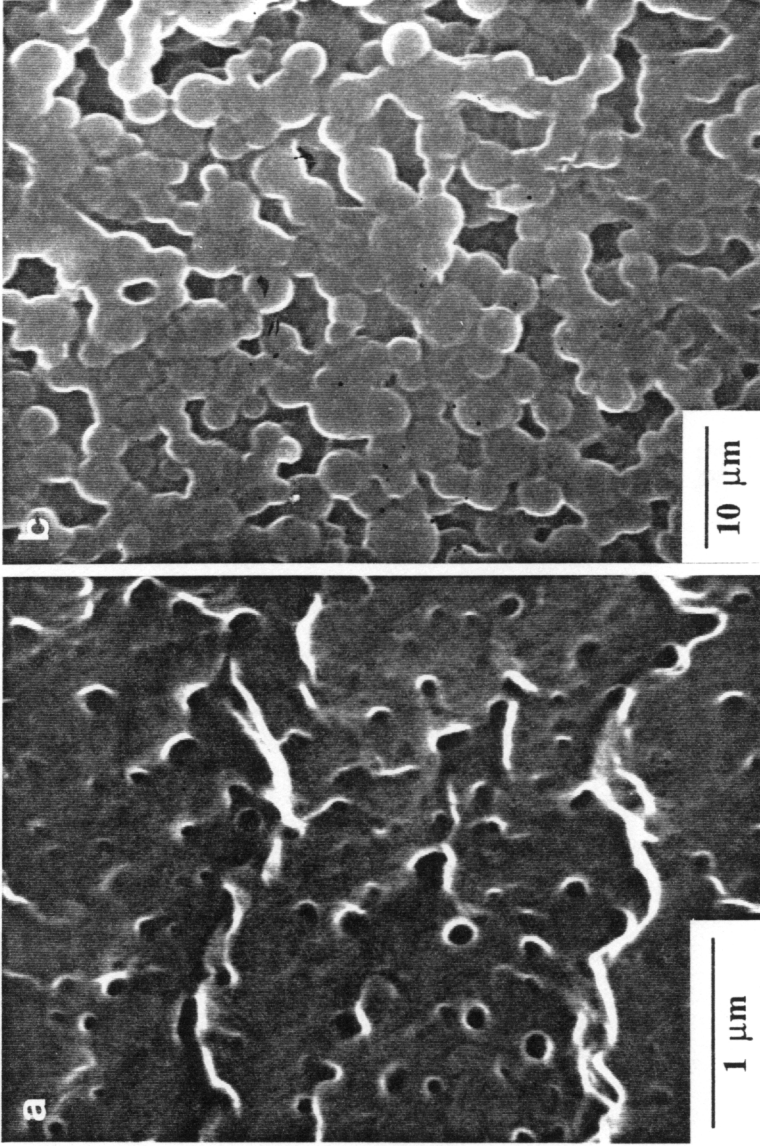


**Figure 2.4.18** SEM photomicrographs showing the effect of temperature of cure on morphology in Quatrex-2010/NMA/DMP-30(2%) system containing 25% by weight of PPG-1025. Cure schedules: (a) room temperature for 7 days, and (b) 150 °C for 3 hours.



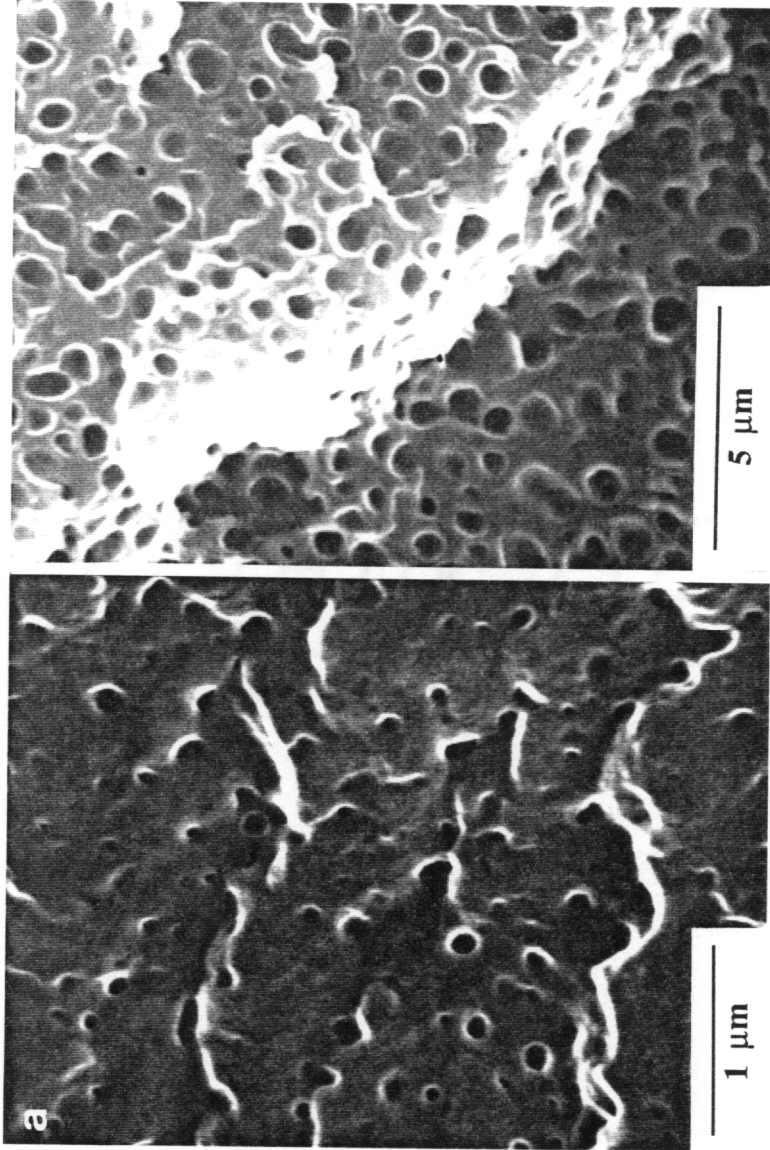


**Figure 2.4.19** SEM photomicrographs showing the effect of post-cure on the room temperature cured Quatrex-2010/NMA/DMP-30(2%) system containing 25% PPG-1025. (a) room temperature for 7 days, and (b) room temperature for 7 days + 150 °C for 3 hours.

The temperature dependence in the PPG-425 modified Quatrex-2710/Bis-S/TMAH(1%) system is displayed on Figure 2.4.20. The PPO content was 25% by weight. The cure temperatures employed were (a) 100 °C for 12 hours, (b) 150 °C for 3 hours, and (c) 200 °C for 1 hour. The behavior in this case is slightly different from that previously seen in the NMA cured system. The phase size increases progressively from  $\sim 0.05 \mu\text{m}$  to  $\sim 0.1 \mu\text{m}$  to  $\sim 0.3 \mu\text{m}$  as the temperature is increased from 100 °C to 150 °C to 200 °C, i. e. no maximum is observed. This may be explained if one considers that in the given temperature range the phase separation is mainly controlled by thermodynamics with the phase size essentially determined by variation in the nucleation rates. This may not be unreasonable to expect since the compatibility between PPO and the Bis-S cured epoxy is limited, and, therefore, the onset of phase separation possibly occurs quite early during polymerization. Moreover, as given on Table 2.4.2(b), the  $p_{\text{gel}}$  of this system is also considerably high. The result is that the characteristic conversion span  $\Delta p$  remains at a substantial level even at the high temperature of 200 °C, and kinetic limitations play a less consequential role in the phase separation process.

#### **2.4.1.6 Effect of PPO Molecular Weight.**

Figure 2.4.21 displays the SEM photomicrographs of the fracture surfaces of three Quatrex-2010/NMA/DMP-30(2%) samples cured at the same temperature of 60 °C for 12 hours containing 10% by weight of three different PPO's: (a) PPG-425, (b) PPG-1025, and (c) PPG-2025. The molecular weights of these PPO's are rated as 0.5K, 1K, and 2K respectively. Clearly, under the given conditions, the compatibility of the system decreases with increasing PPO molecular weight. The morphology of the PPG-425 modified sample is that of single phase with no domain structure. When a same amount of PPG-1025 is

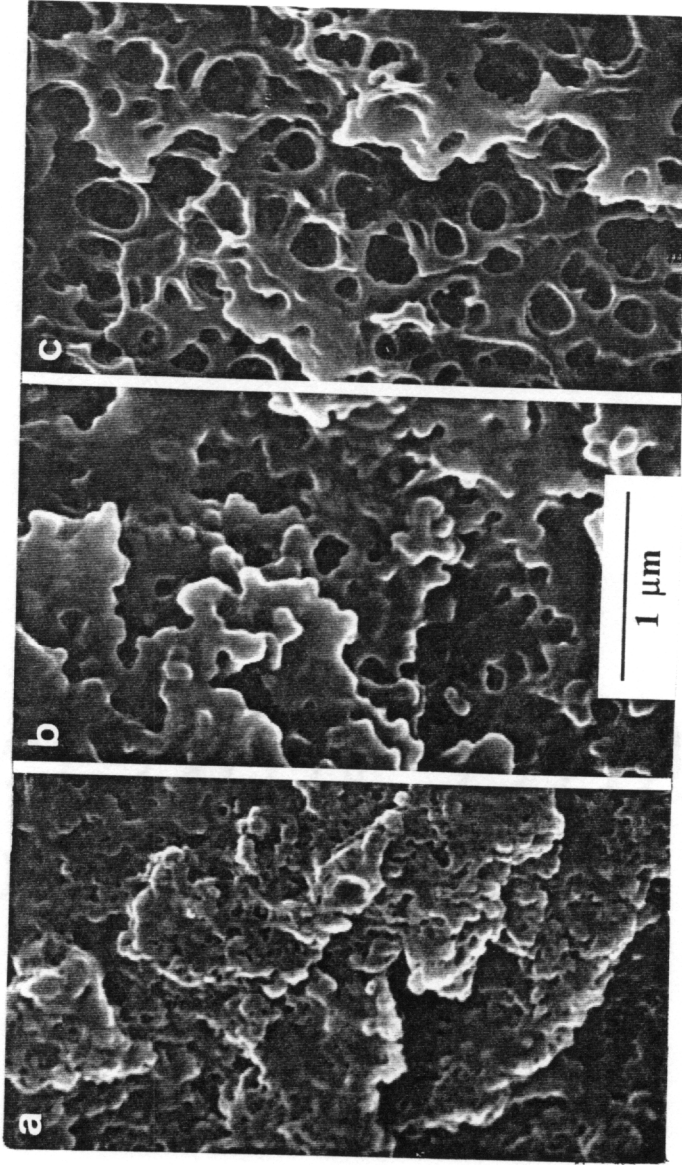


**Figure 2.4.20** SEM photomicrographs showing the effect of temperature of cure on morphology in Quatrex-2710/Bis-S/TMAH(1%) system containing 25% by weight of PPG-425. Cure schedules: (a) 100 °C for 12 hours, (b) 150 °C for 3 hours, and (c) 200 °C for 1 hours.

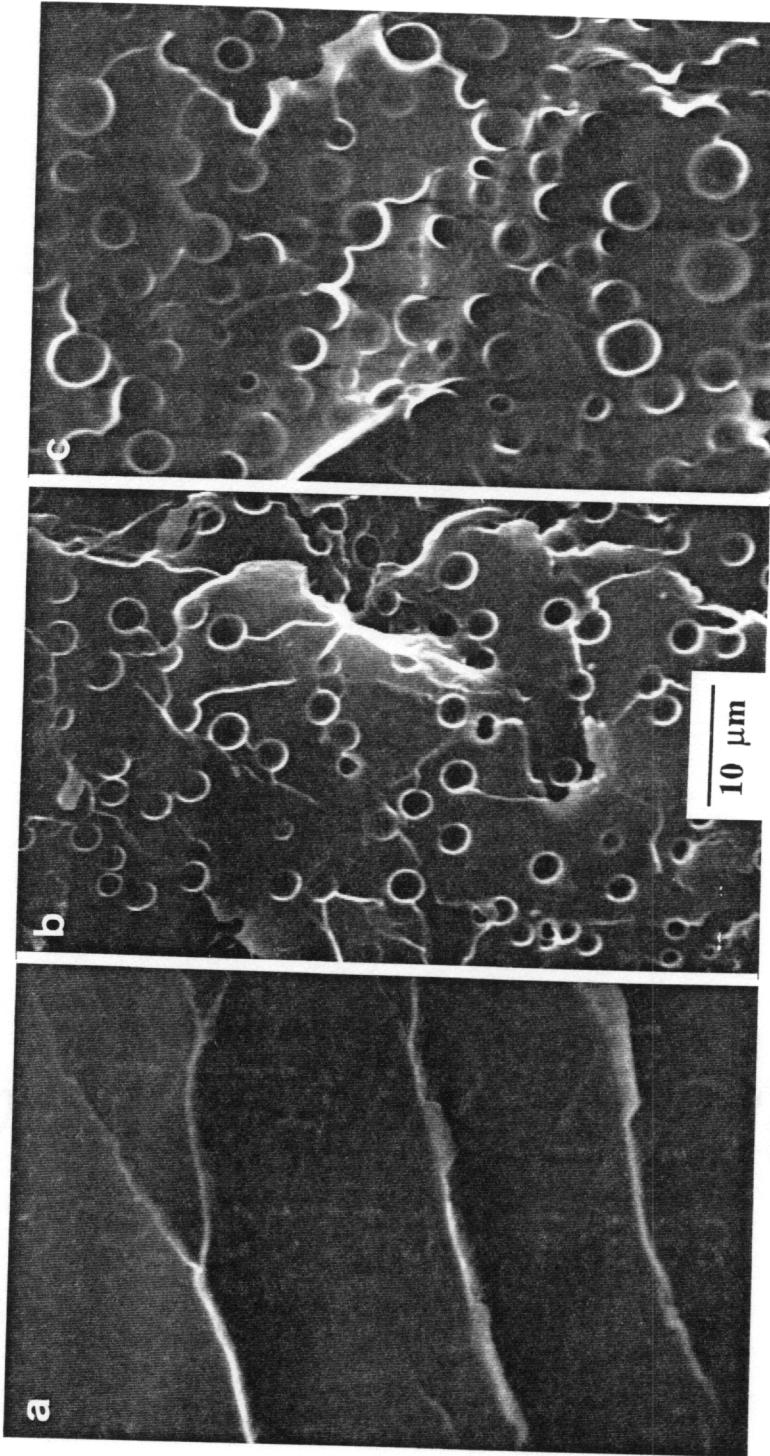


**Figure 2.4.21** SEM photomicrographs showing the effect of PPO molecular weight on morphology in Quatrex-2010/NMA/DMP-30(2%) system cured at 60 °C for 12 hours. 10% by weight of: (a) PPG-425, (b) PPG-1025, and (c) PPG-2025.

used instead, the result is a two-phase morphology with PPO domains of  $\sim 2 \mu\text{m}$ . The domain size increases to a range of 3-4  $\mu\text{m}$  when PPG-1025 is replaced with PPG-2025.

The observed effect of PPO molecular weight on the morphological behavior is consistent with what may be expected from thermodynamic considerations. Equation 2.4.1 suggests that the negative entropic contribution to Gibbs free energy of mixing will be higher if the molar volume of the modifier,  $V_{2,0}$ , increases. Thus, miscibility in the system is favored by the use of a lower molecular weight PPO. In terms of  $p$ - $\phi$  diagrams, this is equivalent to shifting the binodal curve towards higher conversions. The conversion at the onset of phase separation,  $p_b$ , will be greater for a lower molecular weight PPO. Considering the  $p_{\text{gel}}$  to be unaffected, the overall result of decreasing PPO molecular weight is then a reduction in  $\Delta p$ . The tendency for phase separation diminishes as a consequence.

The effect of PPO molecular weight in Quatrex-2710/Bis-S/TMAH(1%) system is shown on Figure 2.4.22. The cure conditions were 150 °C for 3 hours and the two PPO's used were: (a) PPG-425, and (b) PPG-1025. In this case, the change is in the phase structure rather than in the phase size. The discrete phase in the PPG-425 modified sample is PPO, while that in the PPG-1025 modified sample is epoxy. This implies that the phase inversion takes place above 25% PPO in the former and below (or at) 25% PPO in the latter. Referring to Equation 2.4.6, the Flory-Huggins thermodynamics predicts the critical point to be inversely proportional to the square root of the modifier molar volume  $V_{2,0}$ . In other words, a doubling of modifier molecular weight will result in about 29% reduction in the value of critical composition  $\phi_{2c}$ . Thus, if the system is in the right composition range, a phase inversion may be achieved by using a higher molecular weight modifier. The results of Figure 2.4.22 corroborate this theoretical possibility.

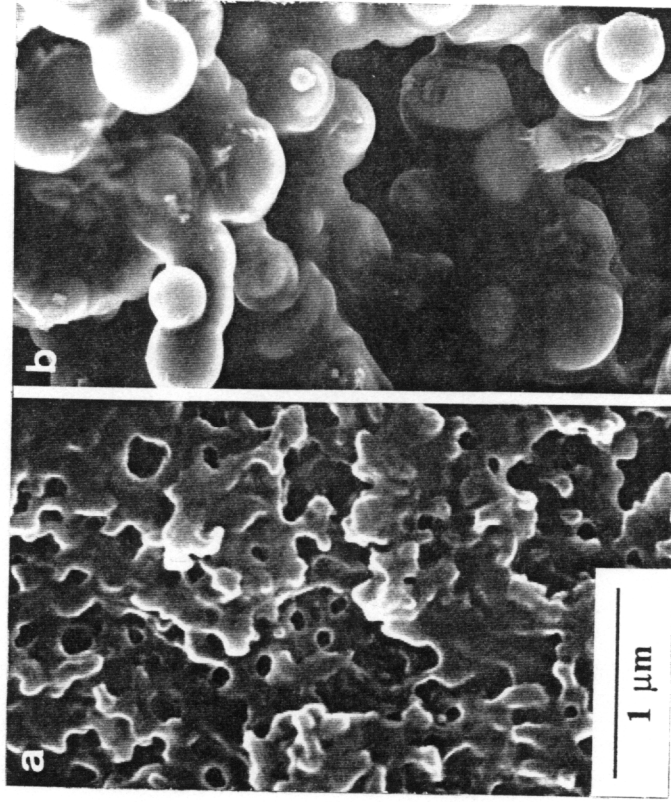


**Figure 2.4.22** SEM photomicrographs showing the effect of PPO molecular weight on morphology in Quatrex-2710/Bis-S/TMAH(1%) system cured at 150 °C for 3 hours. 25% by weight of: (a) PPG-425, and (b) PPG-1025.

#### 2.4.1.7 Effect of Catalyst Concentration.

In all the NMA cured systems discussed so far, the concentration of the catalyst DMP-30 was kept constant at 2% by weight based on the total amount of the epoxy and the hardener (1% by weight corresponds to approximately 0.67% by mole). A comparison of the morphological behavior as this concentration is changed to lower (e. g. 1%) and higher (e. g. 5%) values can be seen on the photomicrographs of Figure 2.4.23. The composition in each was kept identical at 10% PPG-1025 and the curing conditions were 60 °C for 12 hours. By varying the DMP-30 content from 2% to 1%, there is a reduction in the domain size from ca. 2  $\mu\text{m}$  to less than 1  $\mu\text{m}$  together with an increase in the domain density. It also seems from a qualitative evaluation of the photomicrographs that the overall extent of phase separation is also higher in the former than in the latter. At the higher catalyst concentration of 5%, there is no domain structure visible.

The role of catalyst concentration in the phase separation process may be examined on the basis of the concepts developed so far. Assuming that the catalyst only affects the reaction rates and not the reaction chemistry, the  $p_{\text{gel}}$ 's will be independent of the amount of DMP-30 used. Additionally, the onset of phase separation may also be expected to occur at comparable conversions considering that presence of a few percentage of the catalyst does not appreciably change the interactions between the thermoset and modifier. Thus,  $\Delta p$ , the conversion span for phase separation will be similar for each samples. However, what is changed as a result of varying the catalyst concentration is the time allowed for phase separation in the metastable region before gelation. For low catalyst concentrations, the changes occurring in the system are slow. Therefore, the kinetic processes, i. e. nucleation and growth, can be competitive in meeting the thermodynamic requirements for phase



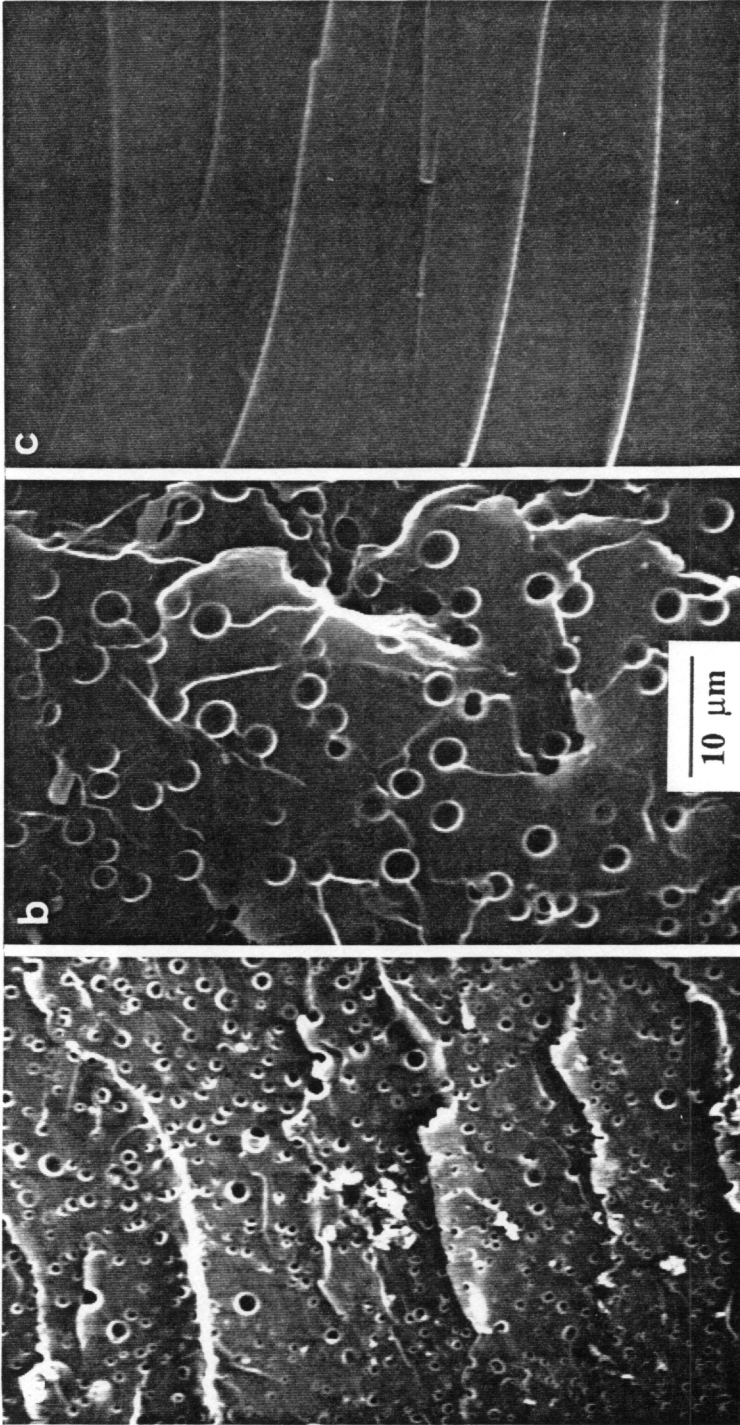


**Figure 2.4.23** SEM photomicrographs showing the effect of catalyst concentration on the morphology in Quatex-2010/NMA/DMP-30 system containing 10% by weight of PPG-1025 cured at 60 °C for 12 hours. DMP-30 % by weight based on total amount of epoxy and hardener: (a) 1, (b) 2, and (c) 5.



separation. As a result, the system may remain fairly close to the equilibrium state and the process is said to be under thermodynamic control. A greater extent of phase separation may be achieved in this case. In the other extreme, if the reaction rates are sufficiently fast, kinetic limitations may allow no phase separation before gelation occurs. In the intermediate range of reaction rates both thermodynamics and kinetics play significant roles in determining the course of phase separation. These three possibilities have been illustrated on Figure 2.4.24 with the help of a  $p$ - $\phi$  diagram. It shows that for a given composition, the cure path splits into three different routes once it enters the metastable region depending on the rate of polymerization. The cure path essentially traces the composition of the continuous phase and thus, gives an indication of the extent of phase separation occurring in the system as a function of conversion. The route I signifies a near equilibrium condition arising from very slow cure. The route III represents the case of extremely fast thermoset polymerization where the cure path is essentially vertical before it meets the gelation line suggesting that no phase separation takes place. The route II belongs to an intermediate case that is most likely to occur in practice. Thus, the extent of phase separation as measured by the volume fraction of the separated phase may be expected to as the catalyst concentration in the system is reduced. However, at the same time, there is an increase in the rate of nucleation. This is due to a decrease in the critical radius of the nucleus when the gap between the actual and the equilibrium states of the system is reduced as demonstrated by Williams and coworkers in their theoretical treatment.<sup>122</sup> In a manner quite analogous to the effect of temperature discussed in Section 2.4.1.5, the combination of increased phase separation and higher domain density will give rise to a maximum in the domain size at a certain intermediate catalyst concentration. In comparison, it may be recognized finally that the 1%, 2%, and 5% DMP-30 systems display behaviors typical to routes I, II, and III respectively.

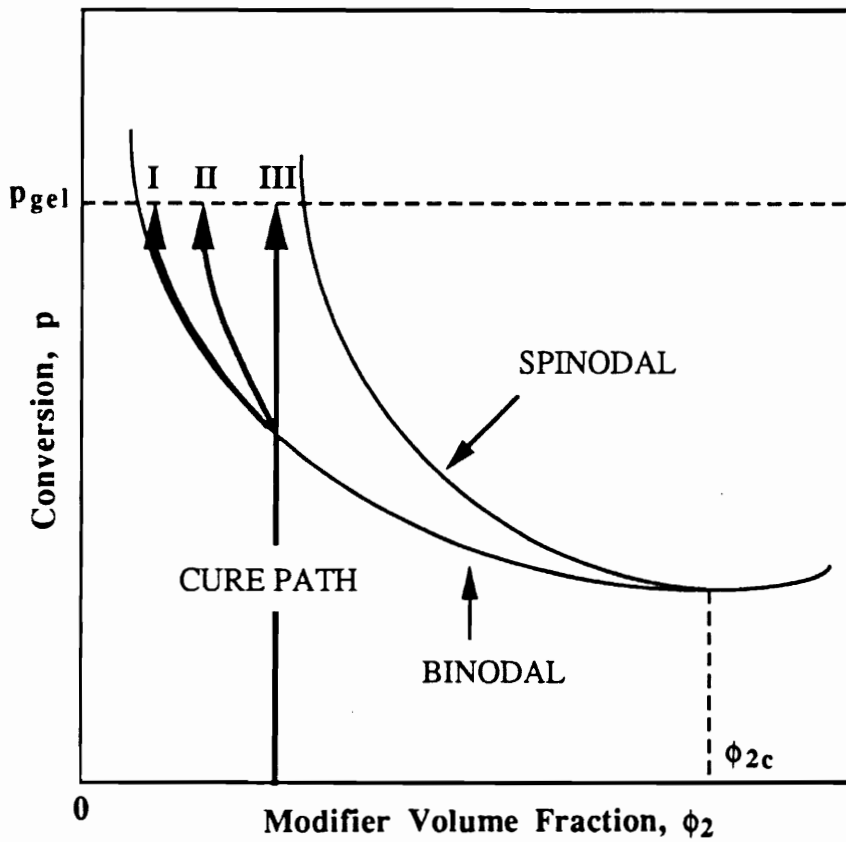


**Figure 2.4.24** A  $p$ - $\phi$  diagram illustrating the different routes followed by the cure path after it enters the metastable region in accordance with the rate of reaction. Route I: slow reaction rates; Route III: fast reaction rates; and Route II: intermediate reaction rates.

## **2.4.2 Cure Behavior.**

The in-situ cure experiments of the neat and 10% PPG-1025 modified Quatrex-2010/NMA/DMP-30(2%) systems using DMA comprised of three consecutive steps:

1. Isothermal cure scan for observation of critical phenomena such as gelation and vitrification;
2. Dynamic cure of the partially cured system from the first step to complete the remaining reaction; and
3. The final dynamic scan to obtain the ultimate properties as a function of the previous cure history.

The results of each step will be discussed, first by taking the neat epoxy system followed by the PPO-modified system. Finally, a compilation of relevant quantitative data from each case will be presented in the form of a TTT diagram.

### **2.4.2.1 Neat Epoxy.**

#### **2.4.2.1.1 Isothermal Cure.**

Figures 2.4.25 displays the DMA resonant frequency and damping behavior of the wire-mesh supported Quatrex-2010/NMA/DMP-30(2%) system cured isothermally at several temperatures ranging from 40 °C to 220 °C. In the resonant mode DMA, the frequency is

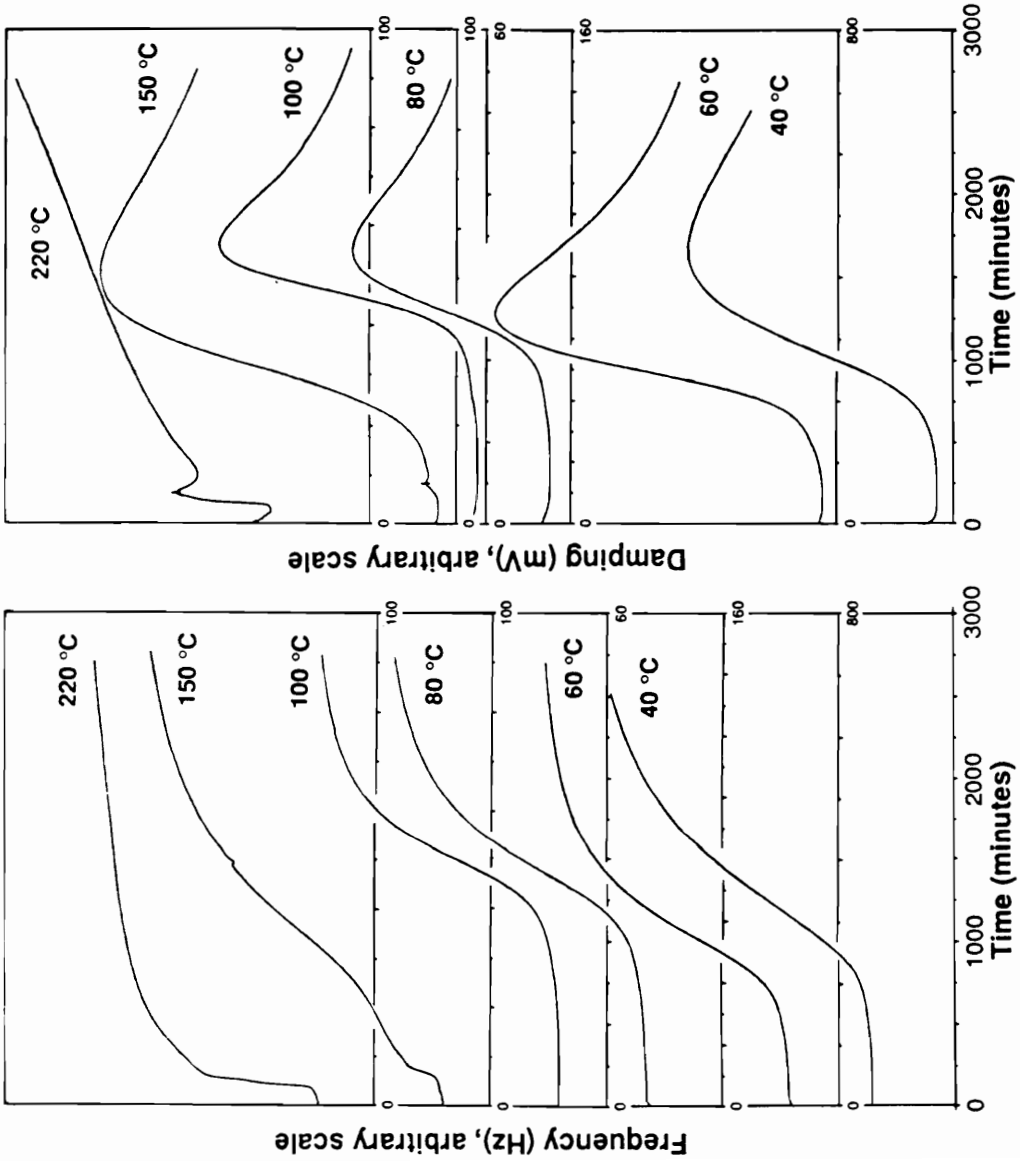
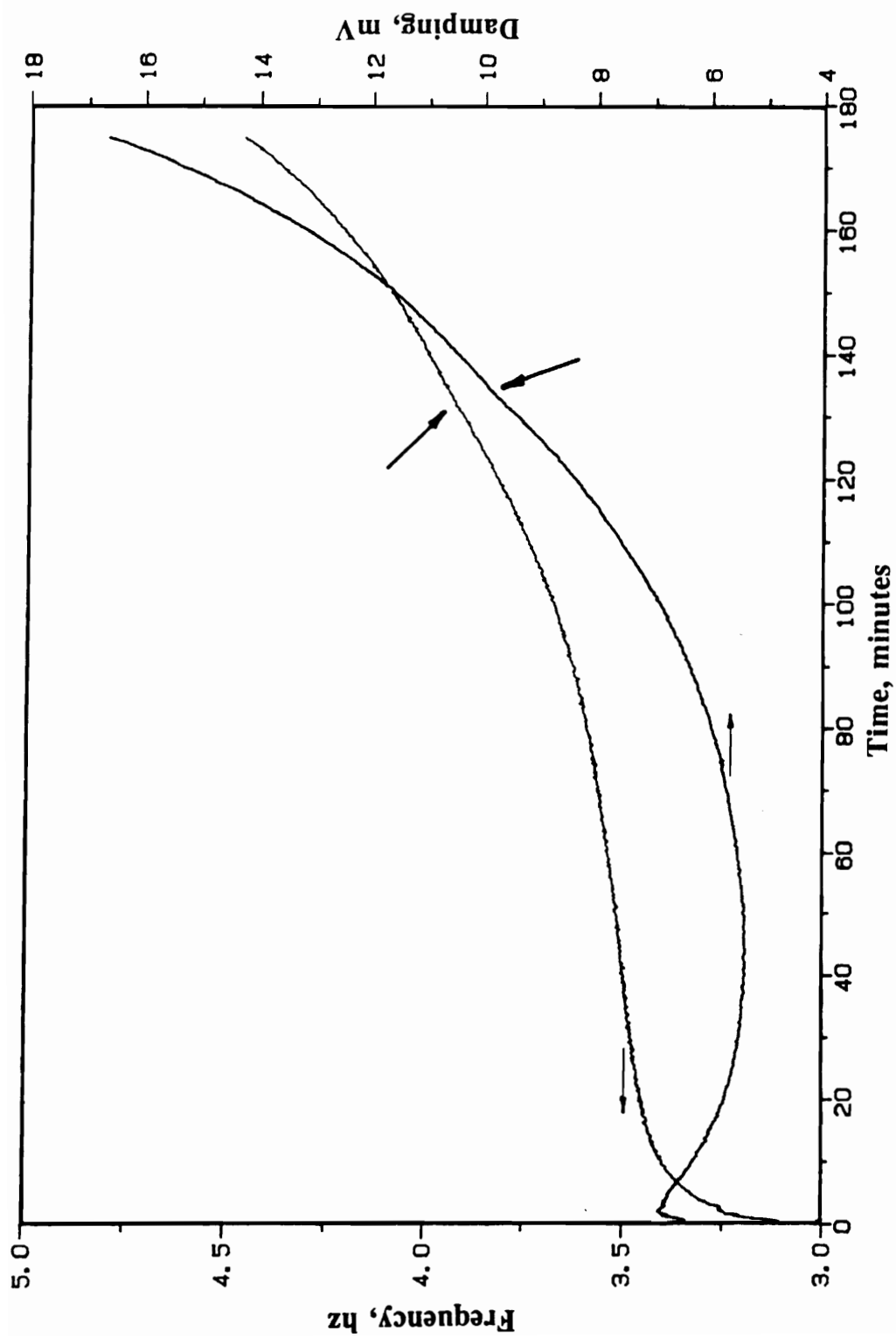


Figure 2.4.25 Isothermal DMA curing curves of the neat epoxy system.

indicative of the modulus of the epoxy during cure, while the damping is related to  $\tan\delta$ , the ratio of loss and storage moduli.<sup>145</sup> Thus, the cure transitions of gelation and vitrification may be expected to be identified by a peak in the damping curve and a stepwise increase in the frequency curve. This can be best seen on the 150 °C curves. The first jump in the frequency curve and the first peak in damping curve at ~8 minutes are both due to gelation (it might be noted here that the term "gelation" is used to mean the macroscopic or rheologically observable change and not the true molecular event, recalling the discussion in Section 2.2.2). The second much broader transitions at ~51 minutes are due to vitrification. At lower temperatures, however, only vitrification points are as clearly discernible. The gel points appear only as *shoulders*, both on frequency as well as damping curves. An example is given on Figure 2.4.26 where an enlarged gel point region of the 60 °C cure is displayed. As pointed to by the arrows, the slopes in the frequency and damping curves change slightly at ca. 130 minutes. Both the presence and the position of these shoulders were well reproduced, supporting their assignment to gelation. The presence of a shoulder instead of a damping peak or a frequency rise may be the result of the partial overlapping of the gelation transition by the broad vitrification transitions.

The gelation shoulders were visible at all temperatures between 40 and 220 °C, at the locations indicated by dotted arrows on Figure 2.4.25. On the other hand, vitrification could be observed at all temperatures, indicated in Figure 2.4.25 by full arrows, except 220 °C where only a single transition representing gelation could be seen. This is due to the fact that 220 °C is well above the glass transition temperature of the fully cured system,  $T_{g\infty}$ , as obtained through the third scan of the three-step DMA run to be discussed later.



**Figure 2.4.26** The gelation region of the 60 °C isothermal DMA curves of the neat epoxy system.

An additional observation that may be made from the frequency curves at each temperature is that after vitrification the modulus continues to rise although at a much slower rate than before. This means that the curing reaction does not terminate completely in the glassy state, but continues to a certain extent under diffusion limitations. The difference between the glass transition temperature and the temperature at which molecular motions are quenched is evident in other phenomena such as sub- $T_g$  annealing also and is predicted by theoretical expressions such as the WLF equation.<sup>181</sup>

#### **2.4.2.1.2 Dynamic Cure.**

The dynamic cure scans at 5 °C/min on samples pre-cured to different levels by the above isothermal scans at different temperatures are shown on Figure 2.2.27. Included are also the frequency and damping curves for a previously *uncured* system. Here, an interesting relationship between the level of initial cure and the subsequent dynamic cure behavior emerges.

For the previously uncured sample, the dynamic scan produces a single well-resolved transition at ca. 150 °C, as indicated by a jump in the frequency curve and a peak in the damping curve. This can be attributed to gelation. Here, the system does not reach vitrification since the sample temperature at all times remains higher than the instantaneous  $T_g$  of the system. For the pre-cured (and pre-gelled) samples, on the other hand, the damping and the resonant frequency spectra show a systematic change from a complex multi-transition to a single-transition phenomenon as one goes from the lowest (40 °C) to the highest (220 °C) pre-cure temperatures. Similar dynamic mechanical responses have

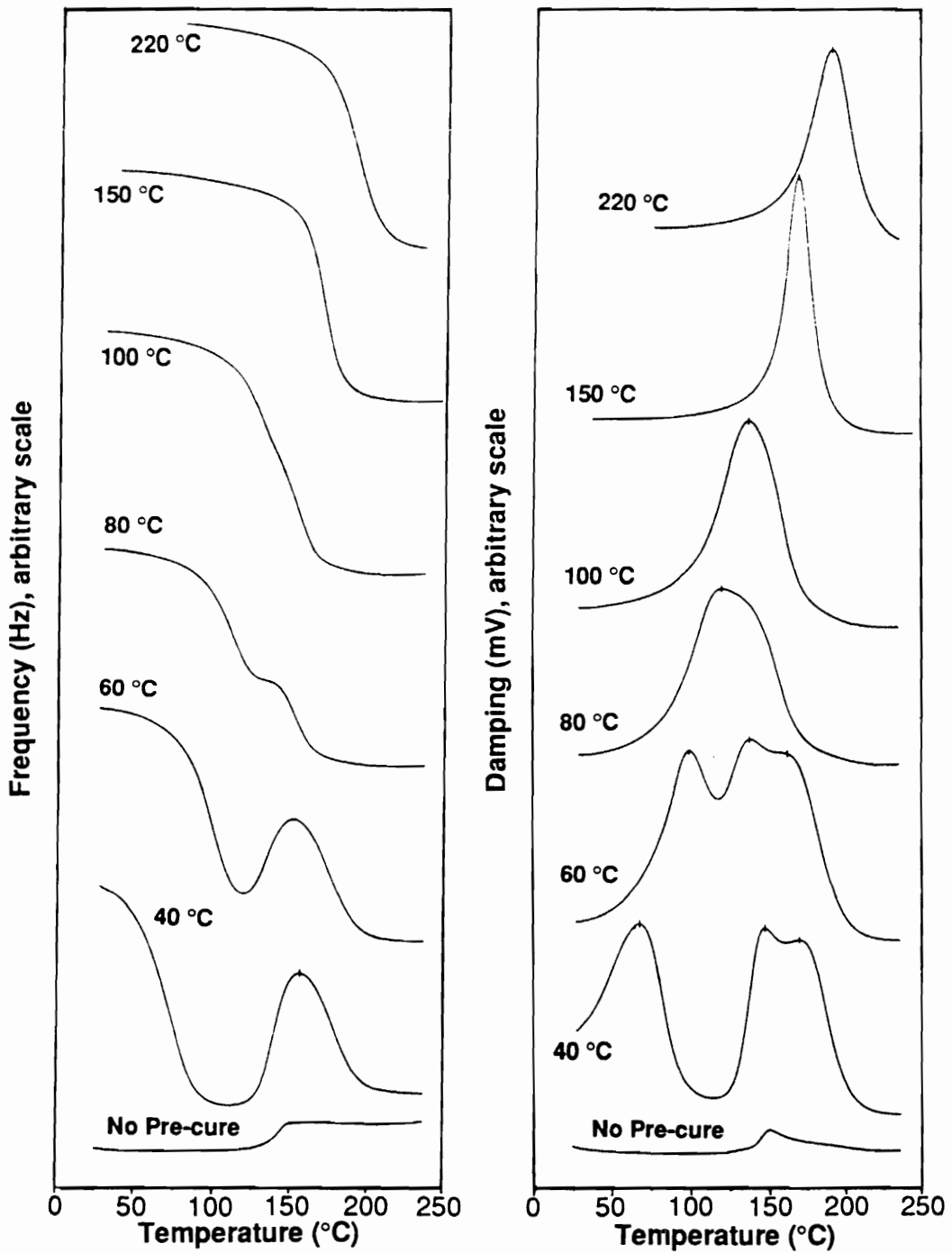


**Figure 2.4.27** 5 °C/minute dynamic DMA scans as a function of pre-cure temperature in neat epoxy.



also been observed before by varying the curing chemistry<sup>161c</sup> and the scanning rate.<sup>215,216</sup>

In a system undergoing dynamic cure, two temperature parameters come into play. The first is the increasing experimental temperature or the temperature of the sample,  $T_s$ . In the present case, the rate of increase of sample temperature is fixed by the DMA scan rate. i. e.  $dT_s / dt = 5 \text{ }^\circ\text{C}/\text{min}$ . The second temperature parameter is the glass transition temperature  $T_g$  of the system. The  $T_g$  of the system is also increasing as further cure takes place during the temperature scan. However, the rate of change of  $T_g$ , i. e.  $dT_g / dt$ , varies according to the rate at which crosslinking takes place at any given point. In addition, it also depends on the conversion at the point: the  $T_g$  rises slowly with respect to conversion in the initial stages, but does so rapidly as it approaches full cure- an experimental evidence<sup>217</sup> well supported by theoretical expressions such as the DiBenedetto Equation.<sup>171</sup>

The rate of reaction in the system itself is dependent on a combination of chemical and physical kinetic restrictions. The chemical kinetics is a function of the concentration of the reacting species through the mechanism of the reaction and on the temperature through the Arrhenius relationship. The physical kinetics is governed by the mobility of the reacting species. The latter can be considered to be a function of the  $(T_s - T_g)$  window. For a negative window, i. e. when the system is in the glassy state, there is little reaction since it is controlled by diffusion limitations. Consequently, the  $T_g$  of the system, being related to the extent of reaction in the system, changes very slowly with respect to the sample temperature  $T_s$ . This allows  $T_s$  to surpass  $T_g$  at a certain point. As this happens, the sample devitrifies and crosslinking reaction resumes. However, the rate of reaction will be dependent on which of the two restrictions, physical or chemical, plays the dominant role.

For a small  $(T_s - T_g)$ , the physical or diffusion controlled kinetics is the rate determining mechanism, whereas at higher  $(T_s - T_g)$ , the chemistry governs the dynamics of the system. Thus, the competition between the sample temperature and the glass transition temperature determines the cure path as well as the accompanying rheological changes.

The above arguments may be elaborated by taking the dynamic cure behavior of the 40 °C pre-cure sample which is reproduced on Figure 2.4.28 together with a proposed model that elucidates the relationship between  $T_g$  and  $T_s$  in the system during the scan. According to the model, the entire scan may be divided into six stages:

*Stage I:* The sample has a  $T_g \geq 40$  °C since it has been pre-cured at that temperature. Starting the scan at room temperature,  $T_s - T_g < 0$ . Therefore, the reaction is diffusion controlled and the  $T_g$  increases very slowly. Frequency and damping responses nearly constant. The result is that  $dT_s / dt > dT_g / dt$ . At the end of this stage,  $T_s$  equals  $T_g$ .

*Stage II:* Devitrification occurs as  $(T_s - T_g) \geq 0$ . Reactions resumes with the controlling mechanism in transition between physical and chemical control. There is a drop in frequency and a peak in damping.  $T_g$  increases at rate faster than stage I. Still,  $dT_s / dt > dT_g / dt$ .

*Stage III:* In the beginning,  $(T_s - T_g) \gg 0$ . The reaction is chemically controlled. Higher temperature and concentrations of the reactant species promote faster rate. As a result,  $dT_g / dt > dT_s / dt$ . Frequency and damping response remain at low levels indicating rubbery nature of the system.  $(T_s - T_g)$  decreases

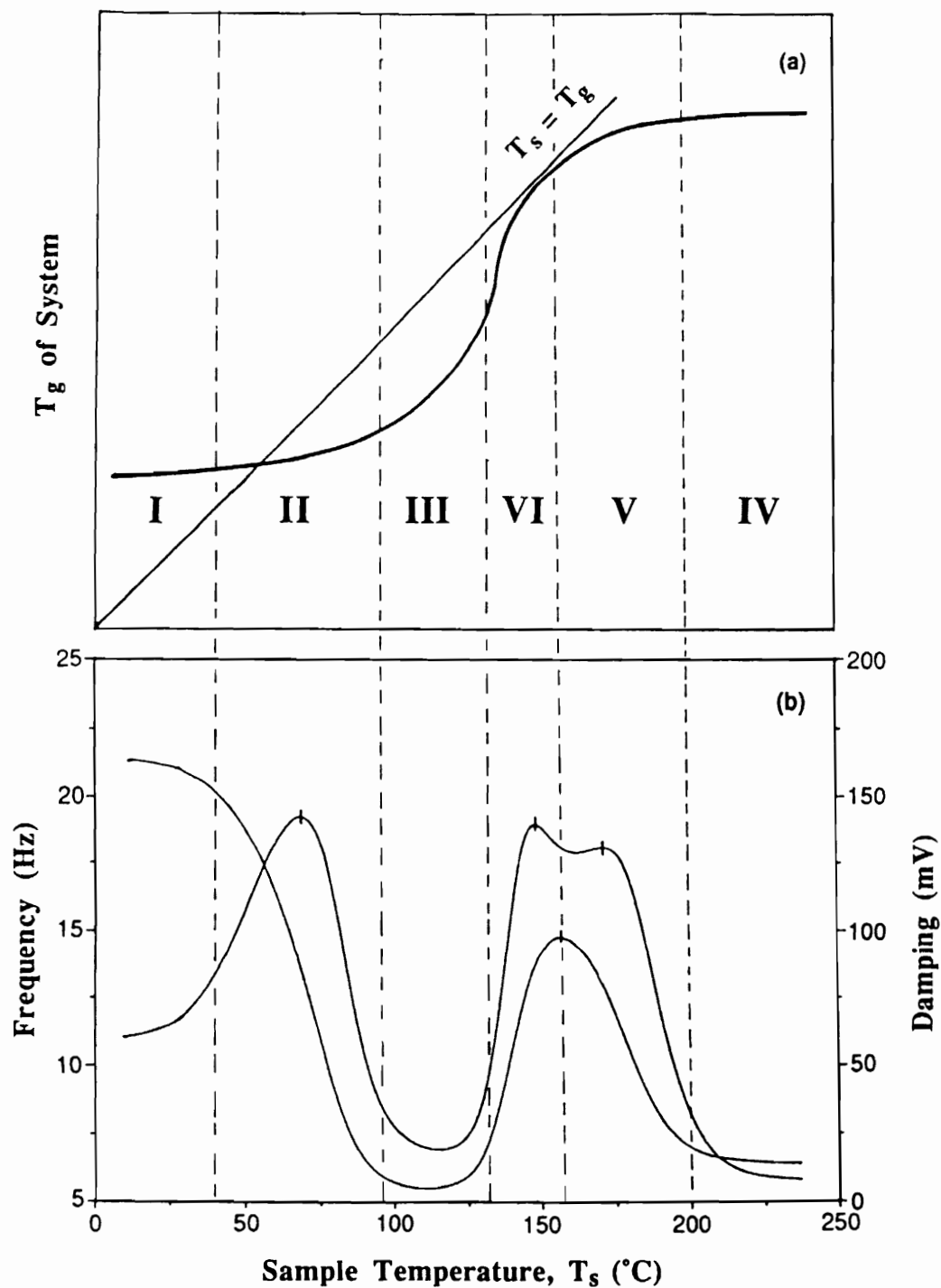


**Figure 2.4.28** (a) Model suggesting various stages in which the glass transition temperature,  $T_g$ , of the system competes with the sample temperature,  $T_s$ , in explanation of: (b) dynamic DMA curves after 40  $^{\circ}\text{C}$  isothermal pre-cure.

and approaches zero, and the controlling mechanism transfers from chemical to physical at the end of the stage.

*Stage IV:* Vitrification occurs as  $T_g$  catches up with  $T_s$  as indicated by a peak in damping and a rise in frequency. However, as the reaction slows down due to vitrification,  $T_s$  once again begins to advance faster than  $T_g$ .

*Stage V:* Before vitrification in stage IV is completed, the gap ( $T_s - T_g$ ) reverses causing a second devitrification, and therefore, a damping peak and frequency drop.

*Stage VI:* The system remains in the rubbery state for the remainder of the scan completing the residual reaction which is not considerable enough to allow the  $T_g$  to further compete with  $T_s$ . The frequency and damping responses remain fairly constant.

The effect on the level of initial cure on this multi-stage behavior is on the breadth and location of the intermediate stages. As one starts with a sample having a higher initial  $T_g$ , or the sample isothermally pre-cured at a higher temperature, the first devitrification transition (stage II) is shifted to the right, while the vitrification (stage IV) and second devitrification (stage V) are shifted towards the left. This can be seen in the 60 °C and 80 °C curves on Figure 2.4.27. For 100 °C pre-cure sample, all three transitions seem to merge together into one broad transition. Finally, at higher pre-cure temperatures of 150 °C and 220 °C, only one devitrification transition is obtained.

### 2.4.2.1.3 Glass Transition Temperature of Fully Cured System.

The glass transition temperature of fully cured samples,  $T_{g\infty}$ , obtained by the third step of 5 °C/min dynamic scan is also a function of the initial temperature of isothermal cure as evident from Figure 2.2.29. There is a minimum in  $T_{g\infty}$  with respect to the pre-cure temperature with the highest values occurring at 40 °C and 220 °C, the two extreme temperatures utilized. TGA data may help partially understand this behavior. Figure 2.2.30 shows dynamic TGA scan on a previously uncured epoxy reaction mixture in nitrogen. It can be seen that the sample loses ca. 4.5% of its original weight during the scan. The weight loss most likely comes from volatilization of NMA since it is the most volatile of the three ingredients of the neat epoxy system. The loss of NMA causes a stoichiometric imbalance in the system. In an epoxy-anhydride system, any deviation in the 1:1 stoichiometry has been found to lower its final  $T_g$ .<sup>218</sup> The nature of the TGA weight loss with respect to the temperature provides a further explanation to the  $T_{g\infty}$  minimum in Figure 2.4.29. At lower temperatures, there is very little weight loss due to insufficient thermal energy. As the scan approaches higher temperatures, a rapid volatilization of NMA is favored, but only to be stopped abruptly when the system reaches its gel point. Analogously, in the isothermal cure, the two extreme temperatures may be expected to promote the least NMA loss and hence the smallest drop in  $T_{g\infty}$ .

In addition to the effect of NMA volatilization, other factors may also have contributed to the variation of  $T_{g\infty}$  with cure conditions. For example, thermo-degradative side reactions may be operative at higher temperatures that can cause an increase in the crosslink density and, therefore, in the glass transition temperature of the system. It is also possible that the cure path affects the formation of network structure<sup>219-221</sup> leading to changes in the  $T_{g\infty}$ .

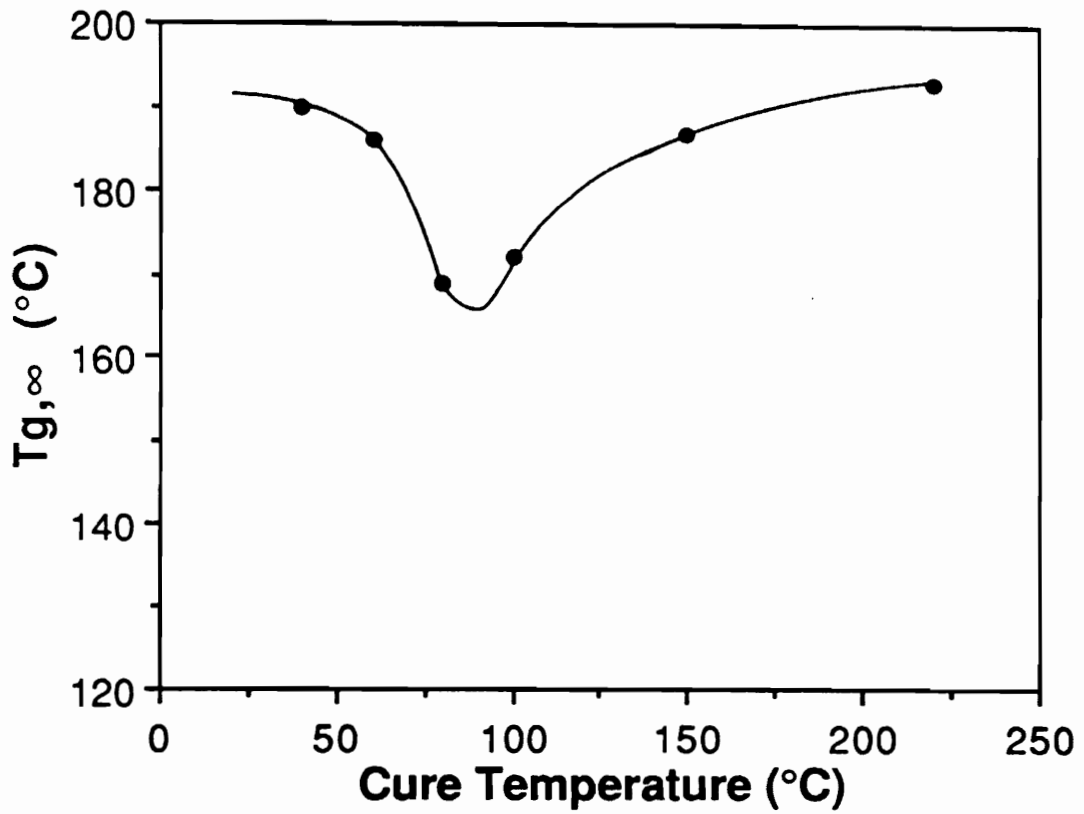


**Figure 2.4.29** Relationship between  $T_{g,\infty}$ , the glass transition temperature of the fully cured system, and the isothermal pre-cure temperature in neat epoxy.

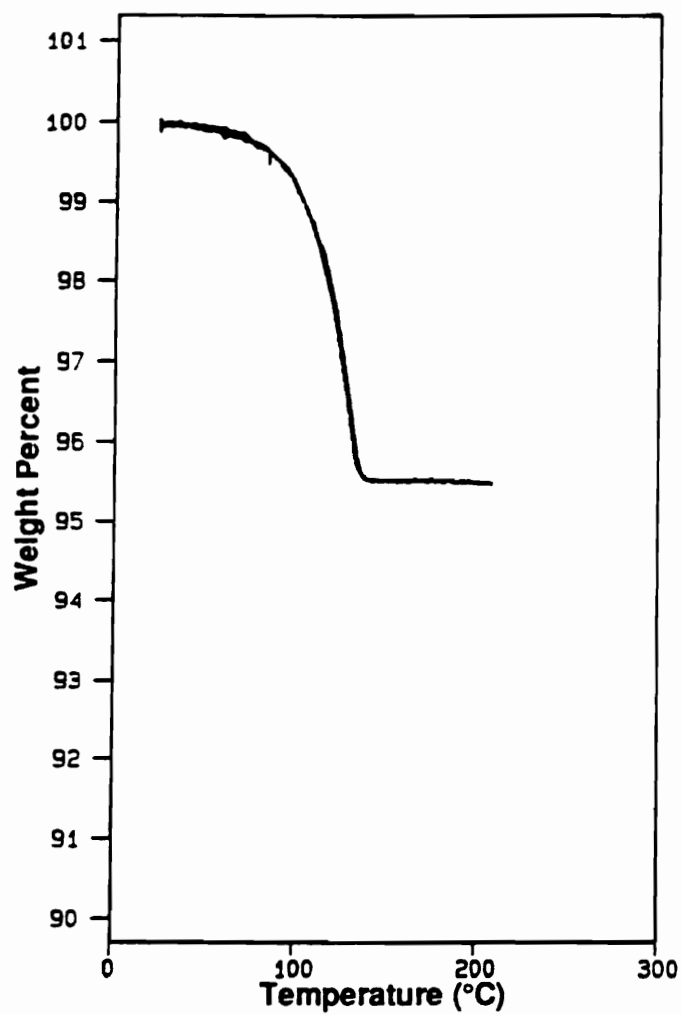


**Figure 2.4.30** 5 °C/minute dynamic TGA scan of previously uncured neat epoxy in nitrogen.

In any case, perhaps the most important observation that can be made from the above results is that one may not expect a single  $T_{g\infty}$  from a given system. The final properties of the thermoset is not only determined by the chemistry of the initial system, but also by the thermal history it encounters during cure.

## 2.4.2.2 PPO-modified Epoxy.

### 2.4.2.2.1 Isothermal Cure.

Figure 2.4.31 displays the isothermal cure scans on 10% PPG-1025 containing Quatrex-2010/NMA/DMP-30(2%) samples at three selected temperatures: 60 °C, 100 °C, and 150 °C. The 60 °C cure curves display two transitions due to gelation and vitrification respectively. The 150 °C cure curves display only gelation since the  $T_{g\infty}$  of the system is reduced below 150 °C due to the presence of PPO (see Section 2.4.2.2.3). The most unusual observation, however, can be made on the 100 °C curves. Here an additional transition occurs between the lower gel point and the higher vitrification point. This can be more clearly seen on Figure 2.4.32 where the 100 °C cure behaviors of the neat and PPO-modified epoxy are compared. The neat epoxy curves show the transitions of gelation and vitrification, whereas the modified epoxy curves display these two as well as an intermediate transition at approximately 35 minutes. Since the only difference between the two systems is that the latter contains 10% PPG-1025, a question arises whether the additional transition in the modified sample is related to the phase separation process. The polymer matrix becomes richer in epoxy during phase separation. As a result, an increase in the overall modulus of the system may be expected. If the modulus change by either of the two critical phenomena, e. g. gelation and vitrification, does not overlap with that due



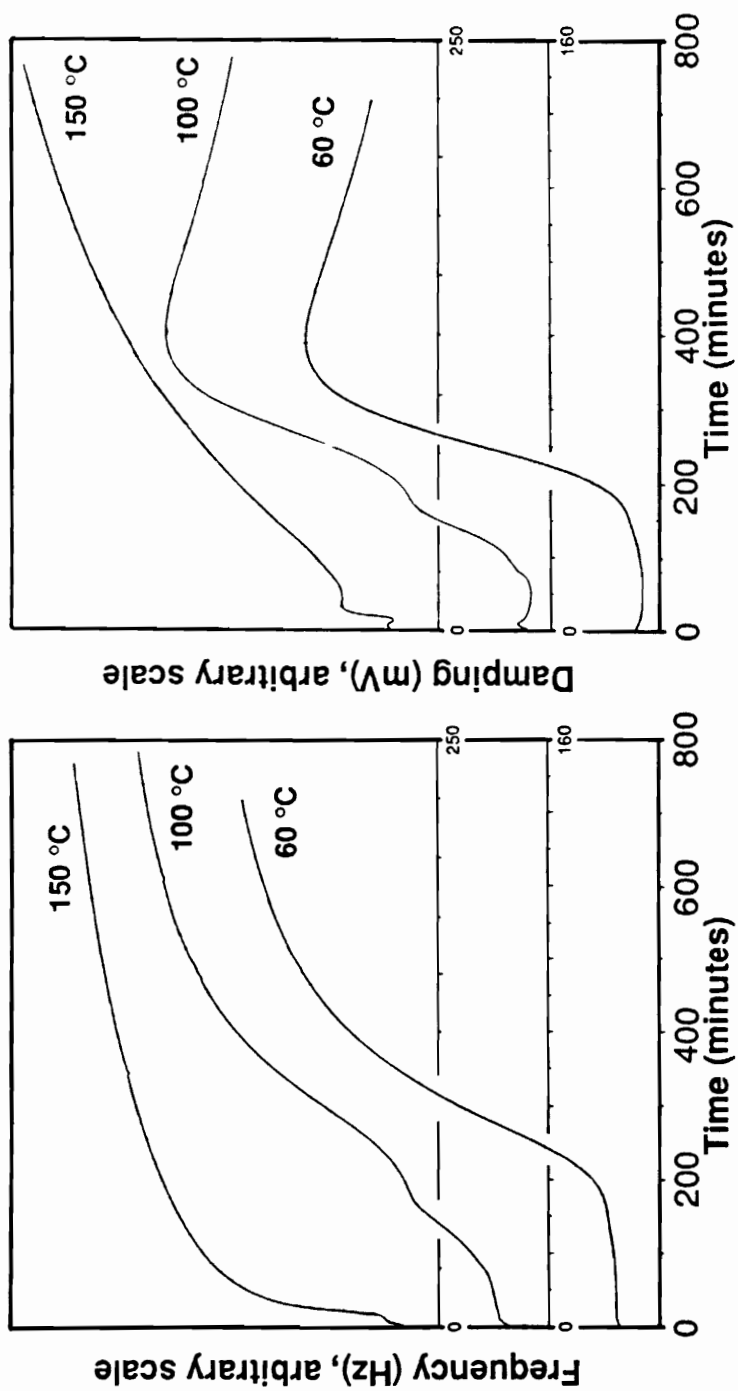


**Figure 2.4.31** Isothermal DMA curing curves of PPO-modified epoxy.

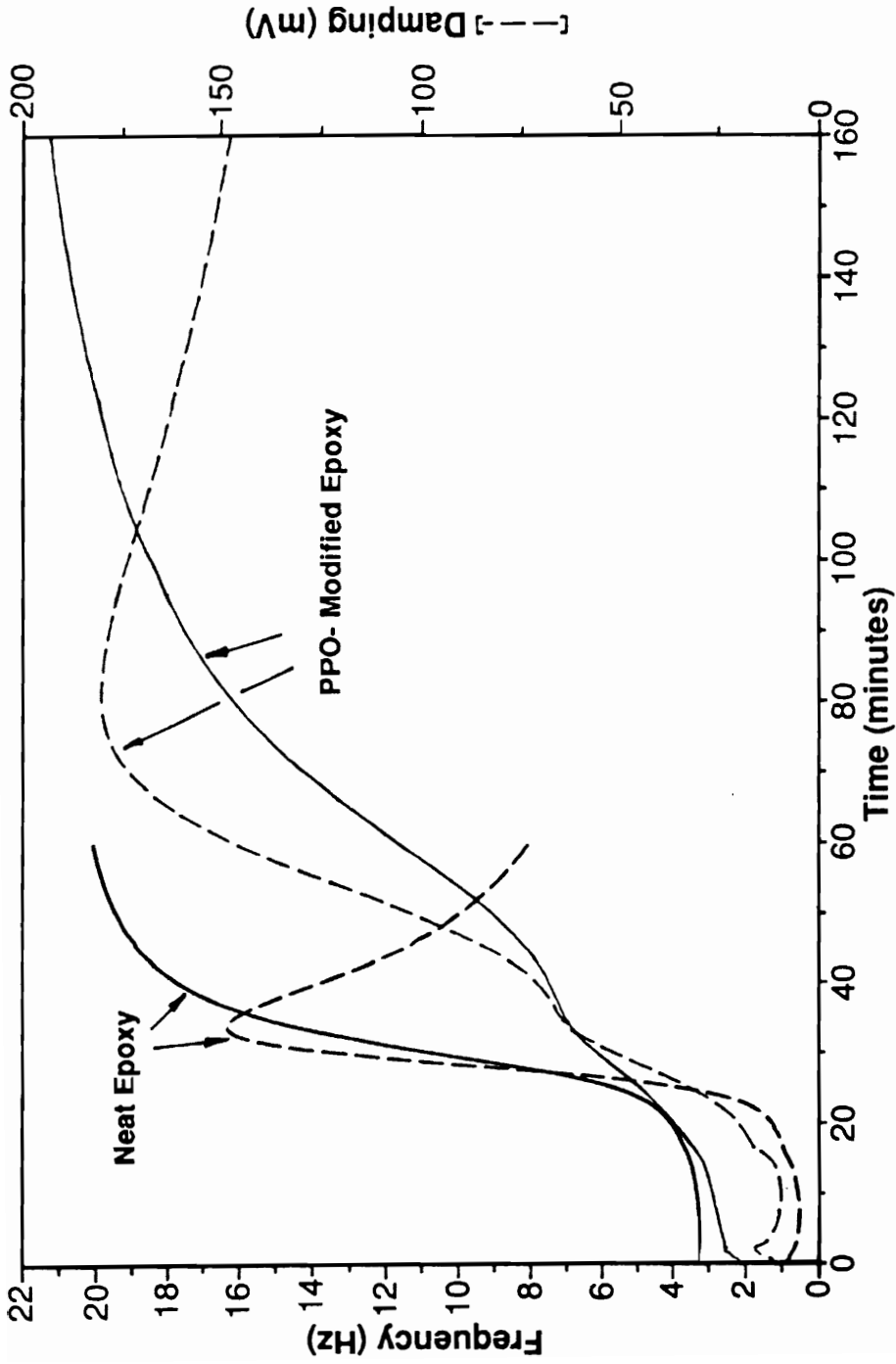
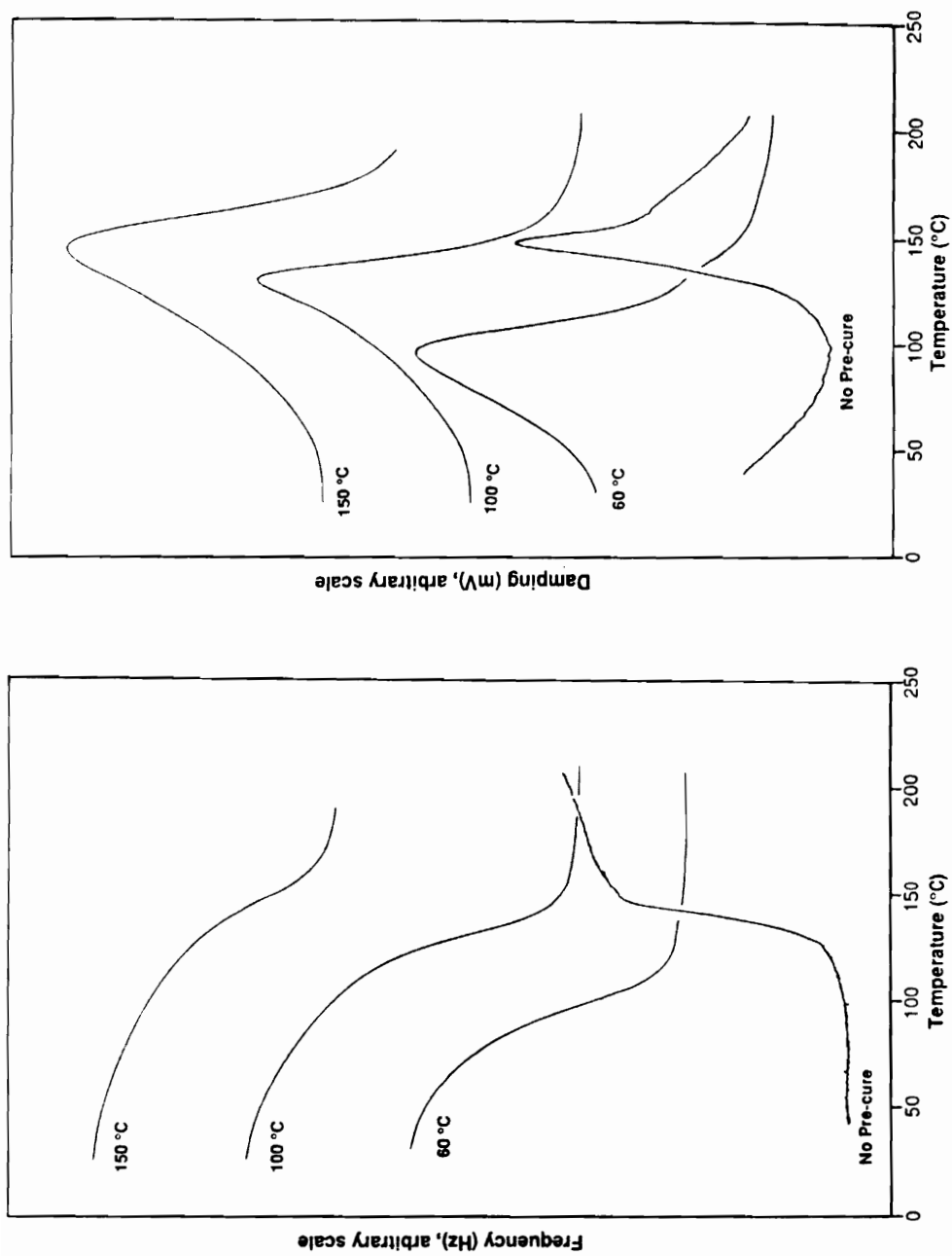


Figure 2.4.32 Comparison of the 100 °C isothermal curing behavior of neat and PPO-modified epoxy.

to phase separation, then an individual transition due the latter may be possible. If this is indeed the true in the present case, this is probably the first time the occurrence of phase separation has been detected via a dynamic mechanical measurement. An another important issue that may be addressed here is the general perception that most of the phase separation occurs well before gelation due to the restriction to diffusion in the high viscosity post-gelation period. As discussed in Section 2.2.1.2, a few instances of morphological changes after gel point have been reported based mostly on light transmission measurements.<sup>129,131,134,137</sup> Whether these changes can be significant enough to offer a major contribution to rheological behavior has not been studied. The results of this study point towards this possibility. However, much more work would be necessary to make any further generalizations.

#### **2.4.2.2.2 *Dynamic Cure.***

Figure 2.4.33 displays the 5 °C/minute dynamic cure scans on the PPO-modified samples with varying degree of pre-cure. Comparison can be drawn to the dynamic cure behavior of the neat epoxy system of Figure 2.4.27. The sample without pre-cure here also shows only one transition which can again be attributed to gelation. On the other hand, the samples pre-cured at 60 °C, 100 °C, and 150 °C do not display the multi-transition behavior, unlike their counterparts in the neat epoxy system. A subtle indication of a secondary transition after the first devitrification is noticeable only on the damping curve of the 60 °C pre-cure sample in the form of a shoulder on the high temperature side. The devitrification transitions in each of the pre-cured samples are rather broad suggesting that some reaction does take place during the scans. Due to the presence of PPO, however, the  $T_g$  does not increase fast enough to compete with the sample temperature  $T_s$ . Therefore,



**Figure 2.4.33** 5 °C/minute dynamic DMA scans as a function of pre-cure temperature in PPO-modified epoxy.

the system remains under chemical control during the entire scan and the additional vitrification-devitrification transitions are not obtained.

#### **2.4.2.2.3 Glass Transition Temperature of Fully Cured System.**

The dependence of the  $T_{g\infty}$  of PPO-modified samples on the pre-cure temperature is depicted on Figure 2.4.34. The behavior is quite different from that of the neat epoxy system seen on Figure 2.4.29. The  $T_g$  increases monotonically with the pre-cure temperature, the highest value of 146 °C being obtained at the pre-cure temperature of 150 °C. In addition to NMA volatilization, the final  $T_g$  will now depend also on the thermal loss of PPO itself and the nature of phase separation of PPO (hence, the extent to which PPO is phase-mixed into epoxy matrix). More work is required to differentiate the various contributions before further explanations can be offered.

#### **2.4.2.3 TTT Diagram.**

The quantitative information obtained from the above DMA experiments can be organized as a TTT diagram as shown on Figure 2.4.35. The  $T_{g0}$ 's, or the glass transition temperatures of the unreacted neat and PPO-modified epoxy mixtures, were obtained from 5 °C/minute dynamic scan on samples without the catalyst. The  $T_{g\infty}$  for the neat epoxy system is shown to be 193 °C which is the highest value obtained in the 220 °C pre-cured sample. As one would expect, the vitrification curve is S-shaped. Also, the gel time decreases as the temperature of cure increases. Both the gel times and vitrification times are higher in case of the PPO-modified system than in the neat epoxy system when compared at the same cure temperature.

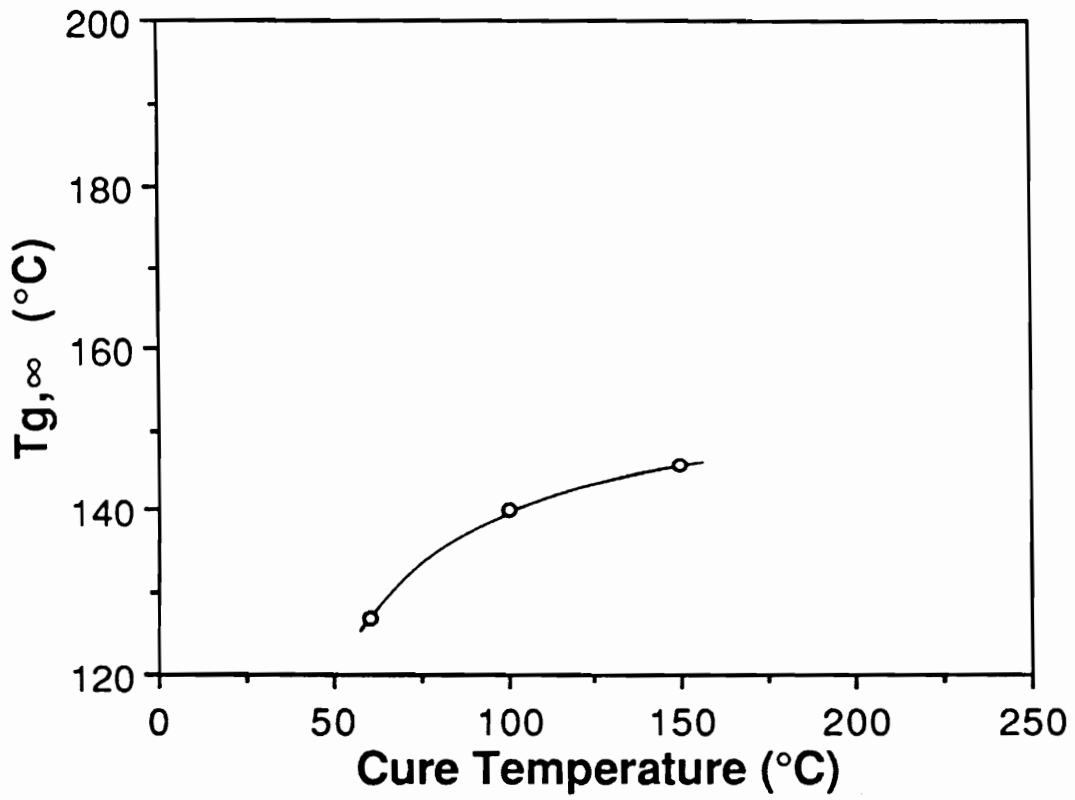


**Figure 2.4.34** Relationship between  $T_{g,\infty}$ , the glass transition temperature of the fully cured system, and the isothermal pre-cure temperature in PPO-modified epoxy.

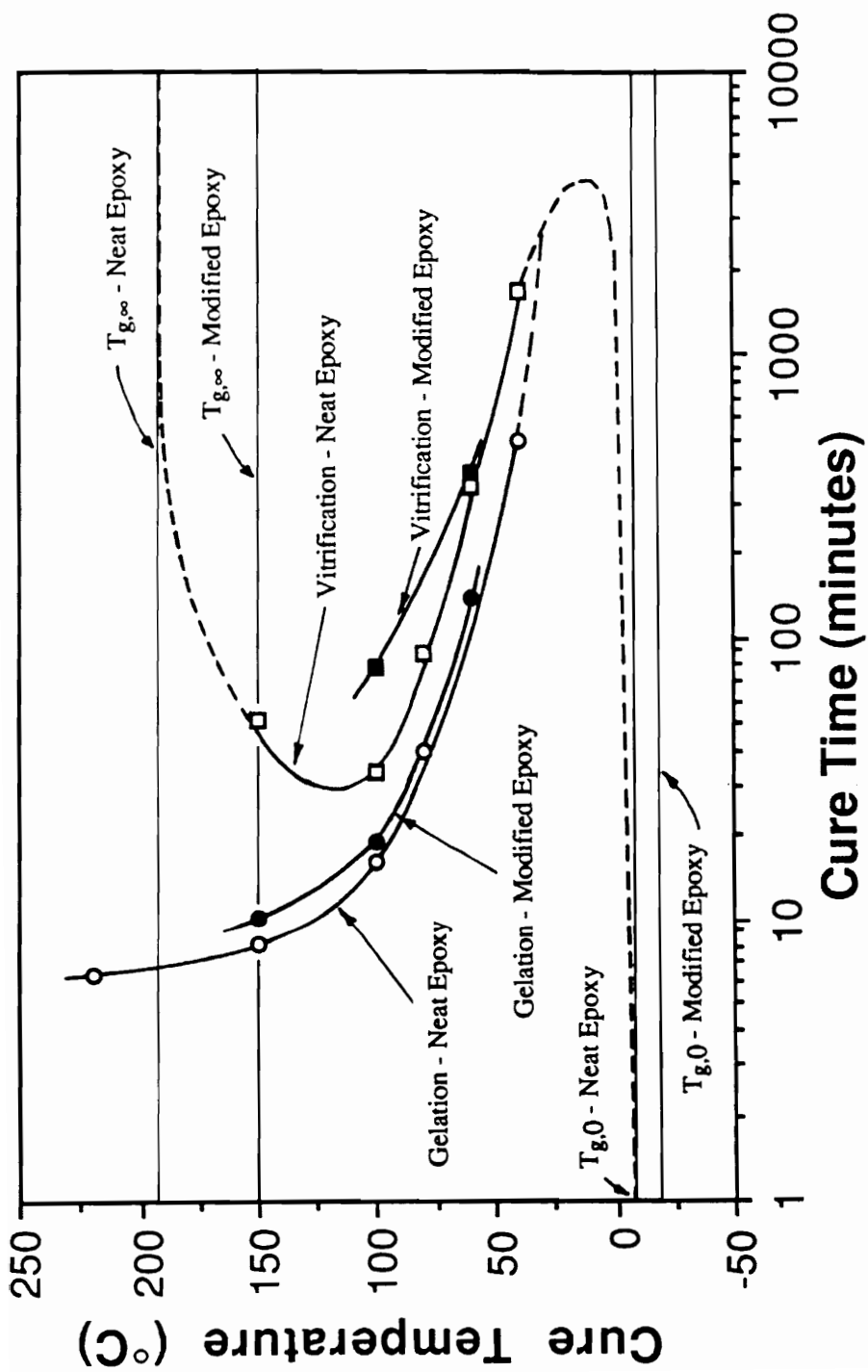


Figure 2.4.35 TTT diagram based on the DMA data of neat and PPO-modified epoxies.

### 2.4.3 Degradation Behavior and Microporosity Development.

In this section, the results of thermal characterization by TGA and DMA in conjunction with scanning electron microscopy are presented with the principal aim to demonstrate the applicability of the two-step approach outlined in Section 2.1 for microporosity development. The epoxy system used in this study was Quatrex-2010 cured with NMA and DMP-30 (2% by weight based on resin plus curing agent). The poly(propylene oxide) used was PPG-1025.

#### 2.4.3.1 Thermogravimetric Analysis.

##### 2.4.3.1.1 *Neat Poly(propylene oxide).*

Dynamic TGA scans of PPG-1025 in air and nitrogen atmospheres are compared in Figure 2.4.36. In the presence of air, PPG-1025 decomposes rapidly after ca. 200 °C. The scan in nitrogen is shifted toward higher temperature, signifying that the degradation is accelerated considerably in the presence of oxygen. This can be seen more clearly from the isothermal scans shown on Figure 2.4.37. At 200 °C, PPG-1025 decomposes completely within 15 minutes or so in air whereas there is very little weight loss in nitrogen even after 12 hours. This difference between degradation rates in air and nitrogen would be an important consideration in case of cured films. The diffusion of oxygen to the bulk will be necessary for efficient conversion of PPO into volatile low molecular weight species. Figure 2.4.37 also displays the degradation characteristics of two lower temperatures in air. The degradation rate is considerably reduced at 150 °C in comparison to 200 °C, while it is practically zero at 60 °C. These TGA results on neat PPG-1025 suggest that 200 °C would



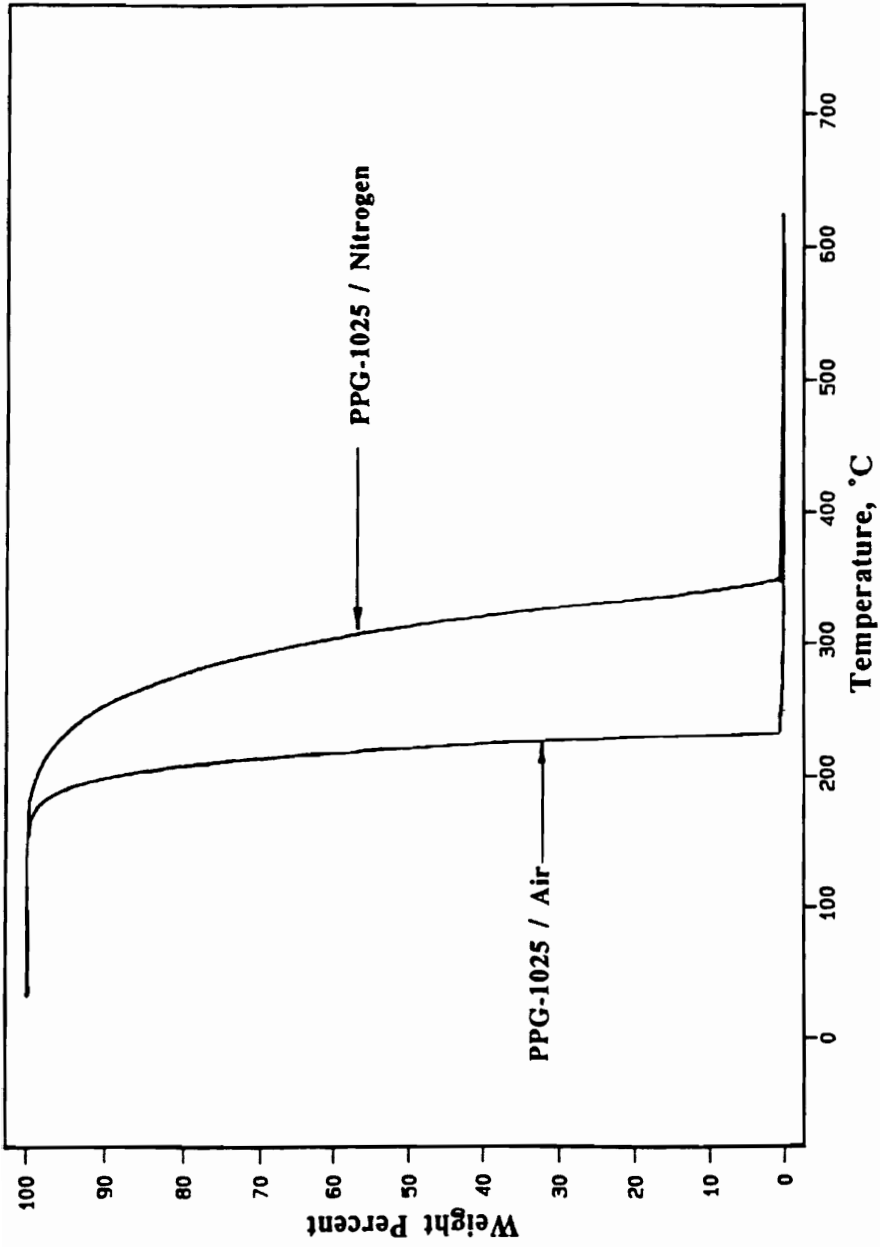
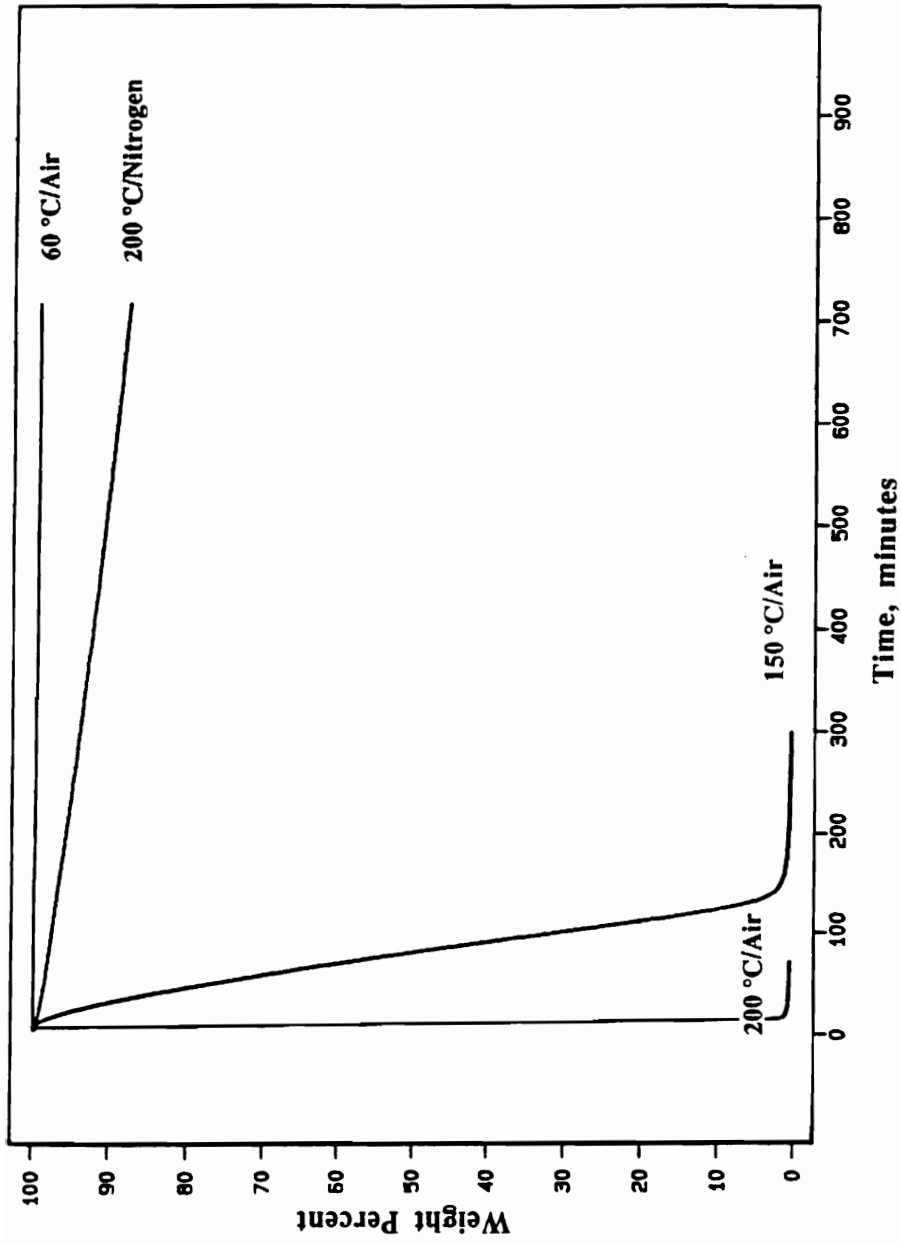


Figure 2.4.36 5 °C/minute dynamic TGA scans of PPG-1025 in air and nitrogen.



**Figure 2.4.37** Isothermal TGA scans of PPG-1025 in air and nitrogen at different temperatures.

be an appropriate temperature for development of porosity in cured systems provided epoxy itself does not show appreciable degradation at this temperature.

#### **2.4.3.1.2 Cured Films.**

Figure 2.4.38 shows the 200 °C isothermal degradation behavior of samples cured at 60 °C for 12 hours plus 150 °C for 3 hours. Two comparisons have been made on this figure: one between neat epoxy and 10% PPG-1025 containing epoxy and the other between bulk films and the relatively thin wire-mesh films (~1 mm vs ~0.125 mm). Both neat epoxy films show significant weight loss. The source of this may be thought to be either the catalyst DMP-30 or some monomeric NMA that may have remained unincorporated in the network after the cure cycle. Alternatively, it may represent low molecular weight volatiles that are usually present in commercial grade epoxies. As would be expected, the weight loss in the PPO-modified samples is considerably greater than that in their neat counterparts. The film thickness can be shown to be an important degradation variable by comparison of scans on PPO-modified bulk and wire-mesh films. The latter shows over 10% weight loss at the end of the experiment (after ~1000 minutes), which is nearly twice as much as that in the former. This is not surprising if one considers the degradation to be controlled primarily by diffusion, both with respect to the required amount of oxygen reaching the phases and the degradation products evolving from the film.

#### **2.4.3.2 Dynamic Mechanical Analysis.**

Figures 2.4.39 and 2.4.40 compare the dynamic mechanical properties of the wire-mesh samples before and after heat treatment at 200 °C for 12 hours. The samples were cured at

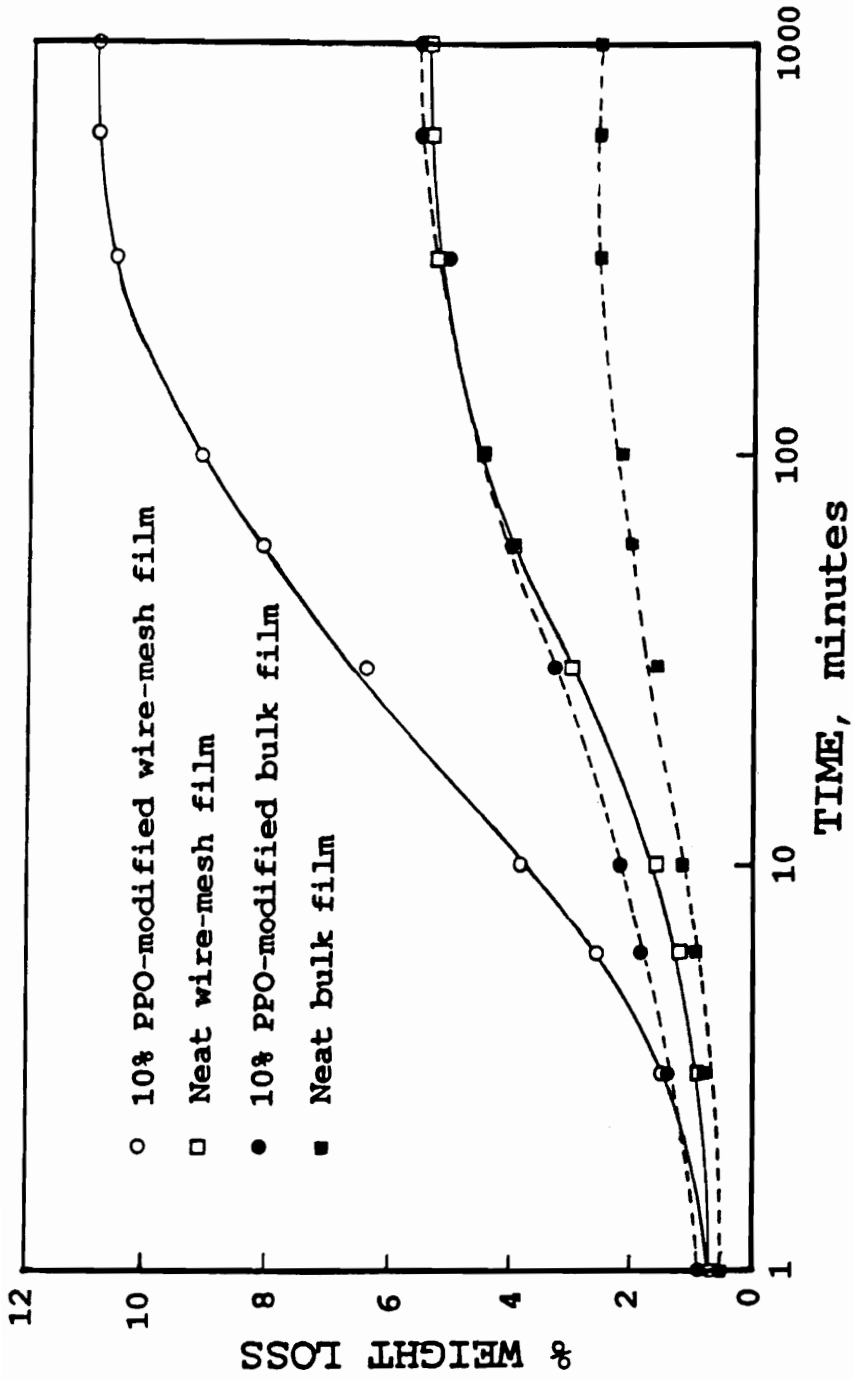


**Figure 2.4.38** 200 °C isothermal TGA scans in air of neat and 10% PPG-1025 containing epoxy systems cured at 60 °C/12 hours + 150 °C/3 hours.

60 °C for 12 hours plus 150 °C for 3 hours prior to the heat treatment. As shown in Figure 2.4.39, the DMA scan on neat epoxy contains two damping peaks, one at 162 °C due to its glass transition and the other in the low temperature region at -44 °C that may be attributed to the  $\beta$ -transition. The scan on 10% PPG-1025 containing sample also shows two damping peaks; however, the low temperature transition, which occurs at the same temperature of -44 °C, is much stronger in this case. This is due to the fact that the main  $T_g$  peak of PPG-1025 overlaps the  $\beta$ -peak of the epoxy matrix. It is also important to note that the damping peak of epoxy  $T_g$  is higher in the neat sample than in the 10% PPG-1025 sample (162 °C vs 150 °C) signifying some phase mixing in the latter. Figure 2.4.40 shows the DMA scans of the two samples *after* the heat treatment. It is quite evident here that the contribution of PPO to the low temperature damping has nearly disappeared. The low temperature zones of both samples look essentially the same. Also the positions of the main  $T_g$  peaks of the epoxy matrix are identical in the two samples. These results strongly suggest that the heat treatment did bring about the degradation and removal of a major portion of the PPO from the epoxy matrix. An another important observation can be made from the initial frequencies displayed by the samples (in the low temperature region below the  $\beta$ -transition of epoxy and the main  $T_g$  of PPO). Before heat treatment, as seen on Figure 2.4.39, the neat and PPO-modified sample both display similar initial frequencies, and therefore similar modulus. However after the heat treatment, as evident on Figure 2.4.40, the initial frequency in the PPO-modified sample is considerably lower than that in the neat epoxy sample. This suggests that after the 200 °C heat treatment, the PPO-modified sample may have become less dense or porous, assuming that the matrix did not collapse after removal of PPO to fill up the voids. The fact that this does not occur was observed with the help of SEM as discussed in the following section.

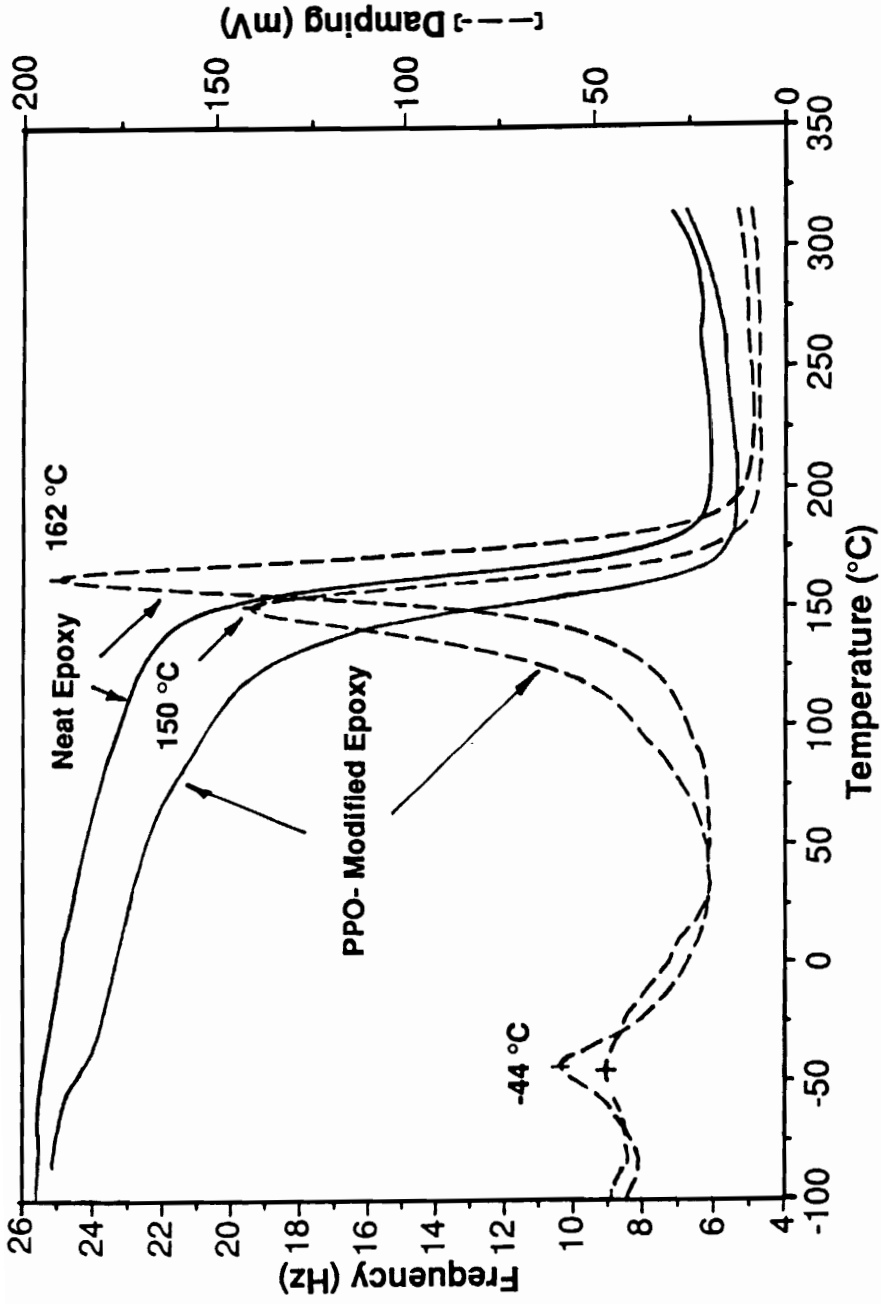


**Figure 2.4.39** 5 °C/minute dynamic DMA scans on wire-mesh films of neat and 10% PPG-1025 containing epoxy systems cured at 60 °C/12 hours + 150 °C/3 hours.

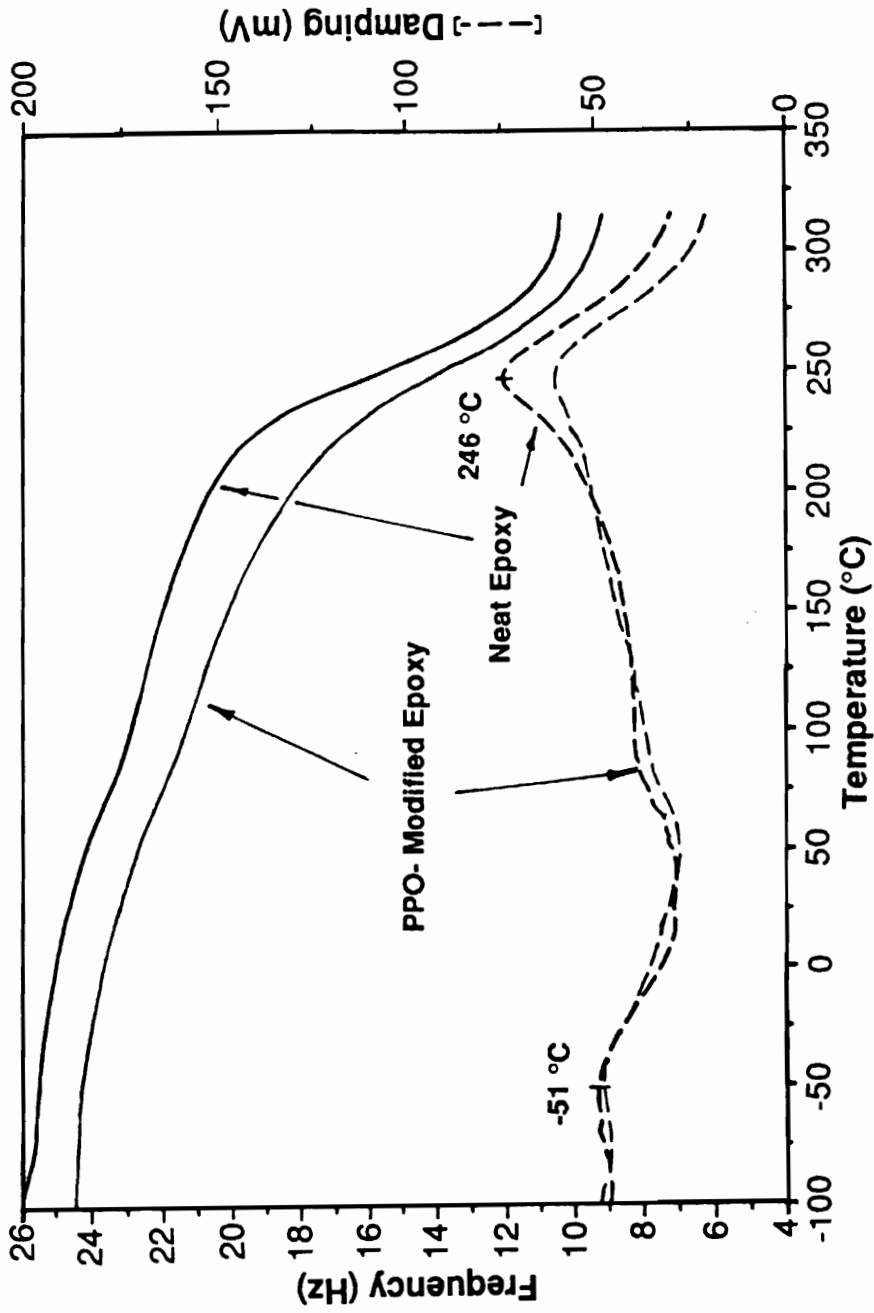


**Figure 2.4.40** 5 °C/minute dynamic DMA scans on wire-mesh films of neat and 10% PPG-1025 containing epoxy systems cured at 60 °C/12 hours + 150 °C/3 hours after heat treatment at 200 °C for 12 hours.

### 2.4.3.3 Scanning Electron Microscopy.

#### 2.4.3.3.1 *Bulk Film.*

Figure 2.4.41 shows the SEM photomicrographs of the fracture surfaces of a 10% PPG-1025 modified epoxy bulk sample cured at 60 °C for 12 hours plus 150 °C for 3 hours (a) before and (b) after heat treatment of 200 °C. Although, there does not seem to be a major difference between the two photomicrographs, a subtle change may be observed. The phase boundaries in Figure 2.4.41(b) are much brighter in comparison to those in Figure 2.4.41(a). Such a high level of contrast between the edge and the interior of the phases in the former may be attributed to absence of PPO. However, by no means this may be used as a positive demonstration of microporosity development. More importantly, the photomicrographs show that on heat treatment at 200 °C, the epoxy matrix does not fill up the empty space that may have been left by the expected removal PPO.

A conclusive evidence of microporosity development can be seen on Figure 2.4.42 where the air-side surfaces, instead of the cross-section, of the above sample before and after the heat treatment are compared. Clearly, the surface of the sample after 200 °C for 12 hour has developed distinct porosity of sizes comparable to the bulk phases of Figure 2.4.41. Thus, the selective degradation of PPO phases from the epoxy matrix is successfully accomplished under the given conditions.



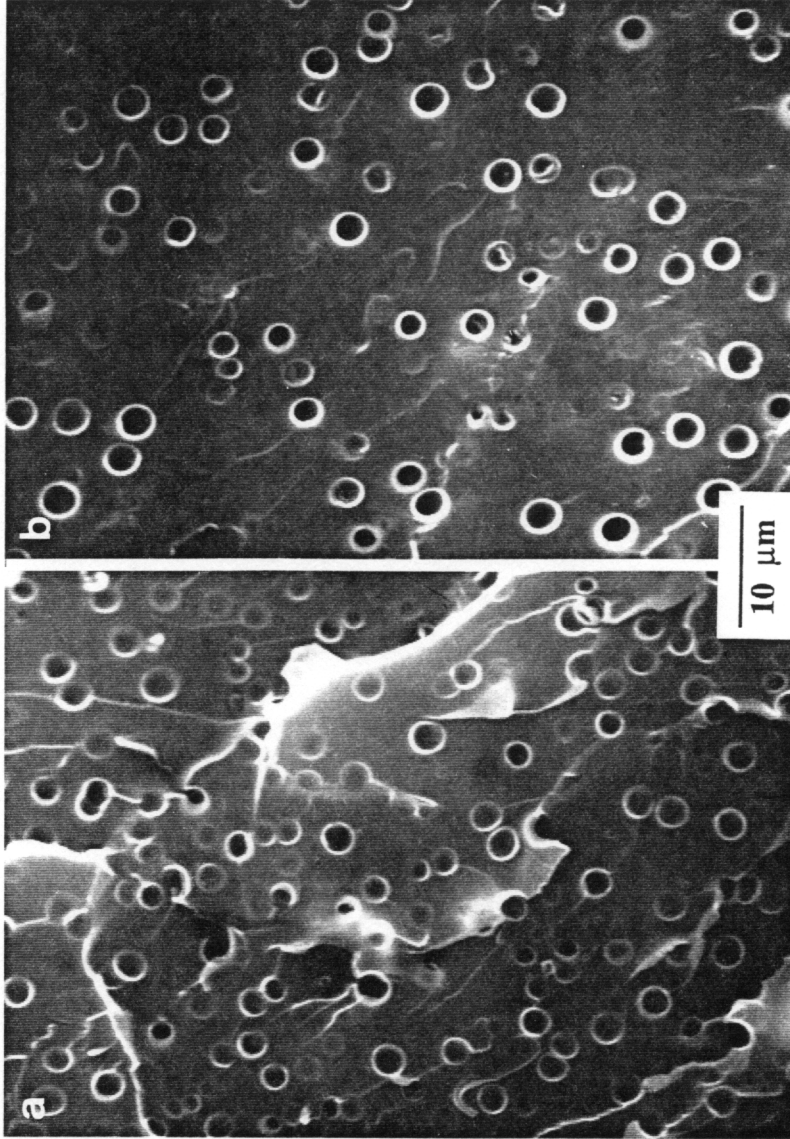


**Figure 2.4.41** SEM photomicrographs showing the effect of heat treatment at 200 °C for 12 hours on the bulk morphology of 10% PPG-1025 containing epoxy sample cured at 60 °C for 12 hours + 150 °C for 3 hours. (a) before heat treatment, and (b) after heat treatment.

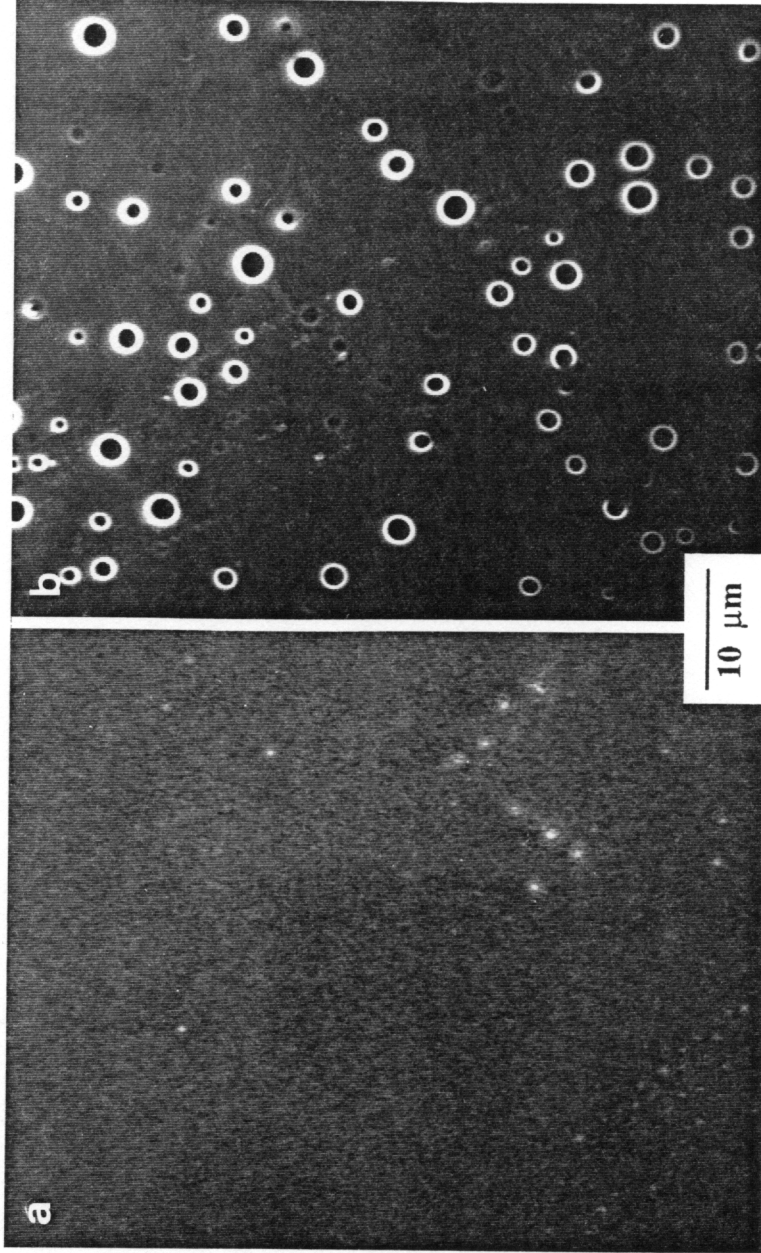


**Figure 2.4.42** SEM photomicrographs showing the effect of heat treatment at 200 °C for 12 hours on the surface of 10% PPG-1025 containing epoxy sample cured at 60 °C/12 hours + 150 °C/3 hours. (a) before heat treatment, and (b) after heat treatment.

#### 2.4.3.3.2 *Disk Coatings.*

The objective for the study of the system as thin coatings was two-fold. The first was to see if the principles developed so far for thick films also hold for films of submicron thickness. The second aim was to demonstrate, as described in Section 2.1, the use of the porosity, if generated, to the practical application of enhancement in lubricant retention in magnetic disks. As described in the experimental section, two formulations were chosen: one containing 10% PPG-1025 and the other containing 25% PPG-1025. For comparison, their respective controls without PPO were also prepared.

*10% PPG-1025 Coating.* At the end of the cure cycle of 60 °C for 12 hours and 150 °C for 3 hours, the 10 % PPG-1025 coating was clear which implied an absence of phase separation. Heat treatment at 200 °C for 12 hours also produced no pores as seen from the photomicrograph of the coating surface on Figure 2.4.43(a). This is indeed in contrast with the morphology of the bulk sample of the same composition as seen so far. In addition, the absence of porosity in the disk coating was also in disagreement with the sample prepared by coating the same solution on a wire-mesh ribbon and curing simultaneously with the disk. Both the surface and the bulk of this thicker coating showed porosity as can be clearly observed from the photomicrographs of Figure 2.4.43(b) and (c) respectively. The thickness, being the only difference between the two cases, seems to be the influencing factor.

The effect of thickness may be direct or indirect. An example of the direct effect that may be considered is how the development of the phases itself is influenced by the thickness of the film, given that all other conditions are the same. When the thickness of the film is in

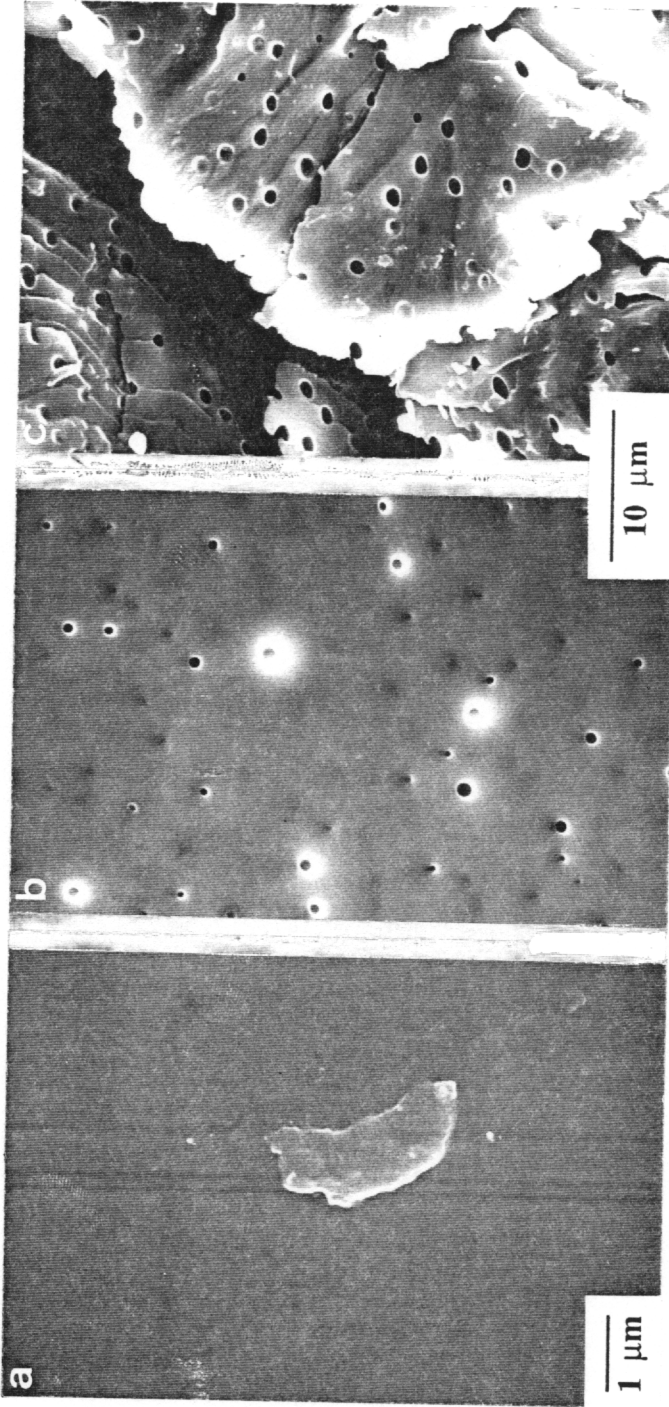


**Figure 2.4.43** SEM photomicrographs showing the comparison of the morphology of 10% PPG-1025 containing epoxy disk-coating with wire-mesh film of the same composition. (a) disk coating surface, (b) wire-mesh surface, and (c) wire-mesh film cross-section.

the same order of magnitude as the expected phase size, it may be possible that instead of discrete spherical phases, the separation occurs in the form of two layers with PPO as the top layer. Heat treatment removes the PPO layer leaving the bottom epoxy layer without any porosity. It may be visualized that the thick films also form a thin PPO layer on the top surface, but underneath this layer there may still be discrete phases. On heat treatment in this case, then, the removal of top PPO layer would expose the underlying discrete phases which in turn may degrade to form pores. An indirect effect of thickness may occur through the way temperature is distributed in a thick film in comparison to a thin film. For instance, the thicker film may attain a higher temperature than the temperature of its environment due to a less efficient disposal of the exothermic heat generated during cure. At this point, these arguments can at best be speculative; a more in-depth study would be required to differentiate the various possible sources that give rise to variation in morphology as a function of thickness under seemingly identical external conditions.

*25% PPG-1025 Coating.* The results of this coating were more positive. After curing at room temperature for 7 days and post-curing at 150 °C for 3 hours, the coating appeared hazy indicating that phase separation had occurred in this case. The coating was then heat treated to 200 °C for 12 hours and analyzed for porosity by SEM. Figure 2.4.44 shows the resulting photomicrographs at two magnifications displaying pores of sizes varying approximately from 0.5 to 3 μm. The presence of porosity was further proved by an enhanced capacity for lubricant retention. The porous PPO-modified coating held 14.0 mg of the lubricant as compared to 3.6 mg in case of the control coating prepared under similar conditions but without PPO. Thus an improvement of nearly four times in lubricant retention was obtained by creating microporosity in the coating.

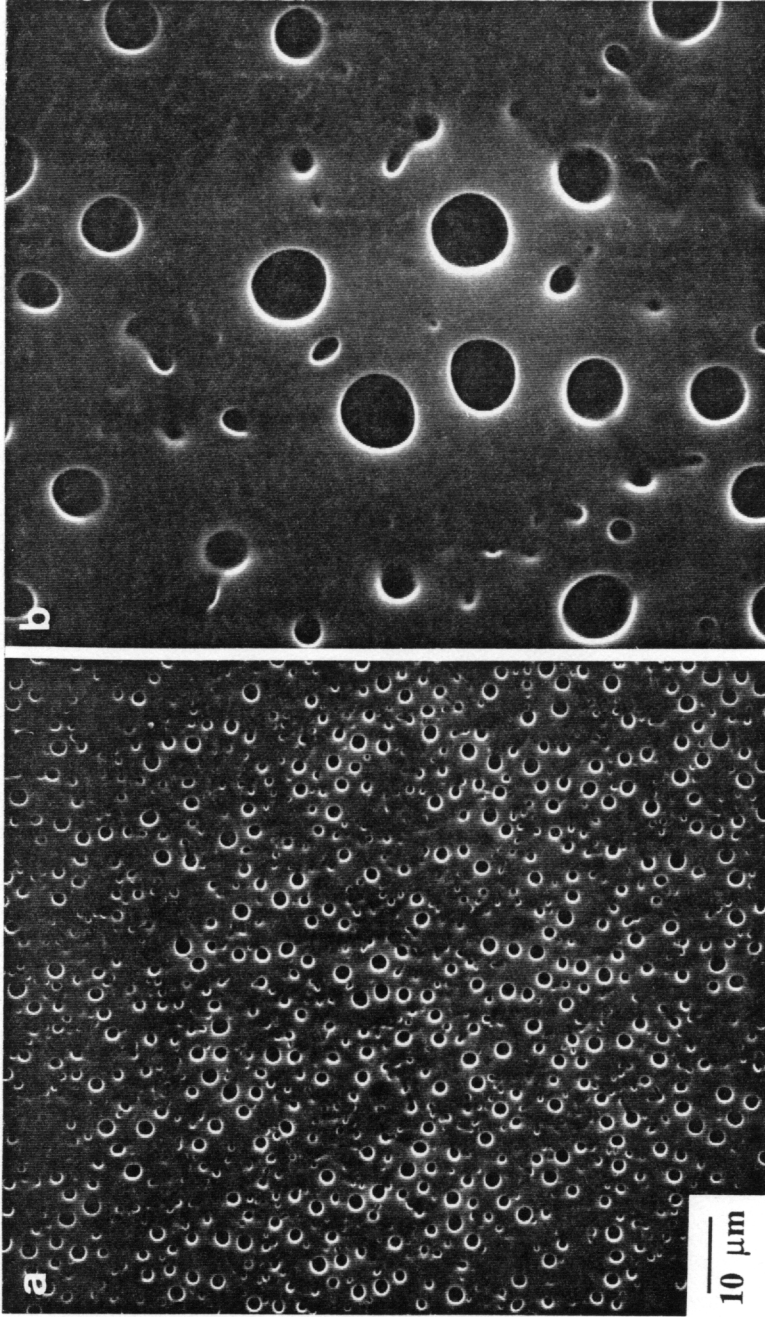


**Figure 2.4.44** SEM photomicrographs showing the surface morphology of 25% PPG-1025 containing epoxy disk-coating showing microporosity development after heat treatment of 200 °C for 12 hours.

## 2.5 CONCLUSIONS

The following general conclusions can be drawn from the three major areas addressed in the present study of poly(propylene oxide)- modified epoxies.

*Phase Separation Process and Morphology Control.* Morphology can be controlled by system variables such as cure chemistry, nature of poly(propylene oxide) end-groups, composition, cure temperature, molecular weight of poly(propylene oxide), and catalyst concentration. With the help of these variables, it was possible to not only obtain a range of phase sizes (from submicron levels to as high as 15  $\mu\text{m}$ ) and phase concentrations (giving rise to separated as well as close-packed domains), but also a change in the nature of the phase structure itself (from poly(propylene oxide)-discrete to epoxy-discrete; from stable micro-phase separated to incompatible grossly phase separated). The observed morphological behavior could be explained on the basis of chemical, thermodynamic, and kinetic factors involved in the phase separation process. It has been shown that the tendency towards phase separation as well as incompatibility may be qualitatively described by the with the help of the parameters that combine these three aspects: (i) the span of epoxy conversion available in the metastable region for phase separation; (ii) the rate of epoxy cure; and (iii) the ability of the poly(propylene oxide) to co-react with epoxy.

*Cure Behavior.* Dynamic mechanical analysis provided an effective means to study the cure behavior of both neat as well as poly(propylene oxide)- modified epoxies. Isothermal cure scans scans displayed the gelation and vitrification transitions. In the poly(propylene oxide)- modified system, an additional transition was also seen which was thought to be related to phase separation. A Complex multi-transition behavior was observed during

dynamic cure scans which was interpreted in terms of the competition between the glass transition temperature and the experimental temperature, the outcome of which governed whether the cure is under chemical or diffusion control. It was found that the glass transition temperature of the fully cured system was not unique but a function of the cure history. The construction of time-temperature-transformation (TTT) diagram from the dynamical mechanical analysis was successfully demonstrated.

*Degradation Process and Microporosity Development.* It was shown with the help of thermal analysis and scanning electron microscopy that it is possible to remove selectively poly(propylene oxide) from the epoxy matrix by heat treatment at 200 °C. It was also demonstrated that thin coatings with microporosity with potential applications in magnetic coatings may be developed by the two-step procedure satisfying the practical objectives of this research. Finally, it was found that the thickness of the film not only affected the degradation of poly(propylene oxide) phases but also the development of the phases themselves when it approached the dimensions typical of the phases.



## 2.6 FUTURE DIRECTIONS FOR RESEARCH

During the course for the present study, several possible future directions for research could be identified with scientific potential both from fundamental as well as practical points of view. The following is a brief summary of some of these topics that may be targeted for further study.

*Morphology Control and Toughened Thermosets.* The results obtained from the study of morphological behavior in poly(propylene oxide)- modified epoxies have demonstrated clearly the versatility of the use of a number of variables that may be independently controlled to give a range of phase sizes and phase concentrations. An obvious extension of this would be to study systematically the effect of the morphology in modified thermosets on their mechanical properties such as toughness. For instance, by being able to vary the size of the domains without changing the composition, one can accurately determine the role of phase size in the toughening behavior. This would also provide an avenue for examining the validity of several toughening mechanisms that have been put forward in the past few years, with a margin for controversies due to a lack of appropriate experimental strategies that provide a broad enough database. The approach taken in this study may be exploited in other systems as well to fulfil this requirement.

*Theoretical Modeling of Phase Separation.* Due to the flexibility in the morphology control, the poly(propylene oxide)- modified epoxy system, particularly when cured by a base catalyzed reaction with an anhydride, would make an attractive system for theoretical modeling. Poly(propylene oxide)s of controlled molecular weights and end-group chemistry may be used as a modifier to epoxies of known functionalities to form model

systems for studying the relationship between experiment and the current theories of phase separation.

*Effect of Thickness in Morphology Development.* A preliminary indication in this study that the thickness may play a role in the how the phase separated morphology develops may be expanded to understand its exact origin. The causes attributable to such experimental factors as temperature control may be differentiated from thermodynamic factors such as interfacial interactions between the polymer and the substrate. This study will help in further generalizing the approach for developing microporosity in thin films.

*Application as Low Dielectric Material.* The epoxy film after development of microporosity by thermooxidative removal of poly(propylene oxide) may be expected to have low dielectric constant since theoretically a portion of its matrix would be replaced with air. Thus, the possible applicability of this method to obtain new materials of low dielectric properties may be worth pursuing.

## APPENDICES

### APPENDIX 2.I

#### Conversion of Hydroxyl End-groups of PPG-1025

Hydroxyl end-groups of PPG-1025 were converted to ester moieties by reaction with benzoyl chloride by the following procedure. After vacuum drying at 80 °C for 2 hours, PPG-1025 was dissolved in freshly distilled tetrahydrofuran to make a ~30% solution. To this was added triethylamine (20% molar excess). Finally, benzoyl chloride (20% molar excess) was added and the reaction mixture was allowed to stay at room temperature for 24 hours. After the reaction was complete, the solvent and unreacted reagents were removed under vacuum. The modified PPG-1025 was dissolved in hexanes to make a 5% solution to which activated charcoal (50 g/l) was added. The mixture was left stirring for about 24 hours and filtered to remove the charcoal together with any impurities. The hexanes were then distilled off under reduced pressure. Finally, the modified poly(propylene oxide), PPG-1025E, was vacuum dried for 12 hours at 80 °C before use.

### APPENDIX 2.II

#### Thermodynamic Relations for Modified Thermosets

##### *Derivation of Equation 2.4.1.*

Combination of Equations 2.2.6 through 2.2.8 gives the Flory-Huggins expression for Gibbs free energy of mixing in a binary polymer mixture:

$$\Delta G_m = RT ( N_1 \ln \phi_1 + N_2 \ln \phi_2 + \chi_{12} N_1 \phi_2 ) \quad (\text{II.1})$$

Dividing each side by the total volume  $v$  of the system to obtain the free energy per unit volume:

$$\Delta G_m^V = RT [ (N_1/v) \ln \phi_1 + (N_2/v) \ln \phi_2 + \chi_{12} (N_1/v) \phi_2 ] \quad (\text{II.2})$$

$N_1/v$  is equivalent to  $\phi_1/V_1$  and  $N_2/v$  is equivalent to  $\phi_2/V_2$ . Substituting in Equation II.2:

$$\Delta G_m^V = RT [ \phi_1/V_1 \ln \phi_1 + (\phi_2/V_2) \ln \phi_2 + \chi_{12} \phi_2 (\phi_1/V_1) ] \quad (\text{II.3})$$

Now for a mixture of thermoset (component 1) and the modifier (component 2):

$$V_1 = V_{1,0} \langle DP_n \rangle \quad (\text{II.4})$$

$$V_2 = V_{2,0} \quad (\text{II.5})$$

Also,

$$\chi_{12}/V_1 = \chi_{12,0}/V_{1,0} \quad (\text{II.6})$$

$$\phi_1 = 1 - \phi_2 \quad (\text{II.7})$$

Using Equations II.4 through II.7 in II.3 gives Equation 2.4.1:

$$\Delta G_m^V = RT \left[ (1-\phi_2) \ln(1-\phi_2) / (\langle DP_n \rangle V_{1,0}) + (\phi_2 / V_{2,0}) \ln \phi_2 + \chi_{12,0} \phi_2 (1-\phi_2) / V_{1,0} \right] \quad (2.4.1)$$

***Derivation of Equation 2.4.6.***

According to classical thermodynamics, the critical point satisfies the following two equalities:

$$\partial^2(\Delta G_m^V) / \partial \phi_2^2 = 0 \quad (2.4.4)$$

$$\partial^3(\Delta G_m^V) / \partial \phi_2^3 = 0 \quad (2.4.5)$$

From Equation 2.4.1 the derivatives of free energy may be derived as:

$$\partial^2(\Delta G_m^V) / \partial \phi_2^2 = RT \left[ 1 / (\langle DP_n \rangle V_{1,0} (1-\phi_2)) + 1 / (V_{2,0} \phi) - 2 \chi_{12,0} / V_{1,0} \right] \quad (II.8)$$

$$\partial^3(\Delta G_m^V) / \partial \phi_2^3 = RT \left[ 1 / (\langle DP_n \rangle V_{1,0} (1-\phi_2)^2) - 1 / (V_{2,0} \phi^2) \right] \quad (II.9)$$

Using Equation II.8 into Equation 2.4.4 and rearranging gives:

$$1 / \langle DP_n \rangle = (1 - \phi_2) \left[ 2 \chi_{12,0} - V_{1,0} / (V_{2,0} \phi_2) \right] \quad (II.10)$$

Similarly, using II.9 into Equation 2.4.5 and rearranging gives:

$$1 / \langle DP_n \rangle = V_{1,0} (1 - \phi_2)^2 / (V_{2,0} \phi_2) \quad (\text{II.11})$$

Combination of Equations II.10 and II.11 and rearrangement gives Equation 2.4.6:

$$\phi_{2c} = [V_{1,0} / (2 V_{2,0} \chi_{12,0})]^{1/2} \quad (2.4.6)$$

## APPENDIX 2.III

### Estimation of Solubility Parameters by Group Contribution Method

The group contribution techniques are based on the assumption that the contribution of the different functional groups to the overall thermodynamic property are additive. The concept has also been extended to estimation of solubility parameters of polymers.<sup>211-213</sup> The working relation for this is given by:

$$\delta = (\rho / M) \sum F_i \quad (\text{III.1})$$

where,  $\rho$  is the density of the polymer;  $M$  = molecular weight of the repeating unit, and  $F_i$  is the Molar Attraction Constant of the group  $i$  as defined by Small.<sup>222</sup>

A consideration must be taken into account when calculating the solubility parameter for a thermosetting polymer, e. g. the solubility parameter will change as the system undergoes cure since new groups with different characteristics are formed as a result. For a valid comparison between various systems, then, a reference state must be used. Here, the *fully* cured system is taken to be that reference. Thus, the repeat units in each of the three

systems may be idealized as the network structures shown in Figures 2.4.1, 2.4.2, and 2.4.3 for Quatrex epoxy cured with NMA, Bis-S, and DDS respectively.

In the following calculations two further approximations were made. First, the density in each case was taken to be 1.2 g/cc which is typical for cured epoxies. Secondly, the molar attraction constant for the (SO<sub>2</sub>) group, not being available in literature, was back-calculated from the knowledge of the solubility parameter of Bis-A polysulfone which is experimentally found<sup>223</sup> to be 10.75 (cal/cc)<sup>1/2</sup>. All other molar attraction constants were taken from those proposed by van Krevelen and Hoftyzer.<sup>212</sup>.

***Calculations for Quatrex/NMA System.***

F<sub>i</sub>'s (J<sup>1/2</sup> cm<sup>1/2</sup> mol<sup>-1</sup>)

1)

---


$$1 (\text{CH}_3) = 1 \times 420 = 420$$

$$7 (\text{CH}_2) = 7 \times 280 = 1960$$

$$7 (\text{CH}) = 7 \times 140 = 980$$

$$1 (\text{C}) = 0 \times 1 = 0$$

$$1 (\text{CO}) = 1 \times 685 = 685$$

$$1 (\text{COO}) = 1 \times 511 = 511$$

$$4 (\text{O}) = 4 \times 235 = 940$$

$$2 (\text{C}_6\text{H}_3) = 2 \times 1240 = 2480$$

$$\Sigma F_i = 420 + 1960 + 980 + 0 + 685 + 511 + 940 + 2480 = 7976 \text{ J}^{1/2} \text{ cm}^{1/2} \text{ mol}^{-1}$$

$$M = 504 \text{ g/mol}$$

$$\rho = 1.2 \text{ g/cc}$$

$$\text{Using Equation III.1, } \delta = 7976 / (504 / 1.2) = 18.99 \text{ (J/cc)}^{1/2} = \mathbf{9.3 \text{ (cal/cc)}^{1/2}}$$

***Calculations for Quatrex/Bis-S System.***

$$F_i\text{'s (J}^{1/2} \text{ cm}^{1/2} \text{ mol}^{-1}$$

1)

---

$$6 \text{ (CH}_2\text{)} = 6 \times 280 = 1680$$

$$2 \text{ (CH)} = 2 \times 140 = 280$$

$$2 \text{ (OH)} = 2 \times 754 = 1508$$

$$4 \text{ (O)} = 4 \times 255 = 1020$$

$$1 \text{ (SO}_2\text{)} = 1 \times 980 = 980$$

$$2 \text{ (C}_6\text{H}_4\text{)} = 2 \times 1380 = 2760$$

$$2 \text{ (C}_6\text{H}_3\text{)} = 2 \times 1240 = 2480$$

$$\Sigma F_i = 1680 + 280 + 1508 + 1020 + 980 + 2760 + 2480 = 10688 \text{ J}^{1/2} \text{ cm}^{1/2} \text{ mol}^{-1}$$

$$M = 582 \text{ g/mol}$$

$$\delta = 10688 / (582 / 1.2) = 22.04 \text{ (J/cc)}^{1/2} = \mathbf{10.8 \text{ (cal/cc)}^{1/2}}$$

***Calculations for Quatrex/DDS System.***

$$F_i\text{'s (J}^{1/2} \text{ cm}^{1/2} \text{ mol}^{-1}$$

1)

---

$$12 \text{ (CH}_2\text{)} = 12 \times 280 = 3360$$

$$4 \text{ (CH)} = 4 \times 140 = 560$$



$$4 (\text{OH}) = 4 \times 754 = 3016$$

$$4 (\text{O}) = 4 \times 255 = 1020$$

$$1 (\text{SO}_2) = 1 \times 980 = 980$$

$$2 (\text{N}) = 2 \times 125 = 250$$

$$2 (\text{C}_6\text{H}_4) = 2 \times 1380 = 2760$$

$$4 (\text{C}_6\text{H}_3) = 4 \times 1240 = 4960$$

$$\Sigma F_i = 3360 + 560 + 3016 + 1020 + 980 + 250 + 2760 + 4960 = 16906 \text{ J}^{1/2} \text{ cm}^{1/2} \text{ mol}^{-1}$$

$$M = 908 \text{ g/mol}$$

$$\delta = 16906 / (908 / 1.2) = 22.34 (\text{J/cc})^{1/2} = 11.0 (\text{cal/cc})^{1/2}$$

## APPENDIX 2.IV

### Conversion at Gelation for Quatrex-2010

#### Cured with Various Curing Agents

Flory<sup>123</sup> derived the following general equation for conversion at gel point in a system of f-functional units reacting with bifunctional units:

$$p_{\text{gel}} = [ 1 / (f-1) ]^{1/2} \quad (\text{IV.1})$$

For simplicity, the average number of epoxide groups per chain of Quatrex-2010 may be rounded off to ~4 from the specified value of 3.6. In case of NMA cured system, then, the problem is of a monomer of functionality 8 reacting with a bifunctional monomer. Substituting  $f = 8$  in Equation IV.1:

$$p_{\text{gel}} \text{ for Quatrex-2010/NMA system} = (1/7)^{1/2} = \mathbf{0.38}$$

For Bis-S cured system,  $f = 4$ . Then,

$$p_{\text{gel}} \text{ for Quatrex-2010/Bis-S system} = (1/3)^{1/2} = \mathbf{0.58}$$

The problem of DDS cured Quatrex-2010 is that of a tetrafunctional monomer reacting with another tetrafunctional monomer. This case has been worked out by Tanaka and Kakuichi.<sup>214</sup> The expression is:

$$p_{\text{gel}} = 2r / 3(1 + r) \quad (\text{IV.2})$$

where  $r$  is the molar ratio of the two species. For stoichiometric reaction between Quatrex-2010 and DDS,  $r = 1$  and,

$$p_{\text{gel}} \text{ for Quatrex-2010/DDS system} = 2 / (3 \times 2) = \mathbf{0.33}$$

## **Chapter III**

### **Polypropylene - Poly(vinyl methyl ether) Blends**

---

#### **3.1 INTRODUCTION**

In this chapter, the results of a preliminary study to probe the nature of physical and/or chemical interactions between polypropylene (PP) and poly(vinyl methyl ether) (PVME) are presented. As mentioned in Chapter I, this study formed a part of a broader objective to search for suitable "compatibilizers" for blends of PP and Nylon 6. Considerable interest exists in developing mechanically compatible blends of these two high-volume, commercially important polymers. PP is relatively inexpensive, hydrophobic and possibly surface active. On the other hand, Nylon 6 possesses high strength and high melting point, but it is moisture sensitive and expensive. The combination of the two polymers is expected to provide an economical route to obtain a new material that assimilates the advantages of its individual components.

When blended by themselves, PP and Nylon 6 display incompatibility with poor mechanical properties as a result of gross phase separation and lack of interfacial adhesion.<sup>224</sup> Therefore, an external means to induce compatibility in the blend is necessary. This can be achieved in a variety of ways, the most common of which is the introduction of a third component, such as a block or graft copolymer, in the blend which could then promote interactions across the interface between the matrix and the dispersed phase. The use of block and graft copolymers as "interfacial agents" have been reviewed in detail by Paul.<sup>225</sup> The compatibilization of immiscible blends by the addition of these copolymers can be compared to the emulsifying effect of surfactants in oil and water mixtures. The early morphological observations of Molau<sup>226-228</sup> clearly demonstrated the ability of block copolymers to emulsify polymer dispersions in solution and thus inhibit gross phase separation. As a result of this work and later studies,<sup>229,230</sup> block copolymers are frequently referred to as oil-in-oil emulsifiers.

More recently, this concept has been extended to melt-blended polymers, by the addition of graft,<sup>231-234</sup> block,<sup>231,235-240</sup> as well as star<sup>240</sup> copolymers. For example, Teyssie *et al*<sup>238</sup> have clearly shown that there is a significant reduction in the dispersed phase size and an increase in the interfacial adhesion as a result of addition of as little as 2% by weight of polybutadiene/polystyrene block copolymer to blends of polyethylene and polystyrene. The presence of the copolymer was also responsible for stabilizing the dispersion against coalescence. In a later publication,<sup>239</sup> Teyssie *et al* further demonstrated that the copolymer was uniformly adsorbed at the interface between the two polymers. Thus, by the virtue of being able to place itself at the interface of the two phases, as schematized on Figure 3.1.1, these additives help to compatibilize a binary blend as a consequence of three main effects

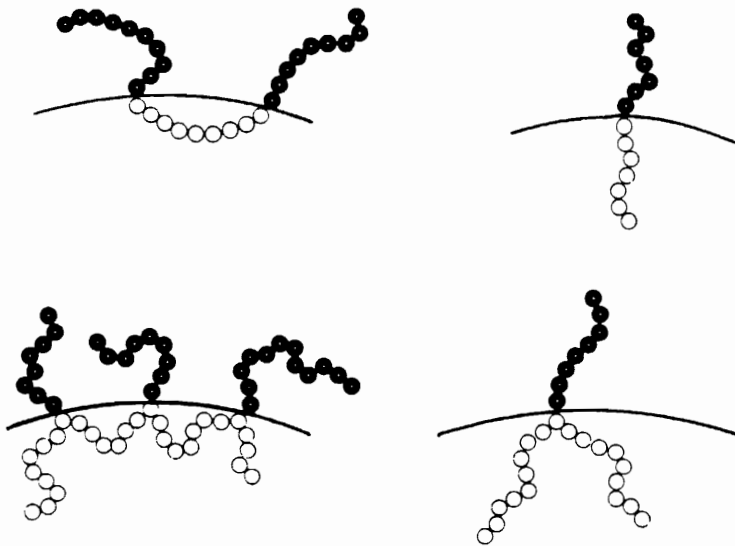


**Figure 3.1.1** Schematic representation of different types of copolymers acting as "interfacial agents". (from reference 22)

described by Maglio and Palumbo,<sup>22</sup> e. g. better dispersion, enhanced adhesion, and phase stabilization.

In order to identify an appropriate block or graft copolymer that is able to compatibilize the blends of PP and Nylon 6, a fundamental approach is proposed in which each homopolymer is paired with a variety of other polymers and studied for their miscibility/immiscibility characteristics. Results from these individual investigations are to be used then to tailor an optimum chemical structure of a block or graft copolymer that would be most effective as an interfacial agent for PP - Nylon 6 blends. The work presented here explores PVME as a potential candidate for interaction with PP. PVME is indeed well-known for its miscibility with polystyrene (PS).<sup>241-243</sup> However, no published literature exists on PVME - PP blends except a patent<sup>244</sup> which alludes to the modification of the properties of PP by addition of a variety of polymeric additives including PVME, with no indication of the precise nature of interactions between the two. The primary objective of the current study was then to take up melt blends of PP and PVME and determine whether miscibility exists between these two polymers.

The principal experimental technique utilized in this study is DSC to observe the crystallization behavior, both under dynamic as well as isothermal conditions, and the subsequent melting points. SEM provides morphological information on the system. Additional supporting data from TGA, FTIR, and solid state NMR are also presented.

## 3.2 EXPERIMENTAL

### 3.2.1 Materials.

Isotactic polypropylene was supplied by Amoco Chemicals, Chicago, Illinois. It was dried at  $\sim 80$  °C for  $\sim 24$  hours before use. Poly(vinyl methyl ether) was purchased from Monomer-Polymer & Dajac Laboratories, Inc., Trevese, Pennsylvania in the form of a 70% solution in toluene. The solvent was removed by keeping it in a vacuum oven at 110-130 °C for  $\sim 48$  hours. An analytical grade mixed xylenes purchased from Fisher Scientific were used for solvent extraction of blends.

### 3.2.2 Methods.

#### 3.2.2.1 *Sample Preparation.*

Two blends having identical compositions (90% PP and 10% PVME) were prepared by using a Haake-Buchler Rheomix blender. The difference between the two blends was the temperature/time utilized for blending: *Blend(210-30)* was prepared at 210 °C with the total residence time of 30 minutes in the blender; similarly, the temperature and time for *Blend(200-15)* were 200 °C and 15 minutes respectively. The total amount of polymer mixture charged into the blender in each case was 50 gm. The blends thus prepared, and neat PP (as control) were pressed into approximately 0.25 mm thick films in a hydraulic press before thermal analyses. Films of *Blend(200-15)* and neat PP were further heat-treated by placing them in a convection oven at 210 °C for different amounts of time. To extract soluble portion of the *Blend(210-30)*, it was dissolved in hot xylenes at 60-70 °C

(approximately 250 ml solvent per 1 gm polymer) and then allowed to cool to room temperature so that the insoluble fraction precipitated out from the solution. The precipitates were separated by filtration, washed with excess xylenes and dried in a vacuum oven at  $\sim 100$  °C for 48 hours, and finally pressed into a film for analysis.

### 3.2.2.2 *Analysis.*

The DSC studies were carried out using a dual cell DuPont 912 DSC coupled to a DuPont Thermal Analyst 2100. The dynamic crystallization and the subsequent melting point measurements were performed by using a three-scan method shown in Figure 3.2.1(a). The first dynamic scan of 10 °C/minute from room temperature to 180 °C and holding at this temperature for 1 minute ensured complete melting of the existing crystals and removal of prior thermal history. The second cooling scan at 2 °C/minute provided the dynamic crystallization behavior. Finally, the third dynamic heating at 10 °C/minute was used to obtain the melting behavior. The isothermal crystallization and the respective melting point measurements were made by using a four-scan method. As shown in Figure 3.2.1(b), the first and the last scans were the same as those of the dynamic method. The isothermal crystallization behavior was obtained from the two intermediate steps, e. g. cooling from 180 °C to 132 °C and then holding at 132 °C to effectuate crystallization. The temperature of 132 °C was chosen as an optimum temperature below which an appreciable amount of crystallization did not occur during the cooling scan and at which crystallization took place at a reasonable rate in all samples so that a proper comparison could be made.

The TGA measurements were performed on a DuPont 951 TGA interfaced to the same data station as DSC. FTIR spectra were collected on a Nicolet MX-1. The  $^{13}\text{C}$  Carbon NMR



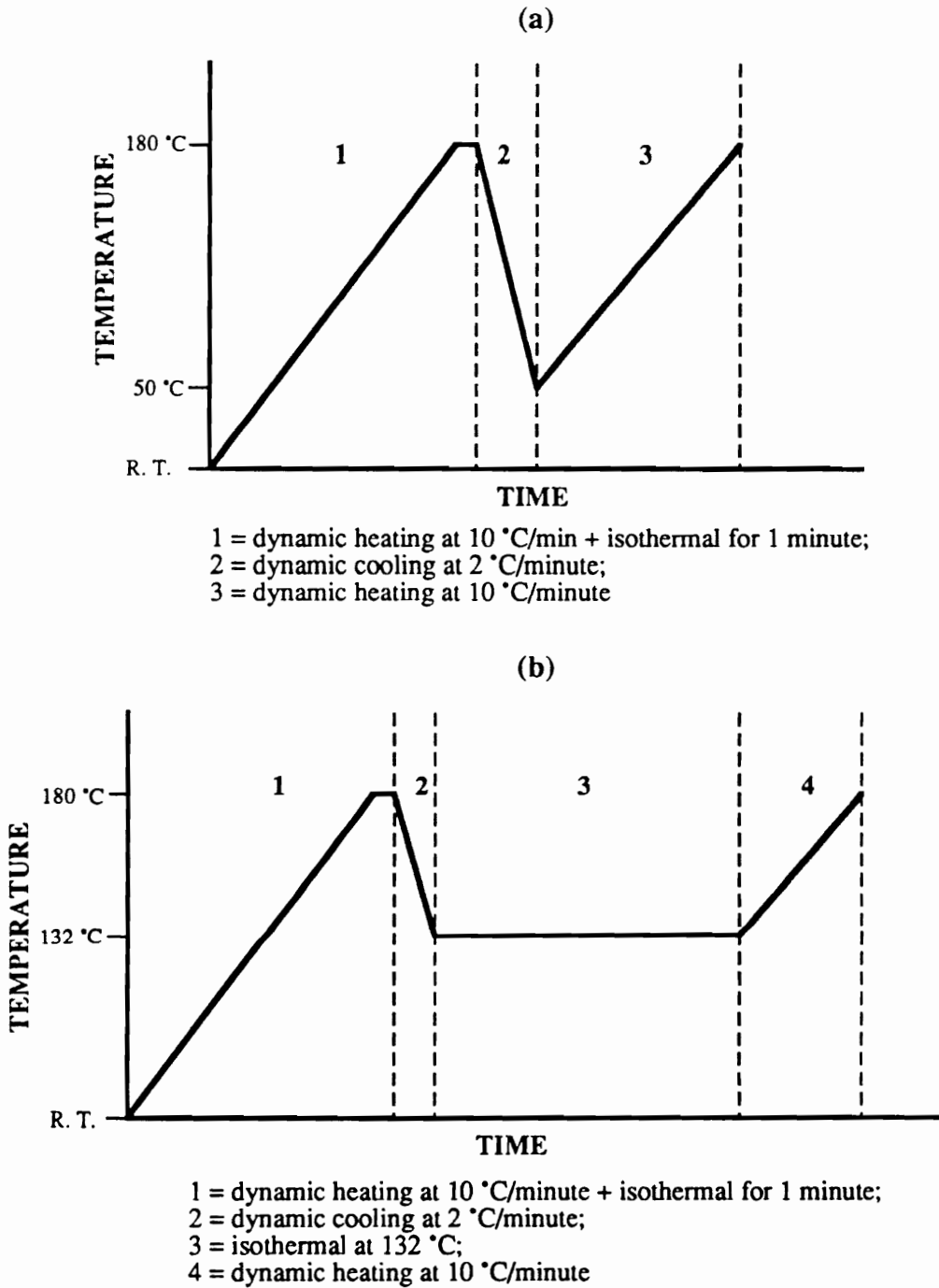


**Figure 3.2.1** DSC methods for study of crystallization and melting behavior in PP - PVME blends. (a) dynamic crystallization; (b) isothermal crystallization.

spectrum was obtained on a Bruker MSL-200 operating at 75.47 Mhz using magic angle spinning with cross polarization (CP/MAS). A Philips EM420 STEM operating at 20 kV was used for scanning electron microscopy. The films were cold-fractured with the help of liquid nitrogen to reveal their cross sections which were then sliced, mounted on the sample probe, and coated with gold-palladium to make them conductive before SEM analysis.

### 3.3 RESULTS AND DISCUSSION

#### 3.3.1 Dynamic Crystallization.

Figure 3.3.1 shows the 2 °C/minute cooling DSC scans of neat PP, Blend(200-15) and Blend(210-30). From the position of endothermic maximum on each curve, it is immediately apparent that the rate of crystallization is higher in Blend(200-15) and lower in Blend(210-30) than that in neat PP. Also listed on Figure 3.3.1 are  $\Delta H_{\text{cry}}$ , the heats of crystallization in each sample measured from the area under the endotherms (the values for the blends are normalized on the basis of unit PP content). There is virtually no difference between  $\Delta H_{\text{cry}}$ 's of neat PP and Blend(200-15), whereas that of Blend(210-30) is lower by 11.3 J/g. This means qualitatively that the degree of crystallinity is lower in Blend(210-30) than either of neat PP and Blend(200-15). Figure 3.3.2 shows the corresponding melting point scans of the three samples after the preceding dynamic crystallization. Once again, the behavior of Blend(200-15) is nearly identical to neat PP- both in terms of the melting points (each at 165 °C) and the heat of fusion,  $\Delta H_f$  (108.9 J/g in the former comparable to 108.1 in the latter). On the other hand, Blend(210-30) displays a significantly different

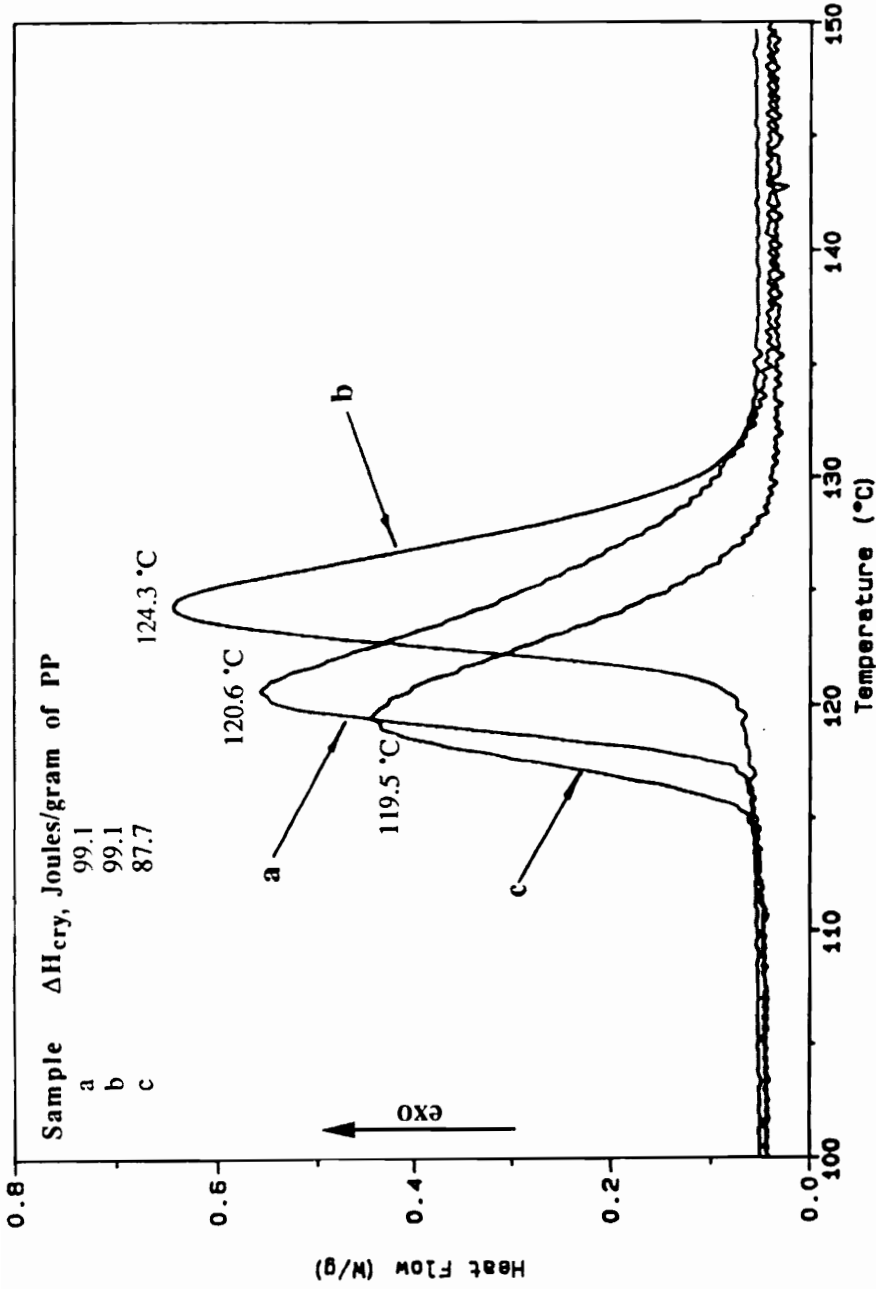


**Figure 3.3.1** Dynamic crystallization behavior of neat polypropylene and polypropylene-poly(vinyl methyl ether) blends. (a) neat polypropylene, (b) Blend(200-15), and (c) Blend(210-30).

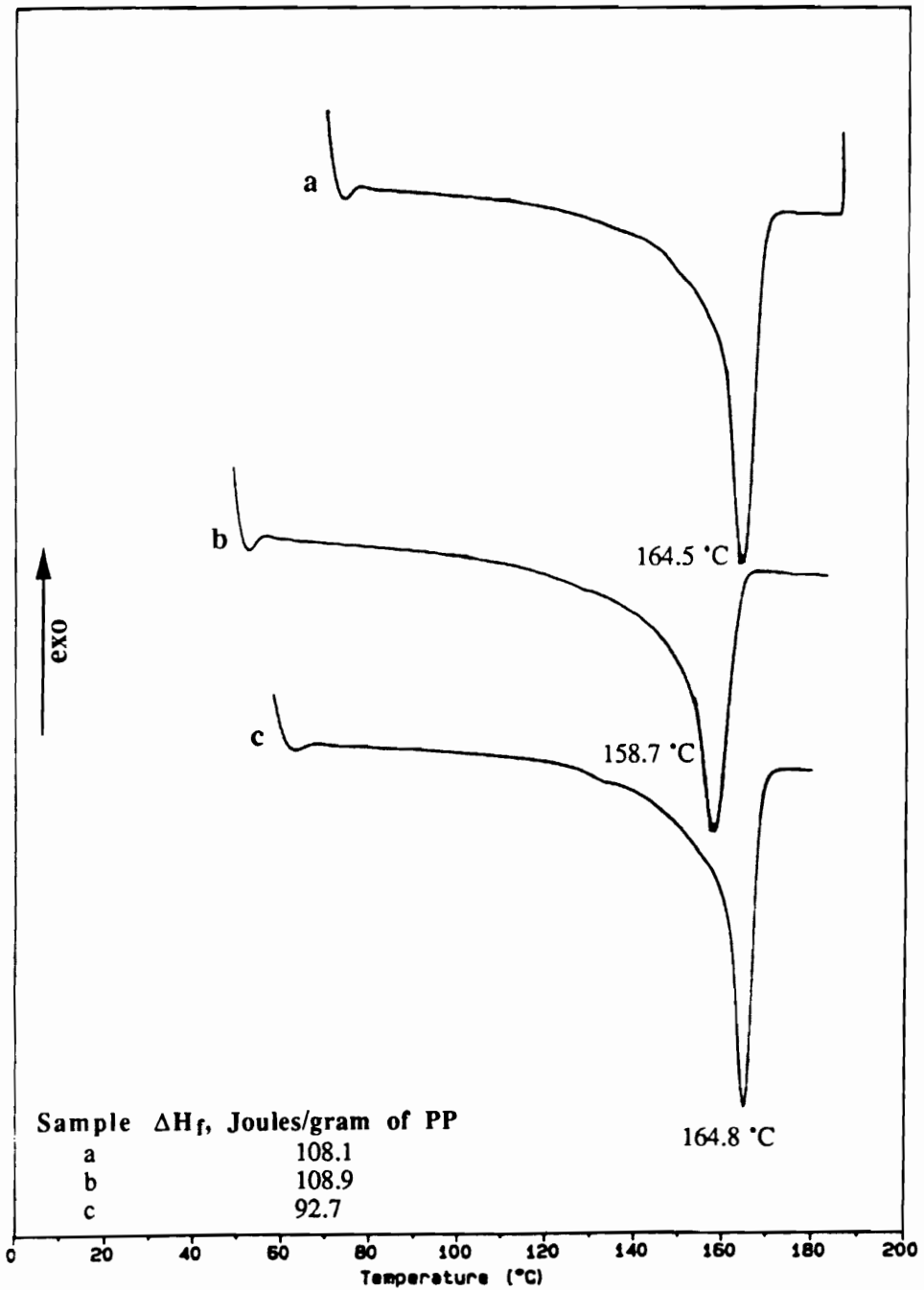


**Figure 3.3.2** Melting point behavior of neat PP and PP - PVME blends after dynamic crystallization. (a) neat PP, (b) Blend(200-15), and (c) Blend(210-30).

melting behavior: the melting point is depressed to 159 °C and the heat of fusion to 92.7 J/g.

The dynamic crystallization and melting point data thus show that the two blends of identical composition but prepared under varying blending conditions display distinctively different properties. The Blend(210-30) behaves in a manner similar to a blend in which the amorphous component is miscible, or partially miscible with the crystallizable component.<sup>245,246</sup> In a miscible polymer mixture, the amorphous component can act as a diluent, leading to a depression in the melting point. Thus, at a particular crystallization temperature, the rate of crystallization in the miscible blend may be expected to be lower in comparison to that in the crystallizable homopolymer alone due to lower undercooling, ( $T_m - T_c$ ), in the former. In addition, the rate of crystallization in a blend is also affected by the glass transition temperature through its influence on the transport properties of the polymer chains. Miscible polymers possess only one  $T_g$ , intermediate between those of the individual components. If the  $T_g$  of the crystallizable component decreases as a result of miscibility, an increase in crystallization rate will ensue, and *vice versa*. However, in general the effect of change in  $T_g$  on crystallization rate is significant only for large undercooling, or when the temperature of crystallization is closer to  $T_g$ . In the system at hand, the  $T_g$ 's of the two components are not too far apart ( $T_g$  of PP =  $\sim$ -10°C, and  $T_g$  of PVME =  $\sim$ -30 °C). Therefore, if miscibility between PP and PVME were to exist, the change in the  $T_g$  of PP as a result of the presence of PVME, specially in the low concentration of 10%, would not be expected to play a major role in crystallization kinetics. In other words, a possible source of both slower crystallization and depression in melting point in Blend(210-30) may be related to *some form* of diluent effect of PVME. However, it may be emphasized that the above data does not necessarily imply miscibility between PP

and PVME. Two other sources related to degradative processes that could occur during blending may also be considered to explain the observed miscibility-like behavior. First is the possibility of molecular weight deterioration of PP from the chemorheological processes in the blender that may bring about a reduction in the crystallization rate as well as the melting point. On the other hand, the same would result if PVME degraded to form smaller monomer-like species or chemical grafts onto PP chains. All of these possibilities will be considered in the remaining discussion.

### 3.3.2 Isothermal Crystallization.

Figure 3.3.3 shows the 132 °C isothermal crystallization behavior of the three samples. The results are in agreement with the trends observed from dynamic crystallization, i. e. Blend(200-15) crystallizes faster and Blend(210-30) crystallizes slower than the neat PP. The melting points of the three sample also are in the same order as those obtained from dynamic crystallization, as shown in Figure 3.3.4: Blend(200-15) and neat PP have identical  $T_m$ 's, while there is a depression of 5 °C in the case of Blend(210-30). Similarly the  $\Delta H_f$  of Blend(200-15) is comparable to that of neat PP, while it is considerably lower in Blend(210-30). The comparison of melting points here may be more valid than those from dynamic crystallization study since each samples have been crystallized at the same temperature, thereby reducing the effect of crystallization temperature on melting point. However, one may note that the even in case of isothermal crystallization, the comparison is at best qualitative since the  $T_m$ 's obtained in this manner are not *equilibrium* values; elaborate experimentation involving several different crystallization temperature and the method of Hoffman and Weeks<sup>247</sup> would have to be performed for this purpose.

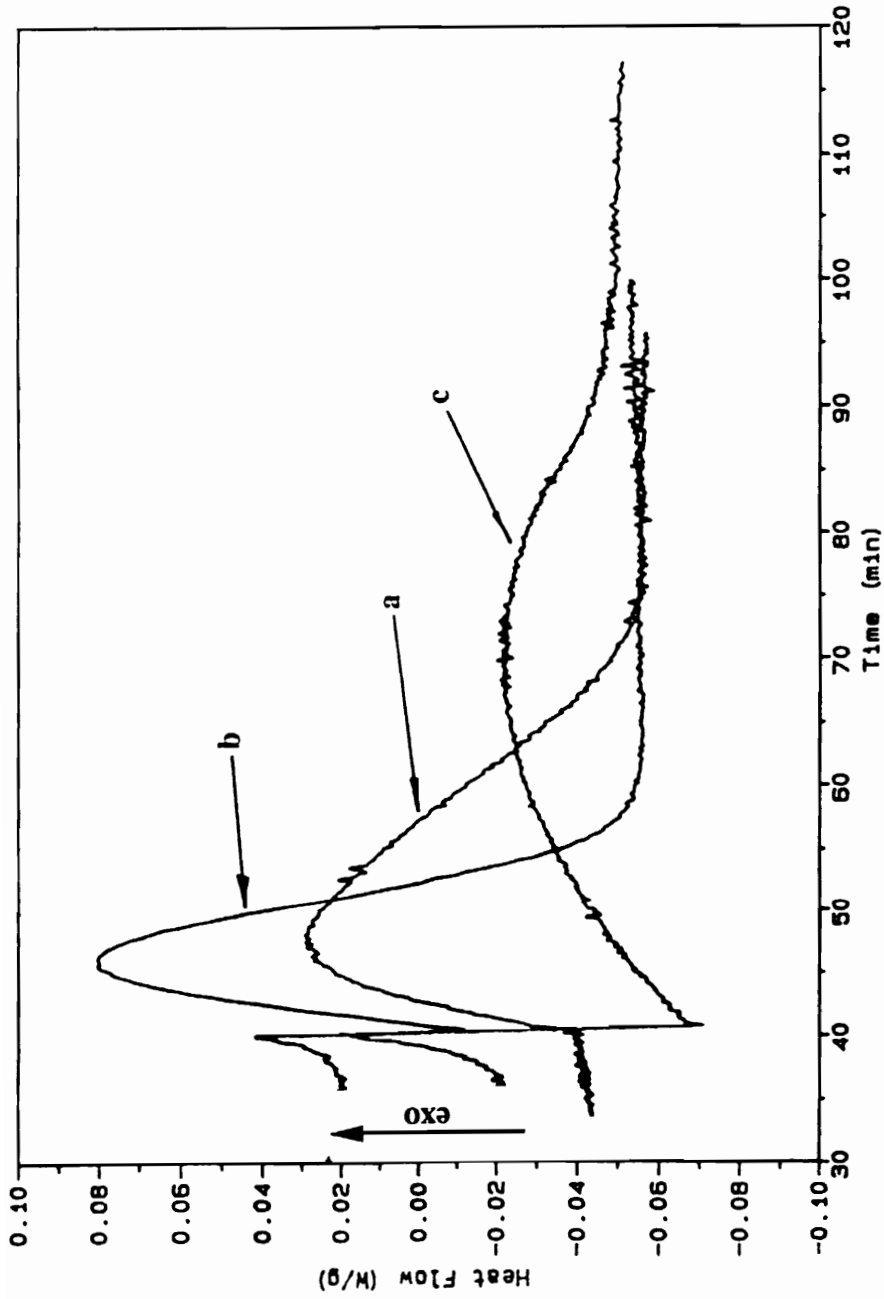


**Figure 3.3.3** 132 °C isothermal crystallization behavior of neat polypropylene and polypropylene-poly(vinyl methyl ether) blends. (a) neat polypropylene, (b) Blend(200-15), and (c) Blend(210-30).

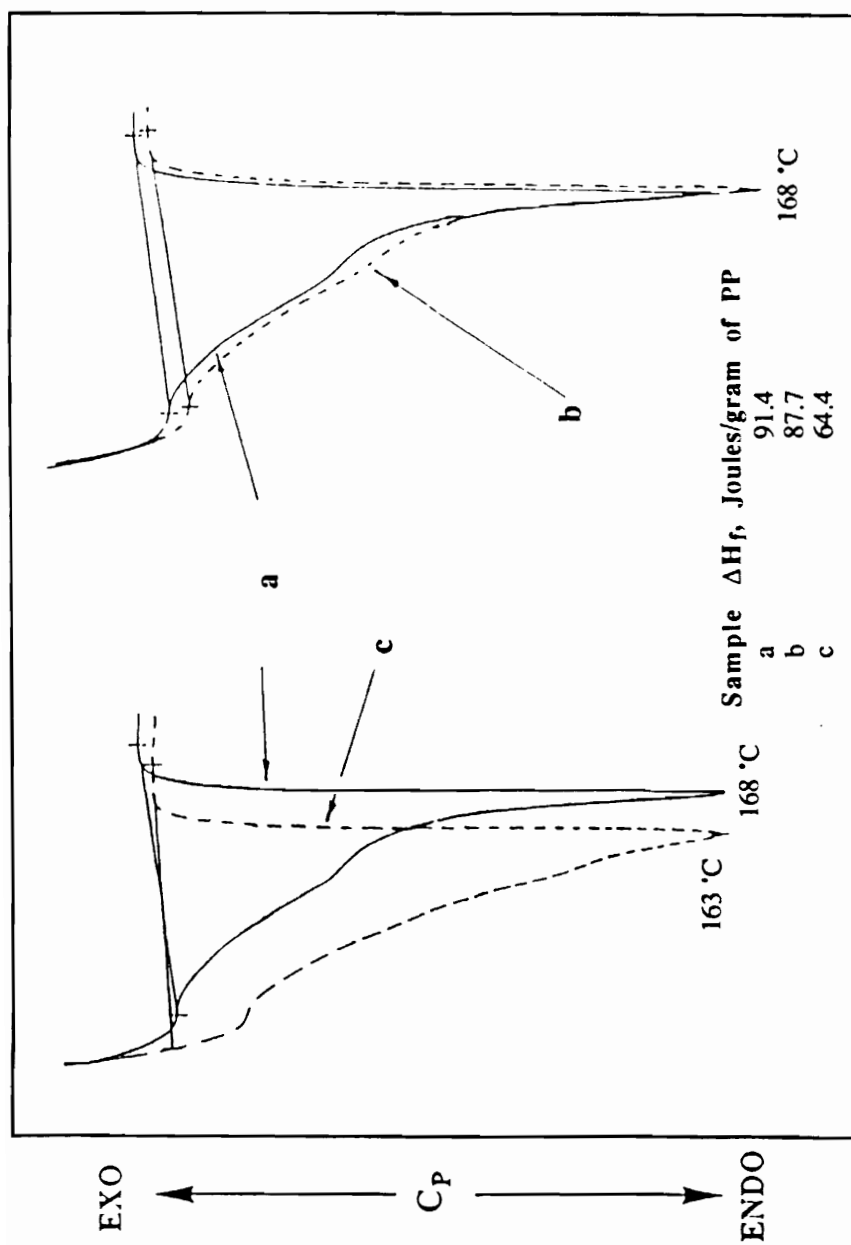


**Figure 3.3.4** Melting point behavior of neat polypropylene and polypropylene-poly(vinyl methyl ether) blends after 132 °C isothermal crystallization. (a) neat polypropylene, (b) Blend(200-15), and (c) Blend(210-30).



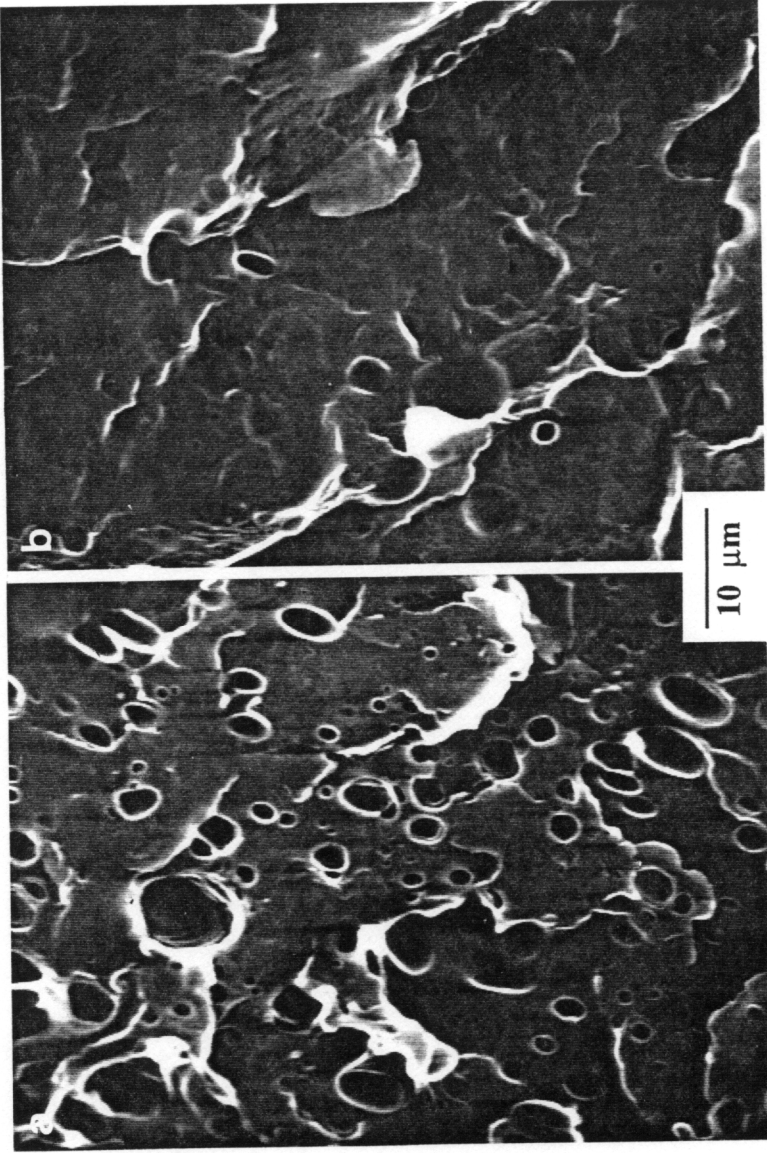
### 3.3.3 Morphology.

Figure 3.3.5 displays the SEM photomicrographs of the fracture surfaces of the two blends. Clearly, there is a considerable difference in the phase structure of the two blends. Evident on the photomicrograph of Blend(200-15) are distinct PVME phases of sizes varying from  $\sim 1 \mu\text{m}$  to  $\sim 6 \mu\text{m}$ . In comparison to this, the phases in Blend(210-30) are comparatively smaller and less numerous. More significantly, however, the phase boundaries seem to be less defined, an indication that there may be some interfacial interaction between the PP matrix and the PVME domains.

In review of the data obtained so far, several questions arise. First is the question of miscibility between PP and PVME. This possibility can be ruled out based on the both the thermal as well as SEM observations of Blend(200-15). However, the behavior of Blend(210-30) does point towards some form of interactions between the two components. Since the only apparent difference between the two blends is the severity (of time and temperature) with which they were prepared, a logical direction that may be pursued to further understand the nature of interactions is to see if there are thermooxidative processes occurring during blending that may give rise to the observed behavior. Along this reasoning, results of two experiments are described next.

### 3.3.4 Effect of Solvent Extraction.

If one considers that there is thermal degradation of PVME during blending, two different ways can be visualized that could be responsible for the observed miscibility-like DSC behavior in Blend(210-30): (i) PVME degrades into smaller monomer like molecules



**Figure 3.3.5** SEM photomicrographs showing the morphology of polypropylene-poly(vinyl methyl ether) blends. (a) Blend(200-15), and (b) Blend(210-30).

which are miscible with PP in the melt state and hence act as a diluent, or (ii) PVME forms free radicals that may quench themselves by forming grafting sites onto nearby PP chains. In each case, the end-effect on the blend would be the same, i. e. reduced crystallization rate and depression in  $T_m$ . To distinguish between which of the two routes is more likely, Blend(210-30) was extracted with hot xylene by the procedure outlined in Section 3.2. The low molecular weight products of PVME as well as the remaining PVME (which is soluble in xylene at room temperature) were expected to be removed from the system by this extraction. If only the first possibility existed, then the post-extraction polymer should display melting point behavior closer to that of the neat PP. However, contrary was found to be true. Figure 3.3.6 shows that the melting points before and after extraction are nearly identical. Thus, it seems that the processes occurring during blending have changed the nature of PP irreversibly. In lieu of this, the second possibility of formation of PVME grafts appears to be more probable.

### 3.3.5 Effect of Heat Treatment.

After the indication of the possibility of thermooxidative processes playing a role in bringing about the reduced crystallization rate and melting point depression in Blend(210-30), the next step was to see if a similar behavior can be induced in the Blend(200-15) by heat treatment at 210 °C in a convection oven. Three different times- 5, 10, and 15 minutes, were utilized. With the polymer being in the thin film form and an ample supply of oxygen, this treatment may be considered to be thermooxidatively more severe than that in the closed environment of the blender (although the role of mechanical energy in degradation mechanism may be significant in the latter). For comparison, similar treatment was also carried out on the films of neat PP.

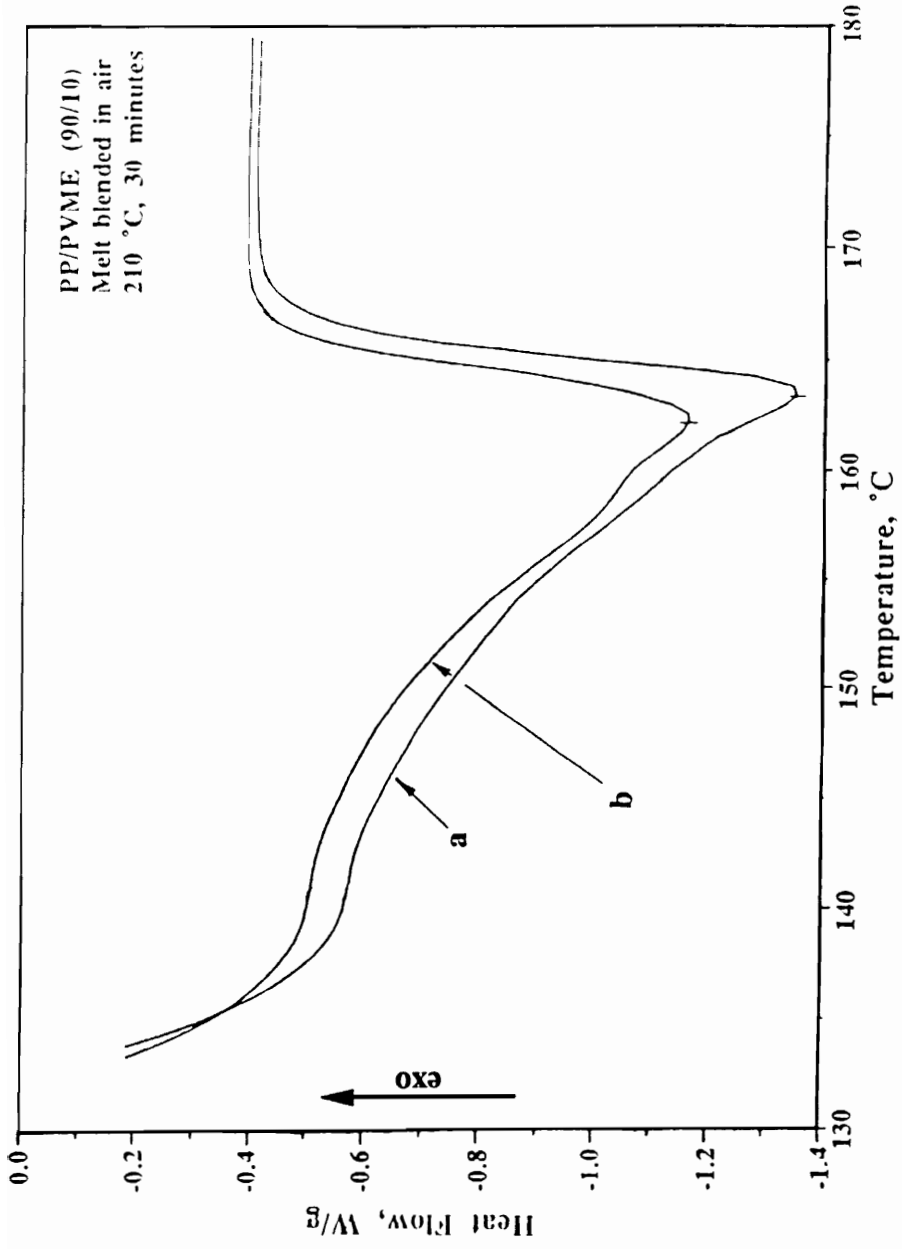


**Figure 3.3.6** Effect of solvent extraction on the melting point behavior following 132 °C isothermal crystallization of Blend(210-30). (a) before extraction, and (b) after extraction.

Figures 3.3.7 and 3.3.8 summarize the results of the effect of heat treatment on isothermal crystallization and melting point behaviors of Blend(200-15) respectively. As the time for heat treatment is increased, the rate of crystallization reduces dramatically as seen on Figure 3.3.7. Similarly, the effect on melting point behavior is also quite obvious. The  $T_m$  depresses from the initial 168 °C to ~160 °C. One may also note that the sharpness of the melting transition has also diminished to a great extent. After 15 minutes of heat treatment, Blend(200-15) behaves fairly close to Blend(210-30) as it is evident on the comparison made on Figure 3.3.9. The corresponding results of heat treatment on neat PP are displayed on Figures 3.3.10 and 3.3.11. It can be seen that neat PP also degrades under the conditions of heat treatment, resulting in both a slower crystallization kinetics as well as melting point depression. However, the changes in both these properties are minimal and not quite as drastic as in case of Blend(200-15). The melting point decreases from 168 °C to 165 °C- a change of 3 °C as compared to nearly 8 °C in Blend(200-15). Similarly, the rate of crystallization remains significantly closer to that of the untreated PP. Also interesting is the fact that due to heat treatment, there is a significant reduction in the  $\Delta H_f$  in the case of Blend(200-15) but not in the case of neat PP. From these results, it may be concluded that PVME plays a major role in the observed thermal behavior of blends- most possibly by chemically grafting onto PP.

### **3.3.6 Thermooxidative Behavior of Poly(vinyl methyl ether).**

Figure 3.3.12 shows the 10 °C/minute TGA scan in air of PVME. The polymer appears to be fairly stable up to ~220 °C after which it begins to degrade steadily. However, this does not mean that below 220 °C, it would not degrade in isothermal conditions. Figure 3.3.13 displays 210 °C isothermal TGA scan of PVME in air as well as nitrogen. In nitrogen, the

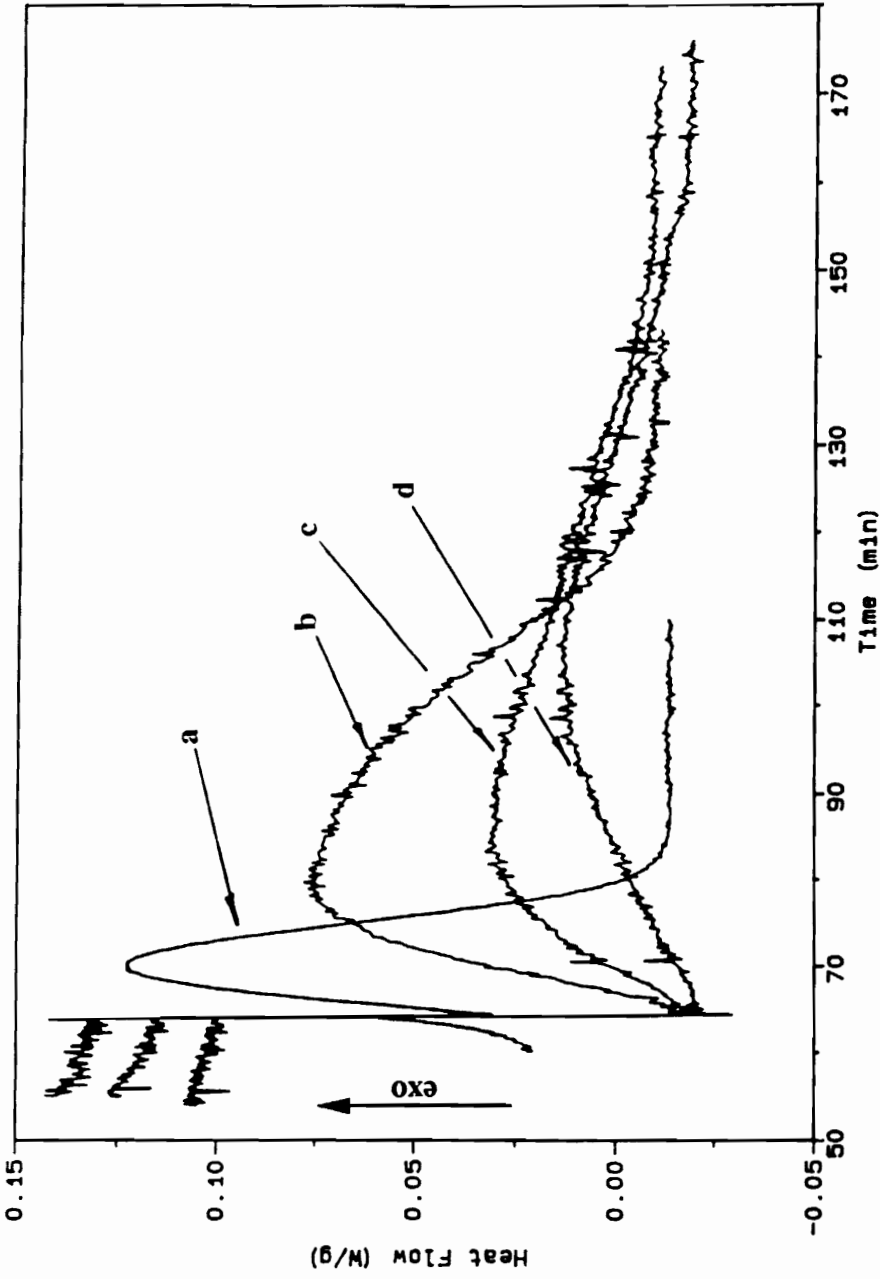


**Figure 3.3.7** Effect of 210 °C heat treatment on 132 °C isothermal crystallization behavior of Blend(200-15). (a) 0, (b) 5, (c) 10, and (d) 15 minutes.

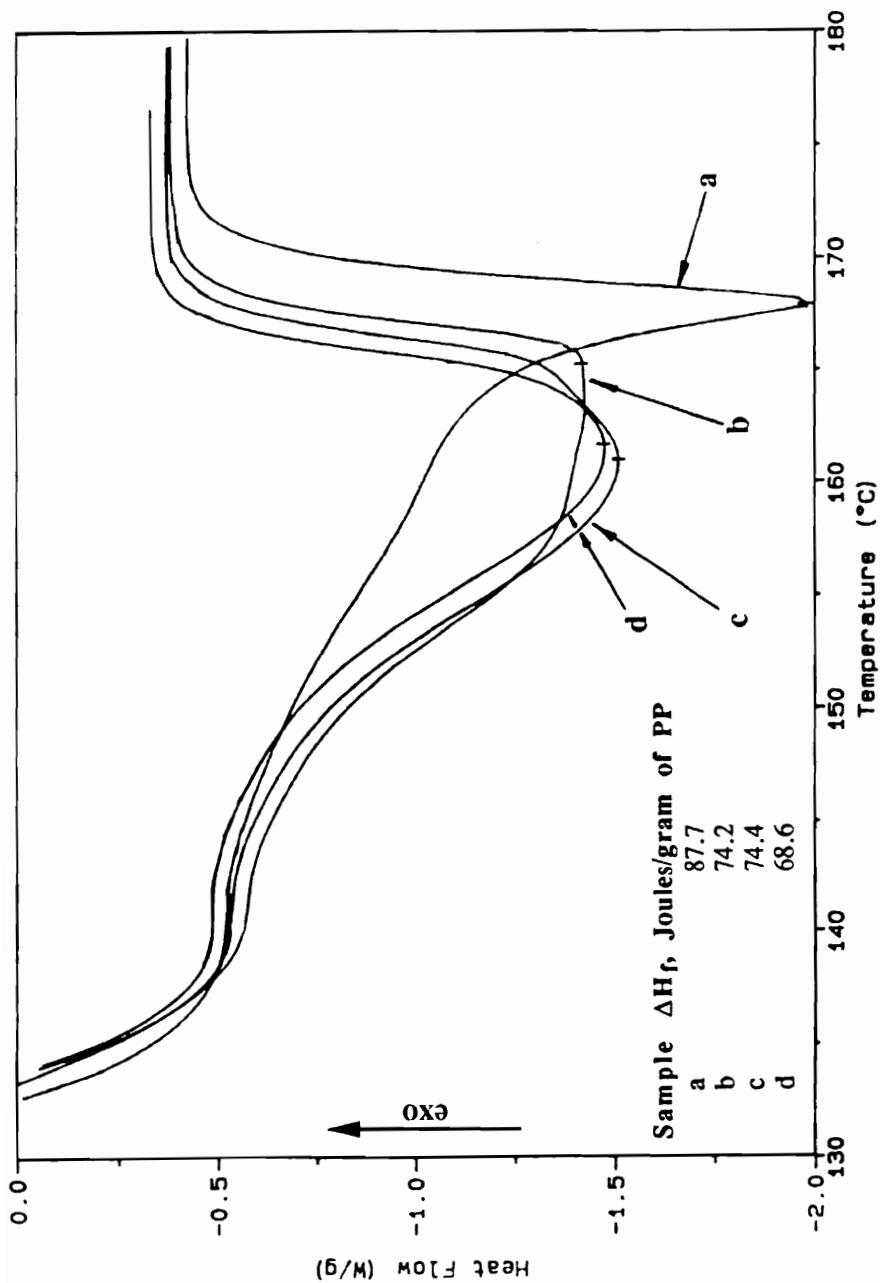


**Figure 3.3.8** Effect of 210 °C heat treatment on melting point behavior following 132 °C isothermal crystallization of Blend(200-15). (a) 0, (b) 5, (c) 10, and (d) 15 minutes.

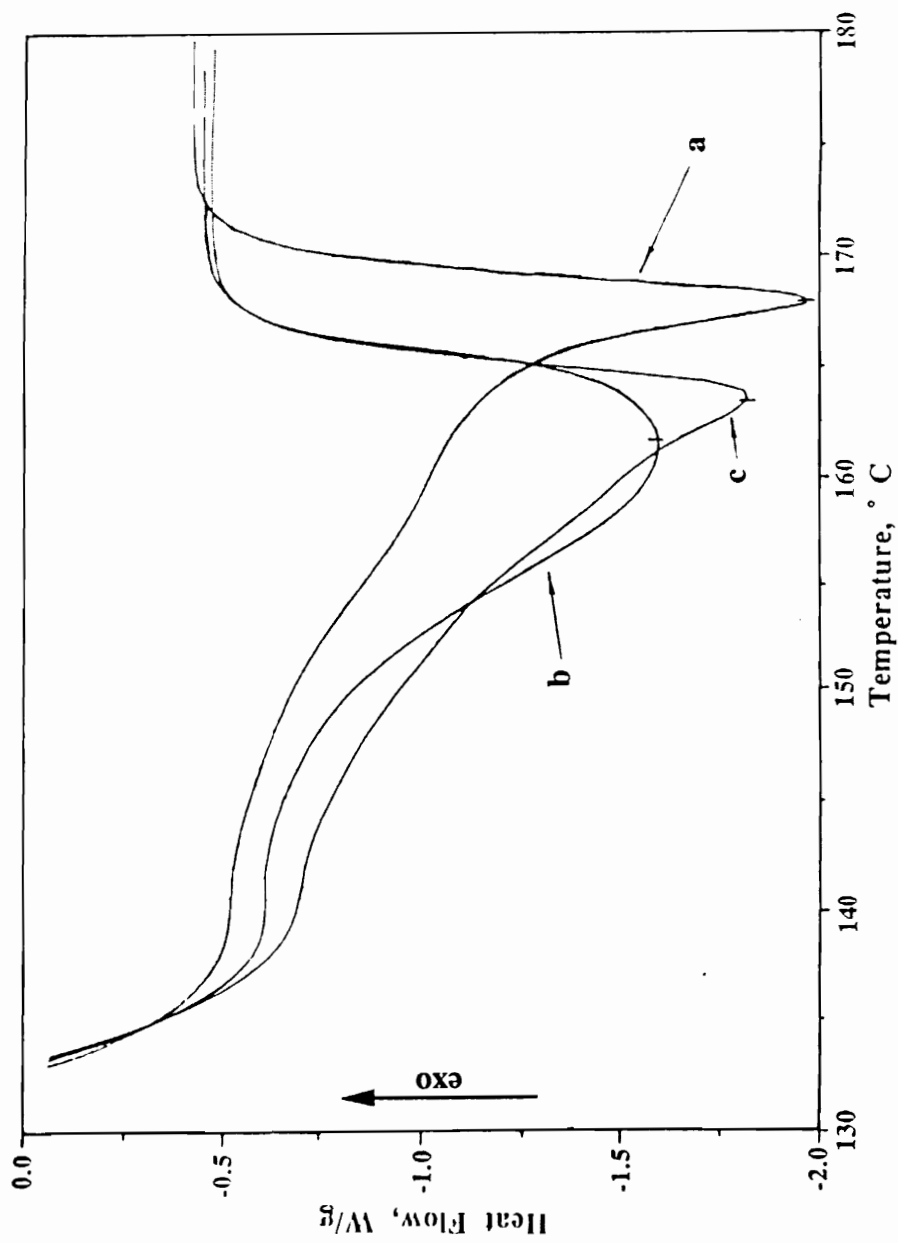


**Figure 3.3.9** Comparison of the melting point behavior after 132 °C isothermal crystallization of (a) Blend(200-15), (b) Blend(200-15) after 15 minutes at 210 °C, and (c) Blend(210-30).



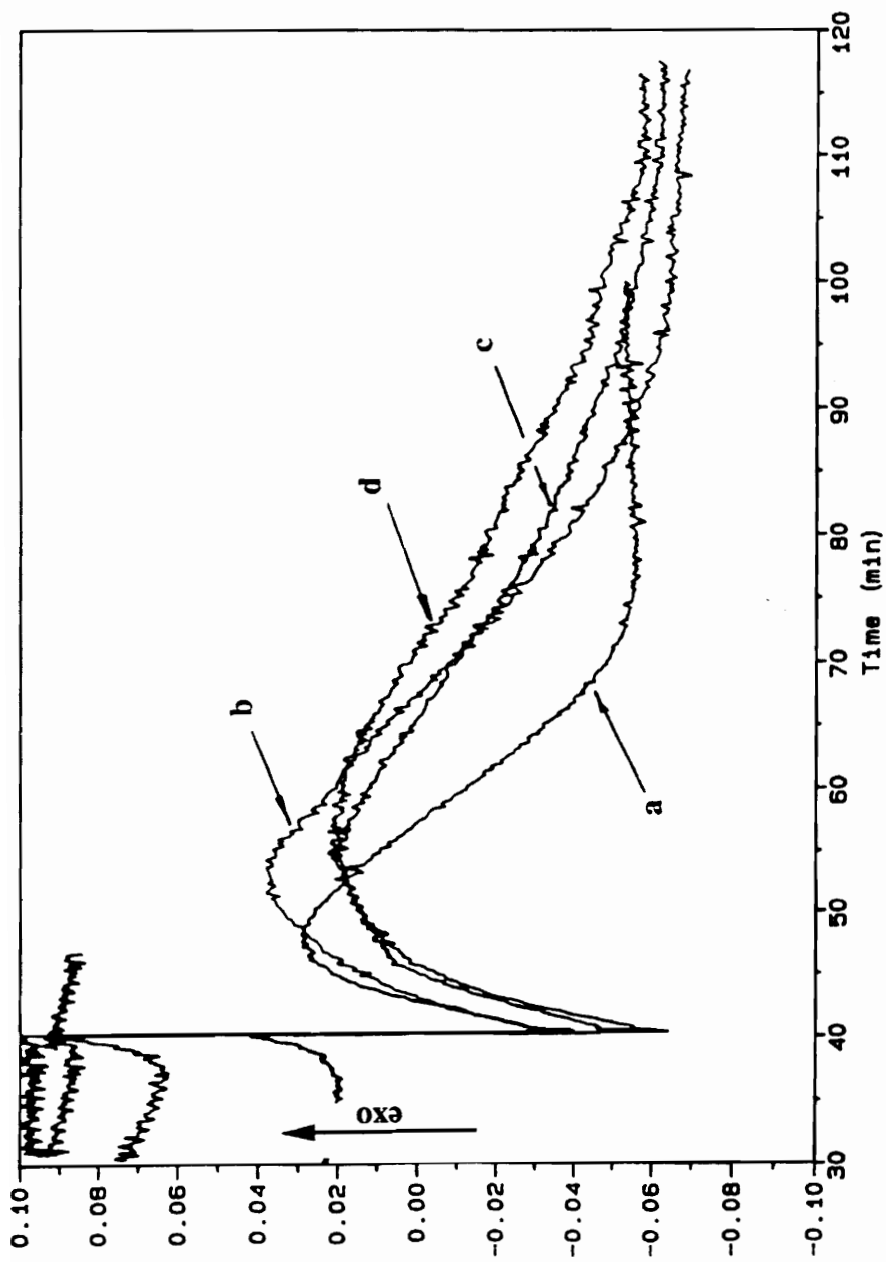


**Figure 3.3.10** Effect of 210 °C heat treatment on 132 °C isothermal crystallization behavior of neat polypropylene. (a) 0, (b) 5, (c) 10, and (d) 15 minutes.

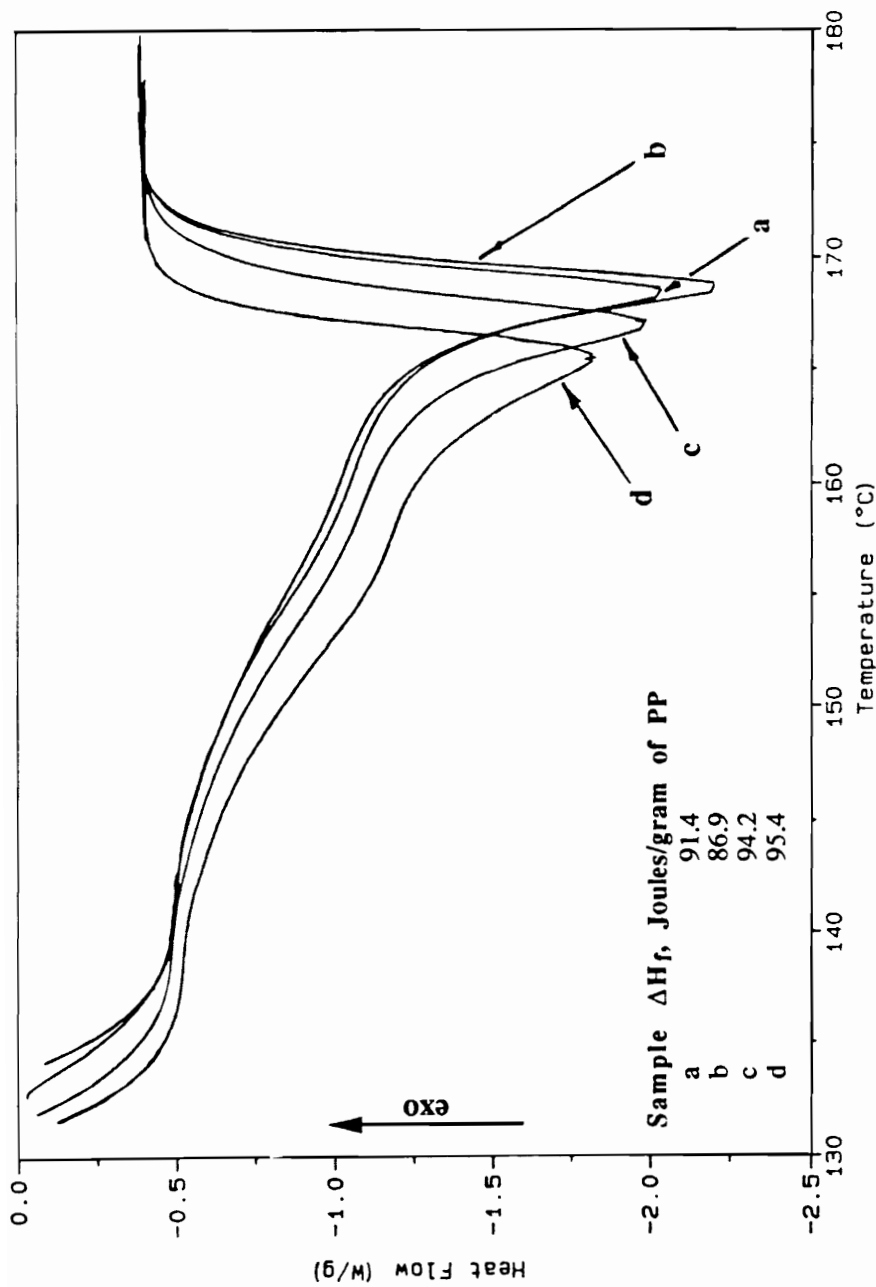


**Figure 3.3.11** Effect of 210 °C heat treatment on 132 °C melting point behavior following 132 °C isothermal crystallization of neat polypropylene. (a) 0, (b) 5, (c) 10, and (d) 15 minutes.

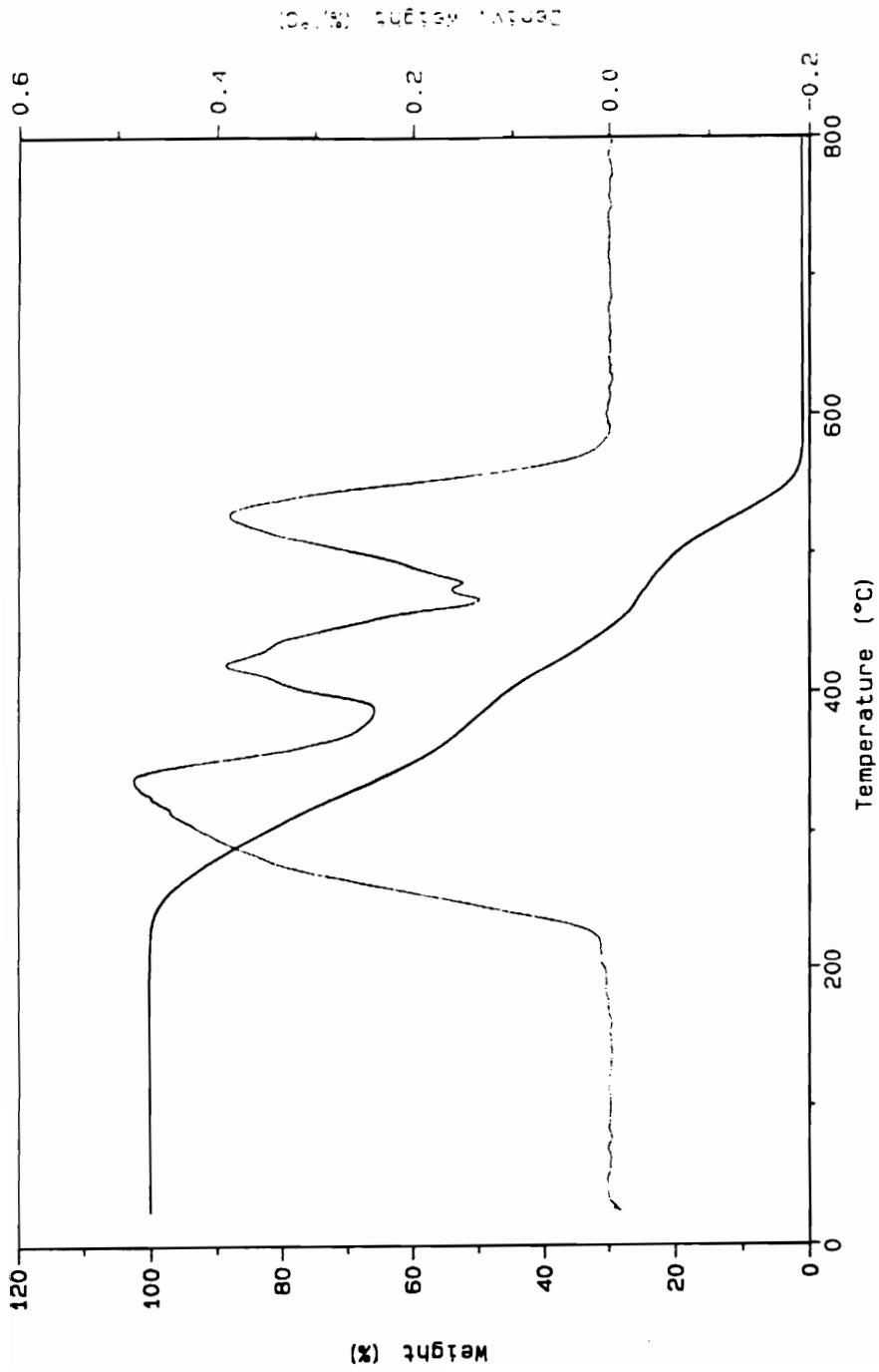


**Figure 3.3.12** 10 °C/minute dynamic TGA scan in air of poly(vinyl methyl ether).

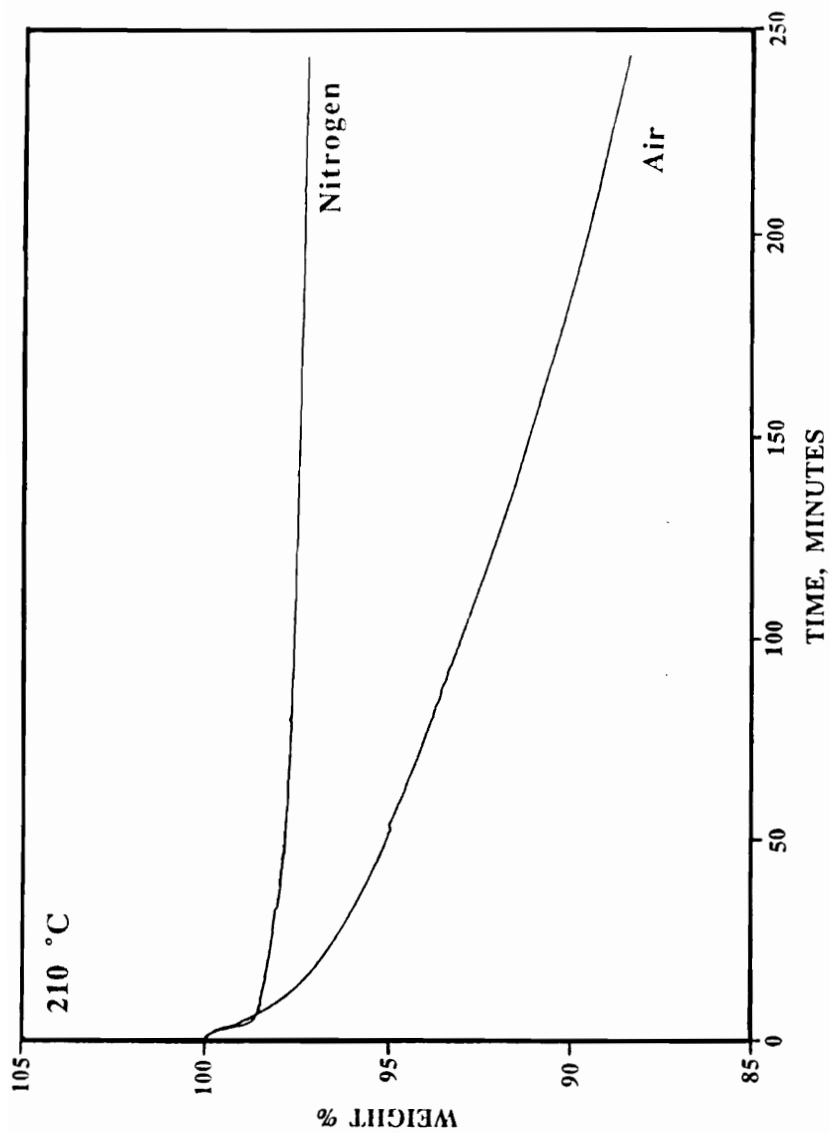


**Figure 3.3.13** Isothermal TGA scans in air and nitrogen of poly(vinyl methyl ether).

polymer remains quite stable after losing some weight initially, possibly due to the presence of some low molecular weight volatiles. In air, on the other hand, there is a continuous loss of weight during the entire experimental period indicating that thermooxidative degradation are possible at 210 °C- given a source for oxygen.

The chemical changes that accompany the thermooxidative degradation can be observed on Figures 3.3.14 and 3.3.15. Figure 3.3.14 compares the FTIR spectra of PVME as-is and after heat treatment of 15 minutes at 210 °C in air. There is an addition of a peak at 1723  $\text{cm}^{-1}$  due to carbonyl in the latter, indicating it to be a product of degradation. After 15 minutes at 210 °C, PVME essentially converted into a crosslinked solid film. Figure 3.3.15 shows the  $^{13}\text{C}$  solid state CP/MAS NMR spectrum run on this crosslinked material. In addition to the peaks attributable to the three carbons of the PVME structure, peaks due to olefinic C=C and carbonyl C=O carbons are also recognized. This is in agreement with a similar previous investigation by Prime *et al.*<sup>248</sup>

From the above, the mechanism for degradation of PVME, as depicted on Figure 3.3.16, may be thought to be as follows. The thermooxidation begins with the abstraction of the methine  $\alpha$ -hydrogen which subsequently leads to the formation of peroxide radical by addition of oxygen. Three routes are then possible in order to stabilize this radical: (a) demethoxylation with the loss of methanol forming ketonic species as a result, (b) main chain fragmentation producing lower molecular weight PVME chains with olefinic end-groups, and finally, (c) crosslinking with the neighboring chains. All three routes are confirmed from FTIR and NMR data as well as the fact that a highly crosslinked material results after degradation. However, the third route seems to be important when considering degradation of PP - PVME blends. In addition to self-crosslinking, the PVME

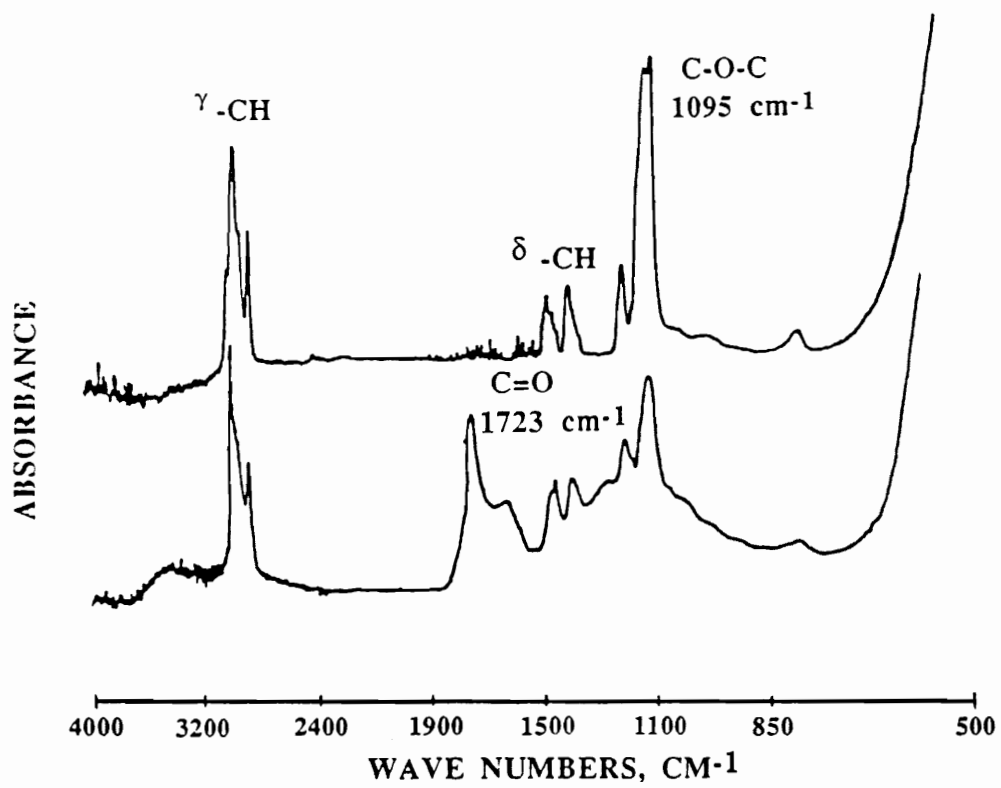


**Figure 3.3.14** FTIR spectra of PVME before and after heat treatment at 210 °C for 15 minutes.

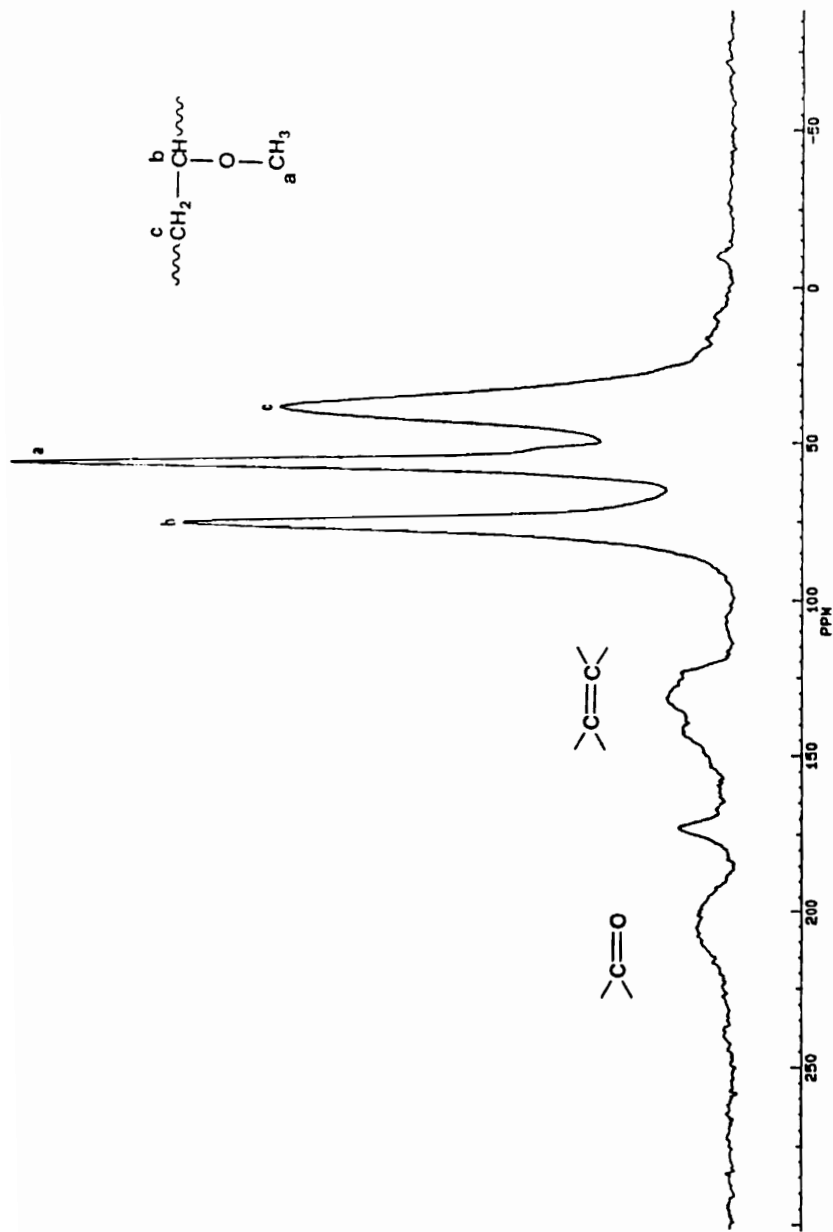


**Figure 3.3.15**  $^{13}\text{C}$  Carbon CP/MAS NMR spectrum of crosslinked poly(vinyl methyl ether) after 15 minutes at  $210^\circ\text{C}$ .

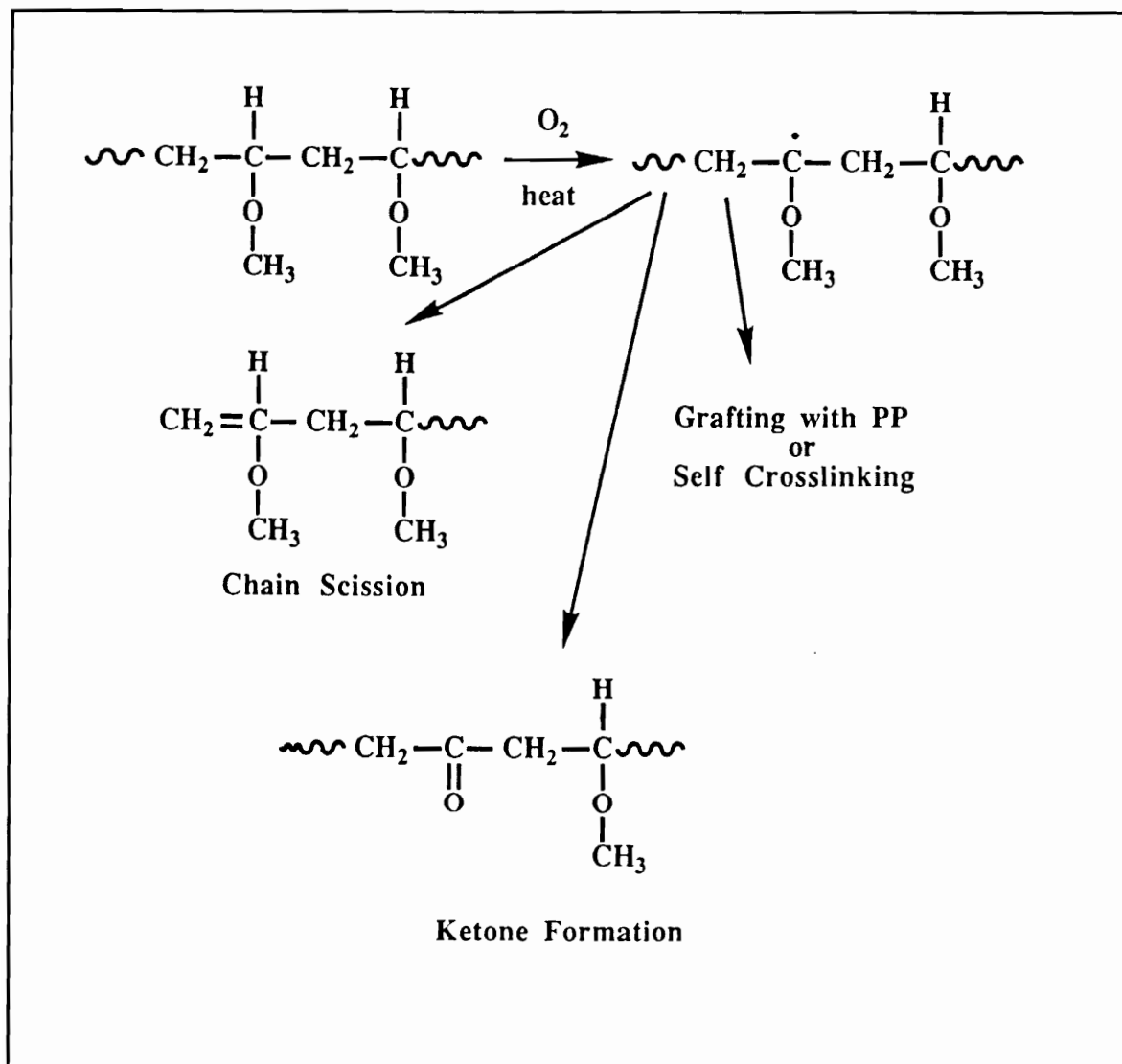


**Figure 3.3.16** Proposed mechanism for thermooxidative degradation of PVME.



chain can also graft onto a nearby PP chain thereby becoming incorporated into the PP matrix, which can then be responsible for miscibility-like behavior observed via DSC.

### 3.4 CONCLUSIONS

Two PP - PVME melt-blends containing 10% PVME prepared under different conditions of temperature and time displayed distinctly dissimilar behaviors. The blend prepared by mixing at 200 °C for 15 minutes indicated an absence of miscibility as judged from crystallization kinetics and melting points from DSC measurements. On the other hand, the blend prepared under slightly more severe conditions e. g., 210 °C for 30 minutes, displayed a DSC behavior suggesting some interactions between PVME and PP; the behavior persisted even after extraction of the soluble PVME fraction from the blend. The morphology of the two blend as examined by SEM varied, corroborating the observations from DSC. Furthermore, the DSC behavior of the 200 °C/15 minute blend could be made to resemble that of the 210 °C/30 minute blend by an external heat treatment. Similar heat treatment did not produce comparable degree of changes in the DSC behavior of the neat PP. Based on these observations and the fact that PVME tends to crosslink as a result of thermooxidative degradation, it is proposed PVME is capable of grafting onto PP chains under the conditions of melt-blending. The chemical attachment of PVME is then thought to be responsible for the display of miscibility-like behavior. Thus, although PP and PVME do not show *physical* miscibility, chemorheological events occurring during the processing of their blends could induce what may be termed as *chemical* miscibility.

### 3.5 FUTURE RECOMMENDATIONS AND IMPLICATIONS

The above preliminary study was at best meant to provide a starting point for further work, both in terms of better understanding of the interactions between PP and PVME as well as exploring the use of these interactions in practical applications. Along these lines, the following areas are recognized as being meritorious for future investigation.

*Optimization of Conditions Leading to Grafting.* The study presented here was limited from the point of view of the control of the blending process. In a melt-blender such as the Haake Rheomix, a number of variables come into play during mixing. Thus, apart from the time and temperature, one may also study, for example, the effects of the rpm of mixing blades, the weight of the polymer charged, and the environment in which the blending is performed. In addition, the properties of the polymers themselves with regards to their molecular weights and presence or absence of stabilizers and antioxidants may make up another set of parameters whose influence on the efficacy of grafting is recommended for further study.

*Analysis of Grafted Polymer.* A more direct evidence of grafting than DSC may shed further light on the mechanism of grafting and therefore, help in the above task of optimization. Model experiments on atactic PP and PVME should allow one to use solution based techniques such as GPC and NMR to monitor changes in molecular weights and chemistry as a result of grafting.

*Extension to Other vinyl ethers.* The higher homologues of PVME such as poly(vinyl ethyl ether) (PVEE) and poly(vinyl butyl ether) (PVBE) may be expected to be more

attractive from the points of synthesis as well their ability for grafting. Work in this direction is currently in progress at Virginia Tech. Initial results with PVBE have shown promise.

*Exploration of Practical Applications.* A number of applications may be identified based on the proposed grafting capability of PVME and its homologues onto PP. A block or graft copolymer with PVME as one of the components will have a potential use as a compatibilizer for PP - Nylon 6 as proposed in the long-term objectives of this project. Grafting at the interface between PP and Nylon 6 would provide the anchoring mechanism necessary for good mechanical properties. Poly(vinyl alkyl ether)s by themselves may also prove to be effective in toughening PP where one would expect to may have both compatibility as well the interfacial adhesion between the two components. One may also visualize a novel method for obtaining compatible blends of PS and PP. The ternary system of PS, PVME and PP should have a two-phase morphology: PS and a minor amount of PVME forming one phase, while PP making up the other. Chemical interactions between PP and PVME across the phase boundary would promote phase stability and adhesion, and therefore, compatibility.

## REFERENCES

---

1. Morton, W. E., and Hearle, J. W. S., *Physical Properties of Textile Fibers*, Butterworth (1962).
2. Filshie, B. K., and Rogers, G. E., *J. Mol. Biol.* , **3**, 784 (1961).
3. Amos, J. L., *Polym. Eng. Sci.*, **14**, 1.(1974).
4. Bucknall, C. B., *Toughened Plastics*, Applied Science Publishers, London (1977).
5. Donattelli, A. A., Thomas, D. A., and Sperling, L. H., in *Recent Advances in Polymer Blends, Grafts, and Blocks*, L. H. Sperling, ed., Plenum Press, p375 (1974).
6. Dobry, A., and Boyer-Kawenoki, F., *J. Poly. Sci.*, **2**, 90 (1947).
7. Bohn, L., *Rubber Chem. Technol.*, **41**, 495 (1968).
8. Krause, S. J., *Macromol. Sci. Rev. Macromol. Chem.*, **C7**, 251 (1972).
9. Olabisi, O., Robeson, L. M., and M. T. Shaw, *Polymer - Polymer Miscibility*, Academic Press, New York (1979).

10. Paul, D. R., Barlow, J. W., and Keskkula, H., *Polymer Blends*, in *Encyclopedia of Polymer Science and Engineering*, **12**, 399 (1989).
11. Fox, D. W., and Allen, R. B., *Compatibility*, in *Encyclopaedia of Polymer Science and Engineering*, **3**, 758 (1989).
12. *Polymer Blends, Volumes I and II*, Paul, D. R., and Newman, S., eds., Academic (1978).
13. Paul, D. R., and Barlow, J. W., *J. Macromol. Sci. Macromol. Chem.*, **C18**, 109 (1980).
14. Barlow, J. W., and Paul, D. R., *Annu. Rev. Mat. Sci.*, **11**, 299 (1981).
15. Paul, D. R., and Barlow, J. W., in *Polymer Compatibility and Incompatibility: Principles and Practice*, K. Solc, ed., MMI Press, Midland, Michigan (1982) p1.
16. Fox, T. G., *Bull. Am. Phy. Soc.*, **1**, 123 (1956).
17. Drake, R. S., and McCarthy, W. J., *Rubber World*, **159**, 51 (1968).
18. Riew, C. K., *Rubber Chem. Tech.*, **54**, 374 (1981).
19. Tran, T-C. H., Ph. D. Dissertation, Virginia Polytechnic Institute & State University, 1984.
20. Dusek, K., Lednicky, F., Lunak, S., Mach, M., and Duskova, D., in *Rubber Modified Thermoset Resins*, C. W. Riew, and J. K. Gillham, eds., *Advances in Chemical Series*, **208**, ACS, Washington, D. C. (1984).p27.
21. Molau, G. E., in *Colloidal and Morphological Behavior of Block and Graft Copolymers*, G. E. Molau, ed., Plenum Press, New York, (1971).p79.
22. Maglio, G., and Palumbo, R., in *Polymer Blends- Processing, Morphology, and Properties, Volume 2*, M. Kryszewski, A. Galeski, and E. Martuscelli, eds., Plenum Press, New York, (1984).p41.
23. Gaylord, N. G., *J. Macromol. Sci., Macromol. Chem.*, **A26**, 1211 (1989).

24. Noshay, A., and McGrath, J. E., *Block Copolymers: Overview and Critical Survey*, Academic Press, New York (1977).
25. *Developments in Block Copolymers - I*, I. Goodman, ed., Applied Science, London (1982).
26. Meier, D. J., *Block Copolymers: Science and Technology*, MMI Press, Midland, Michigan (1983).
27. *Processing, Structure and Properties of Block Copolymers*, M. J. Folkes, ed., Elsevier Applied Science, Barking (1985).
28. Patel, N. M., Dwight, D. W., Hedrick, J. L., Webster, D. C., and McGrath, J. E., *Macromolecules*, **21**, 2189 (1988).
29. Dwight, D. W., McGrath, J. E., Lawson, G. L., Patel, N. M., and York, G., in *Multiphase Macromolecular Systems*, B. M. Culbertson, ed., Plenum (1989) p265.
30. White, R. M., *Scientific American*, **243**(2), 138 (1980).
31. Harker, J. M., Brede, D. W., Pattison, R. E., Santana, G. R., and Taft, L. G., *IBM J. Res. Develop.*, **25**, 677 (1981).
32. Arnoldussen, T. C., and Rossi, E. M., *Ann. Rev. Mat. Sci.*, **15**, 79 (1985).
33. Johnson, D. D., Flores, R., and Vogel, M. J., *U. S. Patent 3,058,844* (1962).
34. Soane, D. S., and Martynenko, Z., *Polymers in Microelectronics: Fundamentals and Applications*, Elsevier, Amsterdam (1989).
35. Kaneko, R., and Koshimoto, Y., *IEEE Trans. Mag.*, **MAG-18**, 1221 (1982).
36. Linder, R. E., and Mee, P. B., *IEEE Trans. Mag.*, **MAG-18**, 1073 (1982).
37. Prime, R. B., *private communication*.
38. Burns, J. M., Auser, W. D., Gutierrez, M. L., and Karmin, M. L., *Proc. NATAS Conf.*, **14**, 534 (1985).

39. Siedl, J., Malinsky, J., Dusek, K., and Weitz, W., *Advan. Polym. Sci.*, **5**, 113 (1967).
40. Guyot, A., and Bartholin, M., *Prog. Polym. Sci.*, **8**, 277 (1982).
41. Miller, J. R., Smith, D. C., Marr, W. E., and Kressman, T. R. E., *J. Chem. Soc.*, 218(1963).
42. Kun, K. A., and Kunin, R., *J. Polym. Sci. A-1*, **6**, 2689 (1968).
43. Jacobelli, h., Bartholin, M., and Guyot, A., *J. Appl. Polym. Sci.*, **23**, 927 (1979).
44. Flodin, P., and Lagerkvist, P., *J. Chromat.*, **215**, 7 (1981).
45. Miller, J. R., Smith, D. C., and Kressman, T. R. E., *J. Chem. Soc.*, 304 (1965).
46. Abrams, I. M., *Ind. Eng. Chem.*, **48**, 1469 (1956).
47. Fujita, F. M., and Soane, D. S., *Polym. Eng. Sci.*, **28**, 341 (1988).
48. Sederel, W. L., and De Jong, G. J., *J. Appl. Poly. Sci.*, **17**, 2835 (1973).
49. *Materials Science of Synthetic Membranes*, D. R. Lloyd, ed., *ACS Symp Ser.*, **269**, ACS, Washington, D. C. (1985).
50. *Reverse Osmosis and Ultrafiltration*, S. Sourirajan, and T. Matsuura, eds., *ACS Symp. Ser.*, **281**, ACS, Washington, D. C. (1985).
51. Meares, P., *Membrane Separation Processes*, Elsevier, Amsterdam (1976).
52. *Synthetic Membranes, Vol. I and II*, A. F. Turbak, ed., *ACS Symp. Ser.*, **153/154**, ACS, Washington, D. C. (1981).
53. Kesting, R. E., *Synthetic Polymeric Membranes: A structural Perspective*, 2nd edition, Wiley-Interscience, New York (1985).
54. Loeb, S., and Sourirajan, S., *Adv. Chem. Ser.*, **38**, 117 (1962).
55. H. Strathmann, in ref. 49, p131.

56. Yoo, Y. T., Kilic, S., and McGrath, J. E., *Polym. Prepr., Am. Chem. Soc., Div. Polym. Chem.*, **28**, 272 (1987).
57. Yoo, Y. T., *PhD Dissertation*, Virginia Polytechnic and State University (1988).
58. Gillham, J. K., *Soc. Plas. Eng. Proc. An. Tech. Conf.*, **38**, 238 (1980).
59. Bolger, J. C., in *Treatise on Adhesion and Adhesives*, R. L. Patrick, ed., Merce Dekker, New York (1973) p1.
60. Pocius, A. V., *Rub. Chem. Tech.*, **58**, 622 (1985).
61. McGarry, F. J., and Sultan, J. N., *Proc. Ann. Tech. Conf. SPI*, **24**, 11-b (1969).
62. McGarry, F. J., and Willner, A. M., *Am. Chem. Soc. Div. Org. Coat. Plast. Chem. Prepr.*, **28**, 55 (1968).
63. Sultan, J. N., and McGarry, F. J., *Poly. Eng. Sci.*, **13**, 29 (1973).
64. McGarry, F. J., *Proc. Roy. Soc. Lond.*, **A319**, 54 (1970).
65. Rowe, E. H., Siebert, A. R., and Drake, R. S., *Mod. Plast.*, **47**, 110 (1970).
66. Siebert, A. R., and Riew, C. K., *Am. Chem. Soc. Div. Org. Coat. Plast. Prepr.*, **31**, 555 (1971).
67. Riew, C. K., Rowe, E. H., and Siebert, A. R., in *Toughness and Brittleness of Plastics*, R. D. Deanin, ed., *Adv. Chem. Ser.*, **154**, ACS, Washington, D. C. (1976) p326.
68. Soldatos, A. C., and Burhans, A. S., in *Multicomponent Polymer Systems*, R. F. Gould, ed., *Adv. Chem. Ser.*, **99**, ACS, Washington, D. C., (1971) p531.
69. Meeks, A. C., *Polymer*, **15**, 675 (1974).
70. Bascom, W. D., Cottington, R. L., Jones, R. L., and Peyser, P., *J. Appl. Polym. Sci.*, **19**, 2545 (1975).
71. St. Clair, A. K., and St. Clair, T. L., *Int. J. Adhes. Adhesives*, **2**, 249, (1981).



72. Kinloch, A. J., Shaw, S. J., and Tod, D. A., in *Rubber Modified Thermoset Resins*, C. K. Riew and J. K. Gillham, eds., *Adv. Chem. Ser.*, **208**, ACS, Washington, D. C. (1984) p101.
73. Shaw, S. J., and Kinloch, A. J., *Int. J. Adhes. Adhesives*, **5**, 123 (1985).
74. McGarry, F. J., Rowe, E. H., and Riew, C. K., *Proc. Ann. Tech. Conf. Reinf. Plast. Compos. Inst. SPE*, **16-C** (1977).
75. Englehardt, J. T., and Nichols, C. S., in *Rubber Modified Thermoset Resins*, C. K. Riew and J. K. Gillham, eds., *Adv. Chem. Ser.*, **208**, ACS, Washington, D. C. (1984) p335.
76. Martin, F. R., in *Developments in Adhesives-I*, Wake, W. C., ed., Applied Science, London (1977) p157.
77. Lees, W. A., *British Polym. J.*, **11**, 64 (1979).
78. Yorkgitis, E. M., Tran C., Eiss, N. S., Jr., Hu, T. Y., Yilgor, I., Wilkes, G. L., and McGrath, J. E., in *Rubber Modified Thermoset Resins*, C. K. Riew and J. K. Gillham, eds., *Adv. Chem. Ser.*, **208**, ACS, Washington, D. C. (1984) p137.
- 78b. Yorkgitis, E. M., *Ph. D. Dissertation*, Virginia Polytechnic Institute and State University (1985).
79. Hill, J. W., *Proc. Ann. Tech. Conf. SPE*, **32**, 301 (1974).
80. Hawthorne, K., Stavinoha, R., Craigie, L., *Proc. Ann. Tech. Conf. Reinf. Plast. Compos. Inst. SPE*, **5-E** (1977).
81. Drake, R. S., Egan, D. R., and Murphy, W. T., in *Epoxy Resin Chemistry II*, R. S. Bauer, ed., *ACS Symp. Ser.*, **221**, ACS, Washington, D. C. (1983) p1.
82. Riffle, J. S., Yilgor, I., Tran C., Wilkes, G. L., McGrath, J. E., and Banthia, A. K., in *Epoxy Resin Chemistry II*, R. S. Bauer, ed., *ACS Symp. Ser.*, **221**, ACS, Washington, D. C. (1983) p21.

83. Saito, N., Nakajima, N., Ikushima, T., Kanagawa, S., and Takahashi, T., *Polym. Mat. Sci. Eng.*, **57**, 558 (1987).
84. Ochi, M., and Bell, J. P., *J. Appl. Polym. Sci.*, **29**, 1381 (1984).
- 84b. Kirshenbaum, S. L., Gazit, S., and Bell, J. P., in *Rubber Modified Thermoset Resins*, C. K. Riew and J. K. Gillham, eds., *Adv. Chem. Ser.*, **208**, ACS, Washington, D. C. (1984) p163.
85. Banthia, A. K., Chaturvedi, P. N., Jha, V., *Polym. Mat. Sci. Eng.*, **57**, 775 (1987)
86. Slysh, R., in *Epoxy Resins II*, H. Lee, ed., *Adv. Chem. Ser.*, **92**, ACS, Washington, D. C. (1970) p108.
87. Noshay, A., and Robeson, L. A., *J. Polym. Sci., Polym. Chem. Ed.*, **12**, 689 (1974).
88. Hedrick, J. L., Yilgor, I., Wilkes, G. L., and McGrath, J. E., *Polym. Bull.*, **13**, 201 (1985).
89. Hedrick, J. L., Ph. D. Dissertation, Virginia Polytechnic Institute and State University (1985).
90. Buckwall, C. B., and Partridge, I. K., *Polymer*, **25**, 639 (1987).
91. Yamanaka, K., Inoue, T., *Polymer*, **30**, 662 (1989).
92. Cecere, J. A., Hedrick, J. L., and McGrath, J. E., *SAMPE Symp.*, **31**, 580 (1986).
93. Cecere, J. A., Ph. D. Dissertation, Virginia Polytechnic and State University (1987).
- 93b. Cecere, J. A., and McGrath, J. E., *Polym. Prepr. Div. Polym. Chem. Am. Chem. Soc.*, **27(1)**, 299 (1986).
94. Buckwall, C. B., and Gilbert, A. H., *Polymer*, **30**, 213 (1989).

95. Kim, S. C., and Brown, H. R., *J. Mat. Sci.*, **22**, 2589 (1987).
96. Recker, H. G., Altstadt, V., Eberle, W., Folda, T., Gerth, D., Heckmann, W., Ittemann, P., Tesch, H., and Weber, T., *SAMPE J.*, **26(2)**, 73 (1990).
97. Sefton, M. S., McGrail, P. T., Peacock, J. A., Wilkinson, S. P., Crick, R. A., Davies, M., and Almen, G., *SAMPE Int. Tech. Conf.*, **19**, 700 (1987).
98. Kinloch, A. J., and Young, R. J., *Fracture Behavior of Polymers*, Applied Science, London (1983).
99. Kinloch, A. J., Shaw, S. J., and Huntson, D. L., *Polymer*, **24**, 1355 (1983).
100. Yee, A. F., and Pearson, R. A., *J. Mat. Sci.*, **21**, 2462 (1986).
101. Kunz-Douglass, S., Beaumont, P. W. R., Ashby, M. F., *J. Mat. Sci.*, **15**, 1109 (1980).
102. Wu, S., *Polymer*, **26**, 1855 (1985).
103. Wu, S., *J. Appl. Polym. Sci.*, **35**, 549 (1988).
104. Kinloch, A. J., in *Structural Adhesives: Developments in Primers and Resins*, A. J. Kinloch, ed., Elsevier Applied Science, London (1986) p127.
105. Gibbs, J. W., *Collected Works Volume I*, Dover Reprints, New York (1961).
106. McMaster, L. P., *Adv. Chem. Ser.*, **142**, (1975) p43.
107. Kwei, T. K., and Wang, T. T., in *Polymer Blends Volumes I and II*, D. R. Paul, and S. Newman, eds., Academic Press, New York, (1978) chapter 4.
108. Keskkula, H., in *Polymer Compatibility and Incompatibility: Principles and Practice*, K. Solc, ed., MMI Press, Midland, Michigan (1982) p323.
109. Sperling, L. H., *Microphase Structure*, in *Encyclopedia of Polymer Science and Technology*, **9**, 760 (1989).
110. Krause, S., in *Polymer Blends Volumes I and II*, D. R. Paul, and S. Newman, eds., Academic Press, New York, (1978) chapter 2.

111. Koningveld, R., Onclin, M. H., and Kleintjens, L. A., in *Polymer Compatibility and Incompatibility: Principles and Practice*, K. Solc, ed., MMI Press, Midland, Michigan (1982) p25.
112. Flory, P. J., *J. Chem. Phys.*, **10**, 51 (1942).
113. Flory, P. J., *Principles of Polymer Chemistry*, Cornell University Press (1953).
114. Huggins, M. L., *J. Am. Chem. Soc.*, **64**, 1712 (1942).
- 114b. Hildebrand, J. H., and Scott, R. L., *The Solubility of Non-electrolytes*, Dover, New York (1964).
- 114c. Hildebrand, J. H., Prausnitz, J. M., and Scott, R. L., *Regular and Related Solutions*, Van Nostrand Reinhold, New York (1970)
115. Koningveld, R., Chermin, H. A. G., and Gordon, M., *Proc., Roy. Soc. Lon.*, **A-319**, 331 (1970).
116. Koningveld, R., Kleintjens, L. A., and Shultz, A., R., *J. Polym. Sci. A-2*, **8**, 1261 (1970).
117. Koningveld, R., and Kleintjens, L. A., in *Polymer Blends and Mixtures*, D. J. Walsh, J. S. Huggins, and A. Maconnachie, eds., Martinus Nijoff Publishers, Dordrecht, the Netherlands (1985) p89.
118. Flory, P. J., Orwoll, R. A., Vrij, A., *J. Am. Chem. Soc.*, **86**, 3515 (1964).
119. Flory, P. J., *Discuss. Far. Soc.*, **49**, 7 (1970).
120. Sanchez, I. C., *Polymer Compatibility and Incompatibility: Principles and Practice*, K. Solc, ed., MMI Press, Midland, Michigan (1982) p59.
121. Sanchez, I. C., *An. Rev. Mat. Sci.*, **13**, 387 (1983).
122. Williams, R. J. J., Borrajo, J., Adabbo, H. E., Rojas, A. J., in *Rubber Modified Thermoset Resins*, C. K. Riew and J. K. Gillham, eds., *Adv. Chem. Ser.*, **208**, ACS, Washington, D. C. (1984) p195.

123. Flory, P. J., *J. Am. Chem. Soc.*, **63**, 3083 (1941).
- 123b. Flory, P. J., *J. Am. Chem. Soc.*, **63**, 3091 (1941).
124. Flory, P. J., *J. Am. Chem. Soc.*, **63**, 3096 (1941).
125. Stockmayer, W. H., *J. Chem. Phys.*, **11**, 45 (1943).
126. Verchere, D., Sautereau, H., Pascault, J. P., Moschiar, S. M., Riccardi, C. C., and Williams, R. J. J., *Polymer*, **30**, 108 (1989).
127. Yamanaka, K., Inoue, T., *J. Mat. Sci.*, **25**, 241, (1990).
128. Drake, R., and Siebert, A., *SAMPE Quat.*, **6(1)**, 11 (1975).
129. Wang, T. T., and Zupko, H. M., *J. Appl. Polym. Sci.*, **26**, 2391 (1981).
130. Hsich, H. S.-Y., *J. Mat. Sci.*, **25**, 1568 (1990).
131. Manzione, L. T., Gillham, J. K., and McPherson, G. A., *J. Appl. Polym. Sci.*, **26**, 889 (1981).
132. Romanchick, W. A., Sohn, J. E., and Giebel, J. F., in *Epoxy Resin Chemistry II*, R. S. Bauer, ed., *ACS Symp. Ser.*, **221**, ACS, Washington, D. C. (1983) p85.
133. Kunz, S. C., Sayre, J. A., and Assink, R. A., *Polymer*, **23**, 1897 (1982).
134. Chan, L. C., Gillham, J. K., Kinloch, A. J., and Shaw, J. S., in *Rubber Modified Thermoset Resins*, C. K. Riew and J. K. Gillham, eds., *Adv. Chem. Ser.*, **208**, ACS, Washington, D. C. (1984) p235.
135. Bucknall, C. B., and Yoshii, T., *Brit. Polym. J.*, **10**, 53 (1978).
136. Nae, H. N., *J. Appl. Polym. Sci.*, **31**, 15 (1986).
137. Visconti, S., Marchessault, R. H., *Macromolecules*, **7**, 913 (1974).
138. Levita, G., Marchetti, A., and Butta, E., *Polymer*, **26**, 1110 (1985).
139. Shaw, S. J., and Tod, D. A., *J. Adhesion*, **28**, 231 (1989).
140. Yamanaka, K., Takagi, Y., and Inoue, T., *Polymer*, **30**, 1839 (1989).

141. Hedrick, J. C., Lewis, D. A., Ward, T. C., and McGrath, J. E., *Polym. Prepr. Am. Chem. Soc. Div. Polym. Chem.*, **29**(1), 363 (1988).
142. Hedrick, J. C., Lewis, D. A., Ward, T. C., and McGrath, J. E., *Proc. Mat. Res. Soc.*, April 1990, in press.
143. Hedrick, J. C., Ph. D. Dissertation, Virginia Polytechnic Institute and State University, 1990.
144. Vasquez, A., Rojas, A. J., Adabbo, H. E., Borrajo, J., and R. J. J. Williams, *Polymer*, **28**, 1156 (1987).
145. Prime, R. B., *Thermosets*, Chapter 5 in *Thermal Characterization of Polymeric Materials*, E. Turi, ed., Academic Press, New York (1981).
146. Chadwick, G. A., *Metallography of Phase Transitions*, Crane, Russak & Co., New York (1972).
147. Burke, J., *The Kinetics of Phase Transformations in Metals*, Pergamon Press, Oxford (1965).
148. Enns, J. B., Gillham J. K., and Small, R., *Polym. Prepr. Am. Chem. Soc. Div. Polym. Chem.*, **22**(2), 123 (1981).
149. Enns, J. B., and Gillham, J. K., in *Polymer Characterization: Spectroscopic, Chromatographic, and Physical Instrumental Methods*, C. D. Craver, ed., *Adv. Chem. Ser.*, **203**, ACS, Washington, D. C. (1983) p27.
150. Gillham J. K., in *Development in Polymer Characterization- 3*, J. V. Dawkins, ed., Applied Science, London (1982) p159.
151. Chan, L. C., Nae, H. N., and Gillham, J. K., *J. Appl. Polym. Sci.*, **29**, 3307 (1984).
152. Peng, X., and Gillham, J. K., *J. Appl. Polym. Sci.*, **30**, 4685 (1985).
153. Gillham, J. K., *Polym. Eng. Sci.*, **26**, 1429 (1986).

154. Enns, J. B., and Gillham, J. K., *J. Appl. Polym. Sci.*, **28**, 2567 (1983).
155. Aronhime, M. T., and Gillham, J. K., in *Epoxy Resins and Composites III*, K. Dusek, ed., *Adv. Polym. Sci.*, **78**, Springer-Verlag, Heidelberg (1986) p83.
156. Lewis, A. F., and Gillham, J. K., *J. Appl. Polym. Sci.*, **6**, 422 (1962).
157. Gillham, J. K., *Polym. Eng. Sci.*, **16**, 353 (1976).
158. Gillham, J. K., *Polym. Eng. Sci.*, **19**, 319 (1979).
159. Gillham, J. K., Glandt, C. A., and McPherson, C. A., in *Chemistry and Properties of Crosslinked Polymers*, S. S. Labana, ed., Academic Press, New York (1977) p491.
160. Gillham, J. K., *AIChE J.*, **20**, 1066 (1974).
161. Stutz, H., and Mertes, J., *J. Appl. Polym. Sci.*, **38**, 781 (1989).
- 161b. Lee, C. Y-C., and Goldfarb, I. J., *Polym. Eng. Sci.*, **21**, 390 (1981).
- 161c. Lee, C. Y-C., and Goldfarb, I. J., *Polym. Eng. Sci.*, **21**, 951 (1981).
- 161d. Lee, C. Y-C., and Goldfarb, I. J., in *Polymer Characterization: Spectroscopic, Chromatographic, and Physical Instrumental Methods*, C. D. Craver, ed., *Adv. Chem. Ser.*, **203**, ACS, Washington, D. C. (1983) p65.
162. Hofmann, K., and Glasser, W., *Proc. NATAS Conf.*, **18**, 240 (1989).
163. Hofmann, K., and Glasser, W., *Thermochim. Acta.*, in print (1990).
164. Zukas, W. X., MacKnight, W. J., and Schneider, N. S., in *Chemorheology of Thermosetting Polymers*, C. A. May, ed., *ACS Symp. Ser.*, **227**, ACS, Washington, D. C. (1983) p223.
165. Toussaint, A., Cuypers, P., and D'Hont, L., *J. Coat. Technol.*, **57(728)**, 71 (1985).
166. Senhaji, A. C., and Harran, D., *Macromol. Chem., Macromol. Symp.*, **30**, 109 (1989).

167. Chambon, F., and Winter, H. H., *Polym. Bull.*, **13**, 499 (1985).
168. Winter, H. H., *Polym. Eng. Sci.*, **27**, 1698 (1987).
169. Feve, M., *Macromol. Chem. Macromol. Symp.*, **30**, 95 (1989).
170. Khanna, Y. P., Kumar, R., and Das, S., *Polym. Eng. Sci.*, **29**, 1488 (1989).
171. DiBeneditto, A. T., *J. Polym. Sci. Part B: Polym. Phys.*, **25**, 1949 (1987).
172. Nielsen, L. E., *J. Macromol. Sci., Rev. Macromol. Chem.*, **C3(1)**, 69 (1969).
173. Adabbo, H. F., and Williams, R. J. J., *J. Appl. Polym. Sci.*, **27**, 1327 (1982).
174. Gordon, M., and Simpson, W., *Polymer*, **2**, 383 (1961).
175. Lunak, S., Vladyka, J., and Dusek, K., *Polymer*, **19**, 931 (1978).
176. Bair, H. E., *Polym. Prepr. Am. Chem. Soc. Div. Polym. Chem.*, **26(1)**, 10 (1985).
177. Matsouka, S., Quan, X., Bair, H. E., and Boyle, D. J., *Macromolecules*, **22**, 4093 (1989).
178. Wisanrakkit, G., and Gillham, J. K., *J. Coat. Technol.*, **62(783)**, 37 (1990).
179. Rabinowich, E., *Trans. Farad. Soc.*, **33**, 1225 (1937).
180. Adams, G., and Gibbs, J. H., *J. Chem. Phys.*, **43**, 139 (1965).
181. Williams, M. L., Landel, R. F., and Ferry, J. D., *J. Am. Chem. Soc.*, **77**, 3701 (1955).
182. Madorsky, S. L., *Thermal Degradation of Polymers*, Interscience, New York (1964).
183. *Thermal Stability of Polymers I & II*, R. T. Conley, ed., Merceel Dekker, New York (1970).
184. *Degradation and Stabilization of Polymers*, G. Geuskens, ed., John Wiley, New York (1975).



185. *Developments in Polymer Degradation I*, N. Grassie, ed., Applied Science, London (1977).
186. Schnabel, W., *Polymer Degradation: Principles and Practical Applications*, Hanser International, Munich (1981).
187. Hawkins, W. L., *Polymer Degradation and Stabilization*, Springer-Verlag, Berlin (1984).
188. Shelton, J. R., in *Polymer Stabilization*, W. L. Hawkins, ed., Wiley-Interscience, New York, (1972) p29.
189. Hansen, R. H., Martin, W. H., and DeBenedictis, T., *Trans. Inst. Rubber Ind.*, **39**, 301 (1963).
190. Wall, L. A., Harvey, M. R., and Tryon, M. J., *J. Phys. Chem.*, **60**, 1306 (1956).
191. Winslow, F. H., in *Durability of Macromolecular Materials*, R. K. Eby, ed., ACS Symp. Ser., **95**, ACS, Washington, D. C. (1979) p11.
192. Madorsky, S. L., and Straus, S. J., *J. Polym. Sci.*, **36**, 183 (1959).
193. Vo Van, K., Malhotra, S. L., and Blanchard, L. P., *J. Macromol. Sci. Macromol. Chem.*, **A8**, 843 (1974).
194. Dulog, L., and Strock, G., *Makromol. Chem.*, **91**, 50 (1966).
195. Kilic, S., and McGrath, J. E., *Polym. Prepr. Am. Chem. Soc. Div. Polym. Chem.*, **28(1)**, 270 (1987).
196. Yoo, Y. T., Kilic, S., and McGrath, J. E., *Polym. Prepr. Am. Chem. Soc. Div. Polym. Chem.*, **XX**, 358 (1988).
197. Gagnon, S. D., in *Encyclopedia of Polymer Science and Engineering*, Volume 6, 2nd Edition, J. I. Kroschwitz, ed., Wiley-Interscience, New York (1986) p273.
201. Jay, R. R., *Anal. Chem.*, **36**, 667 (1964).
202. Shechter, L., and Wynstra, J., *Ind. Eng. Chem.*, **48**, 86 (1956).

203. Dillman, S. H., Seferis, J. C., and Prime, R. B., *Proc. NATAS Conf.*, **16**, 429 (1987).
204. Matejka, L., Lovy, J., Pokorny, S., Bouchal, K., and Dusek, K., *J. Polym. Sci. Polym. Chem. Ed.*, **21**, 2873 (1983).
205. Fischer, R. F., *J. Polym. Sci.*, **44**, 155 (1960).
206. Tanaka, Y., and Kakiuchi, H., *J. Appl. Polym. Sci.*, **7**, 1063 (1963).
207. Antoon, M. K., and Koenig, J. L., *J. Polym. Sci. Polym. Chem. Ed.*, **19**, 549 (1981).
208. Luston, J., and Vass, F., *Adv. Polym. Sci.*, **56**, 91 (1984).
209. Shechter, L., Wynstra, J., and Kurkijy, R. P., *Ind. Eng. Chem.*, **48**, 94 (1956).
210. Smith, I. T., *Polymer*, **2**, 95 (1961).
211. Grulke, E. A., in *Polymer Handbook*, J. Brandrup, and E. H. Immergut, eds., Wiley-Interscience, New York (1989) pVII-519.
212. van Krevelen, D. W., and Hoftyzer, P. J., *Properties of Polymers: Their Estimation and Correlation with Chemical Structure*, Elsevier, Amsterdam (1976).
213. Barton, A. F. M., *CRC Handbook of Solubility Parameters and Other Cohesion Parameters*, CRC Press, Boca Raton, Florida (1983).
214. Tanaka, Y., and Kakiuchi, H., *J. Appl. Polym. Sci.*, **7**, 1951 (1963).
215. Dillman, S. H., *Kinetic Viscoelasticity of Reacting Polymer Systems*, Ph. D. Dissertation, University of Washington, 1988.
216. Wisanrakkit, G., and Gillham, J. K., *Polym. Prepr. Am. Chem. Soc. Div. Polym. Chem.*, **31(1)**, 293 (1990).
217. Pascault, J. P., and Williams, R. J. J., *J. Polym. Sci.: Part B: Polym. Phys.*, **28**, 85 (1990).
218. Galy, J., Sabra, A., and Pascault, J. P., *Polym. Eng. Sci.*, **26**, 1514 (1986).

219. Rosengerg, B. A., in *Epoxy Resins and Composites II*, K. Dusek, ed., *Adv. Polym. Sci.*, **75**, Springer-Verlag, Berlin (1986) p113.
220. Dusek, K., in *Epoxy Resins and Composites II*, K. Dusek, ed., *Adv. Polym. Sci.*, **78**, Springer-Verlag, Berlin (1986) p1.
221. Zukas, W. X., *Polym. Eng. Sci.*, **29**, 1553 (1989).
222. Small, P. A., *J. Appl. Chem.*, **3**, 77 (1953).
223. Kambour, R. P., Romagosa, E. E., and Gruner, C. L., *Macromolecules*, **5**, 335 (1972).
224. Utracki, L. A., Dumonlin, M. M., and Toma, P., *Polym. Eng. Sci.*, **26**, 34 (1986).
225. Paul, D. R., in *Polymer Blends*, D. R. Paul and S. Newman, eds., Academic Press, New York (1978) p35.
226. Molau, G. E., *J. Polym. Sci.*, **A3**, 1267 (1965).
227. Molau, G. E., *J. Polym. Sci.*, **A3**, 4235 (1965).
228. Molau, G. E., and Wittbrodt, W. M., *Macromolecules*, **1**, 260 (1968).
229. Periard, J., and Reiss, G., *Colloid. Polym. Sci.*, **253**, 362 (1975).
230. Reiss, G., Periard, J., and Banderet, A., in *Colloidal and Morphological Behavior of Block and Graft Copolymers*, G. E. Molau, ed., Plenum Press, New York (1971) p173.
231. Ide, F., and Hasegawa, A., *J. Appl. Polym. Sci.*, **18**, 963 (1974).
232. Cimmino, S., Coppola, F., D'Orazio, L., Greco, R., Maglio, G., Minconico, M., Mancarella, E., Martuscelli, E., and Rastoga, G., *Polymer*, **27**, 1874 (1986).
233. Heikens, D., and Barentsen, W., *Polymer*, **18**, 69 (1977).
234. Heikens, D., Hoen, N., Barentsen, W., Piet, P., and Ladan, H., *J. Polym. Sci. Polym. Symp.*, **62**, 309 (1978).

235. Traugott, T. D., Barlow, J. W., and Paul, D. R., *J. Appl. Polym. Sci.*, **28**, 2947 (1983).
236. Fayt, R., Jerome, R., and Teyssie, Ph., *J. Polym. Sci. Polym. Phys.*, **20**, 2209 (1982).
237. Ouhadi, T., Fayt, R., Jerome, R., and Teyssie, Ph., *Polym. Commun.*, **27**, 212 (1986).
238. Fayt, R., Jerome, R., and Teyssie, Ph., *Macromol. Chem.*, **187**, 837 (1986).
239. Fayt, R., Jerome, R., and Teyssie, Ph., *J. Polym. Sci. Polym. Lett.*, **24**, 25 (1986).
240. Fayt, R., Jerome, R., and Teyssie, Ph., *J. Polym. Sci. Polym. Phys.*, **27**, 775 (1989).
241. Bank, M., Leffingwell, J., and Thies, C., *Macromolecules*, **4**, 44 (1971).
242. Bank, M., Leffingwell, J., and Thies, C., *J. Polym. Sci.*, **10**, 1097 (1972).
243. Nishi, T., and Kwei, T. K., *Polymer*, **16**, 285 (1975).
244. Coover, H. W., McCall, M. A., and Guillet, J. E., *U. S. Patent*, **3,121,070** (1964).
245. Fatou, J. G., *Crystallization Kinetics*, in *Encyclopedia of Polymer engineering Science and Engineering*, **Supplement**, 282 (1989).
246. Nishi, T., and Wang, T. T., *Macromolecules*, **8**, 909 (1975).
247. Hoffman, J. D., and Weeks, J. J., *J. Res. Natl. Bur. Stand.*, **66A**, 13 (1962).
248. Prime, R., Whelihan, E., and Burns, J., *SPE Tech. Pap.*, **34**, 1268 (1988).

## Vita

---

Niranjan M. Patel was born in Calcutta, India on February 21, 1957. After attending elementary school in Calcutta, he moved with his family to Jamnagar in the western Indian state of Gujarat where he finished his high school education. Niranjan has a Bachelor's degree in Chemical Engineering from the Maharaja Sayajirao University of Baroda, India. In 1981, he decided to come to the U. S. to pursue graduate studies, among other things, and joined the Chemical Engineering Department at Virginia Polytechnic Institute and State University at Blacksburg, Virginia. He received an M. S. in 1984 specializing in polymer science under the guidance of Professor David. W. Dwight, at which time he left the university to accept a position of Quality Assurance Engineer at the Hysol Electronic Chemicals Division, Dexter Corporation, near Los Angeles, California. After two years of industrial experience there, Niranjan came back to VPI&SU for doctoral work in polymeric materials under Professor James E. McGrath. He received his Ph. D. in Materials Engineering Science in October, 1990. Niranjan currently holds a post-doctoral position at the Thomas J. Watson Research Center, International Business Machines Corporation at Yorktown Heights, New York.